SHAFT   WHIRLING   IN   A   TWIN-SPOOL

JET   ENGINE   SYSTEM

by

H. RATCLIFFE, B.Sc.

A Thesis submitted for the Degree of Doctor
of Philosophy in the Faculty of Engineering
of the University of Glasgow.

Engineering Laboratories
University of Glasgow
Glasgow W2   April, 1971

ProQuest Number: 10647403

ProQuest 10647403

Location Thesis 3536 (Copy 2)	Author: RATCLIFFE, H. Title: Shaft whirling in a twin-spool jet engine system. Date of deposit:

If you remove this volume from the shelf, enter on this
card the reason for removal, the date, and your initials,
and leave the card on the shelf in place of the volume.
Before re-shelving the volume, score through the record
of removal and replace the card in the volume.

Reason for removal	Date	Initials
Reader Consultation	11/9/85	*(signature)*

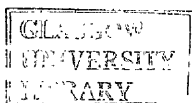| Process	Date	Initials
Accessioned		
Catalogued		
Classified		
Cataloguing checked		
Processed	25/7/84	*(initials)*
Processing checked	—	*(initials)*
Shelved		

SHAFT WHIRLING IN A TWIN-SPOOL

JET ENGINE SYSTEM

Summary of a Thesis submitted by H. Ratcliffe, B.Sc., for the degree of Doctor of Philosophy in The Faculty of Engineering of the University of Glasgow.

Modern jet engines have two co-axial shafts which rotate usually in the same direction but are not coupled mechanically. In common with other types of high speed machinery, shaft vibration, particularly that excited by unbalance and known as whirling, is a serious problem. Despite the enormous investment involved in the design and development of a new type of jet engine, relatively little research has been done on shaft whirling in jet engines. It is believed that no detailed investigation of whirling in a two shaft system has been carried out.

The work described in this thesis was designed to establish the accuracy with which the whirling frequencies could be predicted and in particular to examine how these were influenced by the speeds of the two shafts as a result of gyroscopic effects.

The experimental rig constructed for this investigation was a simple full size model of the rear half of a typical twin-spool jet engine. After extensive testing of the components of the rig, a computer model was developed which would predict the natural frequencies of the rig to an accuracy of better than $5^{o}/o$. It was concluded that this accuracy was not likely to be

approached in the prediction of the frequencies of an actual
jet engine and such calculations should not be relied on in
the design of an engine to ensure that whirling did not
occur within the working speed range.

The computer model was used to explore the variations
of the frequencies over a wide range of combinations of
shaft speed.   Under certain conditions the frequencies were
found to be influenced greatly by the speed of one or both
shafts.   At certain combinations of shaft speed the
character of the mode of vibration of the two shafts was
changed drastically by relatively small variations in the
shaft speeds.   Methods of determining the critical points
of vibration in the working range of a typical jet engine
were examined.   It was found that each frequency which
lay within the working range was liable to be excited by
the unbalance of either shaft.   The results suggest that
more critical points of vibration are likely to be
encountered in the working range of an engine in which the
shafts rotate in opposite directions.

In the course of the investigation a careful examina-
tion of reverse whirl, in which the bent form of the shaft
rotates in the opposite direction to the shaft rotation,
was conducted.   A plausible explanation of the cause of
this phenomenon is given which suggests that it deserves
further study.

One of the shafts exhibited a severe vibration which
was unaffected by the unbalance of the shaft.   The mode
of vibration was that of a subharmonic and further examina-
tion suggested that it was caused by non-linearity of the
support of the shaft as a result of bearing clearance.   It
would appear essential that research into the control of
this type of vibration is conducted.

A NOTE TO THE READER

The pages of text are numbered:—

$$C \cdot N$$

where C is the number of the chapter, and N is the page number of that chapter, e.g. page number 2.12 implies the twelfth text page of Chapter 2.

The text of each chapter is followed by the Tables and Figures referred to in that chapter.

CONTENTS

CHAPTER 10   CONCLUSIONS AND SUGGESTIONS FOR
                   FURTHER WORK

ACKNOWLEDGMENTS

SHAFT WHIRLING IN A TWIN-SPOOL

JET ENGINE SYSTEM

Summary of a Thesis submitted by H. Ratcliffe, B.Sc., for the degree of Doctor of Philosophy in The Faculty of Engineering of the University of Glasgow.

———————

Modern jet engines have two co-axial shafts which rotate usually in the same direction but are not coupled mechanically.   In common with other types of high speed machinery, shaft vibration, particularly that excited by unbalance and known as whirling, is a serious problem. Despite the enormous investment involved in the design and development of a new type of jet engine, relatively little research has been done on shaft whirling in jet engines. It is believed that no detailed investigation of whirling in a two shaft system has been carried out.

The work described in this thesis was designed to establish the accuracy with which the whirling frequencies could be predicted and in particular to examine how these were influenced by the speeds of the two shafts as a result of gyroscopic effects.

The experimental rig constructed for this investigation was a simple full size model of the rear half of a typical twin-spool jet engine.   After extensive testing of the components of the rig, a computer model was developed which would predict the natural frequencies of the rig to an accuracy of better than $5^o/o$.   It was concluded that this accuracy was not likely to be

approached in the prediction of the frequencies of an actual jet engine and such calculations should not be relied on in the design of an engine to ensure that whirling did not occur within the working speed range.

The computer model was used to explore the variations of the frequencies over a wide range of combinations of shaft speed. Under certain conditions the frequencies were found to be influenced greatly by the speed of one or both shafts. At certain combinations of shaft speed the character of the mode of vibration of the two shafts was changed drastically by relatively small variations in the shaft speeds. Methods of determining the critical points of vibration in the working range of a typical jet engine were examined. It was found that each frequency which lay within the working range was liable to be excited by the unbalance of either shaft. The results suggest that more critical points of vibration are likely to be encountered in the working range of an engine in which the shafts rotate in opposite directions.

In the course of the investigation a careful examination of reverse whirl, in which the bent form of the shaft rotates in the opposite direction to the shaft rotation, was conducted. A plausible explanation of the cause of this phenomenon is given which suggests that it deserves further study.

One of the shafts exhibited a severe vibration which was unaffected by the unbalance of the shaft. The mode of vibration was that of a subharmonic and further examination suggested that it was caused by non-linearity of the support of the shaft as a result of bearing clearance. It would appear essential that research into the control of this type of vibration is conducted.

CHAPTER 1

INTRODUCTION

SUMMARY

An outline of the development of the understanding of the behaviour of a whirling shaft is presented. Some of the factors which influence the whirling of a shaft, such as gyroscopic effects, shaft and bearing flexibilities and friction are discussed.

The light and complicated structure of a jet engine presents difficulty in the accurate prediction of the whirling speeds. Further difficulty arises in modern jet engines which have two co-axial shafts, which are mechanically independent, and as a result the ratio of the two speeds is not constant.

The purpose of this investigation was to examine the accuracy of prediction of the whirling speeds of a two-shaft model, which resembled part of a jet engine, and in particular to study the effect of the shaft speeds on the whirling behaviour.

CHAPTER 1

INTRODUCTION

1.1   The Phenomenon of Whirling

The violent behaviour which a rotating shaft may display when the speed reaches a certain critical value was originally reported by Rankine in 1869 (Ref.1). Rankine argued that when the speed reached a critical value any small deflection of the shaft would result in a centrifugal loading which would exceed the elastic forces and therefore the shaft would become unstable. He called the phenomenon 'centrifugal whirling' and proceeded to describe how the critical speed could be obtained.

Greenhill published the results of an examination he had made of the stability of a rotating shaft subjected to a twisting moment and an end thrust, as might occur in the screw shaft of a steamer (Ref.2). He showed that it was possible for the shaft to adopt a helical form at a certain speed, but his theory did not reveal the true nature of whirling.

Reynolds examined theoretically the possibility of predicting the whirling speeds of uniform shafts. The work was continued by Dunkerley who reported the results of an extensive investigation into the problem of predicting the critical speeds of uniform shafts carrying one or more pulleys (Ref.3). He found that the critical speeds of a uniform shaft were identical to the frequencies of lateral vibration, when the shaft was not rotating, calculated using the Euler-Bernouilli elastic equations. When he attempted to calculate the critical speeds of a shaft carrying a pulley the theory became too complex to be readily solved in practical cases. Noting the relation which existed between the frequency of vibration of a

spring carrying two masses to the frequencies which occurred when the spring carried each mass in turn, he was led to a relation which gave a very good prediction of the lowest critical speed of a shaft carrying one or more pulleys. In this method of Dunkerley, the frequency of lateral vibration of the shaft alone is combined with the frequencies it would exhibit, if it were massless, when carrying each mass in turn. Dunkerley proceeded to show experimentally that the method gave a very good estimate of the lowest critical speed of a shaft carrying several pulleys.

Some years later the Swedish inventor, de Laval, encountered the phenomenon of whirling in the development of the first practical steam turbine (Ref.4). He discovered that if the shaft could be accelerated sufficiently rapidly, violent motion of the shaft in the vicinity of the critical speed would not have time to develop, and smooth operation was possible above this speed. His turbines were therefore designed to utilise this principle and operated at speeds several times the critical speed.

The theoretical description of a whirling shaft continued to be studied by, among others, Chree, Lees and Jeffcott (Refs.5,6,7). Jeffcott's paper, published in 1918, contained a particularly clear exposition of the behaviour of a whirling shaft.

Jeffcott considered a light uniform shaft, supported freely in rigid bearings at its ends, which carried a mass, m, at the centre of the span. The centre of mass was supposed to be offset a small distance, a, from the axis of the shaft and the motion of the mass was opposed by the surrounding medium in a viscous manner.

The motion of the mass was defined with respect to a stationary system of co-ordinate axes (x,y) in a plane transverse to the axis of the bearings at the centre of the span (Fig.1.1). The origin of the axes, O, lay on the

bearing axis, while the position of the deflected axis.
was defined by point C, which had co-ordinates (x,y).
The position of the centre of mass was defined by point G,
distance, a, from C, such that line CG was inclined at an
angle ωt to the X – axis at time t when the shaft rotated
at an constant angular velocity, ω.

Since no other external forces, other than the
viscous resistance, act on the mass, the equations of motion
in the X and Y directions are given by:–

$$m \frac{d^2}{dt^2} (x + a \cos \omega t) + f \frac{dx}{dt} + kx = 0$$

$$m \frac{d^2}{dt^2} (y + a \sin \omega t) + f \frac{dy}{dt} + ky = 0$$

in which f is the coefficient of viscous resistance and k
is the elastic stiffness of the shaft.

The two equations may be re-arranged in the form:–

$$m \frac{d^2x}{dt^2} + f \frac{dx}{dt} + kx = ma \, \omega^2 \cos \omega t$$

$$m \frac{d^2y}{dt^2} + f \frac{dy}{dt} + ky = ma \, \omega^2 \sin \omega t$$

The first part of the solution of these standard
equations is damped oscillatory and does not depend on the
eccentricity of the mass.   The remaining part of the
solution is

$$x = \frac{ma \, \omega^2}{\sqrt{(k - m \, \omega^2)^2 + f^2 \, \omega^2}} \cos(\omega t - \varphi)$$

$$y = \frac{ma \, \omega^2}{\sqrt{(k - m \, \omega^2)^2 + f^2 \, \omega^2}} \sin(\omega t - \varphi)$$

where $$\tan \varphi = \frac{f\omega}{k - m \, \omega^2}$$

This solution shows that the path of the axis of the shaft is circular, since $x^2 + y^2$ = constant, and at any rotational speed, ω, the line CG subtends a constant angle φ to the line OC. At low speeds the radius of the path of the shaft axis is small and the centre of mass, G, lies outside the path of the shaft axis, C. If the viscous resistance is relatively small, as it usually is in practice, the radius of the path is large when the rotational speed approaches a value equal to $\sqrt{k/m}$, which is the frequency of lateral vibration of the shaft, when it is not rotating, and this speed is called the critical speed. At very high speeds, since the radius approaches the value a, while the angle φ approaches π, the centre of mass tends towards the axis of the bearings, with the shaft revolving around it.

Jeffcott thus showed that the deflection of the shaft in the vicinity of the critical speed was finite, being controlled by the resistance offered by the surroundings, and that stable operation above the critical speed was possible. He also noted that, provided the shaft could be accelerated rapidly to speeds above the critical speed, dangerously large amplitudes would not have time to develop in the vicinity of the critical speed, a principle which de Laval had employed several years earlier.

1.2 Influence of the Bearing Supports

In practice the supports of the bearings are never rigid and they may also offer some frictional resistance to motion. Smith, in a remarkable paper published in 1933, reported his examination of the behaviour of a rotor mounted in flexible bearings containing some frictional resistance (Ref.8). He found that whereas the critical speed would be lowered when the flexibility of the supports was included, the character of the motion was not changed provided the characteristics of the bearing supports were symmetrical.

When the bearing supports were not symmetrical
he found that the rotor had two critical speeds,
corresponding to the frequencies of lateral vibration of
the rotor in the directions of maximum and minimum bearing
stiffness, and the amplitude of motion of the rotor at
these two speeds was still controlled by the friction
applied to the rotor and the bearing supports. Between
these two speeds, the rotor whirled in a sense opposite to
its rotation, and therefore of the unbalance.

When a shaft is mounted in oil lubricated journal
bearings, the oil film might be expected to provide a
contribution to the flexibility and damping characteristics
of the bearing supports. However, the properties of an oil
film in such bearings is complex and certainly non-linear.

Newkirk discovered that a rotor mounted in journal
bearings would exhibit unstable behaviour at speeds above
about twice the critical speed which it would exhibit in
ideal bearings (Ref.9). He argued that since the mean
angular velocity of the oil film was approximately half
the rotor speed, disturbances at this speed were likely to
occur due to the wedging action of the oil film. This
unstable behaviour is of particular importance in very
large alternators, which operate above the first critical
speed, and it continues to demand the attention of research
workers (Ref.10).

1.3 Gyroscopic Effects

Early steam turbine designers found that the whirling
behaviour of a rotor would be influenced significantly by
the gyroscopic effects of turbine wheels (Ref.4).

The gyroscopic effect on the whirling of a rotor may
be demonstrated by considering the motion of a light uniform
shaft mounted as a cantilever in a rigid bearing, which
carries a disc at the free end (Ref.11). When the shaft

is deflected the disc is tilted as shown in Fig.1.2.
The disc has a mass, m, but the centre of mass is
displaced from the axis of the shaft by a distance, a,
as before.   The disc is rigid and uniform, with a mass
moment of inertia about any diameter, A, and about its
axis, C.

Using X–Y co-ordinate axes in a transverse plane
through the mounting point of the disc,(when the shaft is
stationary), the co-ordinates of the centre of mass are,
as before

$$x + a \cos \omega t, \quad y + a \sin \omega t$$

where ω is the rotational speed.

During the supposed whirling motion the disc will
have angular velocities, $\dot{\varphi}_x$ and $\dot{\varphi}_y$, and accelerations,
$\ddot{\varphi}_x$ and $\ddot{\varphi}_y$.   The angular acceleration $\ddot{\varphi}_x$ requires a moment
about the X – axis, $A\ddot{\varphi}_x$, to be applied to the disc.   In
addition, since the rotation of the disc about the Y – axis
will cause a change in the angular momentum, $C\omega$, an
additional moment about the X – axis, $C\omega\dot{\varphi}_y$, must be applied
to the disc.   Therefore the total moment which must be
applied, about the X – axis to the disc to maintain the
supposed motion is:–

$$A\ddot{\varphi}_x + C\omega\dot{\varphi}_y$$

Similarly, the angular velocity, $\dot{\varphi}_x$, and acceleration,
$\ddot{\varphi}_y$, imply that a moment about the Y – axis

$$A\ddot{\varphi}_y - C\omega\dot{\varphi}_x$$

must be applied to the disc.

The deflection, y, and slope, φ_x, of the end of the
shaft are related to the force, F_y, and moment, M_x, applied
to it by equations of the form:–

$$y = r.F_y + s.M_x$$

$$\varphi_x = s.F_y + t.M_x$$

where r, s and t are positive elastic constants of the shaft.   Inversion of these equations gives:—

$$F_y = d.y + e.\varphi_x$$

$$M_x = e.y + f.\varphi_x$$

where again d, e and f are positive quantities.

Similar relations between the loads F_x and M_y, and the movements x and φ_y, of the end of the shaft are found to be:—

$$F_x = d.x - e.\varphi_y$$

$$M_y = -e.x + f.\varphi_y$$

where the signs are found to alter to comply with the sense of the co-ordinate axes.

These loads are required to produce the assumed displacements of the end of the shaft.   Loads opposite to these will be applied to the disc during the supposed motion, and therefore the equations of motion of the disc become:—

$$m \frac{d^2}{dt^2} (x + a \cos \omega t) = -d.x + e.\varphi_y$$

$$m \frac{d^2}{dt^2} (y + a \sin \omega t) = -d.y - e.\varphi_x$$

$$A\ddot{\varphi}_x + C\omega\dot{\varphi}_y = -e.y - f.\varphi_x$$

$$A\ddot{\varphi}_y - C\omega\dot{\varphi}_x = e.x + f.\varphi_y$$

These equations may be combined using complex notation by putting

$$z = x + iy$$

$$\varphi = -\varphi_y + i\varphi_x$$

to give:—

$$m\ddot{z} + d\dot{z} + e\varphi = ma\,\omega^2 e^{i\omega t}$$

$$A\ddot{\varphi} - iC\omega\dot{\varphi} + ez + f\varphi = 0$$

The free vibration of the disc, which in practice decays as a result of damping, may be assumed to be of the form:—

$$z = Z_1 e^{i\lambda t}, \quad \varphi = \Phi_1 e^{i\lambda t}$$

which leads to the conclusion that vibration will occur when the determinant of the coefficients

$$\begin{vmatrix} d - m\lambda^2 & e \\ e & C\omega\lambda - A\lambda^2 + f \end{vmatrix}$$

becomes zero.

Thus the natural frequencies of the rotor are given by the roots of the equations:—

$$(d - m\lambda^2)(C\omega\lambda - A\lambda^2 + f) - e^2 = 0$$

Putting $C = 2A$, for the case when the disc is thin, then gives:—

$$\lambda^4 - 2\omega\lambda^3 - \left(\frac{d}{m} + \frac{f}{a}\right)\lambda^2 + \frac{2d\omega\lambda}{m} + \frac{df - e^2}{Am} = 0$$

The variation of the four roots of this equation with the rotational speed of the rotor, ω, is illustrated in Fig.1.3. When the rotor is not rotating the roots are $\pm\lambda_1$ and $\pm\lambda_2$ so that the free motion of the disc is

$$z = Ae^{i\lambda_1 t} + Be^{i\lambda_2 t} + Ce^{-i\lambda_1 t} + De^{-i\lambda_2 t}$$

and the disc describes an elliptical path, either clockwise or anti-clockwise. The frequencies λ_1 and λ_2 are identical to the natural frequencies of lateral vibration of the rotor when it does not rotate.

The figure shows that when the rotor is rotating it may whirl at two frequencies which are higher than the irrotational frequencies λ_1 and λ_2, and since the values are positive, it precesses in the same sense as the rotation.   (The word 'precess' has been adopted by workers in the field of shaft vibration to mean 'moves in a closed (normally) path').

The rotor may also whirl at two other frequencies which are lower than the irrotational frequencies, and since these are negative, it precesses in the opposite sense to the rotation.

The steady state solution of the motion of the disc due to the unbalance, is assumed to be of the form:—

$$z = Z_2 e^{i\omega t}, \quad \varphi = \Phi_2 e^{i\omega t}$$

and solution of the equations of motion, putting

$$\lambda = \omega \quad \text{and} \quad C = 2A$$

gives

$$Z_2 = \frac{ma\omega^2 (A\omega^2 + f)}{\omega^4 + (\frac{f}{A} - \frac{d}{m})\omega^2 + \frac{e^2 - df}{Am}} \cdot e^{i\omega t}$$

The denominator of this expression has the same form as the frequency equation when $\lambda = +\omega$.   Resonance will therefore occur when the rotational speed of the rotor is equal to a natural frequency of vibration at which forward precession occurs.   The line $\lambda = +\omega$ in Fig.1.3 shows that, for this simple rotor, resonance will only occur at one speed, which is termed the critical speed of forward precession.   This speed is somewhat higher than the lower natural frequency of lateral vibration which the rotor exhibits when it is not rotating, as a result of the gyroscopic effect of the disc.

Some workers have reported that minor resonance may be observed when the rotor speed coincides with a natural frequency at which reverse precession occurs (line $\lambda = -\omega$ in Fig.1.3). The rotor therefore, rather surprisingly, precesses in a sense opposite to that of the unbalance. Stodola (Ref.4) claimed that this behaviour resulted when the fixing of the disc to the shaft became loose.

Whenever the influence of gyroscopic effects on whirling is discussed in the literature the possibility of reverse whirl is usually given as an aside. den Hartog, an authority with a vast experience of practical vibration problems, reports how he 'looked around and asked his friends for fifteen years about it and was just about to conclude that it was imaginary when a case actually occurred' (Ref.12). He was forced to conclude after many tests, using several shafts and discs, that it was unaffected by unbalance or asymmetry of the shaft cross-section, and its real cause was unknown.

Whenever reverse whirl has been observed by research workers its amplitude has always been small. Whereas, at the forward whirling speed, the bending of the shaft does not fluctuate and therefore internal hysteresis does not act so as to control the vibration, at the reverse whirling speed the shaft bending fluctuates at a frequency equal to twice the speed and control of the vibration is assisted by internal hysteresis.

1.4   The Influence of Internal Friction

The discussion of gyroscopic effects showed that the frequency of vibration of the rotor was affected by the rotational speed. Whirling is a peculiar type of vibration in that a distinction has to be made between the rotational speed of the bent form of the rotor, i.e. its movement or precession, and the rotational speed of the rotor about its own axis.

An effect discovered by Kimball in 1926, which illustrates this peculiar aspect of whirling, is that a frictional mechanism within the rotor, due to hysteresis or movement of clamp fixing used in its construction, may cause instability (Ref.13).

If a non-rotating shaft is bent to and fro, internal hysteresis will cause the load/deflection diagram to traverse a loop as shown in Fig.1.4(a). Imperfect clamp fixings which slip as the shaft bends, Fig.1.4(b), will also cause the diagram to form a closed loop. Both mechanisms absorb energy and convert it to heat and are therefore classed as damping.

If the shaft rotates, while being held in a stationary deflected position, as shown in Fig.1.4(c), the imaginary fibres of the shaft will undergo alternate tension and compression. The fibres marked 1 and 3 will experience maximum strain and therefore maximum tension and compression respectively, while fibres 2 and 4 will be unstrained. But when the strains of these fibres are related to the hysteresis loop, Fig.1.4(a), it can be seen that fibre 2 is in compression while fibre 4 is in tension. When all the fibres are considered it is found that the unstressed fibres lie along the dashed line in the figure, which is not at right angles to the shaft deflection. The internal friction, therefore, produces a tangential force, F_h, which tends to drag the shaft in the direction of rotation. This force is, in some way, related to the shaft deflection and its rotational speed.

When the shaft is free to vibrate, and therefore free to precess at a rate λ, as shown in Fig.1.4(c), internal friction results in a tangential force acting on the shaft, the direction of which depends on the difference between the shaft speed, ω, and the speed of precession, λ. When the shaft speed is less than the critical speed, λ, the tangential force acts opposite

to the direction of precession and therefore assists
the normal friction exerted on the shaft by the
surrounding medium.   At the critical speed, when $\omega = \lambda$,
the force due to internal friction is zero since the
fibres do not experience cyclic strain.   When the shaft
speed exceeds the frequency, λ, the tangential force due
to internal friction opposes the external frictional
force, F_e, and at sufficiently high speeds will overcome
the latter and instability results (Ref.8).

When gyroscopic effects are present in a rotor the
forward whirling speed is still not controlled by internal
friction.   But when the reverse whirling speed is
encountered the internal friction may provide a strong
influence since the shaft fibres are cycled at a frequency
equal to twice the rotor speed.

1.5   The Prediction of Critical Speeds

The prediction of critical speeds is carried out by
determining the natural frequency of lateral vibration of
the rotor, with an appropriate correction being made for
gyroscopic effects when the rotor contains large discs.

Sometimes the rotor configuration is such that it
may be assumed to approximate to a uniform light shaft
carrying several discs in which case a reasonable estimate
of the lowest speed may be obtained using either the
Rayleigh or Dunkerley methods.   In large steam turbines
the cross-section of the rotor is large in comparison
with the span and varies appreciably along the span, and
no such simplification of its form can be made to ease
the analysis.

Designers realised that steam turbine rotors could
be analysed by a 'lumped - mass' technique but the
computation involved was considered prohibitive (Morris,
working in the field of aircraft design, had some success
in devising efficient methods which reduced the

computational labour (Ref.14)).   A graphical method,
normally used for determining the deflection of loaded
beams was employed.   A deflection curve for the rotor,
supposed to be whirling at a certain speed, was assumed,
from which the centrifugal loading along the span was
obtained.   The true deflection of the rotor under this
loading was then determined graphically and compared with
the assumed deflection curve to produce a better estimate
of the critical speed.   The method was limited since it
was only convergent for the lowest critical speed
(Ref.4).

In 1945 Prohl outlined a method which was analogous
to the Holzer method of determining the frequencies of
torsional vibration of shafts (Ref.15).   Starting with a
guessed value for the critical speed and the boundary
conditions at one end of the rotor, a simultaneous step --
wise integration of the shear force, bending moment, slope
and deflection is carried out along the rotor.   The
conditions obtained at the other end of the span are then
compared with the true boundary conditions to obtain a
better estimate of the critical speed.

Prohl's method was suitable for calculating critical
speeds higher than the first, which was an advance over
existing methods, but was still tedious.   However, this
drawback was soon resolved by the advent of digital
computers.

The computational facility offered by computers also
permitted the calculation of critical speeds to be
formulated in a more elegant manner as an eigenvalue
problem.

1.6   The Jet Engine

One of the first successful applications of the gas turbine to aircraft propulsion was designed and developed by Sir Frank Whittle, who called it simply, a jet engine.   Whittle used a centrifugal compressor since it was lighter and more robust than the axial type and a wealth of experience on small centrifugal compressors for supercharging piston engines already existed.

Later, when the efficient design of axial flow compressors became feasible, the axial type superseded the centrifugal compressor for all but the smallest jet engines.

The development of the axial compressor to obtain even higher compression ratios was found to lead to handling difficulties.   Since the blade row diameters are approximately the same, the compressor must be designed to have almost constant axial velocity of air flow in order to obtain reasonable blade angles.   As the speed is reduced, because the delivery pressure falls more rapidly than the mass flow, the near constant axial velocity is not maintained with the result that the blades in the front stages stall and rapid deterioration in performance, known as surge, results (Ref.16).

The handling difficulties inherent in high compression ratio axial compressors were in some cases overcome by arranging for some of the air flow to be bled from the later stages of the compressor at low speeds. This remedy is wasteful and not always completely successful in avoiding surge throughout the speed range. A better solution is to divide the compressor into two mechanically independent units, driven by separate turbines as shown diagrammatically in Fig.1.5.   The arrangement shown is typical of modern bypass jet engine design. About half the mass flow delivered by the low pressure compressor is diverted around the engine to be mixed with

the remaining air just before the propelling nozzle, thus achieving a high propulsive efficiency with a significant reduction in jet noise.

1.7   Balancing of Jet Engines

Since very high rotational speeds are used in jet engines, balancing of the rotors is extremely important. During the assembly of an engine each rotor is balanced carefully at several stages during assembly.   Current balancing methods are capable of balancing a rotor dynamically to within 1/10 oz. in.   The centre of mass of a typical turbine rotor weighing 100 lbf. would therefore lie only 0.00006 in. from the axis of the bearings.   (Although the eccentricity would seem very small, the out of balance force developed at a speed of 12000 rpm would be 25 lbf).

The fine degree of balance achieved during assembly is almost certainly lost when the engine reaches operating temperatures, due to differential expansion and consequent movement of the parts of the assembly.   In service the rotors are liable to receive some damage which destroys the balance of the rotors.   The ingestion of ice, stones or even birds into the compressor intake, or the uncommon turbine blade failure, may not result in catastrophic failure of the engine, and it is therefore essential that the engine should continue to operate without serious rotor vibration even when seriously unbalanced by such damage.

Serious rotor vibration or whirl is normally avoided since the resultant cyclic bending of the shaft may eventually lead to shaft failure.   But in jet engines the flexibility of the bearing mountings is usually appreciable so that the bending of the shaft under vibration may not be so serious as the movement of the rotor in relation to the casing of the engine.

As with all turbine engines the clearances
between the blades and the casing are designed to be
as small as possible.   In addition the metering of the
vital cooling air supply to the turbine discs is controlled
by labyrinth seals between the rotors and the casing, which
again have very small clearances.   Appreciable movement
of the rotors due to vibration must be avoided otherwise
serious damage may occur at any of these small clearances –
and if titanium blades, which are sometimes used in the
compressor, do rub, catastrophic fires usually result.

1.8   Rotor Damping in Jet Engines

The complexity of a co–axial engine means that the
rotors usually consist of two or more sections which are
coupled by splined connections.   Since large torques are
transmitted by these splines, any flexing of the shaft could
result in a degree of internal damping in addition to that
which occurs at the numerous clamp fits employed at various
points in a complex rotor.   Thus there is the possibility
of a rotor becoming unstable at high speeds, as originally
pointed out by Kimball.   No investigation of this aspect
appears to have been carried out on jet engines.

1.9   Occurrence of Whirling in Jet Engines

The prediction of critical speeds in a jet engine
is more complex than in other types of turbo machinery
because the quest for lighter construction results in the
flexibilities of the casing and the bearing supports, and
the attachment of the engine to the aircraft, having a
significant effect on the vibration of the rotors.   In
the larger types of engine the critical speeds cannot,
as a result, be placed above the maximum speed, and
instead the flexibility of the bearing mountings is often
deliberately exploited in order to place the lowest critical
speed below the idling speed of the engine.

Further complications arise in multi—shaft engines.   A typical plot of the variation of shaft speeds with thrust in a twin—spool engine is shown in Fig.1.6.   Both shafts rotate in the same sense otherwise the bearing between the two would have a relative speed equal to the sum of the shaft speeds, which is a difficult requirement to demand of such high duty components.   If, as already stated, the critical speeds were designed to be below the respective idling speeds of the shafts, then it would seem that whirling within the operating range of speeds would be avoided (assuming the next highest critical speeds were above the maximum shaft speeds).   However, if the critical speed (which is the speed at which the natural frequency of the rotating shaft equals the rotational speed) of the high pressure shaft were at 5000 rpm, say, it might be expected that the natural frequency of the shaft would rise to perhaps 6000 rpm when it rotated at 11000 rpm, due to gyroscopic effects.   But under these conditions the low pressure shaft is rotating at 6000 rpm.   There is, therefore, the possibility that the H.P. (high pressure) shaft may be excited by the unbalance of the L.P. (low pressure) shaft.   Thus in a twin—spool engine it is not sufficient merely to consider the position of the conventional critical speeds in relation to the operating speed range of the engine.

In conventional jet engines the gyroscopic couples exerted by the rotors during manoeuvres can be contained by the large aerodynamic forces available in high speed aircraft.   But in vertical take-off aircraft, adequate control of the attitude of the aircraft during take off, either by swivelling of the nozzles or by air jets at the extremities of the machine, is not easily obtained.   As a result, contra—rotating engines may be necessary for such applications to reduce the gyroscopic couples.   But then the reverse whirling mode of shaft vibration, formerly regarded as of little importance, must be examined.

Although the rotor of a jet engine may never operate at a speed which coincides with its natural frequency, the possibility of excitation from other sources must not be overlooked.   It seems likely that many vertical take-off aircraft will use banks of small engines to provide lift.   If vertical control is provided by throttling some of the engines while the remainder operate at full thrust, unbalance of a throttled engine may conceivably excite vibration of a nearby engine which is running at full speed.

External excitation of a rotor may also be provided by an auxiliary shaft which is driven by the rotor through gearing.   The most serious occurrence of this excitation would exist in turbo-prop engines as a result of the fluctuating forces exerted by the propellor.

1.10   Aims of this Work

The writer spent several years working in an aircraft engine company, Rolls-Royce Ltd.   Although he was only briefly engaged on jet engine development he was aware, through discussions with colleagues, of the problems of shaft vibration on several types of aircraft engine.

The first major axial flow engine built by the company, about 1952, had a single shaft and was plagued by 'rough running' in the early stages of development. The trouble sponsored a detailed investigation of the methods of the prediction of critical speeds and resulted in the formation of the computer department.

The first twin-spool engine, built about 1955, was found to have serious shaft vibration which was recognised as whirling and caused serious mechanical damage due to rubbing between the two shafts.   The whirling speeds had been predicted to lie above the maximum speed of the engine but it was later found that the influence of the

flexibilities of the bearing supports, which had been
neglected in the calculation, were not negligible.

The shaft vibration troubles encountered on these
two engines were eventually overcome during development
and both became very successful engines in service.
How the troubles were overcome is difficult to establish.
Certainly much effort was devoted to improving balancing
techniques, the location and fits of the components of
the rotors and altering the clearances and mountings of
the bearings.   But at the same time other engine
components were also being continually modified during
the course of development.   Thus, although the vibration
troubles were overcome, it would be difficult to specify
which of the many modifications had been responsible.

In the late 1950's, a new twin-spool engine began
development.   As a result of experience gained on its
predecessors, the flexibility of the bearing mountings
was designed to ensure that the critical speeds were at
the lower end of the operating speed range so that the
shafts normally operated with the centre of mass tending
to lie close to the bearing axis, as had been done on
de Laval's turbines.   Whirling was not found to be a
serious problem on this engine.   Instead, severe
vibration, resembling instability, was encountered at
speeds approaching the maximum operating speed.   The
phenomenon was unusual since it was not 'triggered'
until the engine had been operating for some minutes at
high speed, suggesting that thermal effects were involved.
Despite intensive development on several prototype engines
the problem was never solved and it was fortuitous that
a competitor's engine was eventually chosen for the
aircraft concerned.

The vibration trouble encountered on the single shaft engine resulted in an investigation into shaft vibration being carried out on a model engine by Purdy at Cambridge (Ref.17). The model was very complex since it was designed to investigate the vibration behaviour of the complete engine. Partly as a result of the complexity, the experimental work was limited to determining the many frequencies of vibration. These were not predicted with much accuracy and in this writer's opinion the work did not advance understanding of the problem.

Aircraft engine manufacturers have at times carried out their own investigations into shaft vibration on experimental models but these appear to have been restricted to single shafts mounted in flexible bearing mountings and were only intended to confirm that accurate predictions of critical speeds could be carried out for such simple models.

It would seem surprising that no detailed research into the vibration of aero engine shafts has been carried out when the huge investment in such engines is considered. From a shaft vibration point of view, these engines differ markedly from other rotating machinery in that the rotors are quite complex in construction (many of the parts, such as compressor blades, are often not rigidly connected to the rotor) and run at relatively high speeds in very light, and therefore flexible, casings.

An important aspect which demands study is the accuracy of prediction of critical speeds. This question does not appear to have been resolved by aero engine designers, probably because the prototype engine appears perhaps two years, at least, after the last critical speed survey was carried out, during which time many design changes may have been made which were not thought to require a further assessment of critical speeds. As a

result any check on the accuracy of the original calculations is not valid. The writer has invited the opinions of engine designers on the possible accuracy of prediction with little success. He believes that the accuracy achieved may not be better than 10%.

Since most engines currently being designed have at least two co-axial shafts there seems to be a strong case for examining the behaviour of co-axial arrangements of shafts, containing considerable gyroscopic effects, and rotating in either the same or opposite sense.

As suggested earlier, the rotors in aero engines contain many possible sources of internal damping. Since it is known that this can prove to be a cause of instability, and one engine may have shown behaviour of this nature, an evaluation of the possible magnitude of this internal damping, in relation to the external damping acting on the rotors, ought to be undertaken.

The influence of the bearings on the vibration of a rotor can be significant. But the investigation of this aspect is again difficult to conduct in a rational manner during the course of development of an aero engine.

In embarking on this investigation the writer considered which factors could be investigated conveniently on one model. The vibration behaviour of co-axial shaft systems was considered to be the most important aspect since no work appeared to have been done on such systems. But as this aspect could not be carried out properly without a mathematical analysis of the model, it was decided that the accuracy of prediction of critical speeds could be usefully examined at the same time.

An examination of the influence of rotor damping would have involved the construction of complex rotors with special devices to represent the presence of torque loaded splines. It was decided that an examination of

the effect of rotor damping would have increased the
complexity of a two rotor model to such a degree that
a successful examination of the above two aspects would
be difficult.

The influence of bearing parameters on a co-axial
system would not be expected to be markedly different to
that on a single shaft system.   In any case, such an
investigation would be best carried out on a single shaft
model.   It was decided that no attempt would be made to
examine the bearing aspect in detail on the proposed model.

In conclusion, the object of this work was to design
and build a co-axial shaft system which had some resemblance
to an aero engine, to determine the accuracy with which the
critical speeds could be predicted, and to examine the
variation of these over a reasonably wide range of shaft
speeds.

Fig.1.1

(a)

(b)

$$r = \sqrt{x^2 + y^2}$$

(c)

$$\sqrt{\frac{k}{m}}$$

ω

a
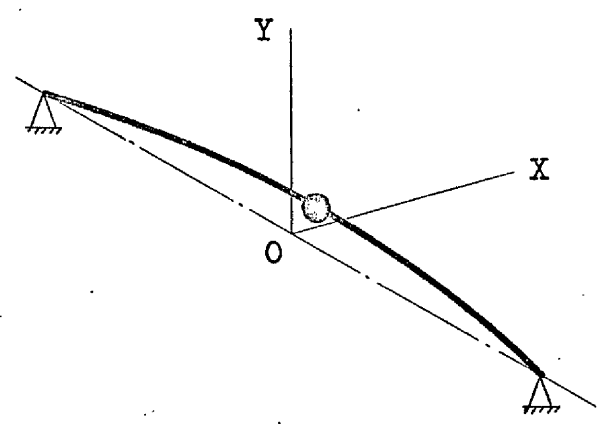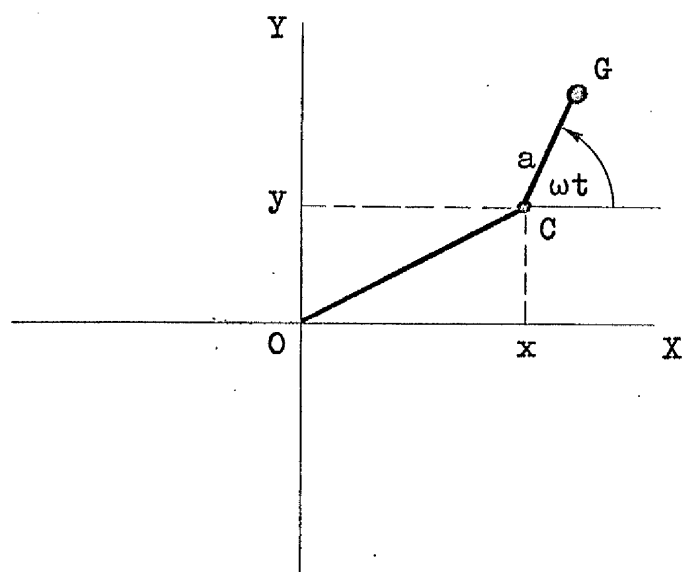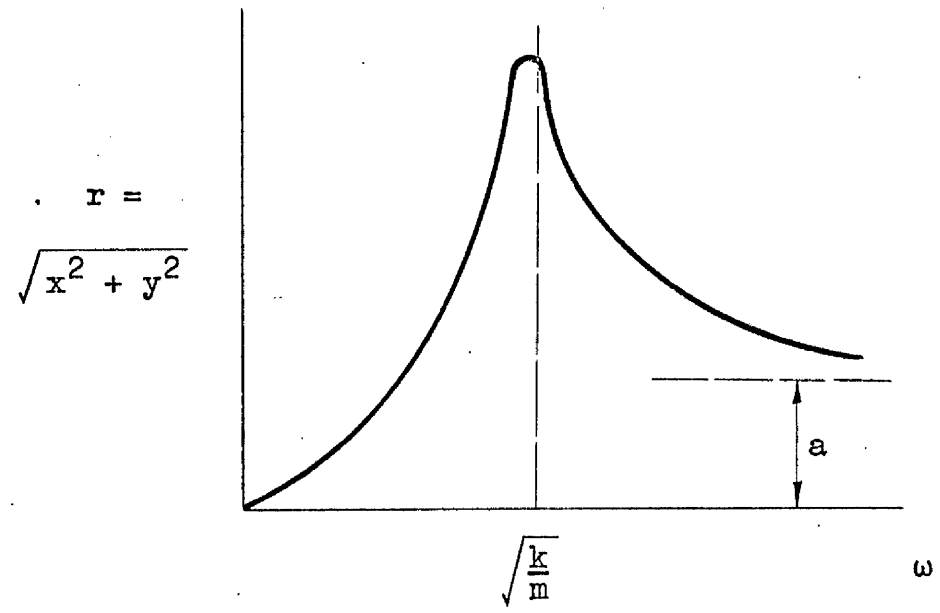
Fig.1.1   Whirling of a simply supported shaft carrying a point mass at the centre.
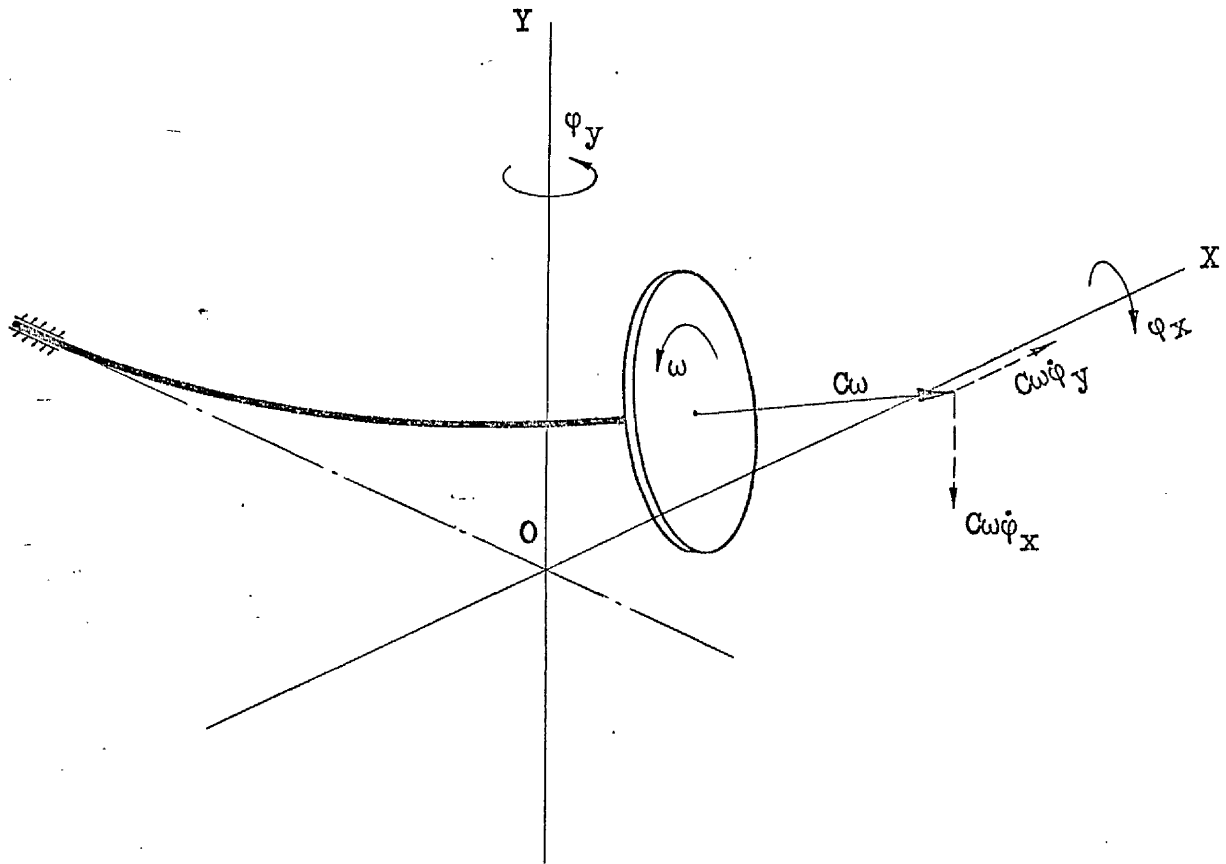
Fig.1.2

Fig.1.2 Whirling of a cantilevered shaft
carrying a disc at the free end.
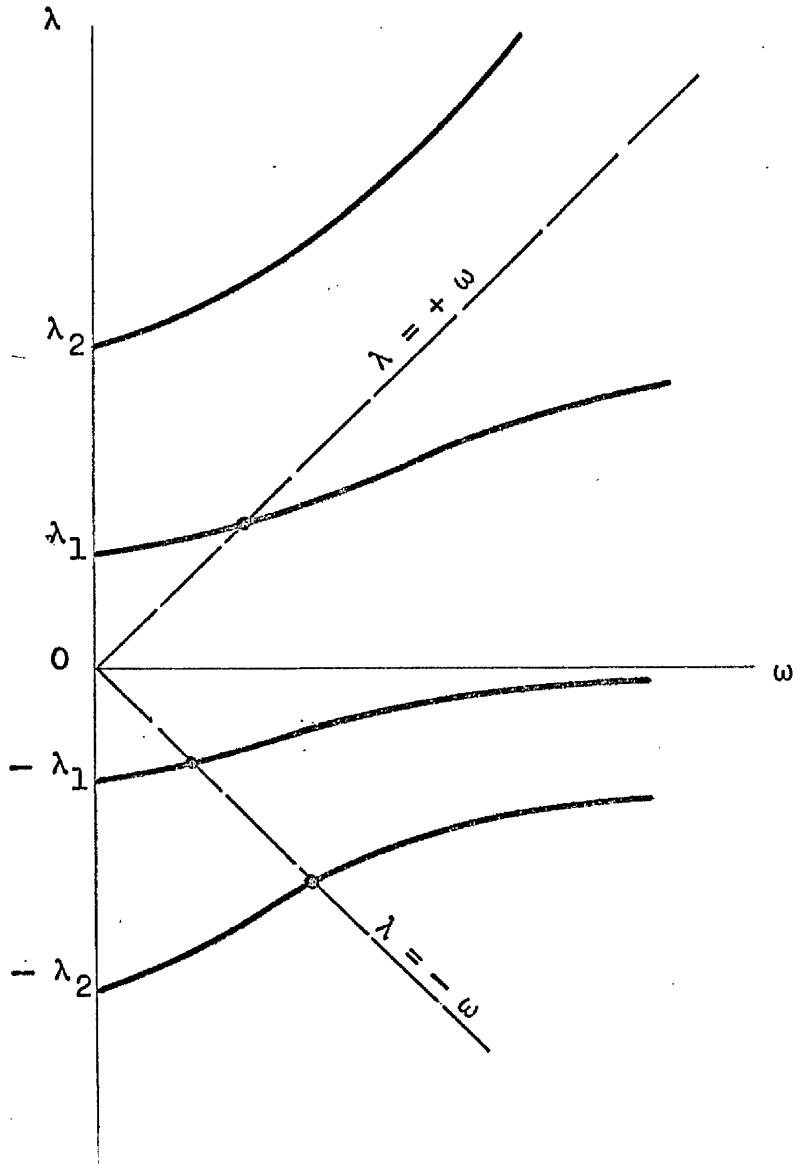
Fig.1.3

Fig.1.3 Natural frequencies of cantilevered shaft/disc system versus rotational speed, ω.

Fig.1.4

Load

1

4

Deflection

2

3

(a)

(b)

Y

F_h

ω

2

1

λ

3

4

F_e

O

X
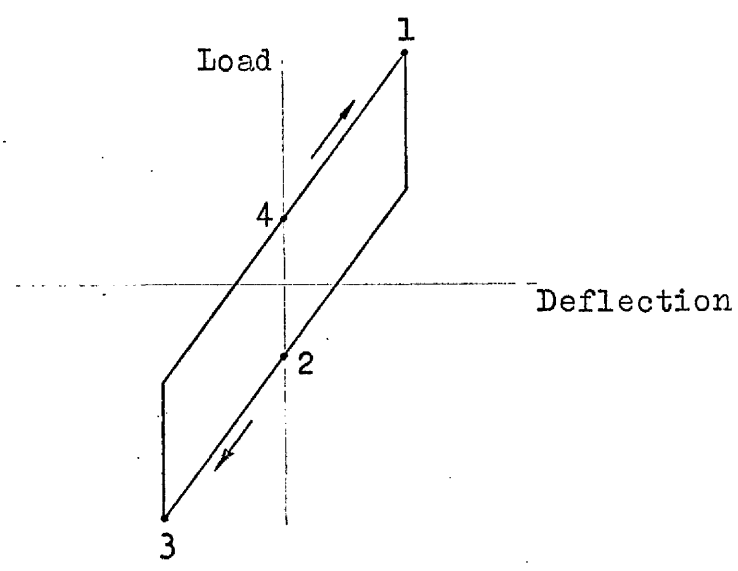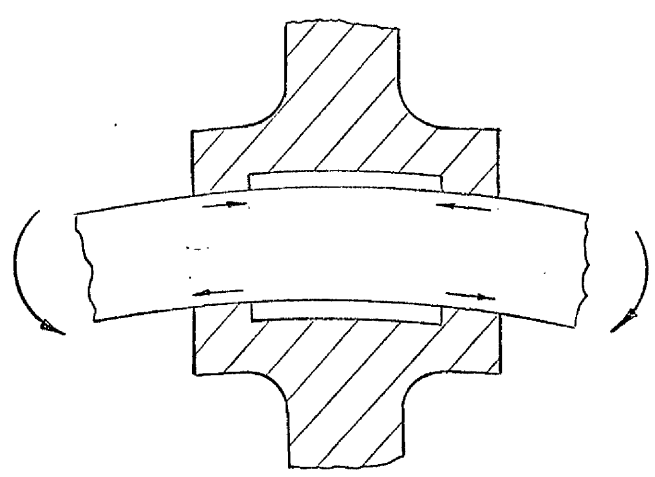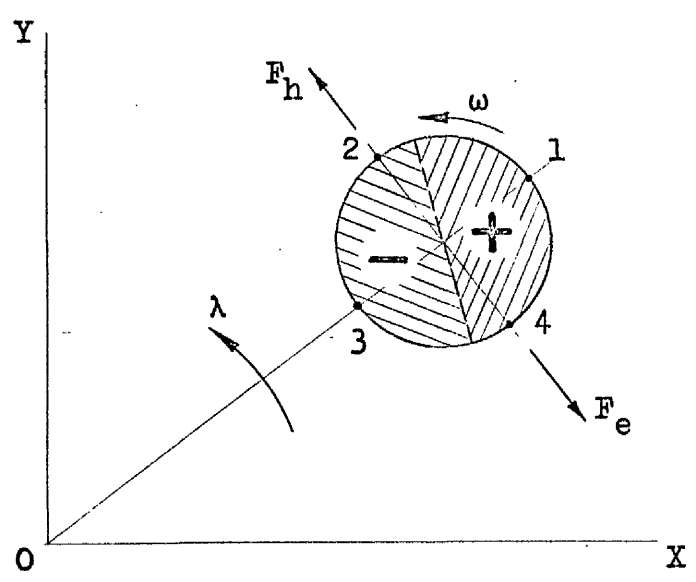
(c)

Fig.1.4   The action of internal friction, caused
by hysteresis or rotor friction, on the
whirling of a shaft.

Fig.1.5

L.P. Rotor

H.P. Rotor

Bearings

Splines
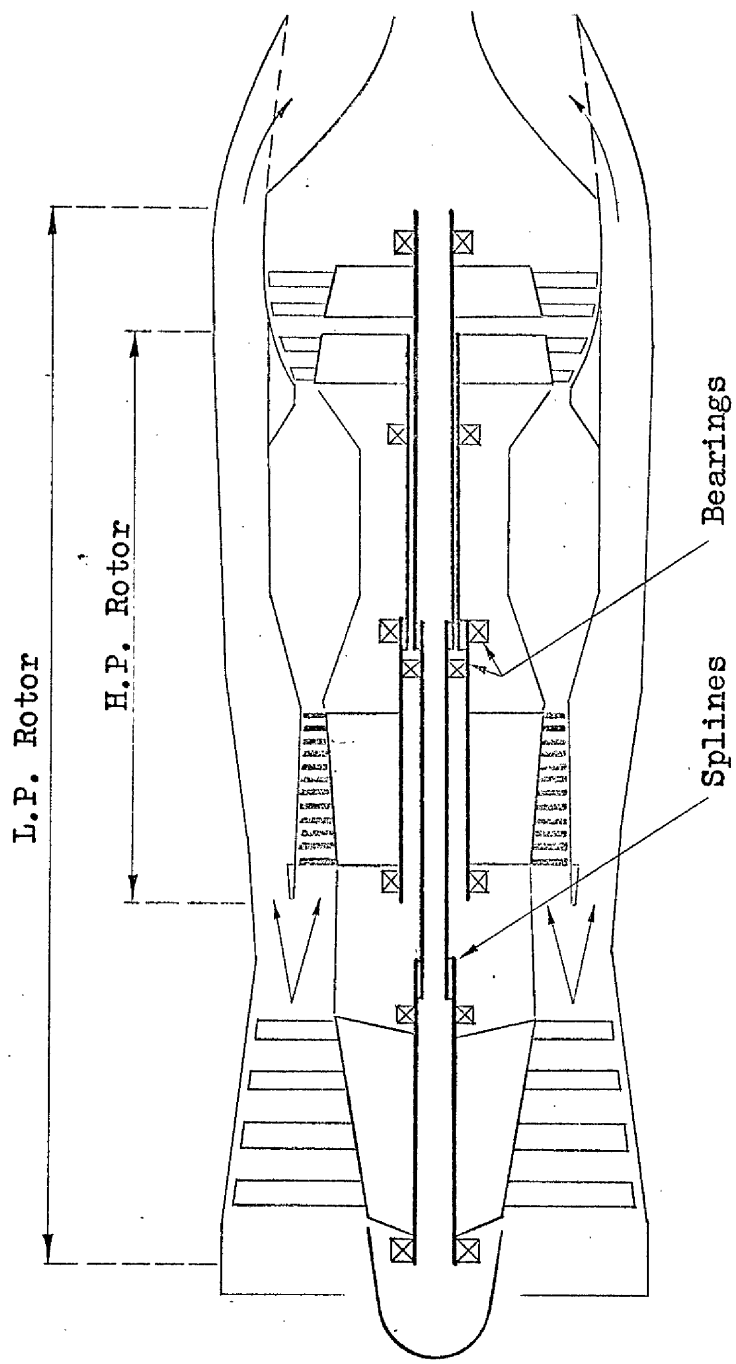
Fig.1.5   Diagrammatic arrangement of typical twin-spool bypass jet engine.
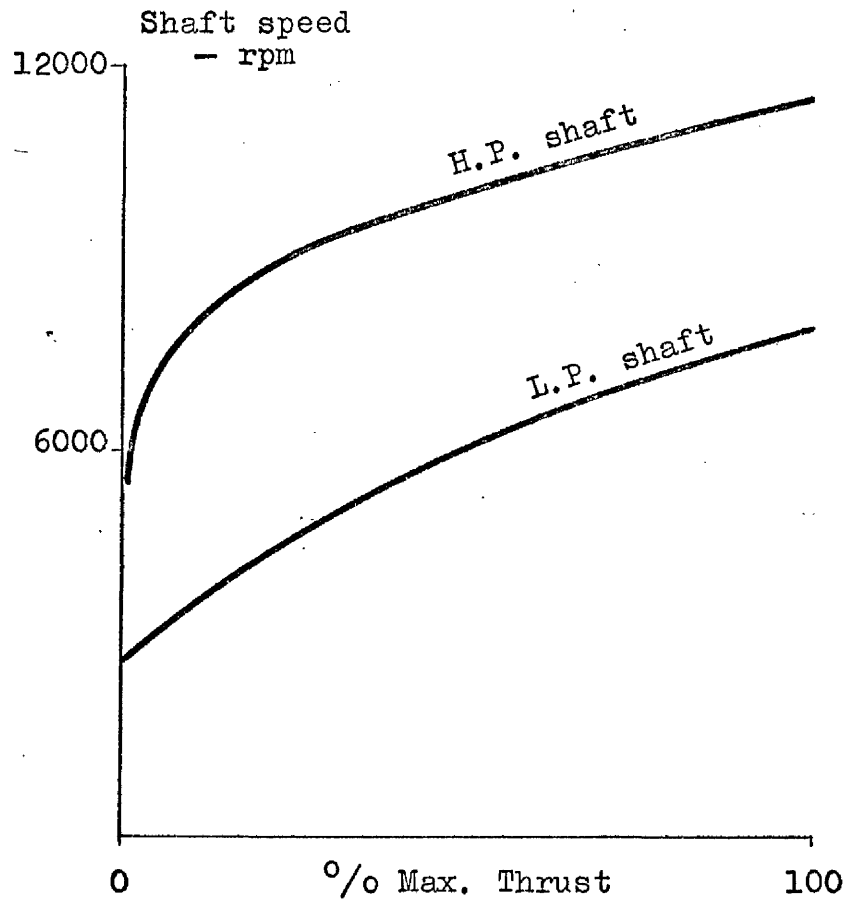
Fig.1.6

Fig.1.6   Typical variation of H.P. and L.P. shaft
speeds with thrust in a twin-spool jet
engine.

CHAPTER 2

THE EXPERIMENTAL RIG

SUMMARY

The configuration and the choice of the major dimensions of the experimental rig are presented. Details of the main features of the rig are described.

The instrumentation system used to monitor the vibration behaviour of the rig is described. An explanation of the technique used to balance the rotors is given.

CHAPTER   2

THE EXPERIMENTAL RIG

2.1   General Requirements of the Rig

The main object of the investigation was an
examination of the vibration behaviour of the co-axial
shaft arrangement used in modern jet engines.   While it
was desirable that the experimental rig should bear some
resemblance to a jet engine, it was particularly important
that the gyroscopic properties and mountings of the rotors
should be representative.

Since the vibration behaviour of co-axial shafts did
not appear to have been examined before, it was likely that
novel vibration behaviour, peculiar to this system, might
be found.   If the work was to be useful to aero engine
designers, it would be necessary to demonstrate whether such
behaviour could be predicted.   Therefore it was essential
that an accurate mathematical simulation of the rig should
be made.   Purdy's work (Ref.17) had indicated that an
accurate simulation of a rig which attempted to represent
the intricate constructional features of a jet engine would
be extremely difficult.   As the complexity of construction
could not be expected to have a great influence on the
general behaviour of a co-axial system, it was decided that
the construction should be as simple as possible while still
retaining the main features of the rotors, and bearing
supports, used in jet engines.

A simple but faithful representation of the complete
rotor system in a jet engine was considered possible, but
would raise certain difficulties.   The shafts used in practice
consist of several sections connected by splined couplings.
No information on the flexibility and damping properties of

these couplings appeared to be available, and so any simulation of these on a rig was liable to introduce vibration behaviour which was not representative.

Secondly, the co-axial system presented difficulties in the possible arrangements used to drive the outer shaft (see Fig.1.5). The outer (H.P.) shaft could be driven by a geared or belt drive, which would have to pass through the casing of the model, but either type of drive would almost certainly introduce restraint and possible excitation of the shafts which was not representative. The best solution would have been to construct a simple turbine wheel on the outer shaft, to be driven by compressed air, but fine speed control would be difficult to achieve. (Purdy had used this arrangement but found it was necessary to incorporate an eddy current brake to assist in the control of the shaft speed).

It was therefore decided that the value of the investigation would not be reduced seriously by restricting the rig to represent only the rear half of a jet engine, i.e. only the two turbine assemblies, which could then be conveniently driven by light shaft drives at either end of the rig.

2.2   Choice of Main Model Dimensions

A cast iron bed plate, 6 ft long and 4 ft wide, originally used to mount piston engines on test, had been acquired for this investigation. It appeared possible to accommodate a full size model of the rear half of a typical twin-spool engine on this bed plate. The shaft lengths and the position of the bearings and discs, representing the turbine assemblies, were therefore chosen to be similar to those on a typical twin-spool engine developing a thrust of 10000 lbf (Fig.1.5).

The gyroscopic effects of the turbine assemblies have a profound effect on the critical speeds of a jet engine shaft and had therefore to be simulated with reasonable accuracy. The resultant raising of the critical speeds above the values which would be obtained with equivalent point masses can be expressed, for a given shaft/disc system, in terms of the radius of the discs and the distance between the disc and the nearest bearing (Ref.18). Since the position of the discs and bearings had been specified, the diameters of the discs were chosen in accordance with this requirement.

The diameters of the shafts and the masses of the discs remained to be decided in order to produce the desired critical speeds. The diameters of the shafts were also controlled by the necessity of providing adequate clearance between the two for safe operation at whirling conditions.

The critical speeds of the rig did not need to be similar to those found in jet engines and were therefore chosen from safety considerations and possible driving methods. Servo controlled electric motors were considered to be the most suitable means of driving the shafts satisfactorily and the type chosen was limited to a maximum speed of 7000 rpm under light loads. Since, in modern jet engines the lowest critical speeds are arranged to be near or below the idling speed, and therefore about half the maximum operating speed, the second critical speed may not be far above the maximum speed. As it seemed desirable that the model should be capable of being used to explore the second critical speeds, the lowest critical speeds were chosen to be about 2000 rpm.

As noted earlier, the critical speeds of jet engine rotors are influenced by the flexibility of the bearing supports. Typical shaft dimensions and bearing flexibilities, for an unspecified engine, were kindly

furnished by Mr. L. J. Stone of Rolls—Royce Ltd. These
indicated that the critical speeds would be roughly half
the values expected in rigid bearings, as a result of the
bearing flexibility. Therefore the masses of the discs
and the dimensions of the shafts were chosen to produce
critical speeds of about 4000 rpm, when mounted in rigid
bearings, and the bearing flexibilities then chosen to
reduce these to the desired value of about 2000 rpm.

The final dimensions of the shafts and discs are
shown in Fig.2.1.

2.3 Detail Design of Model

The inner (or L.P.) shaft was made of a length of
3°/o nickel steel, turned and ground to a constant diameter
of 1.125 in. Although great care was taken in trying to
machine the shaft straight, it was found to be bowed about
0.002 in at the mid—span. This fault was subsequently
found to be not serious. A mild steel disc, with a
diameter of 12 in and a thickness of 1 in, was mounted on
the shaft by means of a Fenner Taperlock coupling, to
represent the L.P. turbine assembly (Fig.2.2). The L.P.
rotor was supported in a SKF type 6004 ball bearing at the
front end, and in a SKF type NU 205 roller bearing at the
rear end.

The outer (or H.P.) shaft consisted of a length of
1.75 o.d., 0.0625 in thick, seamless drawn mild steel tube.
The mountings for the disc and bearing housings were
attached to the shaft by press fit and tack welding. The
H.P. disc was made of mild steel, with a diameter of 12 in
and a thickness of 1 in, attached to the end of the shaft
by a special coupling. The front bearing was a Hoffmann
type XLS 2 ball bearing, the rear a Hoffmann type RXLS 2
roller bearing.

The bearings were mounted in the casing on sets of four spring rods clamped in specially designed housings. The flexibility of the bearing mountings could therefore be altered by replacing the rods with others of different diameter. The arrangement of the front bearing assembly and its spring mounting is shown in Figs.2.3 and 2.4.

It was originally intended that the flexibility of the casing should be capable of being modified easily. The main part of the casing was therefore designed as a cage of eight 0.75 in diameter steel rods, which could be changed for ones of different diameter in order to alter the stiffness of the casing (Fig.2.5). The construction also provided easy access to the rotors for vibration measurement and balancing adjustments. However, it was later found that the stiffness of this construction was difficult to represent mathematically due to the uncertainty inherent in the end fixings of the eight rods. The construction was not representative of jet engine construction in any case, and was later replaced by a simple sheet metal cylinder.

The rig was supported at the rear by two simple triangular frames terminating in Rose universal ball joints which connected with the rear aluminium plate of the casing (Fig.2.6). The front of the rig was supported on a single pillar, connected to the front spring housing by a universal ball joint (Fig.2.4). Although the design of the support of the rig was not ideal (the rear aluminium plate is constrained from rotation about the vertical axis, while the front spring housing is constrained from rotation about the horizontal axis) it is similar to the arrangement used in practice for supporting jet engines.

The supports were bolted directly to the cast iron bed plate. The latter, which weighed about 1500 lbf, was mounted on springs to give a vertical natural frequency of about 5 c/s to achieve a satisfactory degree of vibration isolation from external excitation.

2.4   Shaft Drives

The inherent damping of the rig was expected to be
small and therefore significant whirl amplitudes, even
when the rotors were finely balanced, would be expected to
occur over a very small speed range.   The method of driving
the shafts therefore had to be capable of very accurate speed
regulation.

Shunt wound D.C. motors, rated at 0.5 H.P., with feed-
back speed controllers, type MC47, manufactured by Servomex
Ltd., were selected for this duty.   The performance proved
to be satisfactory — the shaft speeds could be controlled to
within 1 rpm even within the difficult range close to a
whirling speed.

The motors were coupled to the shafts by 6 in lengths
of 0.1 in diameter steel rods, which were flexible enough
to avoid appreciable disturbance due to misalignment being
transmitted to the shafts.

2.5   Instrumentation

Tufnol discs, carrying 120 iron segments embedded in
the peripheries, were mounted on the driven end of each
shaft.   Inductance probes, type G308 made by Southern
Instruments Ltd., were mounted close to the Tufnol discs and
the signals fed to Racal type SA 520 digital frequency
counters.   When the counters were set to record cycle/
second, the digital read out indicated twice the shaft speed
in rpm (120 segment discs, resulting in twice the shaft speed
being indicated, were used so that the counters operated in
their most favourable range, and thus giving an accuracy of
$\pm$ 0.03°/o).

The vibration of various points of the rig, and in
particular of the discs, was monitored in the horizontal
and vertical planes by capacitance probes and two distance
meters (type DM 100, manufactured by Wayne-Kerr Ltd).

To be able to observe the motion of several points of the rig, while running at a fixed speed, the probes were fed through a selector switch (type JB 731, manufactured by Wayne-Kerr Ltd). Examination of correction data to be applied when the vibration of curved surfaces was being measured, showed that the error involved when the probes were used to monitor the motion of the discs was negligible.

In the Wayne-Kerr system of measuring vibration, a high frequency voltage is generated by an internal oscillator and the current passed across the probe/surface gap is used to indicate the magnitude of the gap. When the two meters were being used to measure the motion of a whirling disc, the output signals of the meters were fed to the X and Y plates of a single beam oscilloscope (Type 52, Telequipment Ltd) to produce a replica of the generally elliptical path of the disc centre. But a ripple was found to be superimposed on the displayed path. This ripple was eventually shown to have a frequency which was the difference between the two nominally 50 Kc/s oscillators within the meters. The frequency of these could be adjusted to be the same, but the oscillators were not stable enough to prevent a low frequency beat being produced which was able to pass the filters in the feed to the oscilloscope. The difficulty was finally overcome by modifying the meters so that both used the output of the 50 Kc/s oscillator of one·meter, with suitable output transformers to minimise 'cross talk' between the two vibration readings.

Three sizes of probes were used, capable of measuring maximum vibration amplitudes of 0.005, 0.025 and 0.05 in respectively, were used in this work. The last type were usually employed to indicate the disc motion. When coupled to the oscilloscope, set at a sensitivity of 0.01 mV/cm, a disc movement of 0.001 in produced a deflection of approximately 1 cm on the oscilloscope.

The two channel monitoring system finally adopted
is shown in Fig.2.7.   Normally only one oscilloscope was
employed to display the elliptical motion of a particular
point of the model, but a second oscilloscope was installed
so that the motion of two points of the model could be
observed simultaneously.

The instrument console which was designed and
constructed for this project is shown in Figs.2.8 and 2.9.

2.6   Balancing Technique

Each disc had four equally spaced holes drilled
axially near the periphery to take balancing screws.   A
small piece of thin metal foil was glued to the periphery
adjacent to one of the holes, which was then referred to
as the 12 o'clock position.   Whenever the foil passed a
vibration probe it produced a 'kick' on the oscilloscope
representation of the motion of the centre of the disc,
as shown in Fig.2.10.

The disc, shown in Fig.2.10, is rotating clockwise
and the foil is passing the vertical probe.   The
oscilloscope spot is therefore tracing the vertical kick
on the display.   The oscilloscope display, which is also
being traversed in a clockwise direction, shows that the
centre of the disc reached its highest point almost
quarter of a cycle earlier.   Therefore the disc centre
must be displaced from the bearing axis along the 2 o'clock
radius.

If the disc were rotating well below the forward
whirling speed then the phase lag would be small and the
unbalance must lie along the 2 o'clock radius.   This
method of determining the location of the unbalance was
used in the early stages of balancing the rotors.   But a
more accurate method of balance was later employed by
balancing the rotors just below the forward whirling speed.

Under such conditions the unbalance would lead the displacement of the centre of the disc by almost a quarter of a cycle.   Then an oscilloscope display, as shown in Fig.2.10, which shows the disc to be displaced along the 2 o'clock radius, would indicate the unbalance to be one quarter of a cycle ahead, i.e. along the 5 o'clock radius.

Using this method of determining the angular position of the unbalance of the disc, balancing was carried out by a process of trial and error.   As the balance was improved, and the size of the path decreased, the speed was raised closer to the whirling speed to increase the sensitivity. The final balancing was carried out at the whirling speed and as a result extremely good balance was achieved, of the order of 0.02 oz in, compared with that used in the aero engine field of about 0.1 oz in.   Even better balancing could easily be achieved with patience but was impractical since it deteriorated if the shaft was left stationary for a few hours, presumably because the shaft sagged imperceptibly under its own weight.

The metal foil was also employed to give an indication of the phase angle of the vibration and also to indicate the sense of the precession.   For the case shown in Fig.2.10 since the shaft is rotating clockwise, the horizontal kick on the oscilloscope trace must occur after the vertical one. The oscilloscope beam must therefore be traversing the display in the same sense, indicating forward precession. If the horizontal kick had appeared in the upper left quadrant of the display, as indicated, then the display would have indicated that reverse precession was occurring.

2.7   Conclusions

The design and construction of the rig proved to
be satisfactory.   Only one major design change was made
(to the casing), but this resulted from the apparent
difficulty in the representation of the stiffness
properties of the rod cage construction.

When the rig was first assembled the H.P. bearings
appeared to have very little clearance, producing alarming
squeaks when the shaft was turned.   The cause was found
to be due to the distortion of the housings caused by the
spring rod clamping bolts.   Fortunately, it was found
that the efficiency of the rod clamping design was so high
that only a moderate nip on the clamping bolts was neces-
sary, and as a result negligible distortion of the housings
and bearings resulted.

The bearing housings were designed to retain the small
quantity of light oil introduced during assembly.   No
bearing trouble was experienced throughout the experimental
work.

The instrumentation was designed with reliability of
utmost concern.   Once the difficulty of coupling the two
distance meters to the same oscillator was overcome no
further serious trouble was experienced.

Fig.2.1

6.0"

1.125" D

1.0"

12.0" D

1.0"

32.0"

25.625"

18.0"

1.75" O.D
x 0.063" thick tube
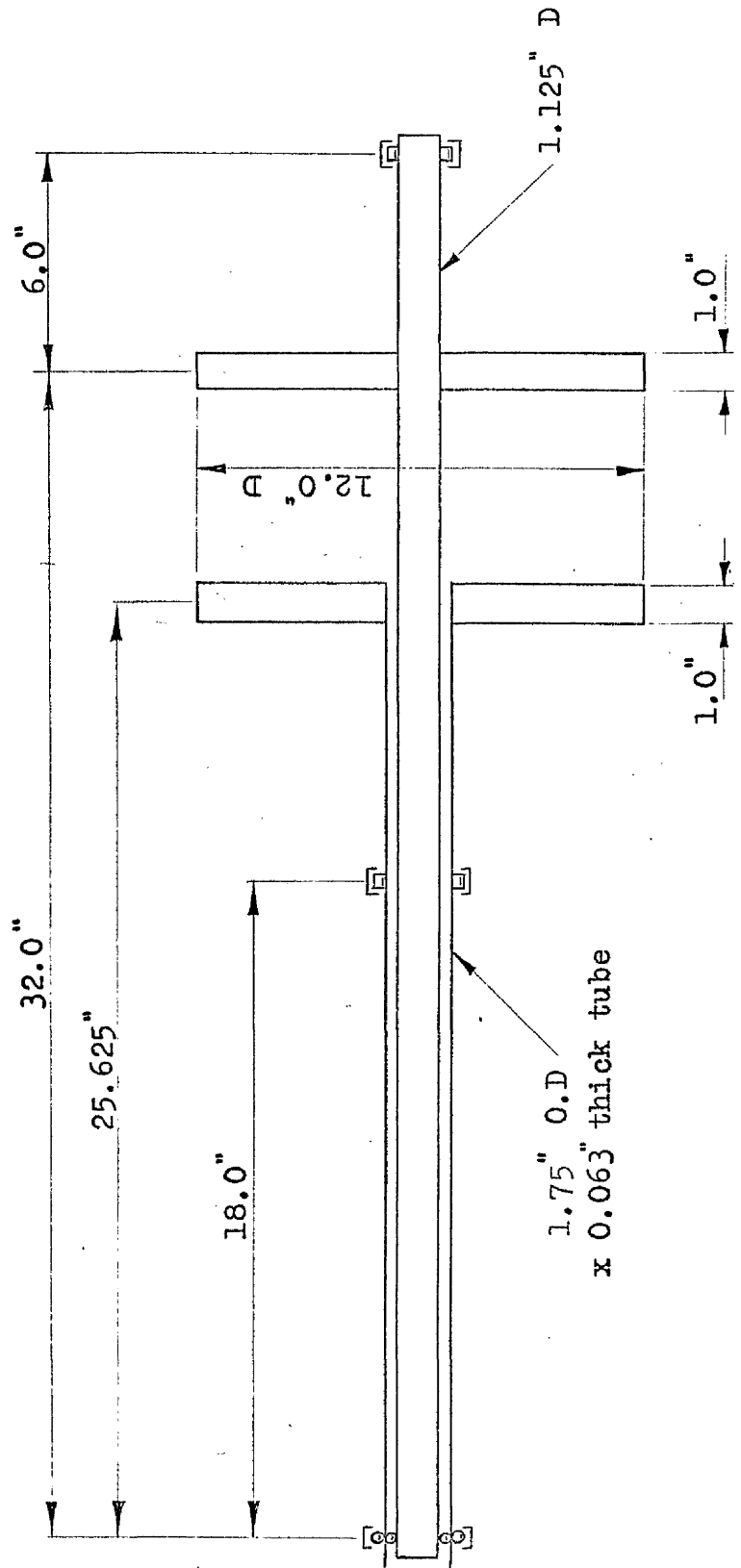
Fig.2.1   Major dimensions of H.P. and L.P. Rotors

Fig.2.3

Clamping bolt

Section A—A

Spring bearing mount

L.P. Shaft

H.P. Shaft

Casing tube

Spring rod

A

A

H.P. Shaft drive

Front bearing housing
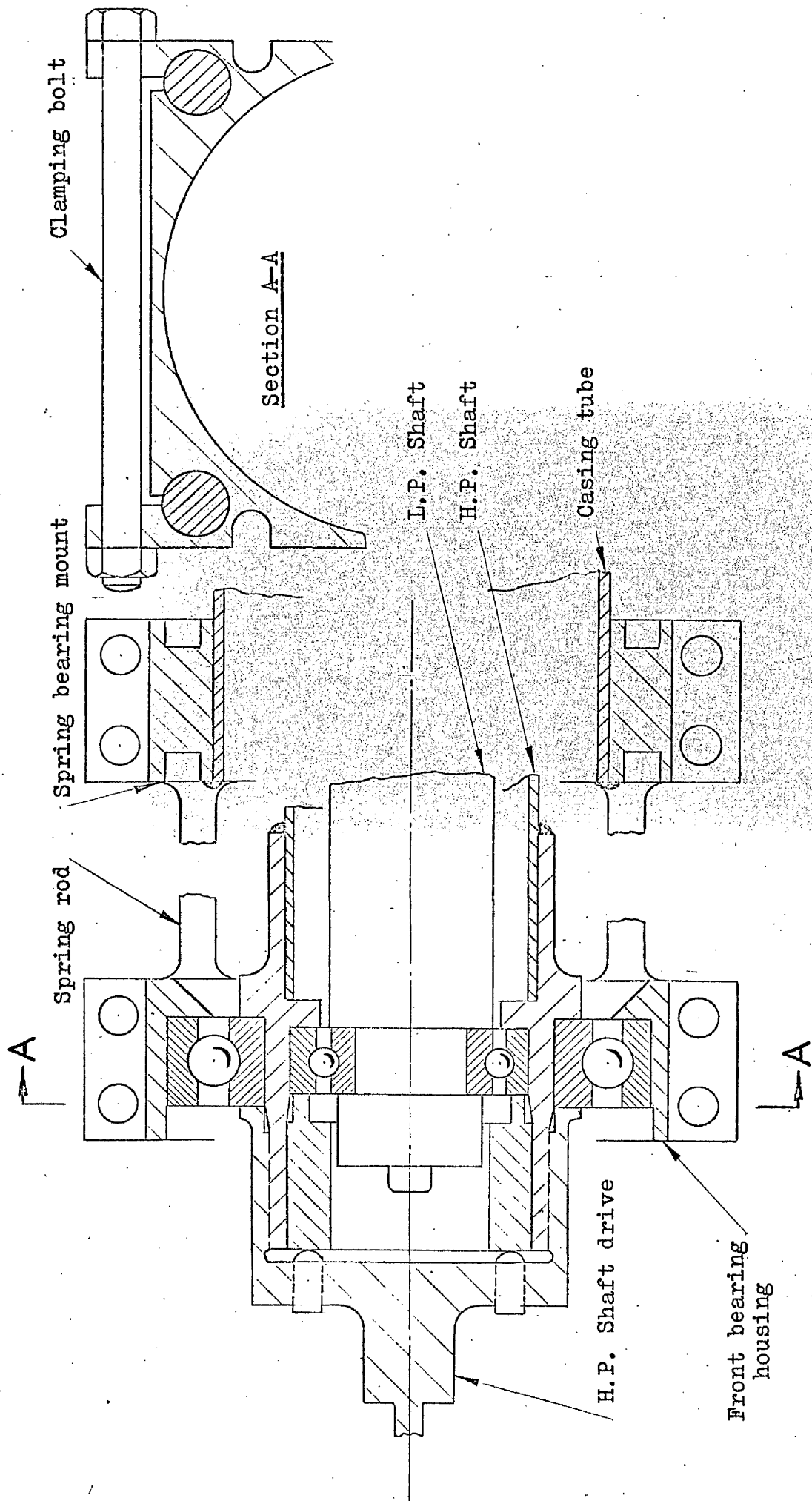
Fig.2.3   Arrangement of front bearing assembly and spring mounting
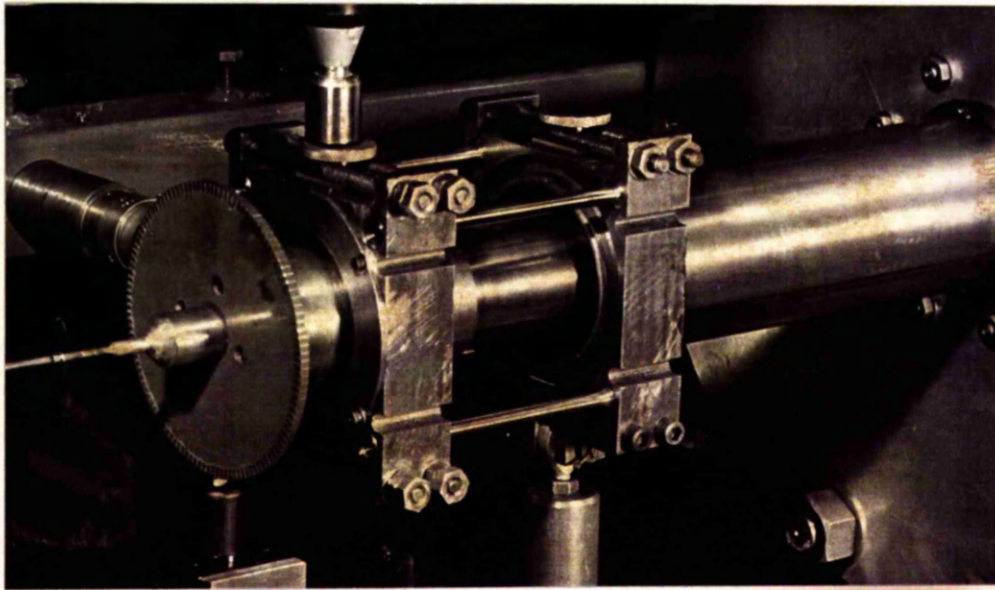
Fig. 2.4

Fig. 2.4   Front bearing housing and
spring support

Fig.2.5

8.66" 21.0" 15.0"

Eight 0.75"D steel rods
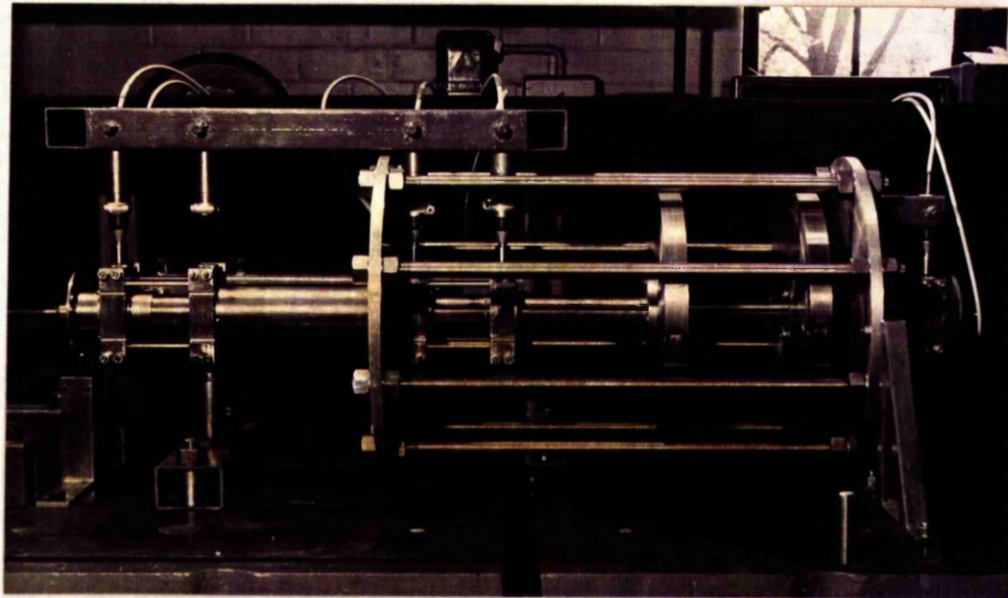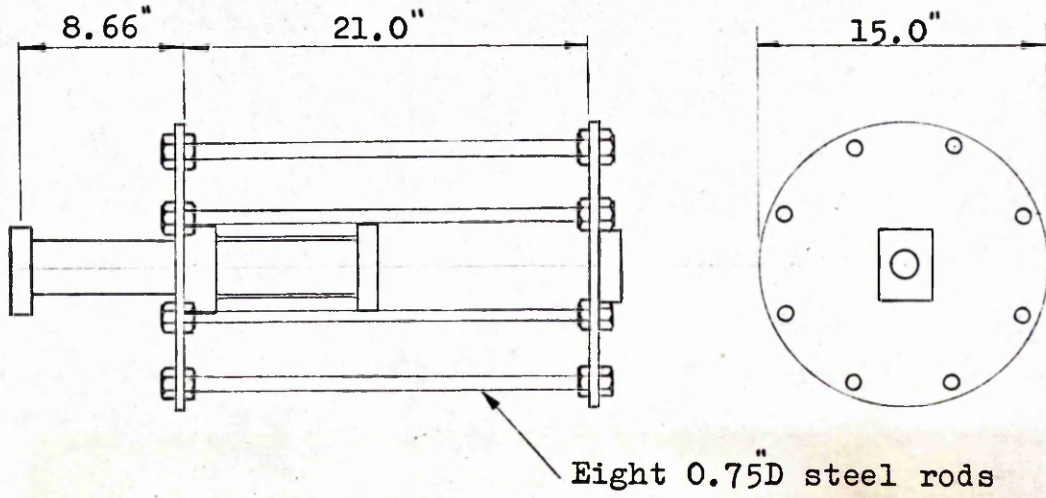
Fig.2.5   Rod cage construction of
the casing
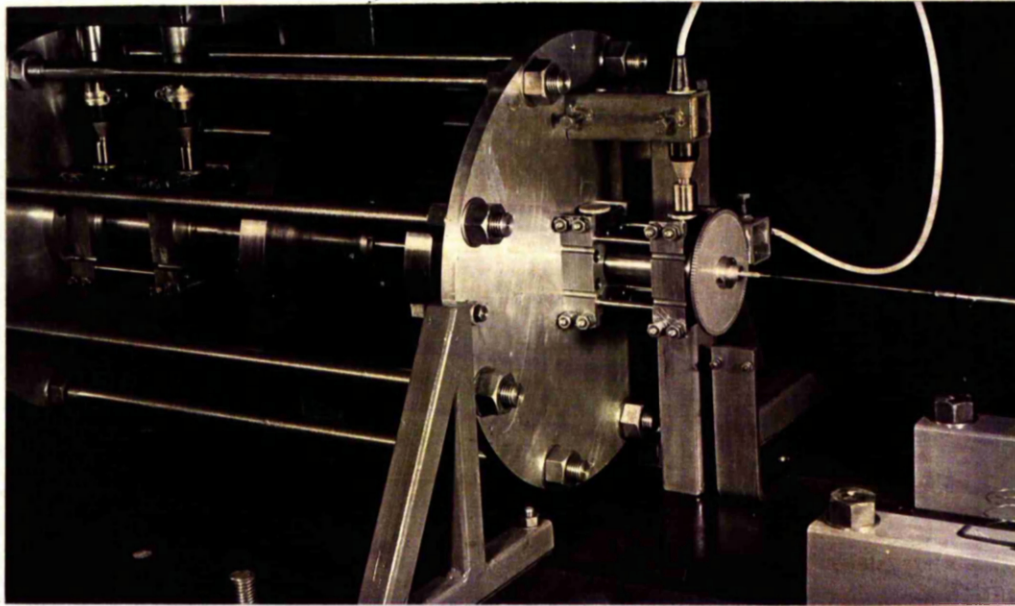
Fig. 2.6

Fig. 2.6   Supports of rig at rear
aluminium plate

Fig.2.7

Vertical probe

Foil marker

Horizontal probe

Whirling disc

Channel selector switches

Oscillator coupling

Distance meters

50 Kc/s filters

Single beam oscilloscopes

Selector switch

Selector switch
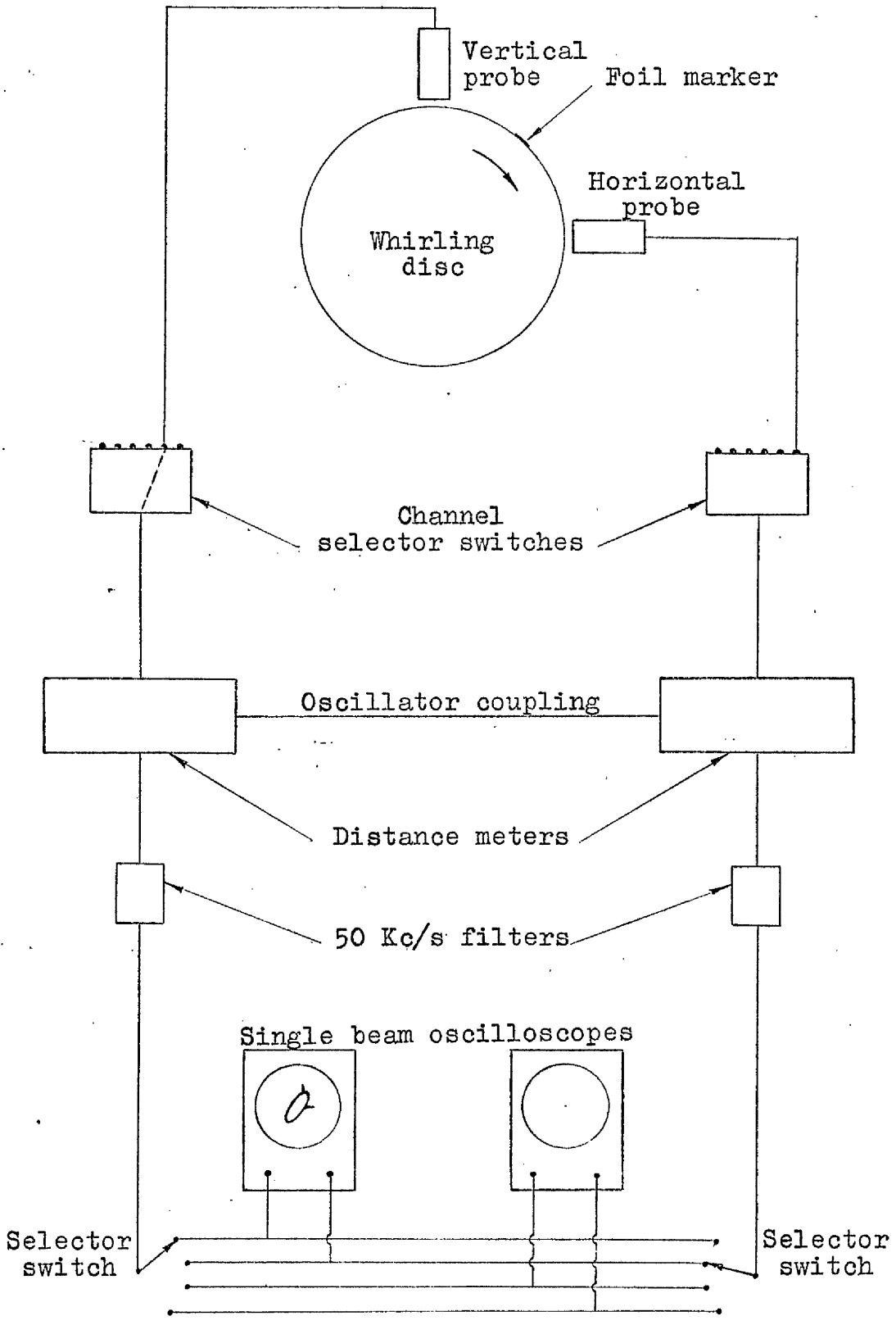
Fig.2.7   Diagrammatic representation of two channel vibration monitoring system.

Fig. 2.8

Oscilloscopes

Frequency
Meter

Frequency
Meter

H.P.

L.P.

Speed
controls

Oscilloscope channel
selector switches

Probe selector switches
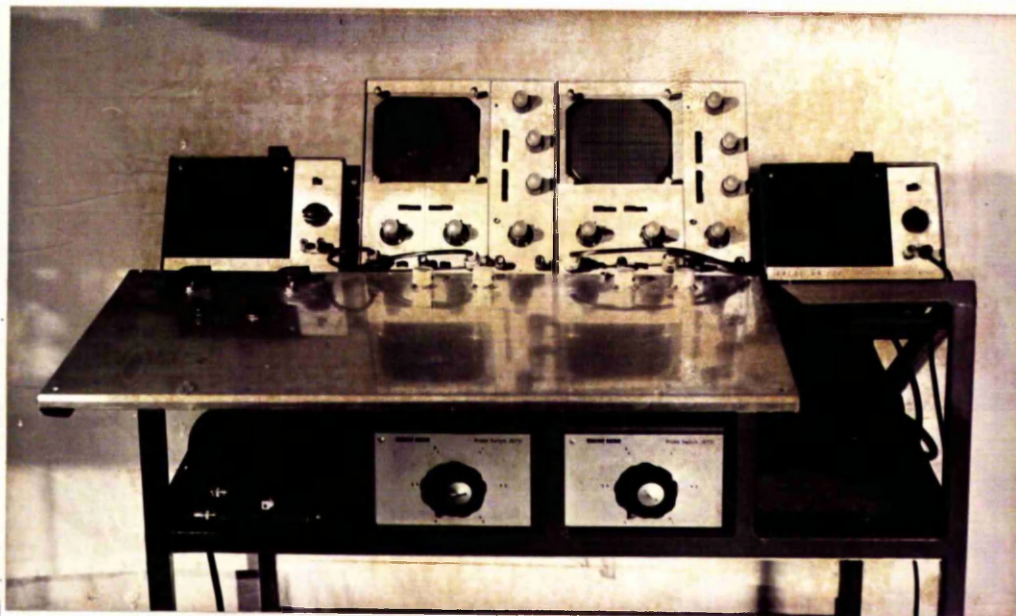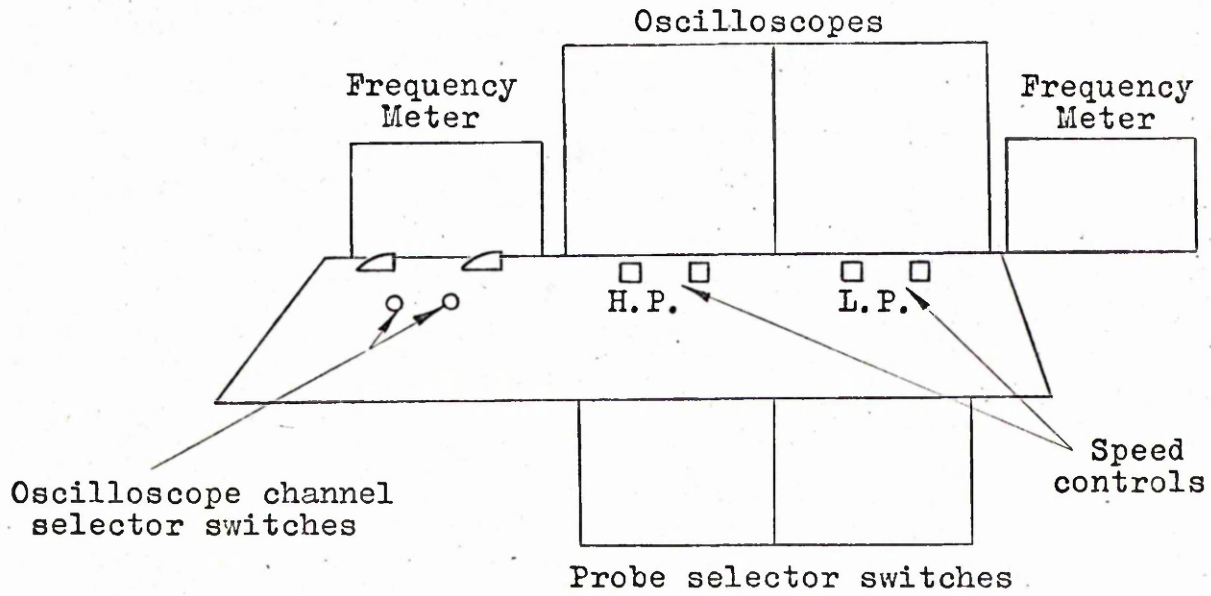
Fig.2.8   Front view of instrument console.

Fig.2.9

Distance
Meters

Output Filters
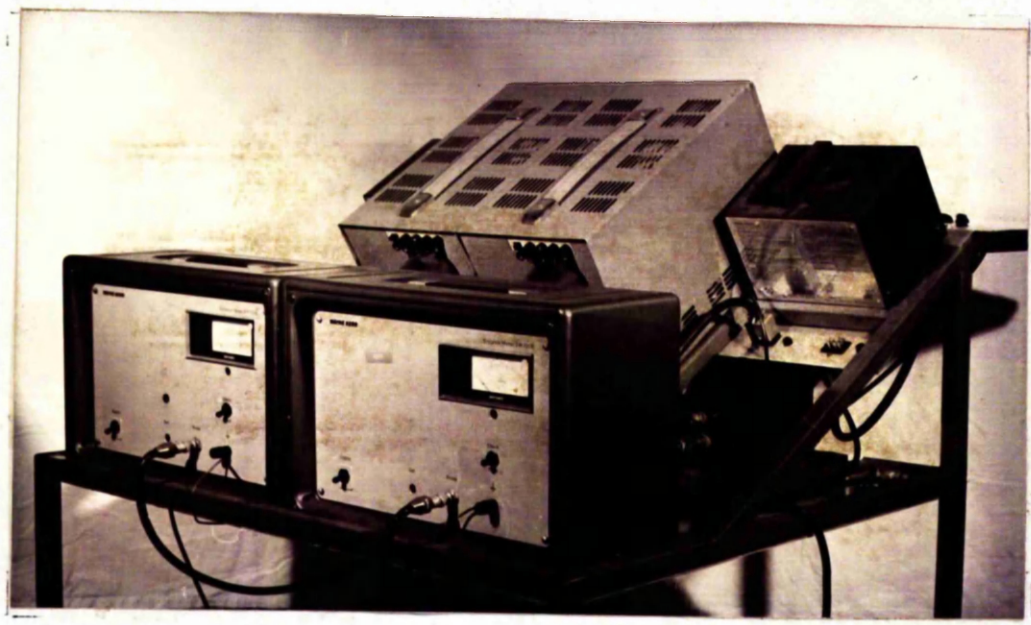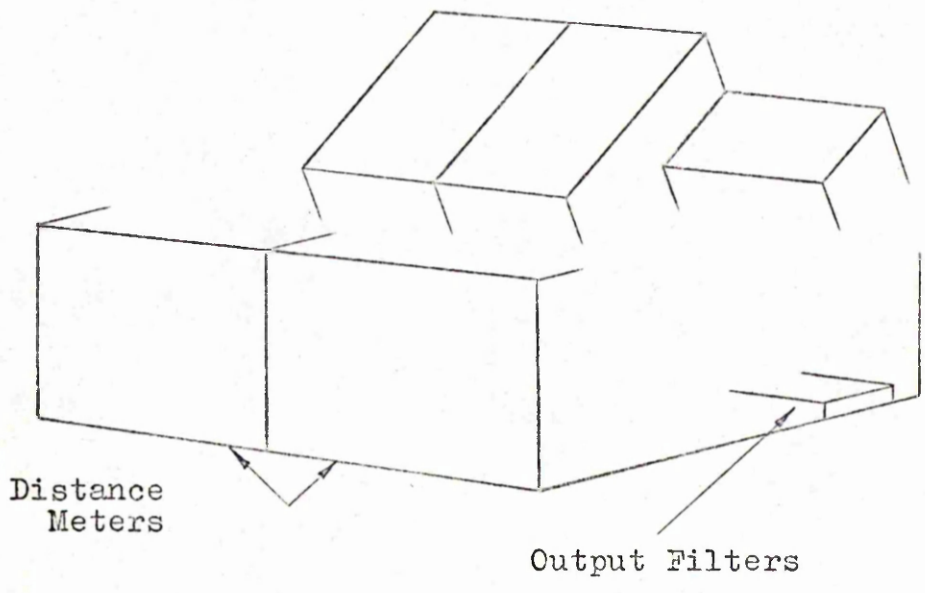
Fig.2.9   Rear view of instrument console.

Fig. 2.10

Vertical
probe

12

Foil
marker

.9

3.

Horizontal
probe

6
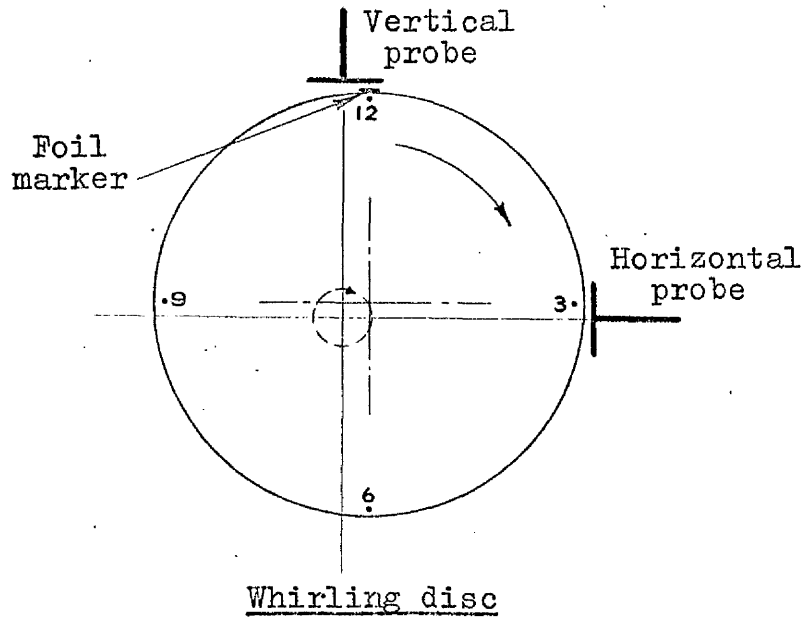
Whirling disc

Position of horiz.
'kick' if reverse
precession occurs

Vertical
'kick'

Horizontal
'kick'

Oscilloscope display
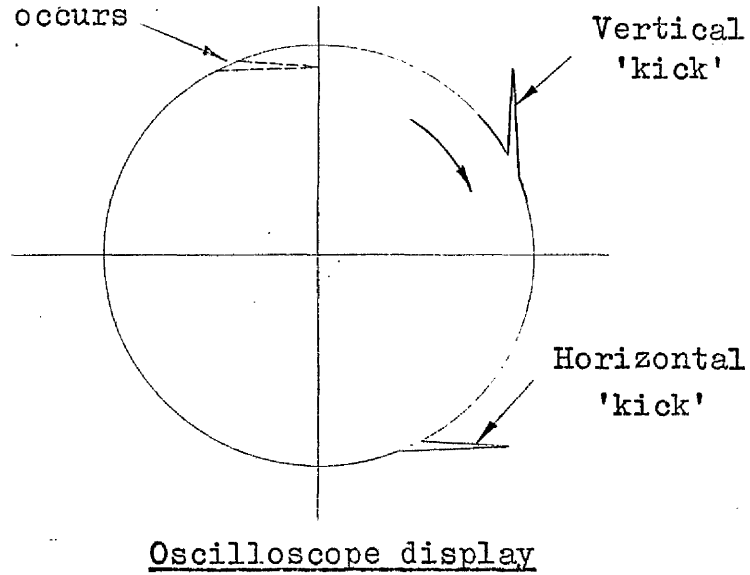
Fig.2.10   Whirling disc and resultant oscilloscope
display of the motion of the centre of the
disc.

CHAPTER 3

FREQUENCY ANALYSIS METHODS

SUMMARY

The frequency analysis of a complicated structure has to be carried out by a lumped-parameter technique. The main features of three of the most usual methods are described.

The prime consideration in the choice of method was that the translation of the physical properties of the structure into numerical form should be as straightforward as possible, thus reducing the likelihood of errors. The transfer matrix method was considered to be the most suitable from this point of view.

CHAPTER 3

FREQUENCY ANALYSIS METHODS

3.1   Introduction

Despite the availability of large computers, the complexity of the structure of a typical jet engine is so great that a complete mathematical representation, from which natural frequencies may be deduced, is not feasible. Instead, the system is imagined to be divided into a number of elements or sections in such a way that the elastic and inertial properties of these may be readily expressed in a simple manner.   One of several methods is then used to combine the properties of the sections into a form from which natural frequencies may be extracted, usually by an iteration technique.   Some of the more usual methods of analysis were therefore examined to determine the most appropriate for this investigation.

The most important consideration was that the treatment of the data for each section must, as far as possible, be the same, otherwise serious errors could be introduced by incorrect programming.

It was intended that the model would be studied in stages of increasing complexity.   It was therefore important to consider which method, from a programming point of view, was easiest to assemble in stages.

In the case of the model it was possible to make a fairly good estimate of at least the lowest natural frequency.   It would therefore be preferable to choose a method which started the iteration from a good estimate of the frequency.

Finally, although the calculation of the frequencies of the model was not expected to involve very large computer storage space it would be unreasonable to choose a method which, when applied to a jet engine calculation, would make excessive storage demands.

3.2   Matrix Force Method

The method often used by the aero engine industry to calculate the natural frequencies has become known as the matrix force method (Ref.19).   The displacements of the sections, expressed as a column matrix $[x]$, are related to the external loads applied to the sections, expressed as a column matrix $[P]$, by a square matrix $[d]$ in the equation:—

$$[x] = [d] . [P]$$

When considering the lateral vibration of a structure, the rotations of the sections, as well as their linear displacements, must be included in the matrix $[x]$. Similarly the matrix $[P]$ includes the torques, as well as the forces applied to the sections.   As a result, if the structure is divided into n sections, the matrix $[d]$ is of order 2n. The elements of the j th column of matrix $[d]$ are the displacements x_i (i = 1, 2n) of the n sections when unit load is applied to the i th section of the structure.

· If the structure vibrates harmonically at an angular frequency ω, the loads applied to the i th section are the 'inertia force', $- m_i \omega^2 x_i$, and the inertia torque, $- A \omega^2 \vartheta_i$.   These can be expressed concisely by the matrix equation:—

$$[P] = - \omega^2 [M] . [x]$$

in which $[M]$ is a square matrix of order 2n containing the 2n inertia forces and torques — the remaining elements

of the matrix being zero. (Since critical speeds are obtained by determining the frequencies of lateral vibration, the inertia torques have to be modified by an additional term to allow for gyroscopic effects).

If there are no other loads acting on the structure, i.e. it is vibrating freely, the displacements of the sections of the structure and the inertia loads can be related by the equation:—

$$[x] = + \omega^2 [d] . [M] . [x]$$

or
$$([d] . [M] - \lambda . I) [x] = 0$$

where I is a unit matrix, and $\lambda = 1/\omega^2$.

The equation is in the standard form of the eigenvalue problem from which the roots λ_i (i = 1,2n) are usually obtained by an iteration technique which produces the roots in descending order of magnitude, i.e. the frequencies, ω_i, in ascending order of magnitude.

The procedure for calculating the elements of the matrix [d] is by no means uniform. Fig.3.1 shows the supposed distorted form of the model when a load is applied to a section of the H.P. shaft. The displacements of the sections of the H.P. shaft, inter and casing are in part due to the distortion of the component concerned but further movement is caused by distortion of the components supporting it. Sections of the L.P. shaft, which is unloaded and therefore undistorted, are also displaced due to the movements of the ends of the casing on which it rests.

Thus the calculation of the deflections of each section differs depending on which component it is part, and where the load is applied to the structure. This complication was considered to be such that serious errors in programming the construction of matrix [d] could be easily introduced and be very difficult to detect.

3.3   Matrix Displacement Method

A similar method has come to be known as the matrix displacement method (Ref.19).   Each section in turn is supposed to have unit displacement imposed on it, while all other displacements are forced to remain zero. Fig.3.2(a) shows this principle for a linear displacement of section j, which requires five loads to be applied to the section and its neighbours to maintain all other displacements zero.   Fig.3.2(b) illustrates the corresponding situation when a unit angular displacement is imposed on section j.   Except for sections of the structure adjacent to a support, the formulation of these loads is uniform.

The results of these calculations are related to the 'inertia loads', as in the previous method by the matrix equation:—

$$- \omega^2 \; [M] \; . \; [x] \; = \; [k] \; . \; [x]$$

where $[k]$ is a square matrix of order 2n containing the loads computed above.

Unfortunately, the above matrix equation is in the form from which matrix iteration would yield the natural frequencies in descending order of magnitude with the interesting lower frequencies being subject to considerable error due to unavoidable rounding errors.   To obviate this the equation is rewritten in the form:—

$$(\; [k]^{-1} \; . \; [M] \; - \; \lambda.I \;) \; [x] \; = \; 0$$

which, since $[k]^{-1} = [d]$, is in the form produced by the previous method.   Thus, although the calculation of the matrix representing the elastic properties of the structure is probably more straightforward and reliable, a matrix inversion has to be performed before iteration can begin.

3.4   Transfer Matrix Method

The transfer matrix method is a modern formulation of the method originally proposed by Holzer and adapted to beam-type problems by Prohl and Myklestad (Ref.19). It is ideal for analysing structures which can be divided into chain-like components.

The simplified diagram of the model, Fig.3.1, can be divided into four parallel beams resting on each other. Considering one of these beams, the conditions to the right of a section i, of the beam, are the deflection and slope of the section y_i and ϑ_i, and the bending moment M_i and the shear force V_i (Fig.3.3).   These are assembled into a column matrix or state vector

$$z_i \quad = \quad \left[y_i \quad \vartheta_i \quad M_i \quad V_i \right]$$

Similarly the conditions to the right of the adjacent element, j, can be represented by a state vector, z_j. A square matrix of order 4, called a transfer matrix, and denoted by t_j can then be constructed which relates the two state vectors according to the matrix equation

$$z_j \quad = \quad t_j \quad . \quad z_i$$

The transfer matrix t_j contains the elastic properties of the section, or the inertial properties, or both.   If the transfer matrix for the next section is t_k, then the conditions to the right of this section are given by the matrix equation

$$z_k \quad = \quad t_k \quad . \quad z_j = t_k \quad . \quad t_j \quad . \quad z_i$$

If the conditions at the left end of the beam, which has been divided into sections a,b,c, ... l,m,n, are represented by state vector, z_o, then the conditions at the right end are given by the state vector

$$z_n = t_n \cdot t_m \cdot t_l \cdot t_k \cdot t_j \cdot t_i \ldots\ldots t_b \cdot t_a \cdot z_o$$

or $$z_n = A \cdot z_o$$

Now the state vectors z_n and z_o both contain two zero quantities, e.g. if the beam is encastré at the left end then y_o and ϑ_o are both zero, and if the right end is simply supported then y_n and M_n are zero. Expanding the matrix equation,

$$\begin{bmatrix} y \\ \vartheta \\ M \\ V \end{bmatrix}_n = \begin{bmatrix} A \end{bmatrix} \cdot \begin{bmatrix} y \\ \vartheta \\ M \\ V \end{bmatrix}_o$$

where $\begin{bmatrix} A \end{bmatrix}$ is a square matrix of order 4 resulting from the successive multiplication of the transfer matrices of the elements.

The first and third equations contained in this matrix equation are:—

$$\alpha_{13} \cdot M_o + \alpha_{14} \cdot V_o = 0$$

$$\alpha_{33} \cdot M_o + \alpha_{34} \cdot V_o = 0$$

Now the elements of the matrix $\begin{bmatrix} A \end{bmatrix}$ contain evidence of the elastic and inertial properties of the beam sections, the latter being functions of ω if the beam is vibrating freely with an angular frequency, ω. Thus, although M_o

and V_o are unknown, these two equations will only be satisfied if the determinant

$$\begin{vmatrix} \alpha_{13} & \alpha_{14} \\ \alpha_{33} & \alpha_{34} \end{vmatrix}$$

becomes zero through a suitable choice of ω, i.e. a natural frequency has been found.

3.5   Conclusions

The transfer matrix method was considered to be the most suitable for analysis of the model. The properties of each element of the structure are calculated by a standard procedure, in all but a few cases, thus removing possible sources of programming errors. The elastic and inertial properties of the whole structure are obtained by a simple repeated matrix multiplication, again reducing the likelihood of errors. The iteration process starts from an estimate of the natural frequency, whereas the other methods start from an estimated modal vector which is not easy to estimate.

In both the matrix displacement or matrix force methods, storage has to be provided for at least a square matrix of order 2n, if the structure has been divided into n sections, e.g. 10,000 storage locations for a system divided into 50 sections. Using the transfer matrix method the same problem would require only 16n, i.e. 800 locations. Although economy of storage was not of prime importance in this investigation, it could easily be so in the more complicated case of an actual jet engine.

Fig. 3.1

L.P. Rotor

Load

H.P. Rotor

Inter

Casing
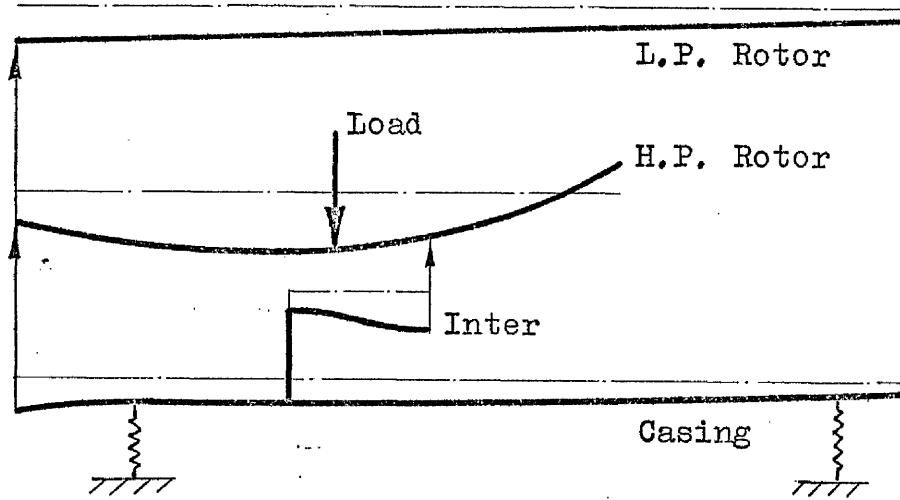
Fig. 3.1   Supposed deflection of model when load
is applied to a point on the H.P. Rotor.
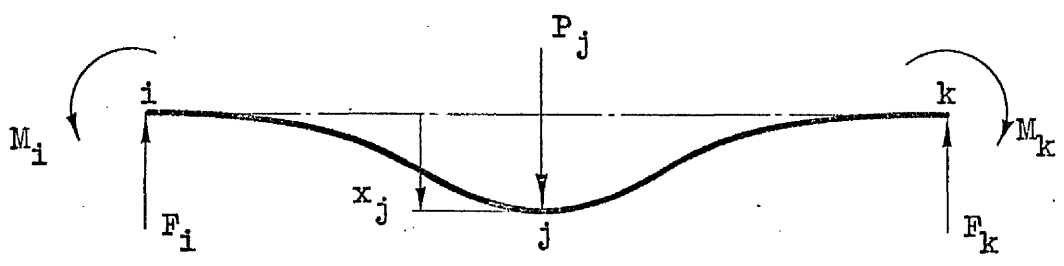
Fig. 3.2

Fig. 3.2(a)   Loads required to impose displacement x_j, under load P_j, while other displacements remain zero.
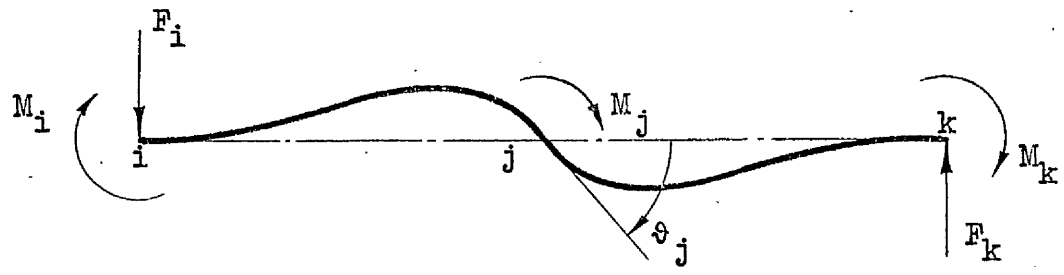
Fig. 3.2(b)   Loads required to impose angular displacement ϑ_j, due to moment M_j, while other displacements remain zero.
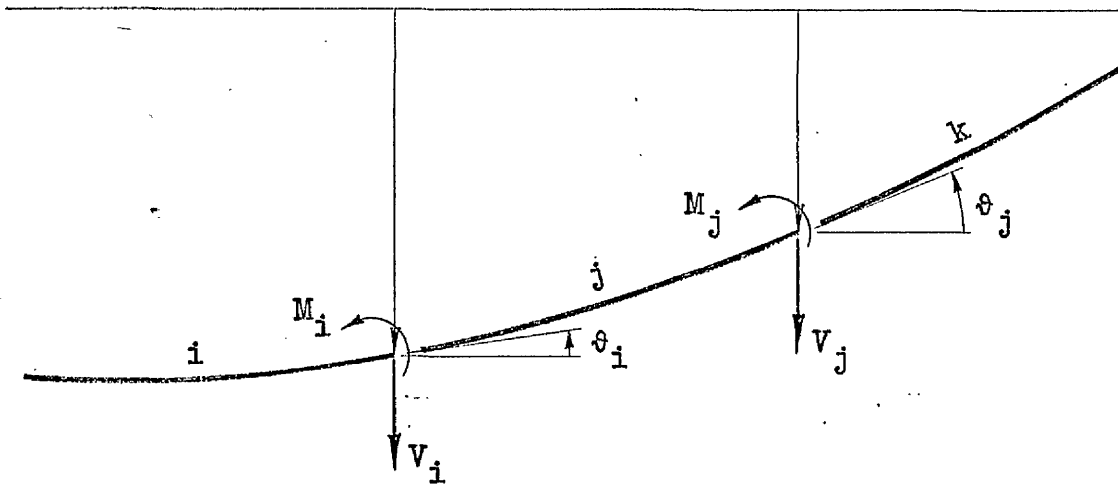
Fig. 3. 3

Fig.3.3   The assumed beam conditions used in the
transfer matrix method.

CHAPTER 4

APPLICATION OF THE TRANSFER MATRIX

METHOD TO THE RIG

SUMMARY

An outline of each of the computer programs designed
to predict the natural frequencies of the components of
the rig, using the transfer matrix method, is presented.
The assembly of these programs to form the computer repre-
sentation of the complete rig is then described.

The proximity of a guessed frequency to the true
natural frequency is judged, in the standard transfer
matrix method, by the magnitude of a determinant. Numerical
difficulties can arise in the evaluation of this determinant.
The application of the modified transfer matrix method, which
is designed to overcome these difficulties, is described.

CHAPTER 4

APPLICATION OF THE TRANSFER MATRIX

METHOD TO THE RIG

4.1   Introduction

The transfer matrix method is especially suitable
for the lumped parameter analysis of a chain-like system
such as a beam or a rotating shaft.   The system is divided
into a suitable number of sections and the changes in
deflection, slope, bending moment and shear force produced
across the section by the loading can be conveniently
represented by a 4 x 4 matrix.   (The derivation of the
transfer matrices used in this work is presented in the
appendix to this chapter).   Sequential multiplication of
the matrices of each section results in a 4 x 4 matrix
which links the conditions at each end of the system.

The final matrix, in the case of vibrating systems,
may be used to locate the natural frequencies and the
associated modes of vibration of the system.

In this chapter an outline is given of the application
of the transfer matrix method to the prediction of the
natural frequencies of the components of the experimental
rig and finally to the complete assembly.

4.2   The L.P. Rotor

The rotor was approximated by dividing it into eight
sections as indicated in Fig.4.1.   The first section was
represented by a flywheel, with the mass and diametral
moment of inertia of the front bearing and its mounting,
resting on a spring.   The transfer matrix representing
the inertial and elastic properties of the section was of
type 1 (see Appendix 4).   The remaining sections were

represented by massless beam sections carrying a flywheel
at their right ends, the mass of each being equal to that
of the section, and the moment of inertia being equal to
that of the section about a diameter through the right end
of the section.   The transfer matrix used for these
sections was of type 2, with the spring support being used
only for section 8 when the rear bearing was spring mounted.

4.3 L.P. Rotor mounted in Rigid Bearings

The initial case of the shaft mounted in rigid
bearings was treated as a beam simply supported (no lateral
deflection at the ends, but non-zero slopes allowed).
Using the subscript R8 to represent the state vector at the
right end of section 8, and L2 for the vector representing
conditions at the left end of section 2, the conditions at
the ends of the beam are given by

$$
\begin{bmatrix} y \\ \vartheta \\ M \\ V \end{bmatrix}_{R8}
= \begin{bmatrix} A_{4,4} \end{bmatrix} \cdot
\begin{bmatrix} y \\ \vartheta \\ M \\ V \end{bmatrix}_{L2}
$$

where $\begin{bmatrix} A_{4,4} \end{bmatrix}$ is a square matrix of order 4 resulting from
sequential multiplication of the transfer matrices for the
sections, i.e.

$$
\begin{bmatrix} A_{4,4} \end{bmatrix} = t_8 \cdot t_7 \cdot t_6 \ldots\ldots t_2
$$

Inserting the boundary conditions

$$
y_{L2} = M_{L2} = y_{R8} = M_{R8} = 0
$$

the matrix equation becomes:—

$$
\begin{bmatrix} 0 \\ \vartheta \\ 0 \\ V \end{bmatrix}_{R8}
=
\begin{bmatrix} a_{11} & a_{12} & a_{13} & a_{14} \\ a_{21} & a_{22} & a_{23} & a_{24} \\ a_{31} & a_{32} & a_{33} & a_{34} \\ a_{41} & a_{42} & a_{43} & a_{44} \end{bmatrix}
\cdot
\begin{bmatrix} 0 \\ \vartheta \\ 0 \\ V \end{bmatrix}_{L2}
$$

The first and third equations from this are:—

$$
a_{12} \cdot \vartheta_{L2} + a_{14} \cdot V_{L2} = 0
$$

$$
a_{32} \cdot \vartheta_{L2} + a_{34} \cdot V_{L2} = 0
$$

and the coefficients a_{12}, a_{14}, etc. are all functions of the assumed circular frequency, ω. If the beam is vibrating, these equations will only be satisfied if ω assumes a value which corresponds to a natural frequency, in which case the determinant of the coefficients becomes zero.

A block diagram illustrating the planning of the computation is shown in Fig.4.2. The top two rows of each transfer matrix, containing the elastic properties of the beam section are calculated from the length and section inertia of the beam section. An initial estimated value of the circular frequency of the beam, ω, is then inserted and together with the gyroscopic factor h, is used to complete the lower two rows of the matrix. The sequential product of the matrices, $\begin{bmatrix} A \end{bmatrix}$, is then computed, from the elements of which the value of the determinant above is computed.

Calling the value of this determinant R_0, a second value is obtained by repeating the calculation using a slightly higher value of ω, ω_1 , leading to a corresponding determinant, R_1. Using the two trial values of ω, i.e. ω_0 and ω_1, and their corresponding determinants R_0 and R_1, a closer approximation to the correct value of ω corresponding to a natural frequency can be obtained by the Newton iteration relation:-

$$\omega_2 = \omega_1 + R_1 \left(\frac{\omega_1 - \omega_0}{R_0 - R_1} \right)$$

Iteration was continued until two successive values of ω corresponded to a difference of < 1 rpm.

The first calculation for the forward whirling speed of the shaft made no allowance for shear deformation of the shaft and the mass moment of inertia of the shaft sections was ignored. A speed of 2472 rpm was obtained.

Since the division of the shaft into 8 sections was possibly only a crude approximation to a slender shaft, the calculation was repeated using 38 sections, and yielded a value for the whirling speed of 2437 rpm. Repeating this calculation, taking into account the moment of inertia of the shaft sections and making allowance for shear deformation, altered the whirling speed only slightly to 2434 rpm. It was therefore concluded that division of the shaft into only 8 sections was sufficient and that shear deformation was of negligible effect.

4.4 L.P. Rotor with Sprung Rear Bearing

For this case the transfer matrix t_8 was altered to include a spring support of stiffness k_2, which was fed in with the initial value of the whirling speed and the gyroscopic factor h. The conditions to the right of

section 8 now became:—

$$M_{R8} \quad = \quad V_{R8} \quad = \quad 0$$

giving the matrix equation

$$\begin{bmatrix} y \\ \vartheta \\ 0 \\ 0 \end{bmatrix}_{R8} = \begin{bmatrix} A \end{bmatrix} \cdot \begin{bmatrix} 0 \\ \vartheta \\ 0 \\ V \end{bmatrix}_{L2}$$

from which the natural frequency is determined when the determinant

$$\begin{vmatrix} a_{32} & a_{34} \\ a_{42} & a_{44} \end{vmatrix}$$

becomes zero, the iteration to this being carried out as before.

4.5   L.P. Rotor with both bearings spring mounted

When the front bearing was spring mounted, the transfer matrix t_1, which contains an allowance for the stiffness of the spring, k_1, is now included in the matrix product $\begin{bmatrix} A \end{bmatrix}$.

The matrix equation relating the conditions to the right of the rear bearing to those to the left of the front bearing then becomes:—

$$\begin{bmatrix} y \\ \vartheta \\ 0 \\ 0 \end{bmatrix}_{R8} = \begin{bmatrix} A \end{bmatrix} \cdot \begin{bmatrix} y \\ \vartheta \\ 0 \\ 0 \end{bmatrix}_{L1}$$

both the bending moment and shear force beyond each bearing being zero.

The last two equations of this matrix equation yield the determinant

$$\begin{vmatrix} a_{31} & a_{32} \\ a_{41} & a_{42} \end{vmatrix}$$

which becomes zero when a natural frequency is obtained.

4.6   Calculation of Mode of Vibration

The calculation of the mode of vibration in each of the above cases was similar and will be illustrated by considering the last case where both bearings are spring mounted.

The first of the equations giving a zero boundary condition to the right of section 8 is:—

$$M_8 = a_{31} \cdot y_1 + a_{32} \cdot \theta_1 = 0$$

from which

$$\theta_1 = - \frac{a_{31}}{a_{32}} y_1$$

Putting, arbitrarily, $y_1 = 1.0$, and using b_{ij} to represent the elements of the successive matrix product

$$t_b \cdot \ldots t_3 \cdot t_2 \cdot t_1$$

the deflection at section b becomes:—

$$y_b = b_{11} - b_{12} \cdot \theta_1$$

$$= b_{11} - \frac{a_{31}}{a_{32}} \cdot b_{12}$$

Thus the deflection of each section, when vibrating at the natural frequency found, can be calculated.   In particular, the relative values of the deflections of the bearings and the disc, which were to be monitored on test, could be obtained.

4.7   The Casing

The casing was divided into 17 sections as shown in
Fig.4.3.   Sections 1, 3 and 17 were treated as disc masses,
using transfer matrix of type 1, with section 3 being mounted
on a spring of stiffness k_1.   Sections 7 and 15 were ori-
ginally treated as disc masses, representing the aluminium
plates, but when it was found that the flexibility of the
plates was appreciable this factor was incorporated by using
a transfer matrix of type 4 to represent their properties.
All other sections were treated as beam sections with mass
(transfer matrix type 2).

4.8   Deflection of casing under a point load

The normal frequency type program was modified by
making $\omega = 0$ to eliminate the inertia loading, in order to
calculate the deflected shape of the casing when a point
load was applied to the front aluminium disc.   In order to
eliminate the large deflections of the bearing springs, the
casing was considered to be mounted on rigid supports at the
front and rear bearing spring supports.

Since the front bearing spring support is simply
supported, the known conditions to the left of section 4 are
$y_{L4} = M_{L4} = 0$ leaving ϑ_{L4} and V_{L4} as unknowns together with
the only external load P, applied to the front aluminium
plate (Section 6.2).   The conditions at the left of
section 4 are then given by:—

$$
\begin{bmatrix} y \\ \vartheta \\ M \\ V \end{bmatrix}_{L4}
=
\begin{bmatrix} 0 & 0 & 0 \\ 1 & 0 & 0 \\ 0 & 0 & 0 \\ 0 & 1 & 0 \end{bmatrix}
\cdot
\begin{bmatrix} \vartheta \\ V \\ P \end{bmatrix}_{L4}
$$

Sequential multiplication of this 3 x 4 matrix by the transfer matrices then gave the conditions at section 7 in terms of ϑ_{L4}, V_{L4} and P. The loading P at this point was then introduced by making the fourth element of column 3 unity. Further sequential multiplication by the remaining transfer matrices finally gave the conditions to the right of section 15 as

$$\begin{bmatrix} y \\ \vartheta \\ M \\ V \end{bmatrix}_{R15} = \begin{bmatrix} A \end{bmatrix} \cdot \begin{bmatrix} \vartheta \\ V \\ P \end{bmatrix}_{L4}$$

where again since section 15 was simply supported, y_{R15} and M_{R15} are both zero.

Now, since the coefficient a_{31} is zero, (physically the bending moment cannot be affected by the initial slope ϑ_{L4}), the third equation of this matrix equation is:—

$$a_{32} \cdot V_{L4} + a_{33} \cdot P = 0$$

giving

$$V_{L4} = - \left(a_{33} / a_{32} \right) \cdot P$$

Since y_{R15} is zero, the first equation gives, using the above relation

$$a_{11} \cdot \vartheta_{L4} + a_{12} \cdot \left(- a_{33} / a_{32} \right) \cdot P + a_{13} \cdot P = 0$$

giving

$$\vartheta_{L4} = \left(a_{12} \cdot a_{33} / a_{32} \right) \cdot P - \left(a_{13} / a_{11} \right) \cdot P$$

4.9

Thus the initial conditions to the left of section 4 are now known in terms of P. Therefore, if b_{ij} are the elements of the sequential product of the transfer matrices $t_i \cdot \ldots \ldots t_5 \cdot t_4$, then the deflection y_i is given by:—

$$b_{11} \cdot \vartheta_{L4} + b_{12} \cdot V_{L4} + b_{13} \cdot P$$

i.e. in view of the above relations, y_i is given in terms of the external load P.

4.9 Natural frequency of casing on rigid supports

The calculation of the natural frequencies of the casing mounted on rigid supports at the bearing spring mounts (sections 3 and 15) was carried out in a similar fashion to the corresponding program for the L.P. rotor yielding,

$$
\begin{bmatrix} y \\ \vartheta \\ M \\ V \end{bmatrix}_{R15} = \begin{bmatrix} A \end{bmatrix} \cdot \begin{bmatrix} y \\ \vartheta \\ M \\ V \end{bmatrix}_{L4}
$$

Using the boundary conditions

$$y_{L4} = M_{L4} = y_{R15} = M_{R15} = 0$$

the determinant, which becomes zero when a natural frequency is reached, is:—

$$
\begin{vmatrix} a_{12} & a_{14} \\ a_{32} & a_{34} \end{vmatrix}
$$

4.10 Natural frequency of casing when mounted on spring supports

Again the calculation was similar to that for the L.P. rotor, with the stiffnesses of the spring supports for sections 3 and 15 being introduced with the initial guess of ω.

The matrix equation with the boundary conditions

$$M_{L3} = V_{L3} = M_{R15} = V_{R15} = 0$$

now giving the frequency determinant:—

$$\begin{vmatrix} a_{31} & a_{32} \\ a_{41} & a_{42} \end{vmatrix}$$

4.11 Modified matrix method

When relatively stiff springs are used as supports the elements of the determinant can become very large (Ref.19, p.193) so that the final stage of the evaluation of the determinant can lead to the difference of two very large numbers. This effect was found with the above program. The elements of the determinant were found to be of the order of 10^6 which meant that the value of the determinant was the difference of two numbers of the order of 10^{12}.

The modified transfer matrix method (Ref.19, p.205) which is designed to overcome this difficulty, was examined but it was found that for this particularly simple case it expressed the frequency condition as,

$$\frac{a_{31}}{a_{32}} - \frac{a_{41}}{a_{42}} = 0$$

This is, of course, an alternative arrangement of the determinant which avoids the difference of two large numbers. When this relation was applied, it was found that errors were not being introduced in the original method of evaluating the determinant, at least for the two lowest frequencies.

4.12 H.P. Rotor

A convenient method of investigating the computer representation of the H.P. rotor was to consider it mounted in the front half of the casing as shown in Fig.4.4. The division of the two components into sections for analysis is shown.

The casing was divided into 9 sections. Sections 1, 3, 7 and 9 are masses with transfer matrices of type 1 being used to represent their properties. Sections 4, 5 and 6 are beam masses which require transfer matrices of type 2. Sections 2 and 8 are sections representing the spring rods and required a special type of transfer matrix (type 3). The H.P. shaft was divided into 10 sections of either disc or beam mass as indicated in the figure.

The casing can be considered as a beam, mounted on springs k_1 and k_2. The unknown conditions at the left end are the deflection, y_1, and the slope, θ_1, and the reaction transmitted across the front bearing, R_1. The state vector to the left of section 1 then becomes:—

$$\begin{bmatrix} y \\ \theta \\ M \\ V \end{bmatrix}_{L1} = \begin{bmatrix} 1 & 0 & 0 \\ 0 & 1 & 0 \\ 0 & 0 & 0 \\ 0 & 0 & 1 \end{bmatrix} \cdot \begin{bmatrix} y_1 \\ \theta_1 \\ R_1 \end{bmatrix}$$

This form of the starting state vector was adopted in order to separate the contributions to the deflection, slope, bending moment and shear force due to y_1, ϑ_1 and R_1.

Sequential multiplication of this matrix by the transfer matrices for sections 1 to 9 gives, with the addition of a further column to represent the shear force change due to the rear bearing reaction, R_2, gives the state vector to the right of section 9:—

$$\begin{bmatrix} y \\ \vartheta \\ M \\ V \end{bmatrix}_{R9} = \begin{bmatrix} a_{11} & a_{12} & a_{13} & 0 \\ a_{21} & a_{22} & a_{23} & 0 \\ a_{31} & a_{32} & a_{33} & 0 \\ a_{41} & a_{42} & a_{43} & 1 \end{bmatrix} \cdot \begin{bmatrix} y_1 \\ \vartheta_1 \\ R_1 \\ R_2 \end{bmatrix}$$

In a similar way, the state vector representing the conditions to the left of section 11 on the H.P. rotor is:—

$$\begin{bmatrix} y \\ \vartheta \\ M \\ V \end{bmatrix}_{L11} = \begin{bmatrix} 1 & 0 & 0 \\ 0 & 1 & 0 \\ 0 & 0 & 0 \\ 0 & 0 & -1 \end{bmatrix} \cdot \begin{bmatrix} y_1 \\ \vartheta_2 \\ R_1 \end{bmatrix}$$

where it is assumed that the deflection of the H.P. rotor, at the front bearing, is the same as that of the bearing housing.

Sequential multiplication of this matrix by the transfer matrices for sections 11 to 16 then gives the state vector representing the conditions at the rear bearing housing:—

$$
\begin{bmatrix} y \\ \vartheta \\ M \\ V \end{bmatrix}_{R16} = \begin{bmatrix} b_{11} & b_{12} & b_{13} \\ b_{21} & b_{22} & b_{23} \\ b_{31} & b_{32} & b_{33} \\ b_{41} & b_{42} & b_{43} \end{bmatrix} \cdot \begin{bmatrix} y_1 \\ \vartheta_2 \\ R_1 \end{bmatrix}
$$

The top row of this relation gives the deflection of the shaft at the rear bearing, which will later be assumed to be the same as the deflection of the housing, given by the top row of the matrix defining the conditions at the right end of the casing.

The reaction, $- R_2$, transmitted to the shaft by the rear bearing housing is now introduced by augmenting the matrix to give:—

$$
\begin{bmatrix} y \\ \vartheta \\ M \\ V \end{bmatrix}_{R16} = \begin{bmatrix} b_{11} & b_{12} & b_{13} & 0 \\ b_{21} & b_{22} & b_{23} & 0 \\ b_{31} & b_{32} & b_{33} & 0 \\ b_{41} & b_{42} & b_{43} & -1 \end{bmatrix} \cdot \begin{bmatrix} y_1 \\ \vartheta_2 \\ R_1 \\ R_2 \end{bmatrix}
$$

Multiplication of this matrix by the transfer matrices for sections 17 to 20 then gives the conditions to the right of section 20 as:—

$$
\begin{bmatrix} y \\ \vartheta \\ M \\ V \end{bmatrix}_{R20} = \begin{bmatrix} c_{11} & c_{12} & c_{13} & c_{14} \\ c_{21} & c_{22} & c_{23} & c_{24} \\ c_{31} & c_{32} & c_{33} & c_{34} \\ c_{41} & c_{42} & c_{43} & c_{41} \end{bmatrix} \cdot \begin{bmatrix} y_1 \\ \vartheta_2 \\ R_1 \\ R_2 \end{bmatrix}
$$

The boundary conditions to the right of section 9 of the casing are $M_{R9} = V_{R9} = 0$, and for the right end of the shaft, $M_{R20} = V_{R20} = 0$. In addition, the deflections of the bearing and housing are assumed to be equal, i.e. $y_{R9} - y_{R16} = 0$. Extracting the equations representing these conditions and combining them into matrix form gives:—

$$
\begin{bmatrix}
a_{31} & a_{32} & a_{33} & 0 & 0 \\
a_{41} & a_{42} & a_{43} & 0 & 1 \\
c_{31} & 0 & c_{33} & c_{32} & c_{34} \\
c_{41} & 0 & c_{43} & c_{42} & c_{44} \\
a_{11} - b_{11} & a_{12} & a_{13} - b_{13} & -b_{12} & 0
\end{bmatrix}
\begin{bmatrix}
y \\
\vartheta_1 \\
R_1 \\
\vartheta_2 \\
R_2
\end{bmatrix}
= 0
$$

The determinant of the coefficients of these five equations would, of course, become zero at a natural frequency. However, it was expected that since the determinant was of larger order than in the case of the casing alone, and large spring stiffnesses were involved, numerical difficulties might be encountered. Indeed it was found that the final computation in the evaluation of the determinant involved the difference of two numbers of the order of 10^{14}.

To obviate any hidden inaccuracy the modified transfer matrix method was adopted. The deflection, y_1, was given an arbitrary value of 1.0 and rough estimates of 0.1 were assigned to ϑ_1 and ϑ_2, and 10^4 to the reactions R_1 and R_2. Using x_1, x_2, x_3 and x_4 to denote the corrections to be added to these to give the true values at a particular frequency, ω, the above matrix equation becomes:—

$$
\begin{bmatrix} & \\ & A & \\ & \end{bmatrix} \cdot \begin{bmatrix} & 1.0 & \\ \vartheta_1 & + & x_1 \\ R_1 & + & x_2 \\ \vartheta_2 & + & x_3 \\ R_2 & + & x_4 \end{bmatrix} = 0
$$

where $\begin{bmatrix} A \end{bmatrix}$ is now the 5 x 5 matrix above.

The first four of these equations were solved to give values for the correction factors x_i. The last three of these i.e. x_2, x_3 and x_4, were then used in the fifth equation to give a second estimate of x_1, say x_1', which is normally different to x_1. The value of $x_1 - x_1'$ is used to detect a natural frequency, since it becomes zero under such a condition.

The correct values for ϑ_1, R_1, ϑ_2 and R_2 for a particular guessed value of the natural frequency, are then

$$
\vartheta_1 \quad + \quad \frac{x_1 + x_1'}{2}
$$

$$
R_1 \quad + \quad x_2
$$

$$
\vartheta_2 \quad + \quad x_3
$$

$$
\text{and} \quad R_2 \quad + \quad x_4
$$

When these are used to repeat the calculation the new value of $x_1 - x_1'$ is the same (apart from very small differences due to rounding errors) and does not involve the difference of large numbers, thus avoiding numerical difficulties. Also, the new correction factors, calculated as above, are virtually zero and thus the corrected values for ϑ_1, R_1, ϑ_2 and R_2 can be used as very good estimates for the starting conditions for the next trial value of the frequency, if it is close to the previous value.

Summarising, the standard method of applying the transfer matrix method is a process of step-wise integration of the beam equation. Inappropriate starting conditions of unity are used for the deflection, slope, etc., and understandably can result in ridiculously out of proportion values for the final conditions which leads to numerical difficulties in the assembly and solution of the determinant. The modified matrix method proceeds in a more realistic manner by using, at each trial, very close estimates to the true values of the starting boundary values of deflection, slope, bending moment and shear force, which naturally lead to realistic values for the final conditions, thus avoiding numerical inaccuracy.

4.13 The Complete Rig

The program for the complete rig was essentially an assembly of the previous programs. The rig was treated as an assembly of four beams, divided into sections as before, resting on one another as shown in Fig.4.5. As a result there are four unknown reactions, R_1, R_3, R_4 and R_5, transmitted across the bearings. In addition, since the casing now has to be divided into two parts, the main part transmits an unknown reaction, R_2, and couple, C, to the second beam, referred to as 'Inter', which is the mounting of the H.P. rear bearing housing on the front plate of the casing. For clarity the sections of each component are omitted, being the same as in previous programs, and only the remaining unknowns, y, ϑ_1, ϑ_2, ϑ_3 and the unknown loads are shown.

4.14   Treatment of the Casing

The conditions at the left end of the casing were represented by the matrix product:—

$$\begin{bmatrix} y \\ \vartheta \\ M \\ V \end{bmatrix} = \begin{bmatrix} 1 & 0 & 0 \\ 0 & 1 & 0 \\ 0 & 0 & 0 \\ 0 & 0 & 1 \end{bmatrix} \cdot \begin{bmatrix} y \\ \vartheta_1 \\ R_1 \end{bmatrix}$$

The conditions at the front plate were then obtained by sequential multiplication of this matrix by the transfer matrices for the sections up to the front plate.   The reaction, R_2, and couple, C, were then introduced by adding two columns to the matrix to give the conditions to the right of the plate thus:—

$$\begin{bmatrix} y \\ \vartheta \\ M \\ V \end{bmatrix} = \begin{bmatrix} a_{11} & a_{12} & a_{13} & 0 & 0 \\ a_{21} & a_{22} & a_{23} & 0 & 0 \\ a_{31} & a_{32} & a_{33} & 1 & 0 \\ a_{41} & a_{42} & a_{43} & 0 & 1 \end{bmatrix} \cdot \begin{bmatrix} y \\ \vartheta_1 \\ R_1 \\ C \\ R_2 \end{bmatrix} \quad \ldots\ldots (1)$$

Pre—multiplication of this matrix by the remaining matrices for the sections of the casing gave the conditions to the right of the L.P. rear bearing housing as:—

$$\begin{bmatrix} y \\ \vartheta \\ M \\ V \end{bmatrix}_C = \begin{bmatrix} b_{11} & b_{12} & b_{13} & b_{14} & b_{15} & 0 \\ b_{21} & b_{22} & b_{23} & b_{24} & b_{25} & 0 \\ b_{31} & b_{32} & b_{33} & b_{34} & b_{35} & 0 \\ b_{41} & b_{42} & b_{43} & b_{44} & b_{45} & 1 \end{bmatrix} \cdot \begin{bmatrix} y \\ \vartheta_1 \\ R_1 \\ C \\ R_2 \\ R_5 \end{bmatrix}$$

with an additional column to introduce the bearing reaction, R_5.

The known conditions from this equation are

$$M_c = V_c = 0$$

and also the deflection y_c must equal the deflection of the L.P. rear bearing, y_L.

4.15 Treatment of the H.P. Bearing Support ('Inter')

The conditions at the left end of this beam are those given by equation (1) with —1.0 replacing 1.0 in the new columns to allow for the unknown loads —R_2 and —C. Multiplication of this matrix by the transfer matrices for the Inter sections, with a further column added to introduce the H.P. bearing reaction, R_3, gave the conditions to the right of the H.P. bearing housing as:—

$$\begin{bmatrix} y \\ \vartheta \\ M \\ V \end{bmatrix}_I = \begin{bmatrix} c_{11} & c_{12} & c_{13} & c_{14} & c_{15} \\ c_{21} & c_{22} & c_{23} & c_{24} & c_{25} \\ c_{31} & c_{32} & c_{33} & c_{34} & c_{35} \\ c_{41} & c_{42} & c_{43} & c_{44} & c_{45} \end{bmatrix} \cdot \begin{bmatrix} y \\ \vartheta_1 \\ R_1 \\ C \\ R_2 \\ R_3 \end{bmatrix}$$

The known conditions from this equation are:—

$$M_I = V_I = 0$$

and the deflection y_I must equal the deflection of the H.P. rear bearing, y_H.

4.16   Treatment of the H.P. Rotor

The conditions at the left end of the H.P. rotor, where reactions $-R_1$ and R_4 are introduced across the bearings were represented by:—

$$
\begin{bmatrix} y \\ \vartheta \\ M \\ V \end{bmatrix}
=
\begin{bmatrix}
1 & 0 & 0 & 0 \\
0 & 1 & 0 & 0 \\
0 & 0 & 0 & 0 \\
0 & 0 & -1 & 1
\end{bmatrix}
\cdot
\begin{bmatrix} y \\ \vartheta_2 \\ R_1 \\ R_4 \end{bmatrix}
$$

Multiplication of this matrix by the transfer matrices for the H.P. rotor sections up to the H.P. rear bearing gave the conditions to the right of the bearing as:—

$$
\begin{bmatrix} y \\ \vartheta \\ M \\ V \end{bmatrix}_{H'}
=
\begin{bmatrix}
d_{11} & d_{12} & d_{13} & d_{14} & 0 \\
d_{21} & d_{22} & d_{23} & d_{24} & 0 \\
d_{31} & d_{32} & d_{33} & d_{34} & 0 \\
d_{41} & d_{42} & d_{43} & d_{44} & -1
\end{bmatrix}
\cdot
\begin{bmatrix} y \\ \vartheta_2 \\ R_1 \\ R_4 \\ R_3 \end{bmatrix}
$$

where the additional column introduces the reaction from the H.P. bearing housing, $-R_3$.   The deflection of the H.P. shaft, $y_{H'}$, at this point must equal the deflection of the H.P. bearing housing, y_I, derived above.

Further multiplication of this matrix by the remaining transfer matrices gave the conditions to the right of the H.P. disc as:—

$$
\begin{bmatrix} y \\ \vartheta \\ M \\ V \end{bmatrix}_{H}
=
\begin{bmatrix}
e_{11} & e_{12} & e_{13} & e_{14} & e_{15} \\
e_{21} & e_{22} & e_{23} & e_{24} & e_{25} \\
e_{31} & e_{32} & e_{33} & e_{34} & e_{35} \\
e_{41} & e_{42} & e_{43} & e_{44} & e_{45}
\end{bmatrix}
\cdot
\begin{bmatrix} y \\ \vartheta_2 \\ R_1 \\ R_4 \\ R_3 \end{bmatrix}
$$

in which the conditions M_H and V_H are known to be zero.

4.17 Treatment of the L.P. Rotor

The conditions at the left end of the shaft are represented by:—

$$\begin{bmatrix} y \\ \vartheta \\ M \\ V \end{bmatrix} = \begin{bmatrix} 1 & 0 & 0 \\ 0 & 1 & 0 \\ 0 & 0 & 0 \\ 0 & 0 & -1 \end{bmatrix} \cdot \begin{bmatrix} y \\ \vartheta_3 \\ R_4 \end{bmatrix}$$

Multiplication of this matrix by the transfer matrices for the L.P. shaft sections gave the conditions to the right of the L.P. rear bearing as:—

$$\begin{bmatrix} y \\ \vartheta \\ M \\ V \end{bmatrix}_L = \begin{bmatrix} f_{11} & f_{12} & f_{13} & 0 \\ f_{21} & f_{22} & f_{23} & 0 \\ f_{31} & f_{32} & f_{33} & 0 \\ f_{41} & f_{42} & f_{43} & -1 \end{bmatrix} \cdot \begin{bmatrix} y \\ \vartheta_3 \\ R_4 \\ R_5 \end{bmatrix}$$

where the additional column introduces the reaction $-R_5$ from the L.P. bearing housing.

The known conditions from this matrix equation are:—

$$M_L = V_L = 0$$

and the deflection, y_L, must equal the deflection of the rear bearing housing, y_C.

4.18 Boundary conditions of complete Rig

There are 10 unknown quantities:—

y ...   . the deflection of the front of the rig

ϑ_1, ϑ_2, ϑ_3 ... . the slopes at the left ends of the casing, H.P. and L.P. rotors respectively

R_1, R_2, R_3, R_4, R_5 . . the reactions transmitted between the components

C ...   . the couple transmitted between the Casing and Inter

The known conditions are:—

$$M_c = M_I = M_H = M_L = 0$$

$$V_c = V_I = V_H = V_L = 0$$

and

$$y_c - y_L = 0$$

$$y_I - y_H' = 0$$

The unknown reaction R_5 can be eliminated by combining the boundary conditions $V_c = V_L = 0$. The shear force to the right of the casing is:—

$$V_c = b_{41} \cdot y + b_{42} \cdot \theta_1 + b_{43} \cdot R_1 + b_{44} \cdot C + b_{45} \cdot R_2 + R_5 = 0$$

The shear force to the right of the L.P. rotor is:—

$$V_L = f_{41} \cdot y + f_{42} \cdot \theta_3 + f_{43} \cdot R_4 - R_5 = 0$$

Addition of these two equations then gives $V_c + V_L = 0$, thus eliminating the unknown reaction, R_5.

Thus the boundary conditions give 9 equations with 9 unknowns as laid out in Fig.4.6. The determinant of the coefficients of these equations would of course become zero when a natural frequency was obtained. However, since the evaluation of this determinant might have led to numerical difficulties, the modified transfer matrix method was adopted.

To describe the application of this procedure the 9 equations of Fig.4.6 can be arranged as:—

$$\begin{bmatrix} D & \vline & E \\ \hline & F \end{bmatrix} \left\{ y \ R_1 \ R_2 \ R_3 \ R_4 \ \vartheta_1 \ \vartheta_2 \ \vartheta_3 \ C \right\} = 0$$

where the matrix has been partitioned for clarity, into a single column matrix, D, a single row matrix, F, and the remaining matrix, E.

If the deflection of the left end of the model, y, is given an arbitrary value of unity and appropriate estimated values given to the unknowns, R_1, R_2, etc., to which correction factors, x_1, x_2, x_3, etc. must be added to give the true values which would occur at the particular frequency being examined, then the first 8 equations of the original matrix become:—

$$\begin{bmatrix} E \end{bmatrix} \cdot \begin{bmatrix} R_1 \\ R_2 \\ R_3 \\ R_4 \\ \vartheta_1 \\ \vartheta_2 \\ \vartheta_3 \\ C \end{bmatrix} = - \begin{bmatrix} D \end{bmatrix} - \begin{bmatrix} E \end{bmatrix} \cdot \begin{bmatrix} x_1 \\ x_2 \\ x_3 \\ x_4 \\ x_5 \\ x_6 \\ x_7 \\ x_8 \end{bmatrix}$$

The solution of these equations gives values for the 8 correction factors, x_1, x_2, x_3, etc. A second value for the correction factor, x_1, namely x_1', may be obtained, using these values inserted in the last equation of the matrix, i.e:—

$$
\begin{bmatrix} & & F & & \end{bmatrix}
\begin{bmatrix} 1 \\ R_1 \\ R_2 \\ R_3 \\ R_4 \\ \vartheta_1 \\ \vartheta_2 \\ \vartheta_3 \\ C \end{bmatrix} = 0
$$

The value of $x_1 - x_1'$ is used to judge the proximity of a natural frequency since it should then become zero.

The corrected values for the unknowns, i.e:—

$$R_1 \quad + \quad (x_1 + x_1')/2$$
$$R_2 \quad + \quad x_2$$
$$R_3 \quad + \quad x_3$$
$$R_4 \quad + \quad x_4$$
$$\vartheta_1 \quad + \quad x_5$$
$$\vartheta_2 \quad + \quad x_6$$
$$\vartheta_3 \quad + \quad x_7$$
$$C \quad + \quad x_8$$

may then be used as very good estimates of the unknowns at the next trial frequency — assuming it to be close to the first.

4.19 Solution of the Simultaneous Equations

The solution of the simultaneous equations to obtain the correction factors in the modified matrix method was carried out with an elegant subroutine devised by Mr. R. Jeffreys, formerly of the Computing Department of Glasgow University.

The subroutine solves the equations

$$A x = y$$

by transforming the matrix A into

$$A = L U$$

where L is a lower triangular matrix, with zero diagonal elements, and U is an upper triangular matrix with non-zero diagonal elements. At each stage of the transformation the rows are interchanged to ensure that the largest element in the pivotal column is used as the current pivotal element, thus minimising arithmetical inaccuracies.

The subroutine was modified to produce an efficient means of evaluating a determinant. The value of the determinant of the matrix A is given by the product of the diagonal terms of U, multiplied by $(-1)^s$, where s is the number of row changes which occur during the triangulation process.

4.20 Iteration Difficulties

A typical variation of the magnitude of the determinant obtained when the standard matrix method was used is shown in Fig.4.7(a). The value was large (of the order of 10^{12} when the H.P. rotor mounted in the casing was being considered, and 10^{20} in the case of the complete rig) and fairly constant until ω was very close to a natural frequency. As a result the location of a particular natural frequency by iteration was not straightforward unless a

very good estimate of the frequency was available as a
starting value.   When this was not possible the computer
program was caused to produce values of the determinant
at small intervals of ω and a plot of the results, as in
Fig.4.7(a), was used to provide a very close approximation
which could then be used to initiate an iterative process.

The modified matrix method was adopted when it was
realised that the final operation in the evaluation of the
determinant was likely to produce arithmetical inaccuracies.
The plot of the remainder (e.g. $x_1 - x_1'$, in Section 4.18)
versus ω, produced by this method is sketched in Fig.4.7(b).
Again the location of a natural frequency by iteration
depended on the calculation commencing with a very good
estimate of the required natural frequency.

The modified matrix method was employed for nearly
all the frequency predictions.   However in later calcu-
lations on the complete rig, at certain combinations of
shaft speeds, and particularly when two frequencies were
very close together, the remainder sometimes diverged to
+ or $-\infty$ as shown at the right of Fig.4.7(b).   Presumably
this condition arose when the determinant of the matrix   E ,
in Section 4.18, became ill-conditioned.   The remedy was
to choose another variable, say R_2, instead of R_1 and use
the difference of the two estimates of its correction
factor, namely x_2 and x_2' , to judge the position of the
natural frequency.   This procedure was usually successful.
However, when higher modes of vibration of the complete rig
were being explored the difficulty was not removed even
after four changes of variable (and four major alterations
to the computer program).   Rather in desperation the
standard matrix method was returned to and despite the very
large values of the determinant satisfactory convergence
was obtained.   But the calculation of the modes was not

accurate, as shown by disagreement of the displacements
of the components at the bearings.   This difficulty was
resolved by arranging for the iteration to proceed until
successive iterations were within 0.1 rpm, instead of
1.0 rpm.
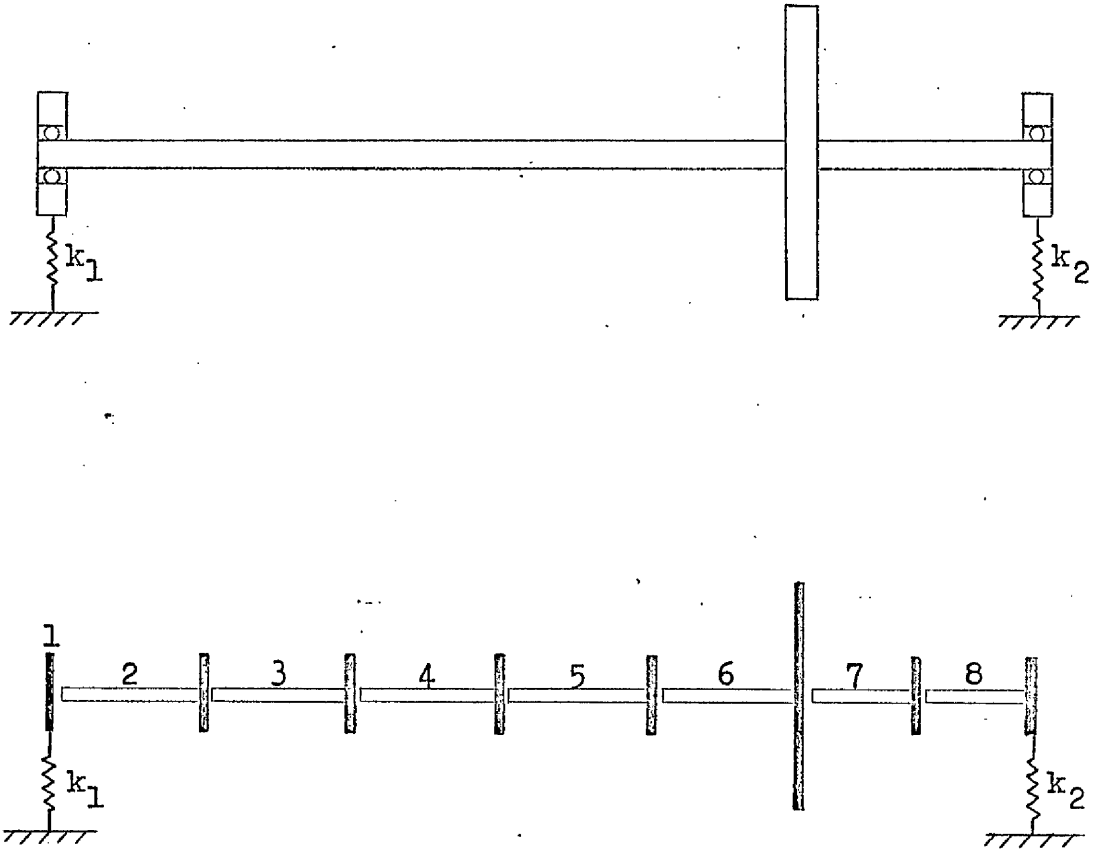
Fig.4.1

Division of L.P. Rotor into 8 sections.

Fig.4.2

Read section data

(ℓ, m, I, J)

Calculate top

rows of T.M.s.

Insert initial

guess ω

$R_0 := 0$

Calculate lower

rows of T.M.s.

Mult. of Matrices

to give $[A]$

$R_0 := R$

$\omega_0 := \omega$

$\omega := \omega + 0.1$

$R := [A]$

$R_0 = 0$? —————————— YES

NO

$R_1 := R, \omega_1 := \omega$

$\omega_2 := \omega_1 + R_1 \left(\dfrac{\omega_1 - \omega_0}{R_0 - R_1} \right)$

$\omega_2 - \omega_1 < 0.01$? —————— YES

NO

$R_0 := R_1, \omega_0 := \omega_1,$

$\omega := \omega_2$

Calculate mode

Output
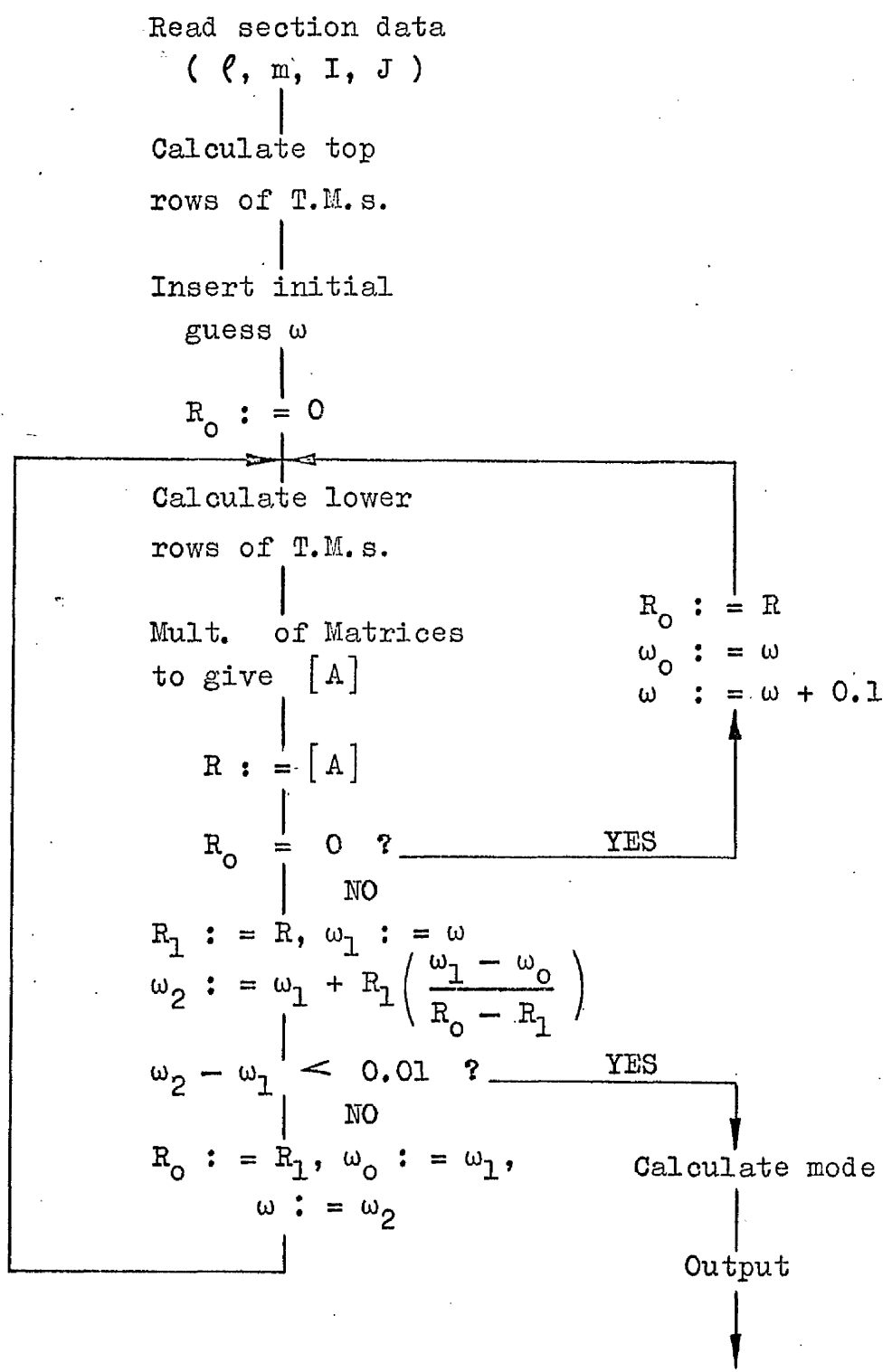
Fig.4.2   Block diagram of computer programme of
transfer matrix calculation.

(The symbol ': =' implies 'adopts the value').
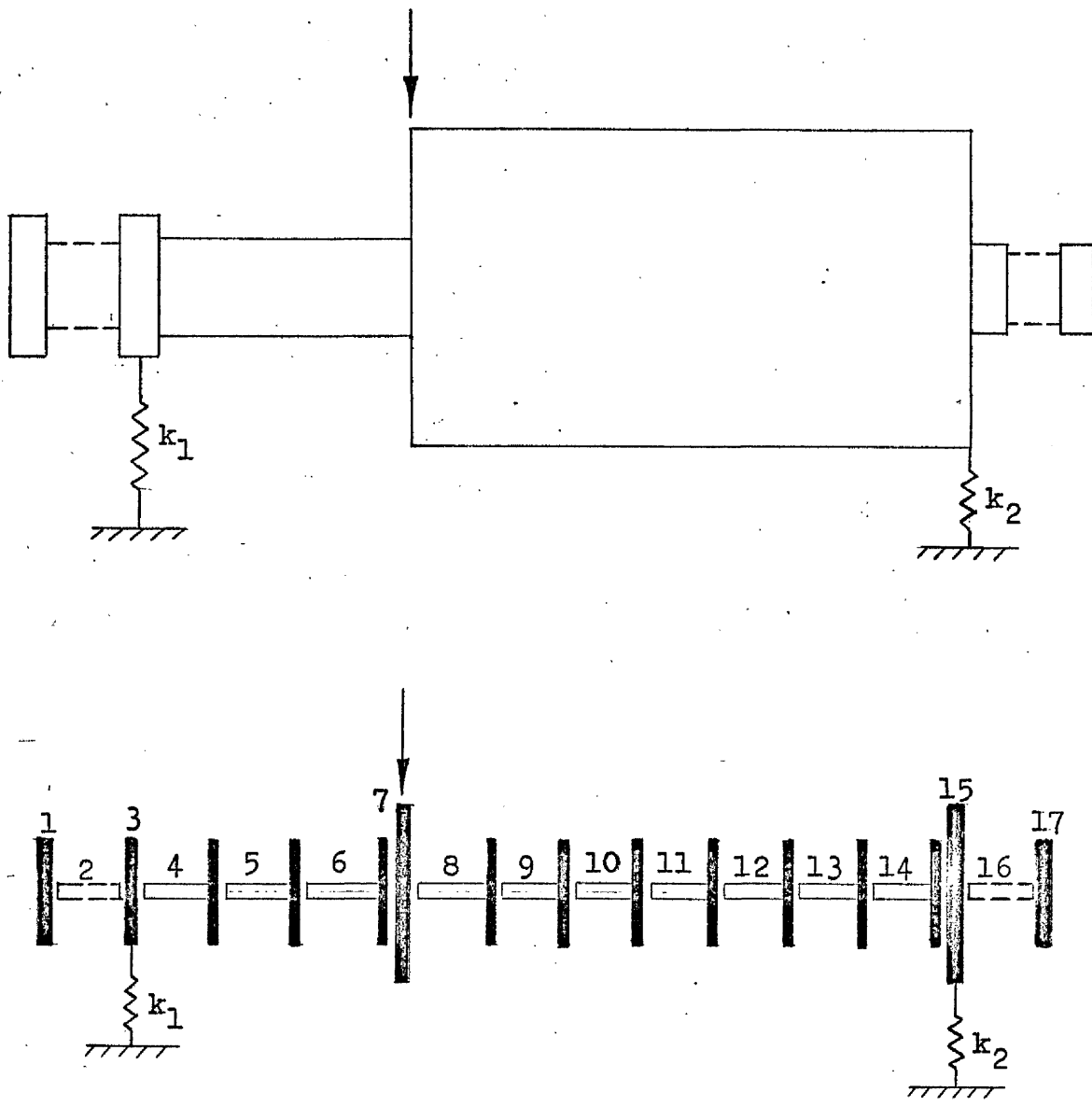
<u>Fig.4.3</u>   Division of Casing into sections.

Fig.4.4

$$k_1$$

$$k_2$$

20

11   17

12 13 14 15 16 18 19

y
ϑ_2

R_1 R_2

7

1   3   9

y
ϑ_1 2   4 5 6   8

k_1

k_2
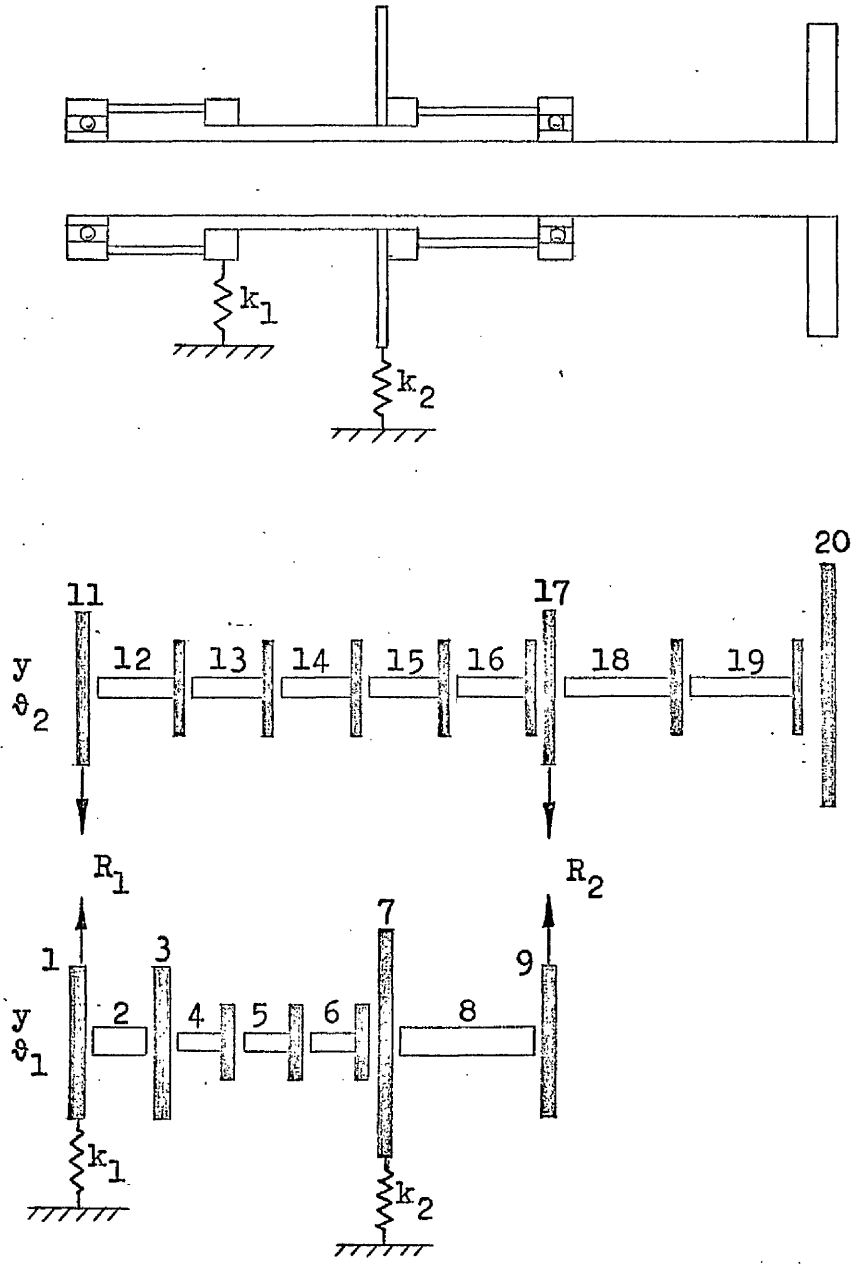
Fig.4.4   Division of H.P. Rotor and front half
of Casing into sections.
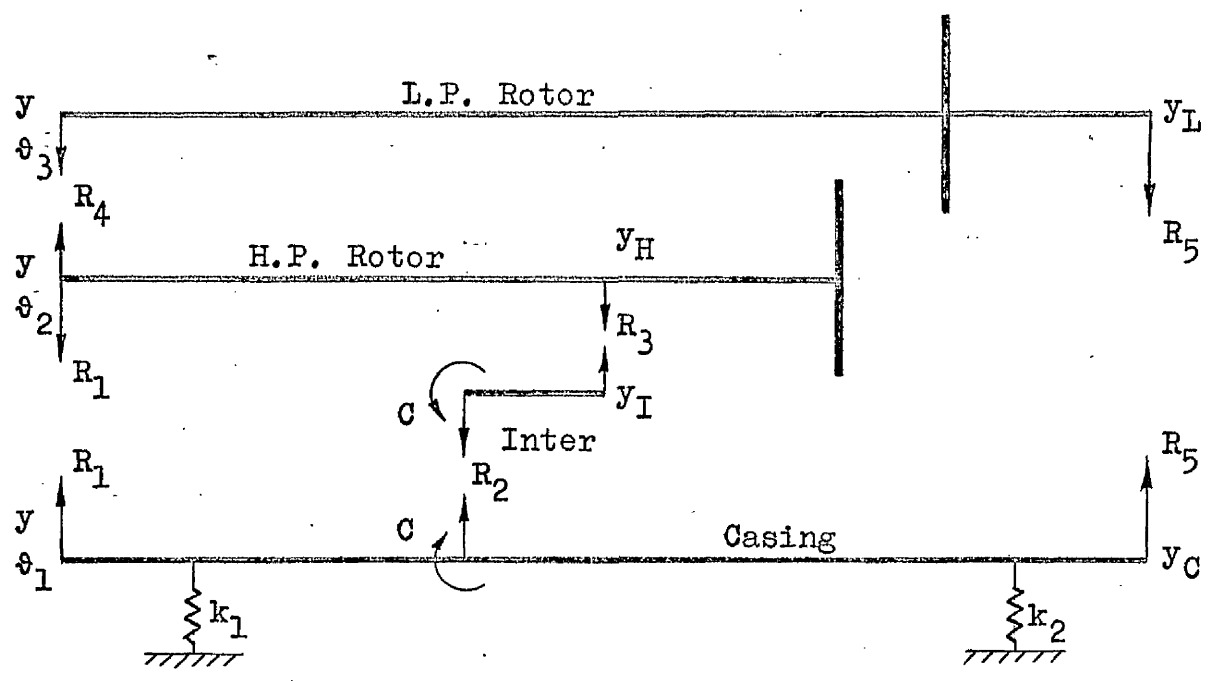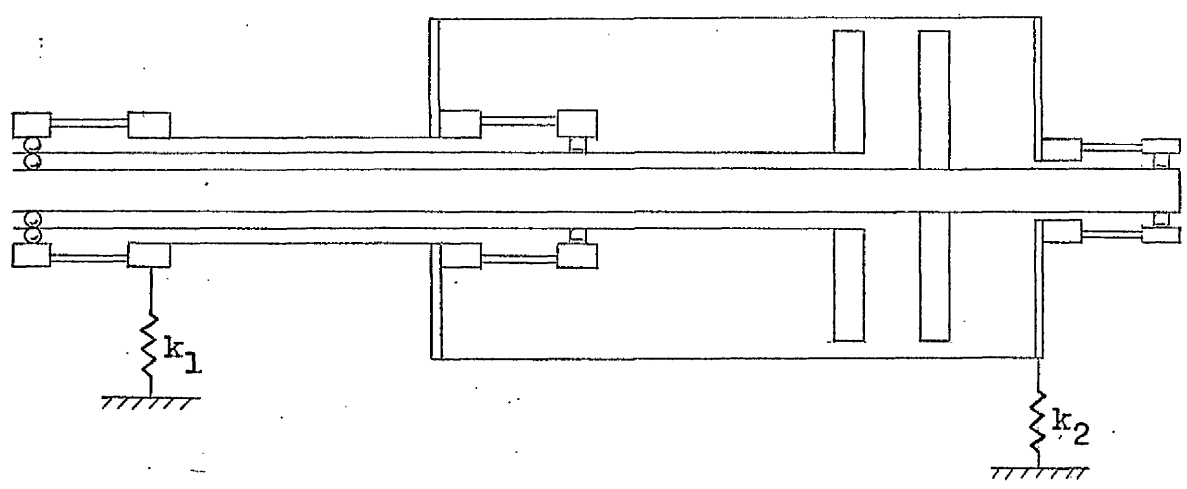
Fig.4.5

Fig.4.5   Breakdown of Complete Model into a
            system of 4 beams.

$$
\begin{bmatrix}
b_{1,1} & b_{1,3} & b_{1,5} & 0 & -f_{1,3} & b_{1,2} & 0 & -f_{1,2} & b_{1,4} \\
c_{1,1} & c_{1,3} & c_{1,5} & -d_{1,3} & -d_{1,4} & c_{1,2} & -d_{1,2} & -d_{1,1} & c_{1,4} \\
b_{4,1} & b_{4,3} & b_{4,5} & -f_{4,1} & -f_{4,3} & b_{4,2} & 0 & -f_{4,2} & b_{4,4} \\
e_{4,1} & e_{4,3} & 0 & e_{4,5} & e_{4,4} & 0 & e_{4,2} & 0 & 0 \\
c_{4,1} & c_{4,3} & c_{4,5} & 1.0 & 0 & c_{4,2} & 0 & 0 & c_{4,4} \\
e_{3,1} & e_{3,3} & 0 & e_{3,5} & e_{3,4} & 0 & e_{3,2} & 0 & 0 \\
f_{3,1} & 0 & 0 & 0 & f_{3,3} & 0 & 0 & f_{3,2} & 0 \\
c_{3,1} & c_{3,3} & c_{3,5} & 0 & 0 & c_{3,2} & 0 & 0 & c_{3,4} \\
b_{3,1} & b_{3,3} & b_{3,5} & 0 & 0 & b_{3,2} & 0 & 0 & b_{3,4}
\end{bmatrix}
\begin{bmatrix} y \\ R_1 \\ R_2 \\ R_3 \\ R_4 \\ \vartheta_1 \\ \vartheta_2 \\ \vartheta_3 \\ c \end{bmatrix} = 0
$$

Fig.4.6   Final matrix equation for the rig.

Fig.4.7
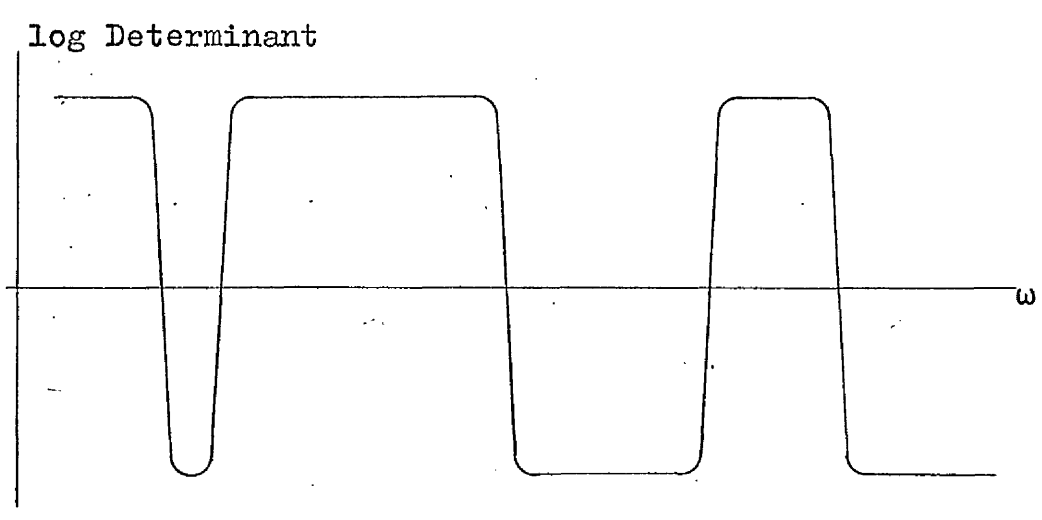
log Determinant

Fig. 4.7(a)   Variation of Determinant with ω.
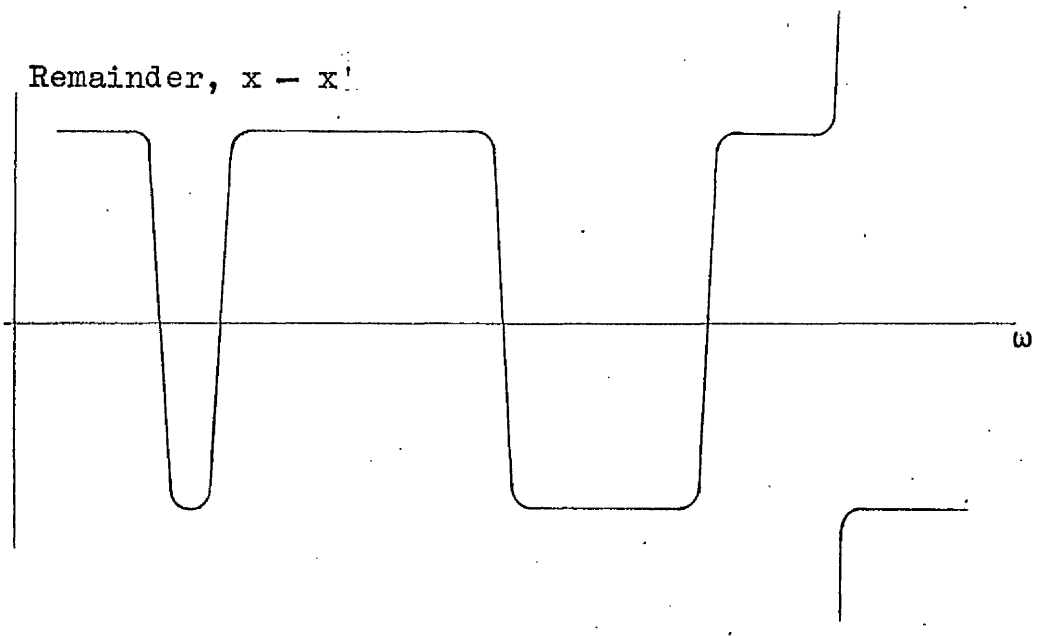
Remainder, x — x'

Fig. 4.7(b)   Variation of Remainder with ω.

APPENDIX 4

DERIVATION OF TRANSFER MATRICES

A4.1 Transfer Matrix Type 1

The Type 1 matrix was used for sections representing the rotor discs, the bearing housings, or bearing spring supports.

The section is considered to be represented by a thin disc of mass m, with a diametral moment of inertia, A, and polar moment of inertia, C.   It is mounted on a beam at a point at which the deflection is y, and the slope is ϑ, as shown in the figure.   If the section is one of the rotor discs it is assumed to be whirling at rate λ, while spinning at rate, ω. If the section is a support of the rig then the support is represented by a spring with a stiffness, k.
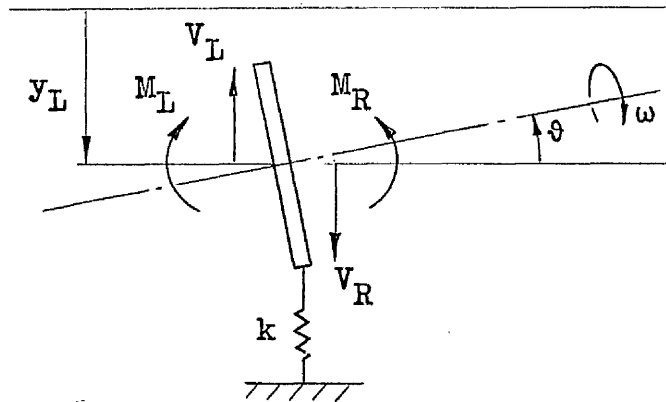
Since the section is assumed to be thin no change in deflection or slope occurs across it, i.e. —

$$y_R = y_L \quad , \quad \vartheta_R = \vartheta_L$$

If the beam is vibrating sinusoidally in the vertical plane at frequency, λ, then the section will apply a vertical loading to the beam of $+ m \lambda^2 y_L$. If the section is mounted on a support then, as a result of the displacement, y_L, an upward force, $k y_L$, will be applied to the section. Thus the change in shear force across the section will be:—

$$V_R = V_L + (m\lambda^2 - k) y_L$$

If the section is at ϑ (anti-clockwise) while vibrating sinusoidally at rate λ, then a torque $- A\vartheta\lambda^2 \sin \lambda t$ (clockwise) must act on the section. The loading on the beam is therefore $+ A\vartheta\lambda^2 \sin \lambda t$ and the bending moment change is given by

$$M_R = M_L - A\lambda^2 \vartheta$$

If the beam is whirling at λ, while rotating at ω, symmetry allows consideration of this case by representing the beam as vibrating in the vertical plane, provided due allowance is made for the actual movement in the horizontal plane resulting in a gyroscopic couple. The additional couple in this case is given by (see Section 1.3):—

$$+ C \omega \lambda \vartheta$$

where C is the polar moment of inertia of the section, and ω is the rotational speed (which may be of opposite sense to the whirl.)

The total change in bending moment across the section is then given by:—

$$M_R = M_L + (-A\lambda^2 + C\omega\lambda) \vartheta$$

The relations expressing the change in conditions across the section are collected in the transfer matrix (Type 1) in the matrix equation:—

$$
\begin{bmatrix} -y \\ \vartheta \\ M \\ V \end{bmatrix}_R =
\begin{bmatrix}
1 & 0 & 0 & 0 \\
0 & 1 & 0 & 0 \\
0 & -A\lambda^2 + C\omega\lambda & 1 & 0 \\
m\lambda^2 - k & 0 & 0 & 1
\end{bmatrix}
\cdot
\begin{bmatrix} -y \\ \vartheta \\ M \\ V \end{bmatrix}_L
$$

A4. 2   Transfer Matrix Type 2

Consider a section consisting of an elastic bar with no mass. The length of the bar is ℓ, its section inertia is J and the material has a Young's Modulus, E. The supposed conditions when the bar is distorted in the vertical plane are shown in the figure:—
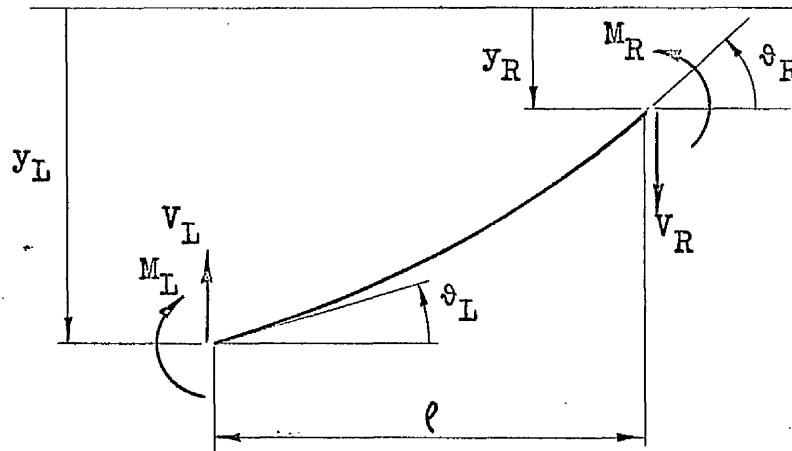
Since there is no load applied to the section equilibrium demands:—

$$V_R = V_L$$

$$M_R = M_L + V_R \cdot \ell$$

If the section is regarded as a cantilever, fixed at the left, then

$$y = - \frac{M \ell^2}{2 E J} + \frac{V \ell^3}{3 E J}$$

$$\vartheta = \frac{M \ell}{E J} + \frac{V \ell^2}{2 E J}$$

ignoring shear deformation.

Combining these relations gives:—

$$y_R = y_L - \ell\,\vartheta_L - (\ell M_L + V_L\,\ell\,)\,\frac{\ell^2}{2\,EJ} + \frac{V_L\,\ell^3}{3\,EJ}$$

$$\vartheta_R = \vartheta_L + (M_L + V_L\,\ell\,)\,\frac{\ell}{EJ} - \frac{V_L\,\ell^2}{2\,EJ}$$

The above relations may be expressed in a concise manner by the matrix equation:—

$$
\begin{bmatrix} -y \\ \vartheta \\ M \\ V \end{bmatrix}_R
=
\begin{bmatrix}
1 & \ell & \dfrac{\ell^2}{2\,EJ} & \dfrac{\ell^3}{6\,EJ} \\
0 & 1 & \dfrac{\ell}{EJ} & \dfrac{\ell^2}{2\,EJ} \\
0 & 0 & 1 & \ell \\
0 & 0 & 0 & 1
\end{bmatrix}
\begin{bmatrix} -y \\ \vartheta \\ M \\ V \end{bmatrix}_L
$$

in which —y has been used to produce positive quantities throughout the matrix.

In the case of a real beam section (with mass) it is regarded as consisting of a massless bar (governed by the above matrix equation) with a thin disc at its right end having inertial properties equal to those of the real beam section as shown in the figure:—

The relation between conditions at the ends of the beam section is then obtained by pre-multiplying the above matrix by a matrix of Type 1, containing the inertial properties. The product is the transfer matrix, referred to as Type 2, in the equation relating the conditions at each end of the section:—

$$
\begin{bmatrix} -y \\ \vartheta \\ M \\ V \end{bmatrix}_R
=
\begin{bmatrix}
1 & \ell & \dfrac{\ell^2}{2\,EJ} & \dfrac{\ell^3}{6\,EJ} \\[2ex]
0 & 1 & \dfrac{\ell}{EJ} & \dfrac{\ell^2}{2\,EJ} \\[2ex]
0 & g\lambda^2 & 1 + \dfrac{g\lambda^2\ell}{EJ} & \ell + \dfrac{g\lambda^2\ell^2}{2\,EJ} \\[2ex]
m\lambda^2 & m\lambda^2\ell & \dfrac{m\lambda^2\ell^2}{2\,EJ} & 1 + \dfrac{m\lambda^2\ell^3}{6\,EJ}
\end{bmatrix}
\begin{bmatrix} -y \\ \vartheta \\ M \\ V \end{bmatrix}_L
$$

where $g = (-\,A\lambda^2 + C\omega\lambda)$.

———

A4.3   Transfer Matrix Type 3

The spring mounting of each bearing was constructed as a cage of four rods clamped between the bearing housing and the spring support, as shown in the figure:—
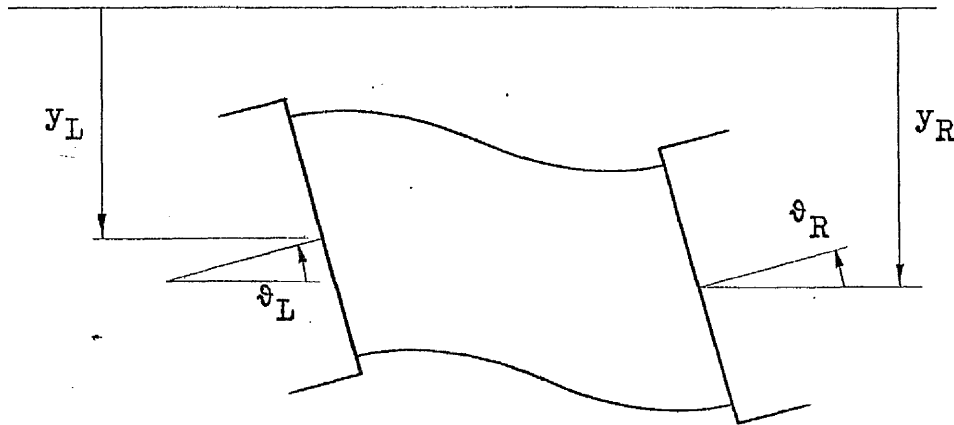
The arrangement was used to ensure that any lateral deflection of the bearing would not cause misalignment of the bearings.   As a result the only change across the section representing the rods was a vertical deflection of $\dfrac{V_L\,\ell^3}{12\,E\,J}$ where J is four times the section inertia of one rod.

The conditions to the right of a rod section were related to those at the left end by a transfer matrix (Type 3) in the equation:—

$$
\begin{bmatrix} -y \\ \vartheta \\ M \\ V \end{bmatrix}_R =
\begin{bmatrix}
1 & \ell & 0 & \dfrac{-\ell^3}{12\,E\,J} \\
0 & 1 & 0 & 0 \\
0 & 0 & 1 & \ell \\
0 & 0 & 0 & 1
\end{bmatrix}
\begin{bmatrix} -y \\ \vartheta \\ M \\ V \end{bmatrix}_L
$$

A4.4 Transfer Matrix Type 4

The aluminium plates forming the ends of the major portion of the casing were originally treated as disc—type masses and the Type 1 matrix was used to represent the change in conditions across the plates. Later it was realised that appreciable distortion of the plates occurred as shown in the figure:—
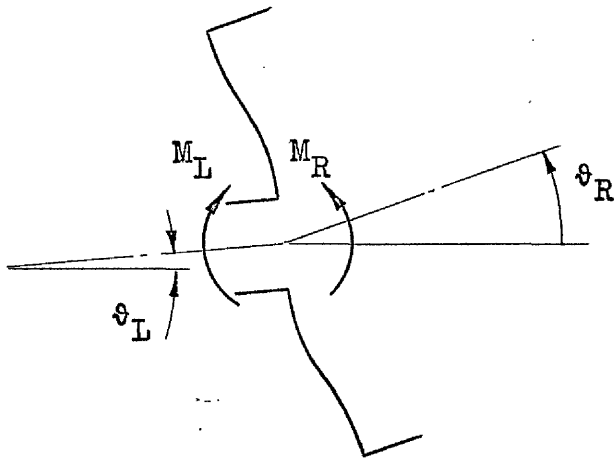
The distortion resulted in a change of slope across the plate which was proportional to the bending moment, and therefore called ϑ_m in the text. The resulting transfer matrix (Type 4) produced the relation between conditions either side of the plates as:—

$$
\begin{bmatrix} -y \\ \vartheta \\ M \\ V \end{bmatrix}_R
=
\begin{bmatrix}
1 & 0 & 0 & 0 \\
0 & 1 & \vartheta_m & 0 \\
0 & -A\lambda^2 & 1 & 0 \\
m\lambda^2 - k & 0 & 0 & 1
\end{bmatrix}
\begin{bmatrix} -y \\ \vartheta \\ M \\ V \end{bmatrix}_L
$$

CHAPTER 5

INVESTIGATION OF THE

WHIRLING BEHAVIOUR OF THE L.P. ROTOR

SUMMARY

Experimental work began with an evaluation of the ability of the transfer matrix method to predict the whirling speeds of the L.P. rotor. The tests showed that satisfactory accuracy was obtained even when the bearing support stiffnesses were varied over a wide range.

The behaviour of the rotor in the vicinity of the forward whirling speed appeared to be influenced by non-linearity of the system. Bearing clearance is shown to be a possible cause of non-linearity.

The whirling motion of the rotor in the vicinity of the reverse whirl was found to be unusual. Tests showed that the amplitude of the reverse whirl was not affected by unbalance of the disc. It is suggested that resonance at the reverse whirling speed is caused by non-circularity of the journals. A theoretical treatment of this aspect is presented in support of this suggestion.

CHAPTER 5

INVESTIGATION OF THE

WHIRLING BEHAVIOUR OF THE L.P. ROTOR

5.1   Introduction to L.P. Rotor Tests

Whenever a lumped—mass technique is used in vibration analysis, the number of sections used in the mathematical model has to be limited to economise on computation.   But the accuracy of the simulations deteriorates if this process is carried too far.   An evaluation of this effect was necessary at an early stage of the work before embarking on the planning of the computer model of the complete rig.

Difficulties can arise in the application of the transfer matrix method whenever the stiffnesses of the supports of the structure become large (Ref.19).   Since the stiffnesses of the bearing supports of the rig were to be an important feature, it was necessary to determine whether these would lead to mathematical difficulties.

Normally only the bending stiffness of a beam—type structure is used in vibration analysis.   But an additional degree of flexibility is always present due to shear deformation.   Whether it was necessary for this effect to be included in the analysis had to be decided.

To resolve these questions before commencing the manufacture of the complete rig, tests were conducted using the L.P. rotor mounted in temporary bearing supports. The bearing housings were outrigged on four 0.212 in diameter spring steel rods, the length of these being adjustable to achieve a reasonable variation in lateral stiffness (Fig.5.1).

5.2   Determination of Bearing Support Stiffness

A loading gauge was designed for the measurement of the lateral stiffness of the bearing supports.   The gauge is shown in Fig.5.2, where it is being used to determine the lateral stiffness of the rear bearing support.   The gauge was calibrated by using it to apply a vertical load to the platform of a laboratory weighing machine.   The tests showed that the flexibility of the gauge was constant, with a value of 0.004 in/lbf, up to its maximum design load of 30 lbf.   At any load the deflection of the gauge, measured by a $2 - 2\frac{1}{2}$ in internal micrometer, was reproducible within $\pm$ 0.0002 in, suggesting that its accuracy was better than $\pm$ 0.3^{o}/o.

The stiffness of the bearing supports was determined by measuring the movement of the bearing housing with a dial micrometer (reading to 0.0001 in) when loads, up to a maximum of 30 lbf, were applied by the loading gauge. (The Wayne-Kerr equipment was also used to determine the deflection of the bearing housing.   Although the most sensitive probe, with a maximum range of 0.010 in, was used, the discrimination of the meter was not better than that of the dial micrometer, nor were the results as reproducible).

The overall accuracy of the stiffness of the bearing support was therefore limited by the discrimination of the dial micrometer.   At a relatively large support stiffness of 16000 lbf/in (producing a deflection of .002 in at the maximum load of 30 lbf), a discrimination of $\pm$ .0001 in on the dial micrometer implied an accuracy of only $\pm$ 5°/o in the determination of the stiffness.   The accuracy was of course improved to a degree by smoothing the results of the loading tests.   When the stiffness of the bearing support was reduced to a relatively low value

of 1600 lbf/in, the deflections obtained were so large
that they could be measured with an accuracy of $\pm$ 0.5%.
Therefore, except at very high values the accuracy of
the determination of the bearing support stiffness was
considered to be of the order of $\pm$ 1%.

5.3   Variation of Whirling Speeds with
       Rear Bearing Stiffness

The forward and reverse whirling speeds of the
rotor were determined with the front bearing rigidly
mounted while the stiffness of the rear bearing support
was varied.   The balance of the disc was adjusted so
that at the forward whirling speed a disc orbit of
approximately 0.020 in radius (determined by the Wayne-
Kerr probes) would be obtained.

The damping of the system was so small (a damping
factor of approximately 0.0007 was inferred) that
significant deflection of the disc occurred over a range
of only 20 rpm.   The true whirling speed was judged to
be that at which a 90° phase shift was indicated by the
oscilloscope display of the disc orbit.

The results of these tests are listed in Table 5.1
and are shown plotted in Fig.5.3 for comparison with the
computer predictions obtained from an 8-section
representation of the rotor.   The experimental results
appear to agree with the computer predictions within
$\pm$ 2%.   However, the results do suggest that the forward
and reverse speeds converge more rapidly than the computer
predicted.   (The forward and reverse whirls could not be
separated when the rear bearing stiffness was set at
2500 lbf/in).   This effect may be an indication that the
influence of the bearing clearance becomes significant
with very flexible bearing supports.   Although the
vertical and horizontal stiffnesses of the bearing
supports were found to be identical within experimental
limits, the stiffness in the horizontal direction, as seen

by the shaft, is reduced by the bearing clearance.
(The journal of the shaft may be considered to be rolling
within a cylinder of a diameter larger than the journal
by an amount equal to the clearance).

The computer model, using only 8 sections, had
predicted a forward whirling speed of 2472 rpm.   When it
was altered to represent the rotor divided into 38 sections,
the rigid critical speed was found to be 2437 rpm — a
reduction of 1.4°/o — suggesting that a division of the
rotor into rather more than 8 sections would be advisable
in later work.

When the 38-section computer model was modified to
allow for shear deformation, the critical speed was
reduced slightly to 2434 rpm showing that it would not be
essential to include the shear deformation effect in future
calculations.

5.4   Variation of Whirling Speeds with Front Bearing Stiffness

Further tests were carried out on the L.P. rotor to
determine the accuracy of the computer model when the
stiffness of the front bearing support was varied.   The
results obtained are shown in Table 5.2.   The forward and
reverse whirling speeds are shown plotted on the computer
predictions in Figs.5.4 and 5.5.   The agreement was again
within ± 2°/o, which was considered satisfactory.

5.5   Experimental Traverse through Forward Whirl

Although the transition through the forward whirl
occurred within a speed range of only 30 rpm (1.5°/o of
the mean speed), attempts were made to observe the
behaviour of the L.P. rotor at several speeds in this
range.

These tests were carried out with the front bearing
mounted rigidly while the rear bearing support had a

stiffness of 16000 lbf/in. The results at small speed intervals through the whirling range are shown plotted in Fig.5.6.

When the radius of the disc orbit exceeded 0.006 in, the rear roller bearing began to rattle. The subsequent increase in radius with rotor speed did not resemble the resonance curve that would be exhibited by a linear system. Furthermore, at a rotor speed of 2169 rpm the disc orbit collapsed suddenly from a radius of 0.033 in to 0.005 in. When the speed was then lowered gradually the radius of the orbit remained virtually constant at 0.005 in down to a speed of 2150 rpm. Unfortunately, the test was terminated at this speed.

A subsequent examination of the rear roller bearing showed that the inner track, which was intended to be a press fit on the shaft, was loose. The fault was corrected by cementing the track to the shaft with Araldite.

The results of a subsequent traverse through the whirling range are shown plotted in Fig.5.7. Again the rear bearing rattled as soon as the disc orbit exceeded 0.006 in. The variation of radius of the disc orbit as the speed increased was almost identical to that observed in the earlier test. The orbit collapsed suddenly at 2175 rpm and reverted to the relatively low radius of 0.005 in. As the speed was lowered the radius remained almost constant, though unsteady, until, at a speed of 2157 rpm, it suddenly 'jumped' to rejoin the rising speed line. Further reduction of speed showed that the orbit radius remained at a relatively large value down to a speed of 2130 rpm. Unfortunately, the test was terminated at this speed but it is thought that if it had continued a second jump to a lower radius would have occurred at a speed just below 2130 rpm.

The strange behaviour of the rotor when passing through the whirling range which was not affected by the fit of the inner track of the bearing was thought to be attributable to some non-linearity within the system. When a vibrating system contains a restoring mechanism which is non-linear, such as the stiffening spring characteristic shown in Fig.5.8(a), the amplitude versus frequency characteristic leans to the right, as shown in Fig.5.8(b). (When the spring stiffness falls as the deflection increases, the characteristic leans to the left). At two points on the characteristic 'jumps' occur depending on whether the frequency is rising or falling, as indicated by the dashed lines in Fig.5.8(b), (Ref.20).

Since the response of the L.P. rotor resembled that of a non-linear system a search was conducted to detect the cause of the possible non-linearity.

A test carried out to check the stiffness of the rear bearing support confirmed that this was constant, at least over the normal range of deflections.

Yamamoto (Ref.21) had reported that a single row ball bearing, which had no self-aligning housing, exhibited a moment versus angular deflection characteristic, Fig.5.8(c) and (d), which steepened rapidly when the shaft deflection exceeded about 0.5^{o}. A test was conducted on the L.P. rotor to establish whether a similar effect would be exhibited by the rear roller bearing. A lateral load was applied to the shaft, adjacent to the disc, and the resulting deflection of the disc noted. The test failed to reveal a non-linearity, although the imposed deflection of the shaft far exceeded that observed in running tests. Presumably the angular deflection of the shaft at the rear roller bearing was too small to exhibit the non-linearity which Yamamoto reported.

The noticeable rattle from the rear bearing whenever the radius of the disc orbit exceeded 0.006 in seemed significant. The radial acceleration of the disc under these conditions would be at least

$$r\,\omega^2 \;=\; \frac{0.006}{12}\;\left(\frac{2\pi}{60}\;2144\right)^2 \;=\; 25\ \text{ft/sec}^2$$

and if the radius had been almost 0.008 in, the acceleration would have exceeded that due to gravity. Thus it seemed almost certain that, whereas at lower amplitudes the shaft would revolve while resting at the bottom of the bearing clearance (Fig.5.8(e)), at larger radii the radial acceleration of the disc would exceed gravity and the shaft would cross the clearance (actually roll around the circumference of the bearing). Considering only the vertical stiffness of the support of the shaft under these conditions, its characteristic would then be expected to exhibit 'back lash' as shown in Fig.5.8(f). This effect was thought to be the source of the suspected non-linearity.

In section 5.1 it was noted that the whirling speeds were judged to be those at which a phase lag of 90° was reached. The variation of phase angle with speed shown in Figs.5.6 and 5.7 suggests that when the speed is increasing the phase change through 90° is delayed. This effect would be expected to occur in a non-linear system with a hardening spring characteristic. As a result the experimental whirling speeds may be perhaps 1°/o higher than they would have been had the bearing had no clearance. (The experimental forward whirling speed when both bearings were rigidly supported was 2475 rpm. The computer model predicted 2472 rpm, when 8 sections were used, and 2437 rpm when 38 sections were used).

Some time after these results had been obtained
the writer received some information from Mr. H. Black
of Heriot-Watt University, describing the work he was
conducting on the problem of the stable operation of
centrifugal pump rotors (Ref.22).   The model he examined
consisted of a uniform shaft, mounted in rigidly mounted
ball bearings, carrying a mass at its mid-span.   A spring
supported bush was mounted adjacent to the mass with a
radial clearance between it and the shaft of 0.020 in
(Fig.5.9(a)).   The response which he observed is shown
in Fig.5.9(b).   Normal whirling resonance was followed by
an increasing amplitude up to approximately 3 times the
whirling speed.   The theoretical treatment Black used to
explain the behaviour included the non-linear restraint
imposed by the bush, (Fig.5.9(c)), produced amplitude and
phase angle variations, (Fig.5.9(d)), which resembled the
observed behaviour of his model.

The striking resemblance between the amplitude and
phase angle variation of Black's model and those of the
L.P. rotor, supports the contention that the observed
behaviour is due to non-linearity of the rotor support.

5.6   Transition through the Whirling Speeds

Sketches of typical oscilloscope displays of the
orbit of the centre of the disc at different speeds in the
neighbourhood of the reverse and forward whirling speeds
are shown in Fig.5.10.   The sketches show the change in
size of the orbit and also the apparent phase change.

The orbit displayed when the speed was well below
the reverse whirling speed is shown in (1).   Since the
disc was rotating clockwise, the kicks produced by the foil
marker on the periphery of the disc indicate that the disc
is precessing in the direction of rotation and that the
unbalance lies along the 12 o'clock radius of the disc.

Sketches (2), (3) and (4) show that as the speed increases the orbit grows and becomes elliptical, which soon closes into a straight line, and then returns to an elliptical form, but with reverse precession.

At stage (5) the orbit has reached its maximum and the kicks have shifted 90° around the orbit. This was judged to be the reverse whirling speed. The disc reaches its highest point when the foil marker passes the horizontal probe, producing the horizontal kick on the display. The deflection of the disc centre from the bearing axis is therefore along the 9 o'clock radius. Since the whirling motion is of reverse precession the motion has apparently a phase lag with reference to the whirl and therefore the kicks on the oscilloscope display must shift clockwise, -i.e. in the same direction as the rotation.

As the speed is increased the elliptical orbit continues to tilt, eventually becoming a straight line, then again elliptical with now almost a 180° phase change, (stages (6), (7) and (8)). At stage (9) the orbit is again circular with clockwise precession, and as a result of the transition through the straight line of stage (7), it has, at (9), regained an orbit almost identical to the initial orbit at stage (1).

With further increase of speed the orbit is circular, and as it grows it lags the precession (and of course the rotation). At (11) the orbit reaches a maximum and the speed is judged to be the forward whirling speed. The display at stage (11) shows that the disc reaches its highest point when the horizontal kick is produced. Once again this indicates that the displacement of the disc centre is along the 9 o'clock radius. But since the whirling motion has positive precession this result is to be expected — the maximum displacement lags the excitation (the unbalance) by 90°.

Further increase of speed, stages (12) and (13) show the collapse of the orbit with further phase change until at stage (13) the orbit is similar to that at stage (1), with a phase lag of 180°. The disc is now whirling with the centre of mass adopting a position between the bearing axis and the geometric centre of the disc.

5.7   Effect of Unbalance on Reverse Whirl

Theoretical analysis, outlined in section 1.3, showed that whereas the gyroscopic action of the disc produces a natural frequency at which the centre of the disc precesses in a sense opposite to the rotation, resonance could not be expected to be caused at this frequency by unbalance.

When the rear bearing was mounted with a stiffness of 11250 lbf/in the mean radius of the disc orbit, at the reverse whirling speed of 1868 rpm, was found to be 0.005 in when the disc was well balanced. When the disc was unbalanced by adding screws of up to 2.22 g mass at the 12 o'clock position (equivalent to moving the centre of mass of the disc up to 0.00083 in), no increase in the radius of the orbit at the reverse whirling speed was found. On the other hand an unbalance produced by a mass of only 0.37 g increased the radius of the forward whirl orbit from 0.002 in to 0.032 in.

The effect of the position of the unbalance on the reverse whirl was tested by fitting a balancing screw of 0.37 g to each of the four balancing positions in turn. In each case the effect on the mean radius of the reverse whirl orbit was negligible.

The alignment of the shaft drive was altered in an attempt to discover the source of the excitation of reverse whirl but again no change was produced.

5.8 Excitation of Reverse Whirl

In Chapter 1 it was noted that resonance at the reverse whirling speed of symmetrical rotor systems has frequently been recorded in the literature but no explanation of its cause has been given. The writer believes that the cause is due to non-circularity of the journals of the shaft. Although no tests have been conducted to test the hypothesis, a theoretical treatment leads to plausible results which explain the curious behaviour of the phase of the reverse whirl shown in Fig.5.10.

Before dealing with the theoretical explanation of reverse whirl it seems reasonable to consider the explanation of forward whirl when some external damping is present.

The equations governing the motion of an unbalanced shaft/disc system, as developed in section 1.3, with a term $\delta\dot{z}$ to include external damping acting on the disc, are:—

$$m\ddot{z} + dz + \delta\dot{z} + e\varphi = ma\omega^2 e^{i\omega t}$$

$$A\ddot{\varphi} - iC\omega\dot{\varphi} + ez + f\varphi = 0$$

Assuming the motion of the geometric centre of the disc to be

$$z = Z e^{i\omega t} \quad , \quad \varphi = \Phi e^{i\omega t}$$

the solution becomes

$$Z = \frac{ma\omega^2 (A\omega^2 + f)}{D}$$

where the denominator, D, is the determinant:—

$$\begin{vmatrix} d - m\omega^2 + i\delta\omega & e \\ & \\ e & -A\omega^2 + C\omega^2 + f \end{vmatrix}$$

which is complex since it contains the imaginary component

$$i \, \delta \, \omega \, (A\omega^2 + f)$$

if we put C = 2A for a thin disc.

Multiplying the top and bottom of the expression for Z by D', the conjugate of D, gives

$$Z = \frac{ma\omega^2 \, (A\omega^2 + f) \, . \, D'}{D.D'}$$

where the denominator D.D' is a real number.

Since D' contains the term $- i \, \delta \, \omega \, (A\omega^2 + f)$, the value of Z is complex since the numerator contains the term:—

$$ma\omega^2 \, (A\omega^2 + f)^2 \, . - i \, \delta \, \omega$$

which is negative. Therefore Z is of the form $R \, e^{-i\psi}$ in which R is real. The movement of the centre of the disc is therefore

$$z = R \, e^{i(\omega t - \psi)}$$

The direction of the displacement of the disc, OC in Fig.5.11, therefore lags the direction of the unbalance, vector CG, by an angle ψ.

Now the denominator of Z, D.D', will only become small (and therefore resonance occur) when the value of ω approaches the forward whirling speed. (In section 1.3, where damping was not considered, the denominator was shown to become zero, and therefore resonance occurred, at the forward whirling speed). Therefore, there is no theoretical reason for resonance being induced at the reverse whirling speed due to unbalance.

Now suppose that one journal is not truly circular and as a result the centreline of the shaft, at the bearing, when viewed from the end, will appear to move in a closed path, which will not be circular. The shaft/disc system will then be subjected to displacement excitation. The simplest form of this which can be assumed will be elliptical so that the displacement of the centreline at the journal will be, say,

$$x' = a \cos \omega t \quad , \quad y' = b \sin \omega t$$

or
$$z' = a \cos \omega t + ib \sin \omega t$$

Putting $\quad a = A' + B' \quad$ and $\quad b = A' - B'$

gives
$$z' = A' e^{i\omega t} + B' e^{-i\omega t}$$

The component $B e^{-i\omega t}$ thus provides an excitation which has the sense which is capable of exciting resonance at the reverse whirling speed. Its magnitude $B' = \dfrac{a - b}{2}$, which is half the vertical motion of the shaft due to non-circularity of the journal would be difficult to establish. But in section 5.6 it was noted that eccentricity of the disc of only 0.0001 in was capable of producing strong resonance at the forward whirling speed. It therefore seems feasible that non-circularity of the journal of less than 0.0001 in (which seems possible) would produce noticeable resonance at the reverse whirling speed.

The reverse precession component $B' e^{-i\omega t}$ of the centreline of the journal, modified by the characteristics of the shaft between the journal and the disc, will therefore lead to equations of the disc motion of the form:—

$$m\ddot{z} + dz + i\delta\dot{z} + e\varphi = kB' . e^{-i\omega t}$$

$$A\ddot{\varphi} - iC\omega\dot{\varphi} + ez + f\varphi = 0$$

where k is the force required to produce unit lateral deflection of the journal with respect to the disc.

Assuming the motion to be

$$z = Z e^{-i\omega t} \quad , \quad \varphi = \Phi e^{-i\omega t}$$

and solving for Z gives

$$Z = kB' \cdot \frac{(-3A\omega^2 + f)}{D}$$

in which, again, C has been replaced by 2A, and D is now the determinant:—

$$\begin{vmatrix} d - m\omega^2 - i\delta\omega & e \\ \\ e & -3A\omega^2 + f \end{vmatrix}$$

As before, Z may be rewritten

$$Z = \frac{kB' \ (-3A\omega^2 + f) \cdot D'}{D \cdot D'}$$

where now the denominator, $D.D'$, will become small, and therefore resonance will occur, when the reverse whirling speed is approached.

The expression for Z is again complex since it contains the imaginary term:—

$$kB' \cdot \frac{(-3A\omega^2 + f)^2 \cdot i\delta\omega}{D.D'}$$

which is now positive. Therefore Z is of the form:—

$$Z = R e^{i\psi}$$

The motion of the disc centre, caused by the excitation $kB' \cdot e^{-i\omega t}$ is therefore of the form:—

$$z = R e^{-i\omega t + \psi}$$

Since the sign of ψ is now positive, the displacement of the centre of the disc must lag the whirl, which has reverse precession. Therefore, the disc displacement must appear to shift in the direction of the shaft rotation, thus confirming the clockwise shift of the kicks on the oscilloscope display when passing through the reverse whirl.

5.9   Conclusions

The forward whirl had been shown to be affected to a degree by non-linearity possibly introduced by the effect of the bearing clearance. However, the accuracy of the prediction of the speed at which it occurred had been shown to be satisfactory over a wide range of bearing support stiffnesses.

Although the suggested cause of resonance at reverse whirl had not been tested, the speed at which it occurred had again been predicted with satisfactory accuracy.

Table 5.1

TABLE 5.1

Effect of Stiffness of Rear Bearing
Support on Whirling Speeds of L.P. Rotor

(Front bearing mounted rigidly)

Rear Bearing Support		Whirling Speeds	
Stiffness — lbf/in	Flexibility $\times 10^4$ — in/lbf	Reverse — rpm	Forward — rpm
Rigid	0	2005	2475
16000	0.625	1910	2170
11250	0.89	1865	2055
6180	1.62	1773	1888
4890	2.05	1717	1779
3760	2.66	1622	1669
2500	4.0	1461	1461

Table 5.2

TABLE 5.2

Observed L.P. Rotor Whirling Speeds
(Both bearings mounted flexibly)

Rear Bearing Support		Front Bearing Support		Whirling Speeds	
Stiffness — lbf/in	Flexibility x 10^4 — in/lbf	Stiffness — lbf/in	Flexibility x 10^4 — in/lbf	Reverse — rpm	Forward — rpm
19250	0.52	4270	2.34	1868	2144
19250	0.52	1335	7.5	1723	1948
4300	2.32	1335	7.5	1538	1593
4300	2.32	4030	2.48	1600	1678
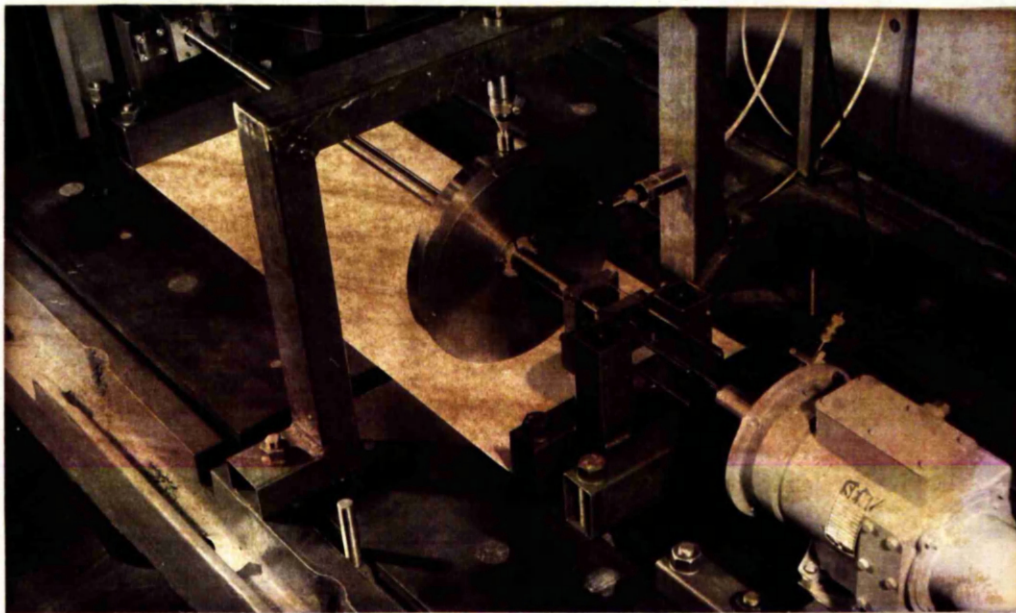
Fig.5.1

Fig.5.1

Fig.5.1   L.P. Rotor mounted in temporary
spring bearing supports

Fig. 5.2

11.5"

2" − 2½" internal
micrometer

1.5" R

1" x ⅛" steel strip

Rig frame

Loading screw
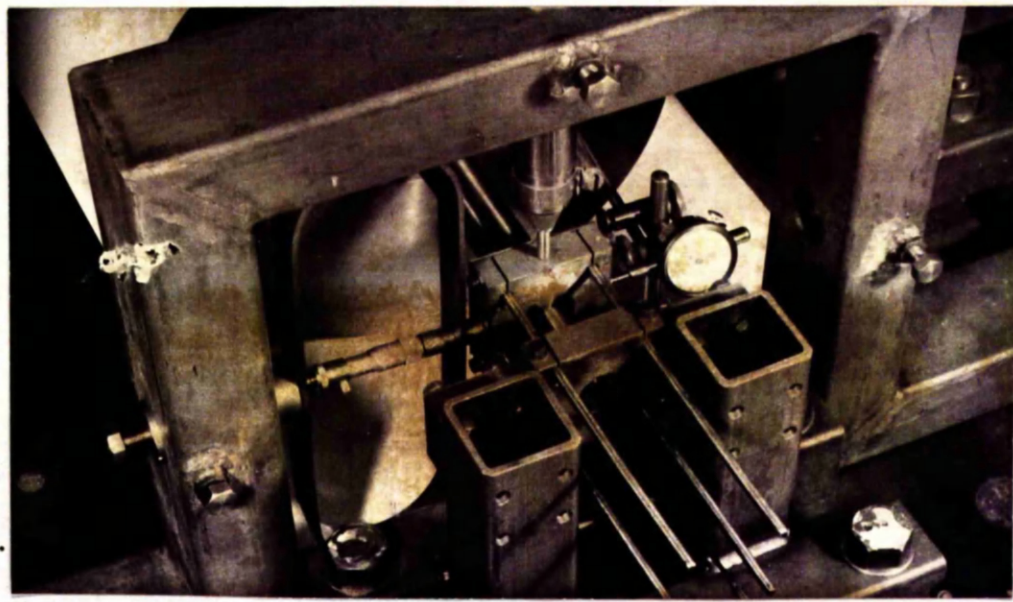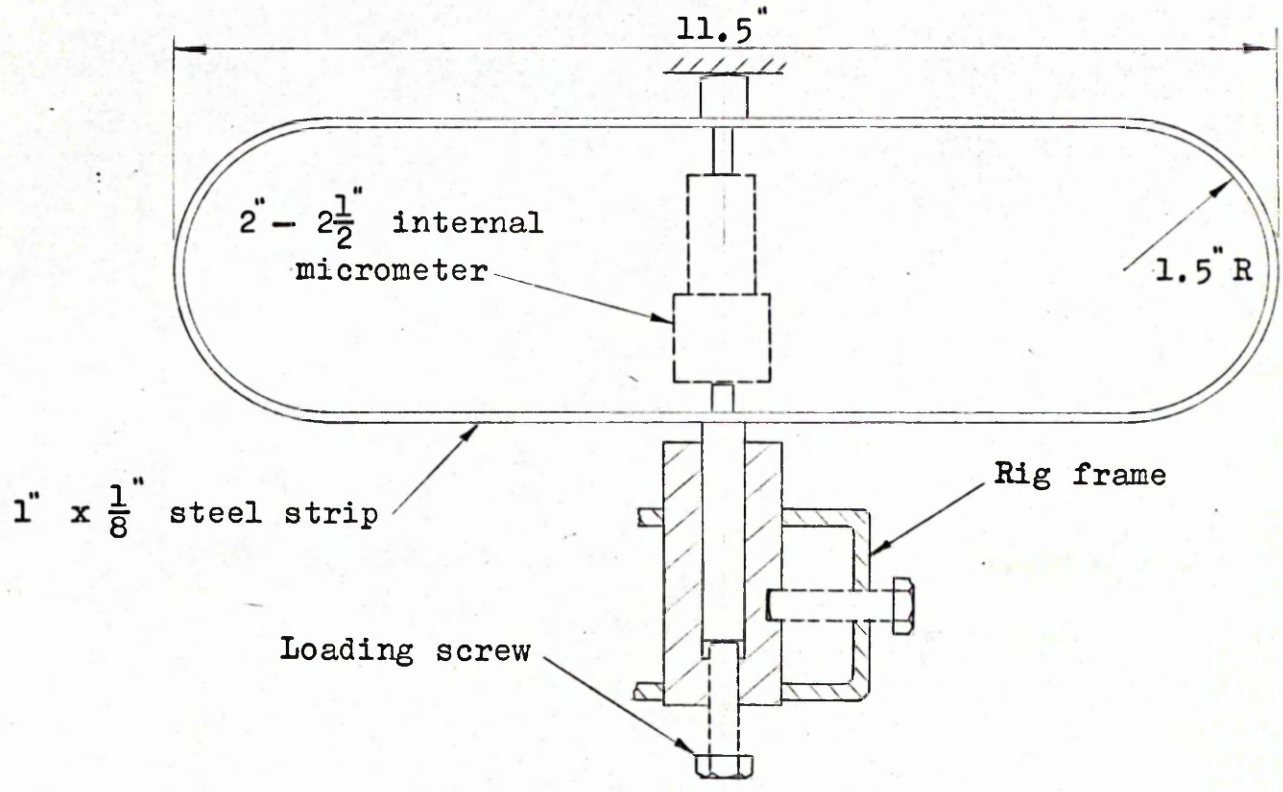
Fig.5.2   The load gauge being used to
determine the stiffness of the
rear bearing support
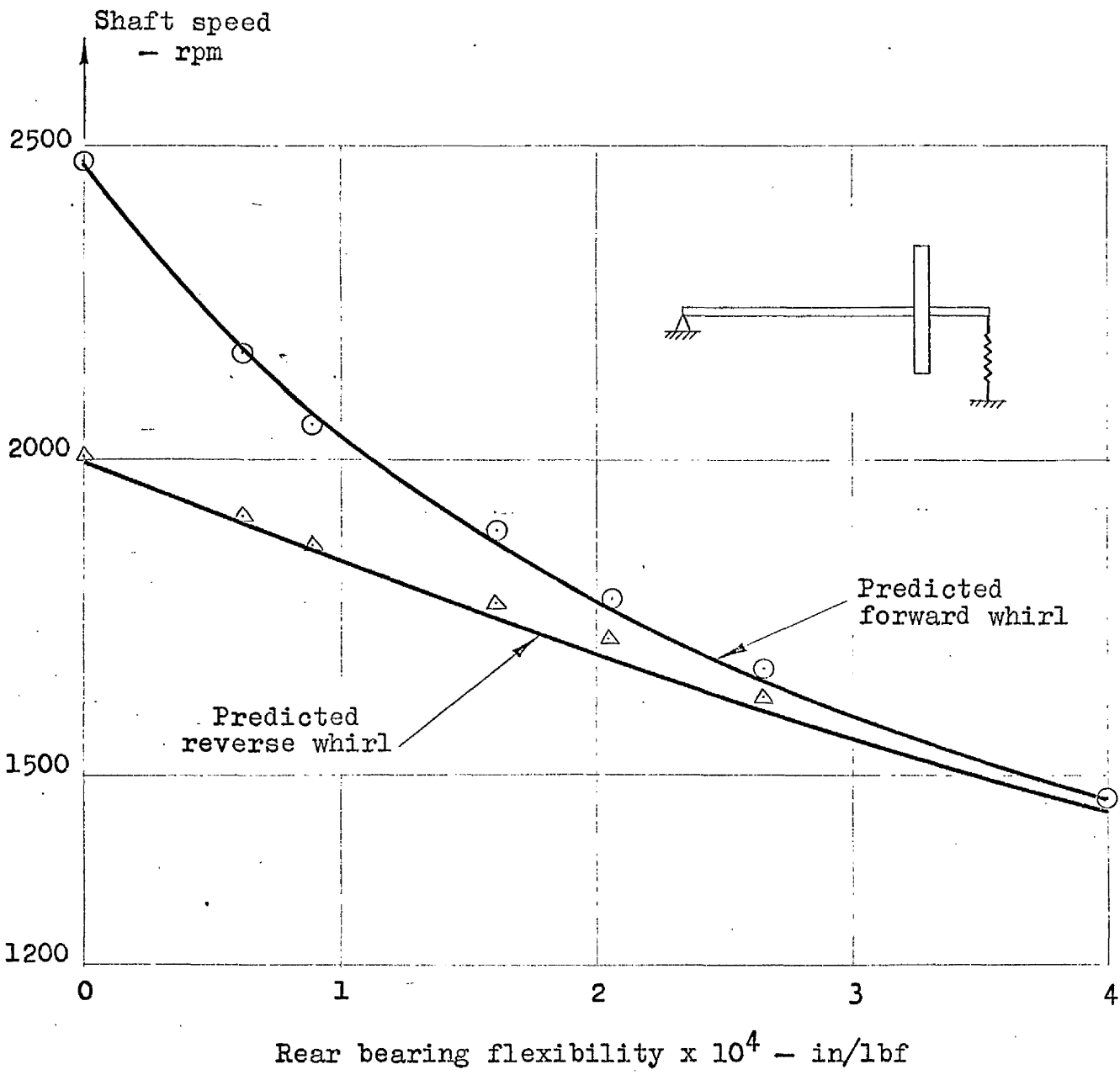
Fig.5.3

Fig.5.3 Comparison of observed and predicted whirling speeds of L.P. rotor with flexible rear bearing support.
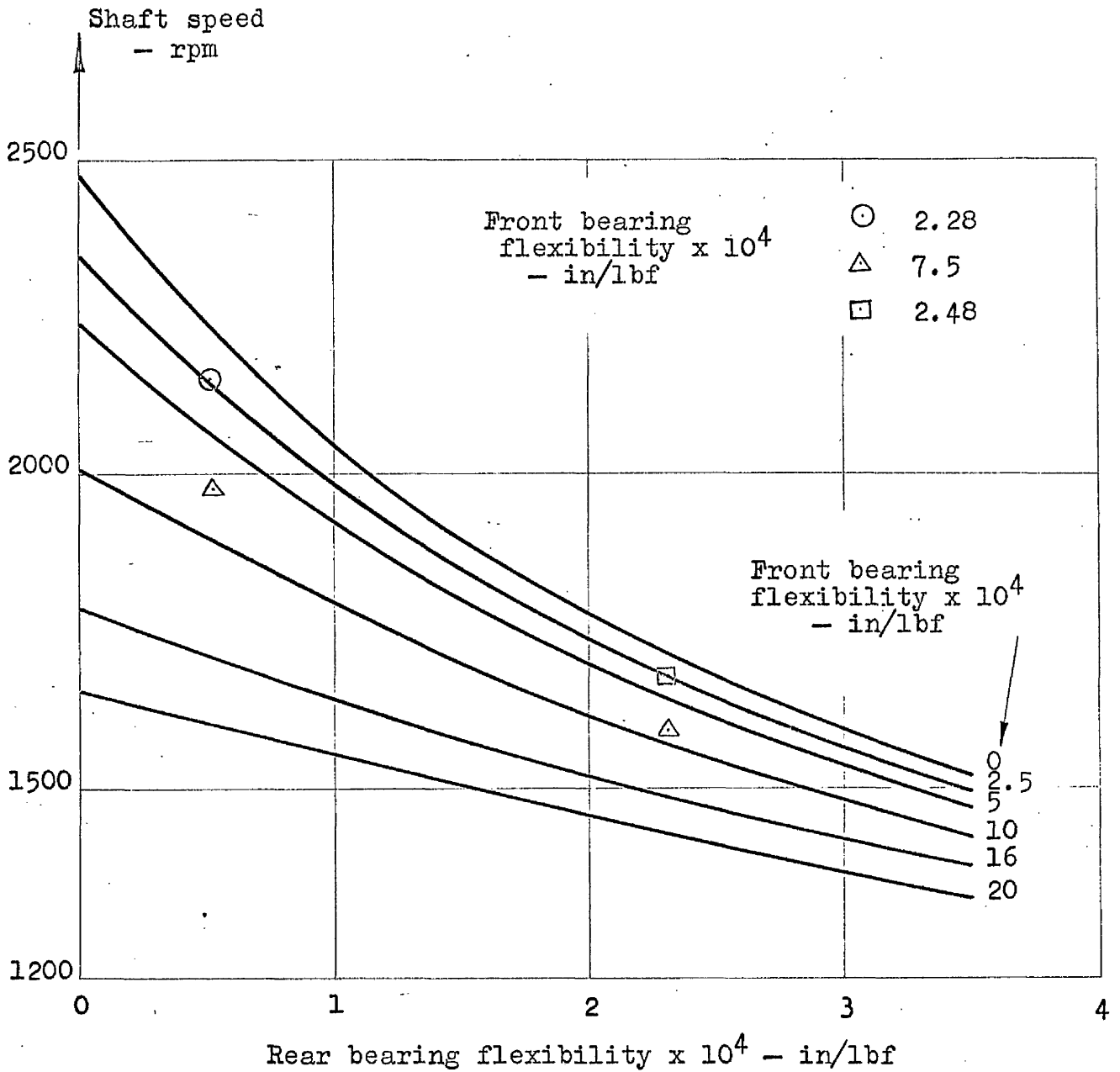
Fig.5.4

Fig.5.4   Comparison of observed and predicted forward
           whirling speed of L.P. rotor with both
           bearings on flexible supports.
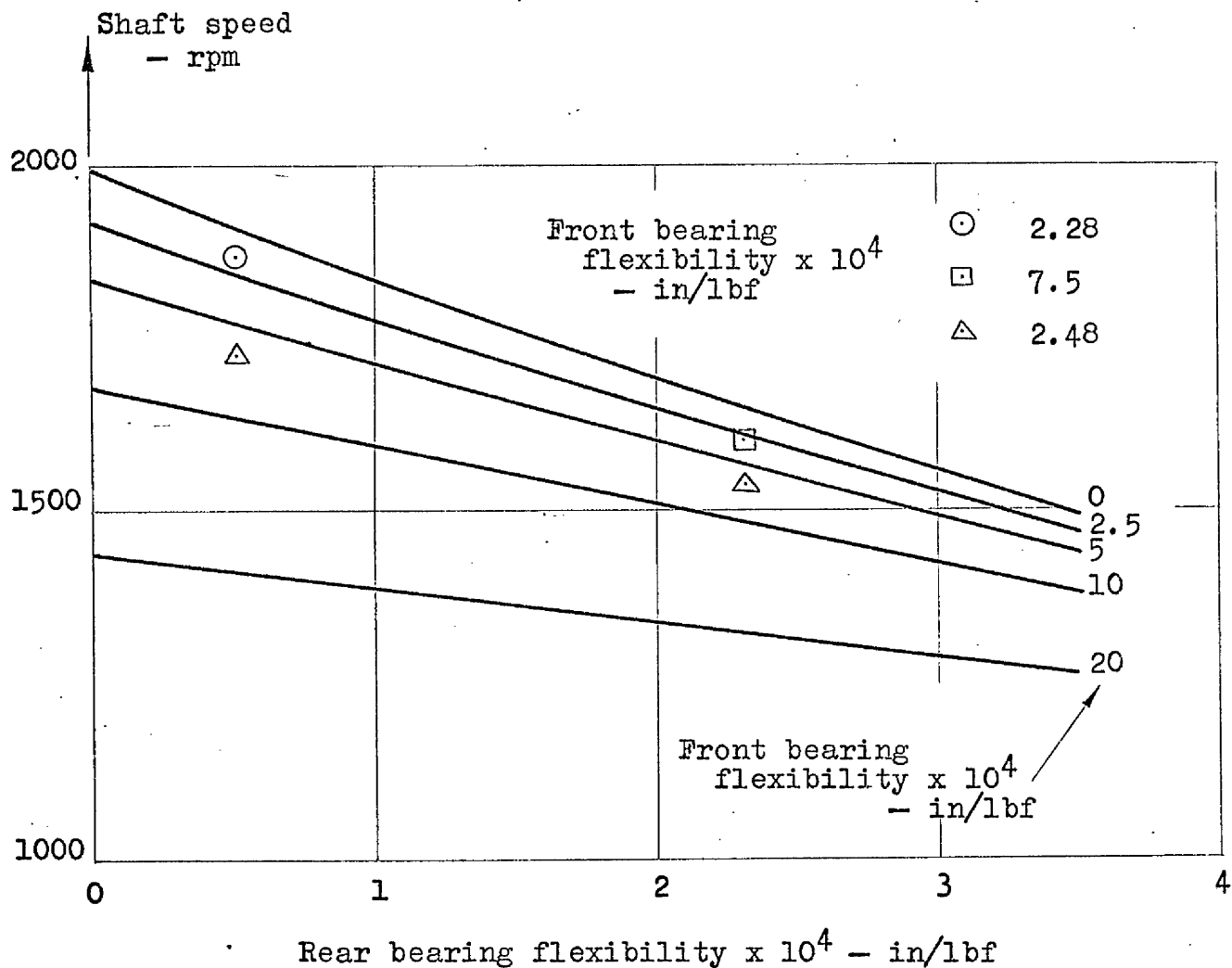
Fig.5.5

Fig.5.5   Comparison of observed and predicted reverse
whirling speed of L.P. rotor with both
bearings on flexible supports.
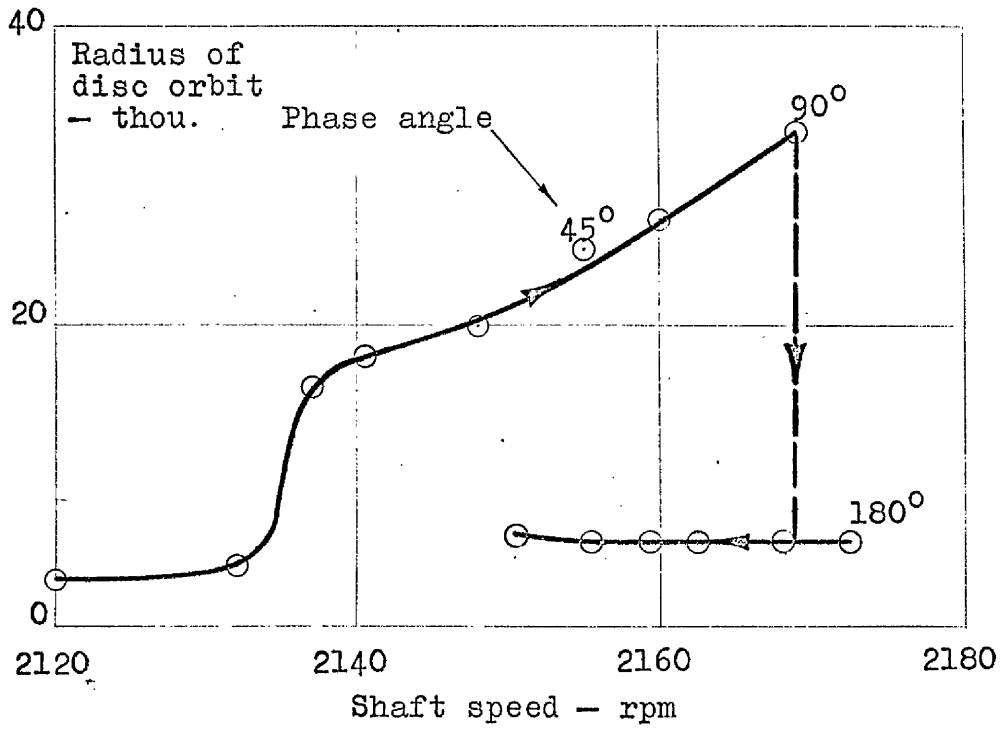
Fig.5.6   Initial traverse through forward
whirl
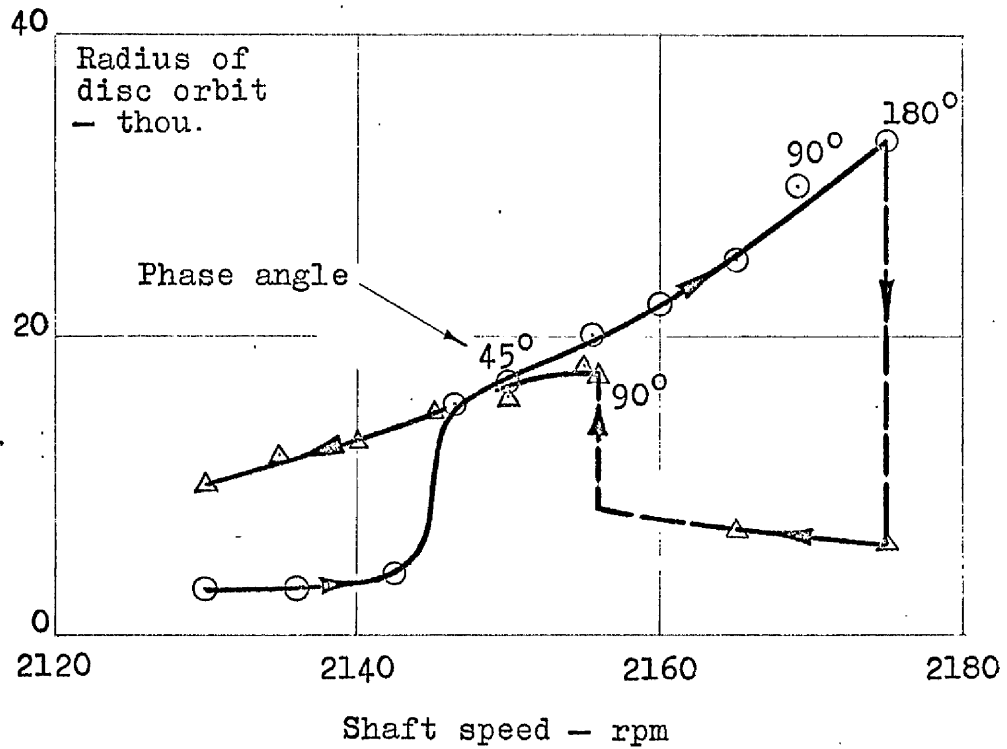
Fig.5.7   Traverse through forward whirl
after repair to rear bearing
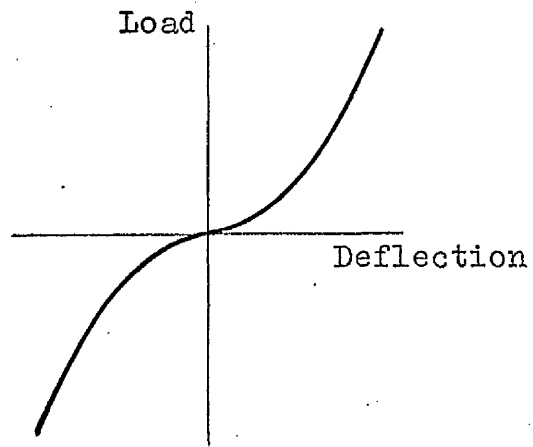
Fig.5.8

(a)
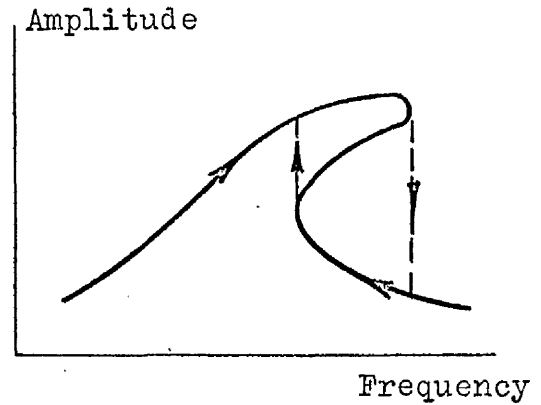
(b)
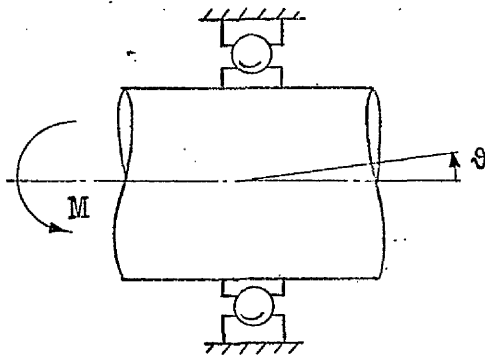
(c)
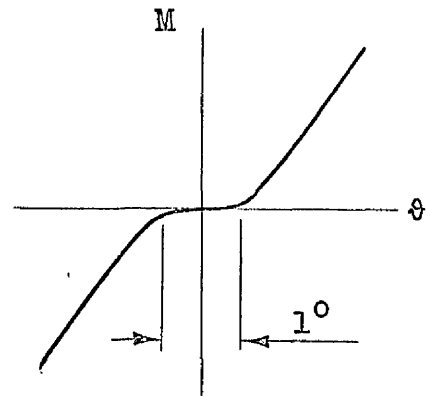
(d)
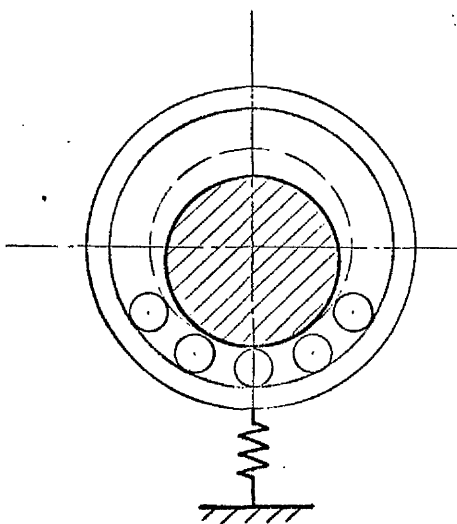
(e)
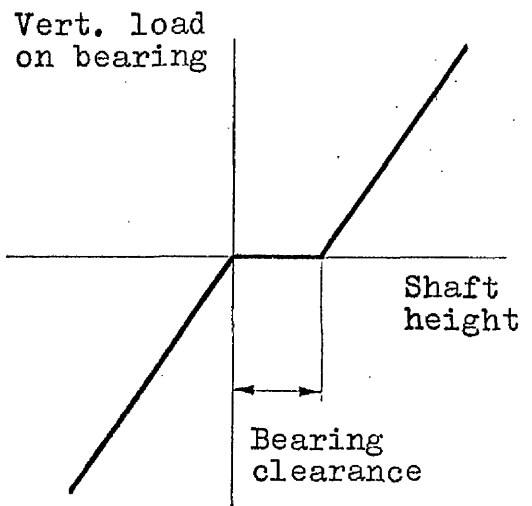
(f)

Fig.5.8   Non-linear characteristics of ball bearings.
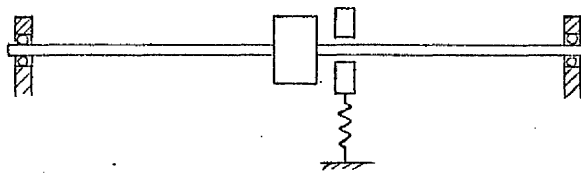
(a)
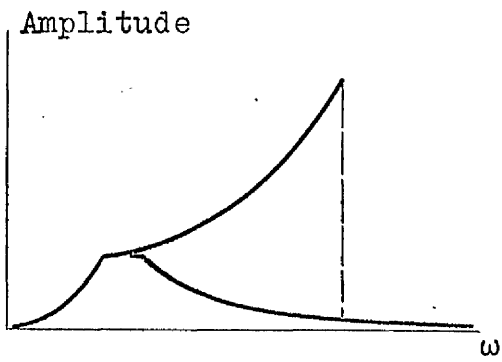
(b)
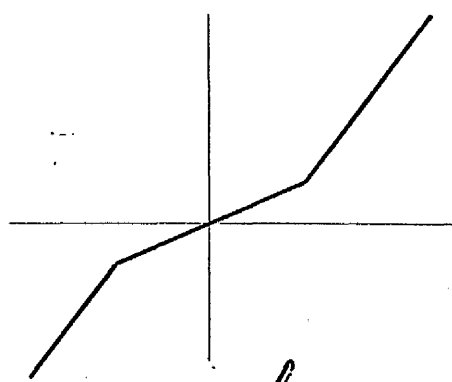
(c)
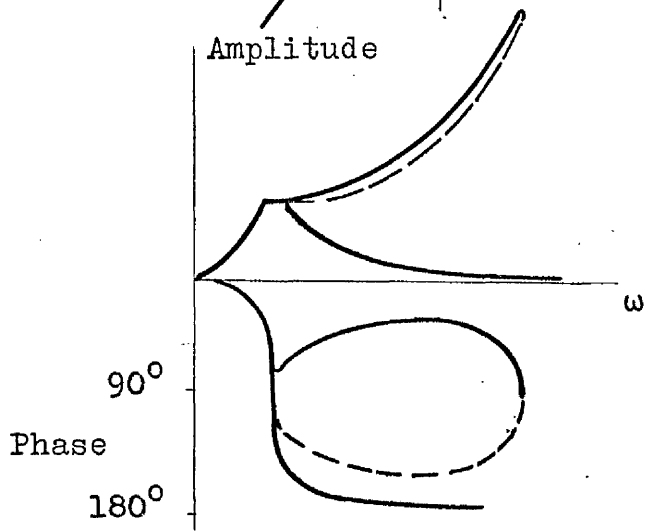
(d)

Fig.5.9   Whirling of a Rotor within a spring
mounted bush.

Foil marker

Disc   Oscilloscope trace

(1)   (2)   (3)   (4)   (5)

(6)   (7)   (8)

(9)   (10)   (11)   (12)   (13)
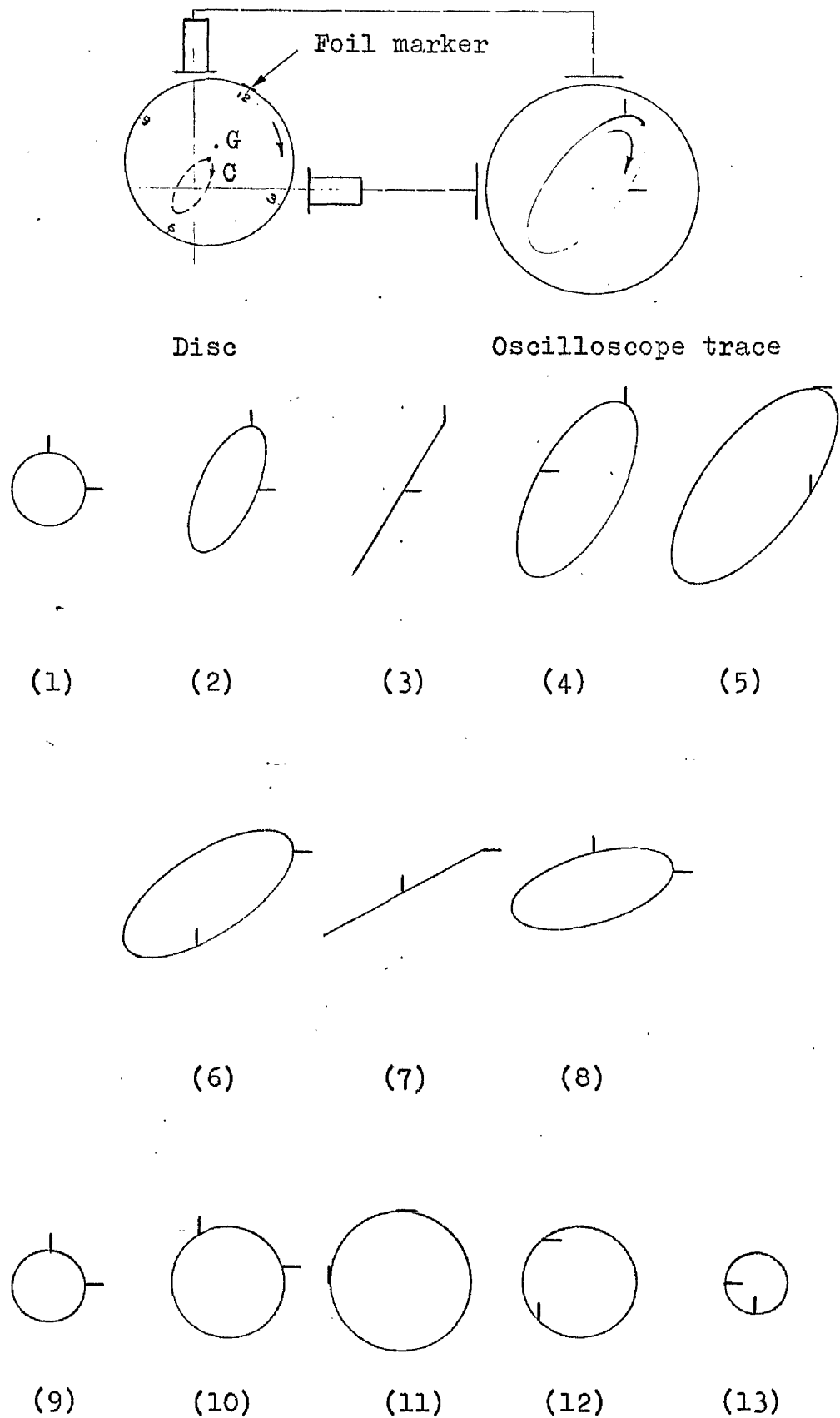
<u>Fig.5.10</u>   Typical oscilloscope traces of path of
disc when rotating at speeds close to the
reverse and forward whirling speeds.
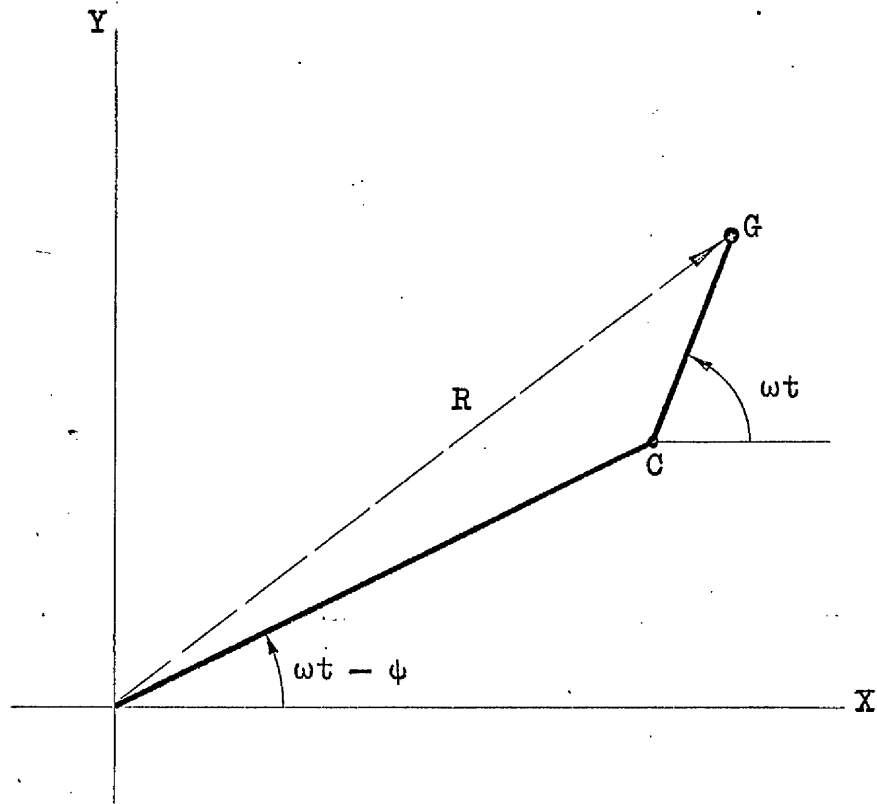
Fig.5.11 Forward whirling of a shaft/disc system.

CHAPTER 6

INVESTIGATION OF THE
VIBRATION BEHAVIOUR OF THE CASING
AND H.P. ROTOR

SUMMARY

The first attempts at prediction of the whirling speeds of the complete rig were unsatisfactory. The vibration behaviour of the casing and H.P. rotor were therefore examined separately in order to isolate the causes of the inaccuracy of the computer model.

The properties of the original design of the casing proved to be too complex. When a more reasonable design was adopted tests showed that the flexibility of the aluminium plates was considerable and its omission was probably the major source of error in the computer model.

A brief examination of the H.P. rotor suggested that the computer representation of its properties was reasonably correct.

CHAPTER 6

INVESTIGATION OF THE
VIBRATION BEHAVIOUR OF THE CASING
AND H.P. ROTOR

6.1   Introduction

When the construction of the whole rig was completed tests were conducted to determine the accuracy of prediction of the whirling speeds.   As described later, in Chapter 7, the results were disappointing.   Further investigation suggested that the computer model of the rig was correct, in principle.   It appeared, therefore, that faults existed in the representation of the properties of the casing and the H.P. rotor, since the representation of the L.P. rotor had been shown to be satisfactory.   Obviously the casing and H.P. rotor would have to be examined separately to reveal any discrepancies.

6.2   Investigation of Properties of the Casing

A computer program was designed to calculate the natural frequencies of lateral vibration of the casing when simply supported at the bearing housings.   The natural frequencies predicted by this program differed widely from those found by lateral excitation of the model.

Since the program was, in principle, identical to that used to predict the whirling speeds of the L.P. rotor it seemed certain that the data representing the elastic and inertial properties of the casing was at fault.

A variety of simple tests were performed on the parts of the casing.   Whereas the stiffness of the front bearing spring rods agreed with the design figure, the rear spring rods were found to be $35^{\circ}/o$ stiffer than intended,

presumably because of the shorter length in relation to the blending section at each end (Fig.2.3).

The stiffness of the cage of eight rods, which formed the major portion of the casing, was checked by clamping the rear plate to the bed plate and applying a lateral load to the front plate as shown in Fig.6.1(a). The stiffness of the cage was found to be about 75°/o of the design figure (which had been used in the computer program).

A further test carried out on a single rod mounted in the rear plate, as shown in Fig.6.1(b), showed that its flexibility was about 20°/o greater than expected. This discrepancy was thought to be caused mainly by the flexibility of the fixing of the rod at the lower end. (The second moment of area of the thread root section of a $\frac{3}{4}$ in B.S.F. rod is only 75°/o of that of the unthreaded rod).

At this stage of the work it was decided that it would be hopeless to attempt an accurate understanding of the properties of the rod cage section. In any case, the construction was not representative of jet engine structures. Instead the section was replaced by a flanged cylindrical steel drum, 0.0625 in thick.

When the computer program had been modified to represent the drum construction, it predicted the lowest lateral frequency to be 73 c/s. A subsequent excitation test on the modified casing showed that the lowest lateral frequency was actually about 50 c/s.

After yet another tedious cross-checking of the computer data, it was concluded that there was still a major source of flexibility which had not been included in the computer model. The computer program was therefore modified to represent the casing mounted on the bearing spring mounts (the flexibility of the bearing springs far

exceeded the flexibility of the rest of the casing) and
to predict the static deflection of the casing when a
lateral load was applied to the front plate (Fig.6.1(c)).
The predicted deflection of the casing under a lateral
load of 80 lbf is plotted in Fig.6.2, line (1).

A loading test conducted to simulate the computer
predictions immediately showed that a major source of
flexibility existed at the front aluminium plate,
Fig.6.2, line (2).

An examination of the flexibility of a disc clamped
at its edge when a moment is applied to a central circular
hole (Ref.23), suggested that the front plate, although
relatively thick, could be expected to have an angular
deflection per unit moment, ϑ_m, of 1.5×10^{-6} rad/lbf in.
The experimental results, line (2), Fig.6.2, indicated a
value of ϑ_m of 0.54×10^{-6} rad/lbf in. The difference was
considered reasonable since the centre portion of the front
plate was obviously stiffened considerably by the mounting
block for the H.P. rear bearing springs.

When the computer program was modified to include
the flexibility, ϑ_m, the resulting deflection curves,
lines (3) and (4) in Fig.6.2, confirmed that it would be
correct to use the experimental value of ϑ_m in the
program.

But the experimental tests had shown that some
flexibility of the supports was evident. Simple loading
tests were carried out to determine the vertical stiffness
of these supports. The stiffnesses proved to be
relatively large and therefore difficult to determine with
any accuracy, but a front support stiffness of 1.2×10^5
lbf/in and a rear stiffness of 1.0×10^5 lbf/in seemed
appropriate values.

The lowest natural frequency of lateral vibration predicted by the computer program containing these stiffnesses was 12.36 c/s compared with the experimental value of 11.42 c/s. The agreement was not particularly good nor were the predicted modes, as indicated in Table 6.1. When various sets of support stiffnesses were inserted in the computer program, it appeared that when both stiffnesses were set at 0.7 x 10^5 lbf/in a fair agreement with the experimental values was obtained.

The values of these stiffnesses, of course, were those which seemed to be appropriate for vibration of the casing in the vertical plane. The corresponding stiffnesses in the horizontal direction could be expected to be different and as a result have some influence on the accuracy of prediction of the whirling speeds of the model.

6.3 Investigation of the Properties of the H.P. Rotor

A satisfactory computer model of the L.P. rotor had been obtained with relatively little difficulty. Since the H.P. rotor had been deliberately designed to be of simple construction it was not expected that an adequate computer representation would be difficult to obtain. Nevertheless, it was considered worthwhile testing the representation of the H.P. rotor before returning to the complete rig.

Ideally the representation should have been tested against the behaviour when the rotor was mounted in bearing supports with readily predictable characteristics. However, it was expedient to mount the rotor in the front half of the casing, with the front plate mounted on the supports built for the rear of the model, as shown in Fig.6.3.

The first computer representation of this arrangement used support stiffnesses of 0.7 x 10^5 lbf/in, i.e. values which had been judged to be appropriate when the casing

was being examined. The predicted lowest frequency of lateral vibration (when the rotor was not rotating) was 1410 c/min, which compared well with the value of 1391 c/min which the system was found to exhibit when it was excited in a vertical direction (Table 6.2).

However, the predicted whirling speeds proved to be widely different to the experimental values. But the tests showed that the forward whirling speed was lower than the lateral frequency when vibrated in the vertical plane!

Careful loading tests carried out on the front and rear bearing spring supports showed that the stiffnesses were symmetrical and within $2^{\circ}/o$ of the design value which had been inserted in the computer program.

Since the supports of the system were very close together and the rotor had a relatively large overhang, the stiffnesses of the supports could be expected to have a profound influence on the whirling speeds. The stiffness of the rear supports, in the vertical direction proved, on examination, to be lower than expected — a value of 0.5×10^5 lbf/in being indicated. The vertical stiffness of the front support was again checked and the results suggested that a stiffness of 0.7×10^5 lbf/in was not inappropriate. (The determination of these stiffnesses with great accuracy was not possible without elaborate test equipment.)

During the tests on the front support it was realised that the considerable side-play at the ball joint of .015 in was likely to have a significant effect on the whirling behaviour of the rotor. It was therefore eliminated by shimming with washers. The whirling speeds exhibited by the rotor after this correction were raised about $7^{\circ}/o$ as a result, with only a small change in vertical lateral frequency (line 2, Table 6.2) and now the forward whirling speed was higher than the lateral frequency.

Although the stiffness tests had been carried out
in the vertical plane the stiffnesses were not determined
in the horizontal direction.   This was not considered a
serious omission since the forward whirling appeared to
occur at only one speed, whereas had the vertical and
lateral stiffnesses been significantly different in the
vertical and horizontal directions, two distinct resonances
would have been expected.

When the new value of the rear support stiffness was
used in the computer representation, the predicted whirling
speeds were found to be only $2^o/o$ higher than the test
values, while the predicted lateral frequency was about
$1.5^o/o$ lower (line 4, Table 6.2).

6.4   Conclusions

The investigation of the characteristics of the
casing and H.P. rotor could have been carried out in a more
elegant manner.   But the object of the work was to develop
a reasonably accurate computer model of the complete rig in
order to investigate the behaviour of a 2-shaft system, and
therefore expediency was the rule throughout this stage of
the work.

During this part of the investigation progress was
often delayed by the development of the computer program,
in particular of the modified transfer matrix method, which
was adopted to obviate numerical difficulties which appeared
possible.

The predictions of the frequencies of the casing and
H.P. rotor had been shown finally to be within $2^o/o$ of the
test values.   This accuracy was considered sufficient to
suggest that a further attempt on the complete model might
be successful.

Table 6.1

TABLE 6.1

Lowest Natural Frequency of Casing
Mounted on Spring Supports

Front Support Stiffness $\times 10^5$ $-$lbf/in	Rear Support Stiffness $\times 10^5$ $-$ lbf/in	Lowest Natural Frequency $-$c/s	$\dfrac{A_f}{A_p}$ *	$\dfrac{A_r}{A_p}$ **
Experimental values		114.2	0.27	0.15
1.2	1.0	123.6	0.21	0.14
1.0	1.0	121.8	0.24	0.13
0.7	0.7	116.0	0.32	0.2
0.6	0.6	112.9	0.36	0.23

* $\dfrac{A_f}{A_p}$ = $\dfrac{\text{Amplitude of Front Support}}{\text{Amplitude of Front Plate}}$

** $\dfrac{A_r}{A_p}$ = $\dfrac{\text{Amplitude of Rear Support}}{\text{Amplitude of Front Plate}}$

Table 6.2

TABLE 6.2

Comparison of Predictions of H.P. Shaft
Frequencies with Model Tests

Configuration	Reverse Whirl — c/min	Lateral Frequency — c/min	Forward Whirl — c/min
Initial model test	1180	1391	1285
Final model test (corrected front support)	1265	1378	1392
Computer prediction (rear support stiffness 0.7 x 10^5 lbf/in)	1337	1410	1483
Computer prediction (rear support stiffness 0.5 x 10^5 lbf/in)	1292	1357	1424
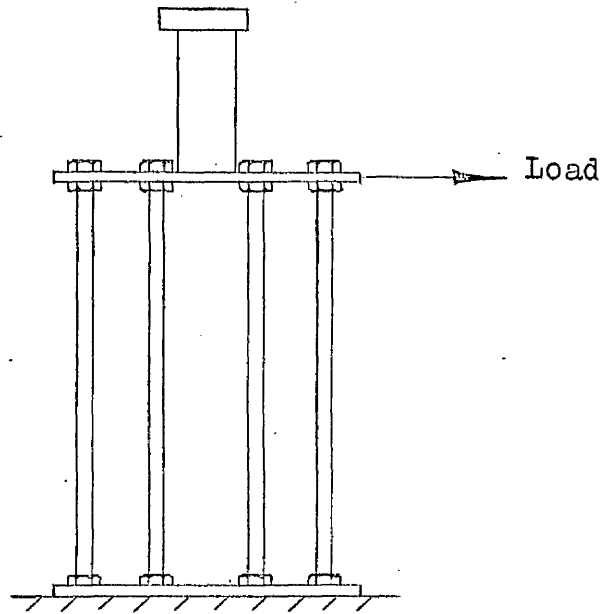
Fig.6.1

(a)
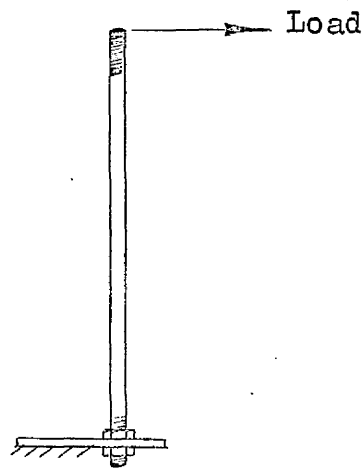
(b)
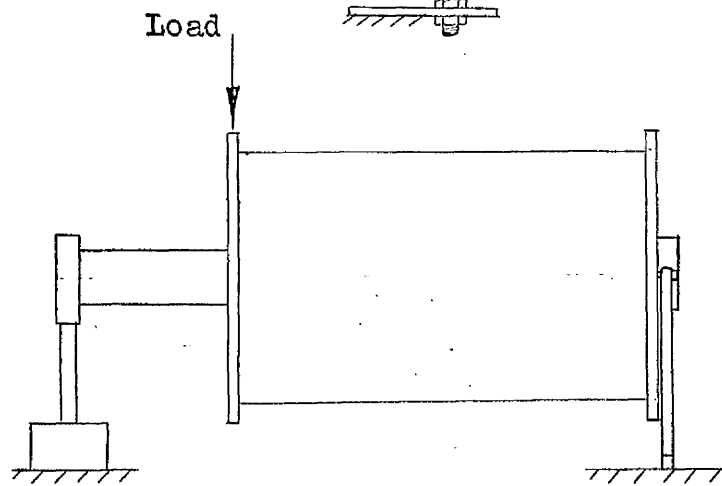
(c)

Fig.6.1   Static load tests carried out
on the casing
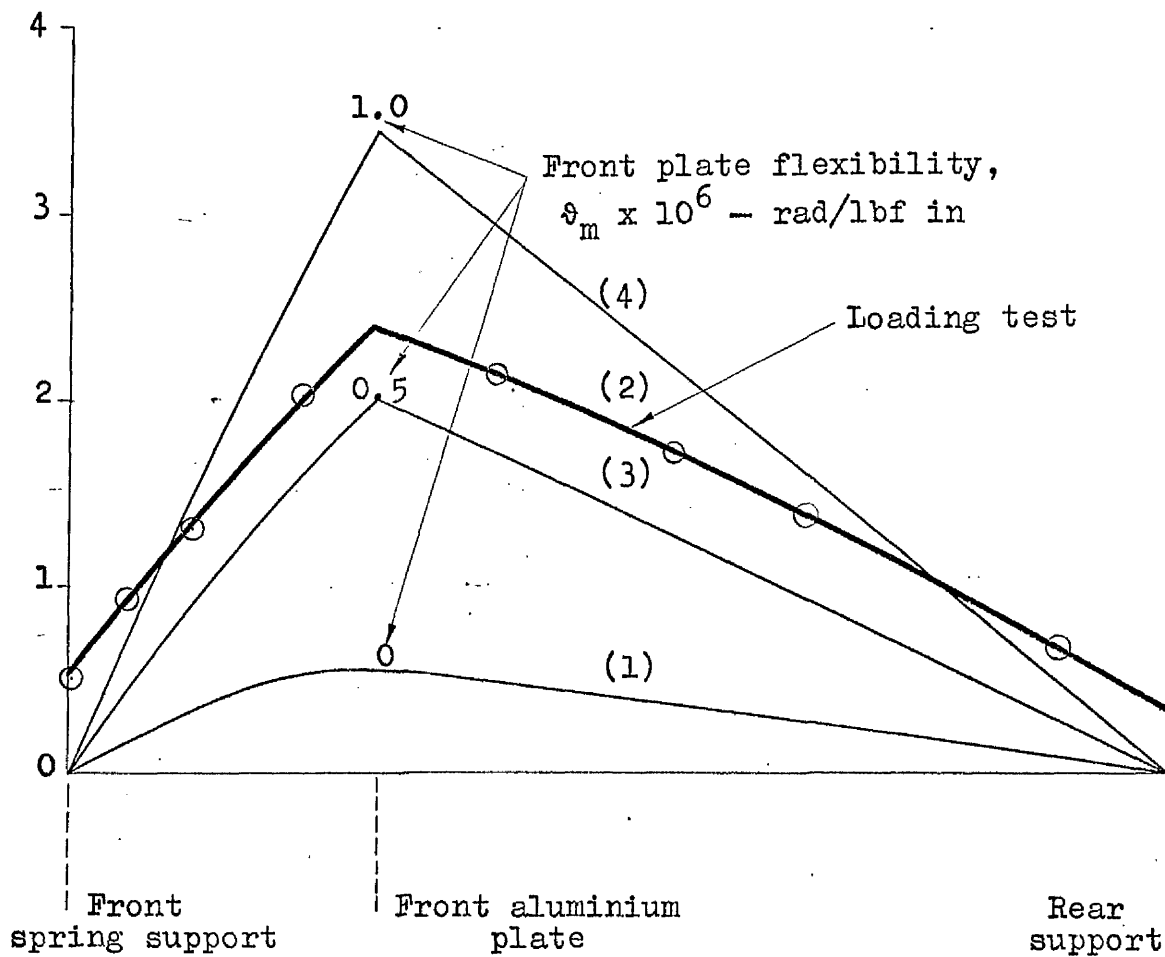
Fig.6.2

Fig.6.2 Comparison of measured deflection of casing with computer predictions
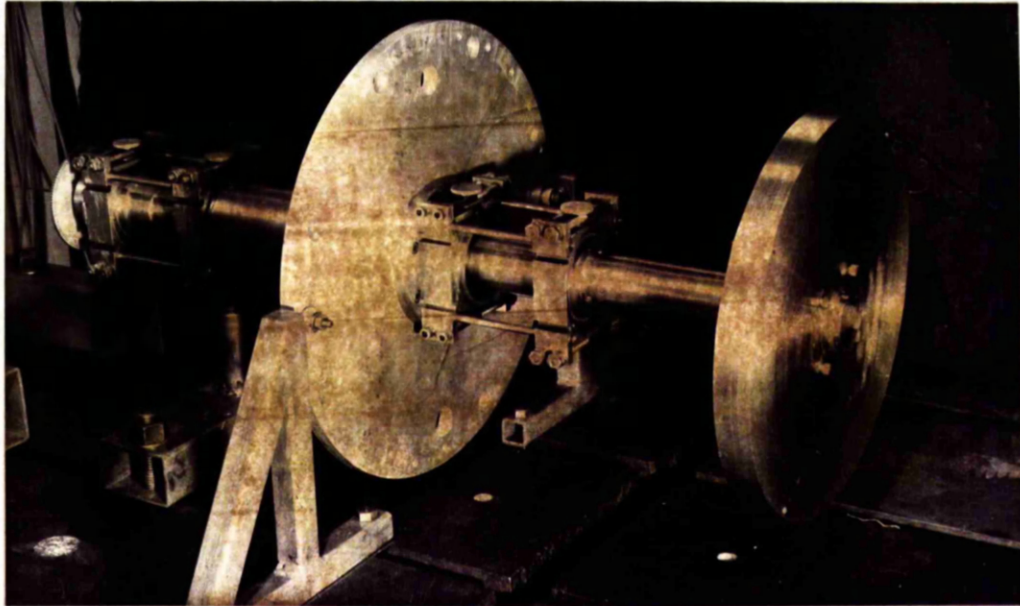
Fig. 6. 3

Fig.6.3   H.P. Rotor mounted in front half
of casing for whirling tests

CHAPTER 7

EVALUATION OF THE ACCURACY

OF THE COMPUTER MODEL OF THE COMPLETE RIG

SUMMARY

The first attempts at predicting the whirling speeds of the complete rig were disappointing. Independent calculations made by the representatives of two aero engine companies also produced poor results.

Later predictions, which incorporated the corrections suggested by the tests conducted on the casing and H.P. rotor, were satisfactory. The H.P. and L.P. whirling speeds were predicted within $4^{\circ}/o$ and $1^{\circ}/o$ respectively.

The sensitivity of these predictions to variations of the rig parameters was explored. No large changes in whirling speeds were found which could not be explained. The computer model of the rig was shown to predict, with fair accuracy, an increase in H.P. whirling speeds of about $20^{\circ}/o$ which resulted when the rear bearing stiffness was made almost 10 times the design value.

CHAPTER 7

EVALUATION OF THE ACCURACY

OF THE COMPUTER MODEL OF THE COMPLETE RIG

7.1 Initial trials of the Computer Model of the Rig

When the first build of the rig was completed, tests
were conducted to determine the accuracy of the computer
model. Experience indicated that the vibration of various
points of the model, including the discs, was most stable
when both shafts rotated at the same speed in the same
direction. This particular shaft speed relation was
therefore adopted for comparison purposes.

The first tests were extremely disappointing.
Considerable effort was therefore devoted to checking the
computer input data, representing the physical characteristics
of the model, and the programing of the calculation.
Comparison of the predicted whirling speeds and modes with
those exhibited by the model failed to indicate the cause
of the discrepancies.

The computer program had been designed to employ the
standard transfer matrix method in which the evaluation of
a final 9 — th order determinant was used to locate the
particular frequency. On examination of this process it
was found that the final operation involved the subtraction
of two large quantities, both of the order of 10^{16}, even
when the iteration process was within 1 rpm of the whirling
speed. It was suspected that hidden numerical difficulties
due to rounding errors were responsible for the poor computer
predictions. The computer program was therefore altered to
employ the modified transfer matrix method, which avoids
such difficulties, but no improvement was found.

The final predictions of the computer model, using the standard and modified transfer matrix methods, are shown compared with the test values in the first two columns of Table 7.1.

During this period of the investigation, three representatives from Rolls-Royce Ltd., Derby, visited the University to discuss the investigation. They were delighted to find a rig on which they could test the accuracy of their own methods of predicting critical speeds, and they were therefore given full details of the rig to use. The details were also sent by a representative of the Allison Division of General Motors (who was attached to Rolls-Royce Ltd under a liaison agreement) to the engineering division of Allison's for evaluation. The predictions which these two companies produced are also shown in Table 7.1. The accuracy was little, if at all, better than that achieved by the writer. But the figures do support the writer's contention that aircraft engine companies cannot predict critical speeds with great accuracy.

7.2   Final predictions of the frequencies of the Rig

Following the disappointing results of the first attempt at predicting the critical speeds of the rig, a detailed examination of the properties of the casing and H.P. shaft was made (Chapter 6). When the results of this examination were used to correct the computer model, the predictions of the two lowest lateral frequencies (when the shafts were not rotating) and the four lowest whirling speeds (when the shafts were rotating in the same direction at the same speed) were found to agree well with the frequencies exhibited by the model, (Table 7.2). (The lateral frequencies are not strictly comparable since the model values were obtained by exciting the model using the unbalance of one of the shafts, i.e. the 'H.P. lateral' was excited by the L.P. shaft rotating at 1383 rpm. As

will be seen later, in Chapter 8, the variation of H.P. frequency with L.P. speed under these conditions, is small.)

It can be seen that the predictions for the H.P. shaft are about $4^{\circ}/o$ low. The discrepancy is thought to be due to the neglect, in the computer model, of the local stiffening of the H.P. shaft by the inner track of the H.P. rear bearing. The tests conducted on the H.P. shaft mounted in the front half of the casing had suggested a discrepancy of about $2^{\circ}/o$ but there had been uncertainty about the influence of the flexibility of the front plate.

The L.P. shaft frequencies were predicted with satisfactory accuracy comparable with that achieved in the earlier investigations of the L.P. shaft.

7.3   Modes of Vibration

An attempt was made to determine the accuracy of the predicted mode of the vibration when both shafts were rotating in the same direction at the same speed. Vibration probes of suitable range were mounted to monitor the vertical movement of the bearing housings, model supports and the discs. The signals from each probe were, in turn, displayed on the Y-axis of the oscilloscope to be compared with the horizontal motion of the L.P. disc, which was fed to the X plates of the oscilloscope. It was·hoped that this procedure would nullify the effect of fluctuations of the model when operating close to a whirling speed. The results of three tests carried out with both shafts rotating at 2170 rpm in the same direction are shown in Table 7.3 compared with the computer predictions.

Although the accuracy of measurement of the mode of vibration was not expected to be good the results achieved show a fair resemblance to the computed values — which are, of course, for undamped vibration.

7.4   Variation of Model data

The success of a frequency analysis of a
complicated structure depends on the accuracy of the
data used to represent the properties of the model.   The
data may be numerically correct but, as a result of
omissions or faulty presentation, fail to represent faith-
fully the properties of the system.   This aspect, of
course, could not be evaluated but an indication of its
serious nature had been shown by the failure to include
the flexibility of the aluminium plates of the casing in
the initial calculations of the frequencies of the rig.
But it was thought useful to examine the sensitivity of
the computer model to numerical inaccuracies in the data,
now that it appeared to be correct in principle.   This
aspect was tested by computing the change in forward
whirling speeds which resulted when selected parts of the
data were altered, in turn, by $10^{\circ}/o$.   The results which
were obtained are listed in Table 7.4.

The predicted speeds are relatively insensitive to
the stiffness and inertial properties of the casing.
Even the plate stiffnesses appeared to have little
influence on the whirling speeds although they had been
found to be significant in the work carried out on the
casing alone.   However, when the computer model, now
apparently correct, was used to predict the speeds when
both front and rear plates were rigid, the L.P. speed rose
$1.2^{\circ}/o$ while the H.P. speed rose $17.1^{\circ}/o$, thus confirming
the large influence of the plate flexibilities particularly
on the H.P. speed.

The accuracy of the computer model was tested further
by determining the change in whirling speeds which would
be expected to result when the stiffness of the H.P. rear
bearing was made almost 10 times larger (by replacing the
0.25 in diameter spring rods with ones of diameter
0.4375 in).   The per cent changes in the respective

whirling speeds predicted and later determined from the
modified rig are compared in Table 7.5.   The agreement
following such a drastic change of the model was
considered to be satisfactory.

Table 7.1

TABLE 7.1

COMPARISON OF COMPUTER PREDICTIONS WITH THE
WHIRLING SPEEDS OF THE RIG

Whirling Speed	Rig — rpm	Computer Prediction — rpm	R—R Ltd — rpm	Allison — rpm
H.P. Reverse	1175	1182	880	821
H.P. Forward	1265	1331	924	983
L.P. Reverse	1897	1787	1947	1816
L.P. Forward	2160	2905	2327	2022

Table 7.2

TABLE 7.2

COMPARISON OF PREDICTED LATERAL FREQUENCIES
AND WHIRLING SPEEDS WITH THE RIG VALUES

	Rig Values c/min	Computer Prediction c/min	Computer Error %
H.P. Reverse whirl	1370	1315	− 4.0
H.P. Lateral	1447	1383	− 4.4
H.P. Forward whirl	1498	1453	− 3.0
L.P. Reverse whirl	1890	1864	− 1.4
L.P. Lateral	2029	2010	− 0.9
L.P. Forward	2165	2165	0

Table 7.3

TABLE 7.3

Comparison of vibration mode with predicted
free vibration mode when both shafts are
rotating in the same direction at 2170 rpm
(L.P. forward whirl)

Probe Position	Test 1	Test 2	Test 3	Predicted Value
Front Bearing	.16	.14	0.14	.148
Front Support	.01	.018	.021	.018
H.P. Rear Bearing	.1	.066	.081	.079
H.P. Disc	.08	.09	0.11	.113
L.P. Disc	1.0	1.0	1.0	1.0
L.P. Rear Bearing	.28	.26	.29	.259

Table 7.4

TABLE 7.4

%o Changes in Forward Whirling Speeds
resulting from a 10%o increase in
a parameter

Rig Parameter	%o Change L.P. Forward Whirl	%o Change H.P. Forward Whirl
Front support stiffness	0	0
Casing tube stiffness	0	0.1
Drum stiffness	0	0
All casing masses and inertias	− 0.5	0
Front plate stiffness	0	1.4
Rear plate stiffness	0.15	0
Front bearing stiffness	0.2	0.2
H.P. rear bearing stiffness	0.1	1.4
H.P. shaft stiffness	0	1.0
H.P. disc mass and inertia	0	− 4.3
L.P. rear bearing stiffness	0.6	0
L.P. shaft stiffness	3.5	0
L.P. disc mass and inertia	− 3.2	0

Table 7.5

TABLE 7.5

Actual and predicted $^o/o$ changes in
whirling speeds resulting from increasing
the H.P. bearing stiffness to 9.4 times
the original value

	Model $^o/o$ Change	Computer $^o/o$ Change
H.P. Reverse	16.9	18.0
H.P. Forward	21.8	24.3
L.P. Reverse	1.85	0.75
L.P. Forward	1.1	0.8

CHAPTER 8

EXAMINATION OF THE VIBRATION
BEHAVIOUR OF THE RIG

SUMMARY

The rig was found to exhibit resonances at speeds
other than the so-called critical speeds predicted by the
computer model. The nature of these resonances was
examined by running each shaft at speeds up to 6000 rpm
while the other shaft was stationary.

Several minor resonances were found to occur whenever
the rotating shaft reached a speed which was a simple
fraction of its critical speed. These resonances are shown
to be caused by variations in the driving torque applied to
the shaft.

A minor resonance was observed when the H.P. shaft was
rotating is shown to be caused by bearing excitation, since
it occurred when the precessional speed of the rolling
elements of the bearings coincided with the current
frequency of the shaft.

A severe vibration occurred when the speed of the H.P.
shaft reached 4800 rpm. The shaft vibrated at a frequency
which was exactly $\frac{1}{3}$ of the rotational speed. This type
of vibration is shown to be a sub-harmonic almost certainly
caused by non-linearity of the support of the shaft caused
by the bearing clearance.

CHAPTER 8

EXAMINATION OF THE VIBRATION
BEHAVIOUR OF THE RIG

8.1   Introduction

During the development of a reliable computer model
of the rig, several minor resonances had been observed at
speeds other than the so-called critical speeds.   The
nature and cause of these resonances had to be established
before the investigation was extended.   The behaviour of
each shaft, at speeds up to the maximum possible of 6000
rpm, was carefully examined while the other shaft was
stationary.

8.2   L.P. Shaft

The results of the survey carried out on the L.P.
shaft are summarised in Table 8.1 and illustrated in
Fig.8.1.   The movement of the L.P. disc was measured by
capacitance probes with a maximum range of 0.1 in (the
maximum sensitivity of the subsequent oscilloscope display
was 1 cm per 0.001 in).   Probes of greater sensitivity
were tried but to no advantage.   Irregularities in the
nominally circular circumference of the disc, and
eccentricity of the shaft at the disc mounting, caused the
disc centre to appear to revolve in a path with a radius of
almost 0.001 in, even at very low speeds.   Resonances with
an amplitude as small as 0.001 in could therefore not be
detected with precision.

The forward and reverse synchronous whirls (critical
speeds) of the L.P. shaft were observed to be close to the
predicted values.

Noticeable vibration of the L.P. shaft was observed when its speed coincided with the natural frequency of the stationary H.P. shaft. The H.P. disc, at this condition, traced an elliptic path, deviating as much as 0.004 in from the axis of the bearings. Since the H.P. shaft was not rotating little external damping was available to control its movement.

Vibration of the L.P. shaft was also noticeable at speeds which were approximately $\frac{1}{2}$ and $\frac{1}{3}$ of the critical speeds. Under these conditions the centre of the L.P. disc traced out an approximately circular path twice and three times, respectively, during each revolution. The shaft was therefore vibrating, in each case, at its natural frequency, the value of which was determined by the rotational speed — this speed being a simple fraction of the current natural frequency. These 'fractional whirls' (a term which the writer prefers to adopt to differentiate from similar whirls, which are caused by non–linear effects) will be shown later to be caused by variations in the driving torque applied to the shaft.

When the shaft speed was in the region of 5000 rpm, noticeable vibration was apparent which had the appearance of a reverse whirl. Later computer calculations suggested that a higher mode of vibration could be expected at about this speed and the rig would precess in an opposite sense to the shaft rotation.

When the L.P. shaft speed reached 5800 rpm, moderate vibration was noticed accompanied by a distinct rattle emanating from the L.P. rear bearing. Although the oscilloscope display of the vibration was not clear enough to establish its nature, the apparent amplitude of motion of the disc, at least 0.001 in at this speed, was sufficient to cause the maximum radial acceleration of the

shaft to exceed that due to gravity.   It therefore
seemed certain that at this speed the shaft, which at
lower speeds rotates while resting at the bottom of the
bearing, was lifting, momentarily, off the bearing track
and crossing the bearing clearance.

8.3   H.P. Shaft

The results of a vibration survey when the H.P. shaft
speed was varied up to 6000 rpm, while the L.P. shaft was
not rotating, are listed in Table 8.2 and illustrated in
Fig.8.2.   The forward and reverse synchronous whirls
appeared at the expected speeds, allowing for the fact that
the computer predictions had been found to be some $4^{o}/o$
low.

When the H.P. shaft rotated at 2029 rpm some vibration
was apparent which corresponded to lateral vibration of the
stationary L.P. shaft.   Since the L.P. shaft was stationary,
and therefore subject to little damping, relatively large
deviations, of up to .017 in, from the bearing axis were
observed.

Fractional whirls of the H.P. shaft were observed,
although it was not always possible to distinguish the
sense of the whirl.

At a speed of 3550 rpm moderate vibration of the H.P.
shaft was observed which proved to be insensitive to the
amount of unbalance of the shaft.   This particular
vibration will be shown later to be attributable to
variations in the diameters of the rolling elements of the
bearings.

When the shaft speed reached approximately 4800 rpm
a sudden transition to a severe form of vibration was
observed and was maintained, though with decreasing
amplitude, until a speed of over 5000 rpm was reached.
The strange oscilloscope display, shown in Fig.8.3,

suggested that the H.P. disc centre traversed an almost circular path during the course of three shaft rotations. This peculiar behaviour will later be shown to be almost certainly a result of non—linearity in the system caused by the shaft crossing the bearing clearance.

8.4   Critical Speeds

The computer predictions of the H.P. and L.P. shaft frequencies are shown plotted versus the respective shaft speeds in Figs.8.4 and 8.5.   The predicted L.P. critical speeds show good agreement with the observed results.   The H.P. critical speeds are about $4^{o}/o$ high and are therefore consistent with previous results in which both shafts ran at the same speed.

The tests on the H.P. shaft illustrated the sensitivity to unbalance of the H.P. disc.   During preliminary tests the radius of the orbit of the disc was found to be 0.003 in at the forward critical speed of 1499 rpm and observation of the behaviour in the neighbourhood of this speed was not easy.   The disc was therefore unbalanced by adding a small balancing screw, of mass 0.865 g, which would cause the centre of mass to shift a distance of 0.00033 in.   The resultant amplitude at the same critical speed was then found to be 0.021 in.

The damping acting on both shafts was obviously very small, significant amplitudes being observed over a speed range of about 20 rpm at forward whirl.   As a result quite large fluctuations were present in the oscilloscope display, presumably as a result of variations of the driving torque supplied by the servo—controlled motors. It was therefore impossible to determine a reliable record of the amplitude close to the forward critical speed from which a measure of the external damping acting on the shaft could be obtained.   Instead, the 'kicks' on the oscilloscope display, caused by the metal foil markers

on the discs, were used to determine the speeds at which
phase angles of 45°, 90° and 135° were obtained.   The
results of these tests are tabulated in Table 8.3.

If the whirling speed of the shaft is ω, and the
damping is small, phase angles of 45° and 135° will occur
at $(1 - e)\omega$ and $(1 + e)\omega$ respectively, where e is very
small.   If the damping is viscous and ξ times the critical
value then

$$\tan 45° = \frac{2\xi\,(1 - e)}{1 - (1 - e)^2} = 1$$

and $$\tan 135° = \frac{2\xi\,(1 + e)}{1 - (1 + e)^2} = -1$$

When these relations were applied to the observations listed
in Table 8.3, damping ratios of 0.001 and 0.004 were
indicated for the L.P. and H.P. shafts respectively.

8.5   Fractional Whirls

If a rotating shaft is subjected to a fluctuating
torque it may appear to whirl at speeds which are simple
fractions of the critical speed.   An explanation of this
effect is described in detail by Biezeno and Grammel
(Ref. 24).

The diagram, Fig.8.6, shows the cross—section through
the mid—point of a simply supported shaft which carries a
disc at its centre.   As before, (Chapter 1), the equations
expressing the motion of the centre of the disc, C, are:—

$$m\ddot{x} + kx = ma\,\omega^2\cos\varphi$$

$$m\ddot{y} + ky = ma\,\omega^2\sin\varphi \quad\ldots\ldots\ldots (1)$$

Since the shaft is now assumed to be subjected to a
variable moment, it is supposed to rotate at a mean
angular velocity, p, but with a fluctuation, ϑ, in
addition, so that,

$$\varphi = pt + \vartheta$$

Equation (1) then becomes,

$$m\ddot{x} + kx = ma\,\omega^2 \cos(pt + \vartheta)$$
$$= ma\,\omega^2 (\cos pt \cos \vartheta - \sin pt \sin \vartheta)$$

and assuming that the fluctuation, ϑ, is small, the equation
may be written,

$$m\ddot{x} + kx = ma\,\omega^2 (\cos pt - \sin pt.\vartheta) \ldots\ldots\ldots (2)$$

Now the variable moment may always be expressed as a
Fourier series, of which one term is,

$$M = Mo \cos(npt + \beta)$$

where n is an integer.

Referring to Fig.8.6, the equation expressing the
angular motion of the disc is,

$$C\ddot{\varphi} = M + ka\,y \cos \varphi - ka\,x \sin \varphi$$

where C is the polar moment of inertia of the disc. Biezeno
and Grammel show that, for all practical purposes, the last
two terms may be neglected, to give:—

$$\ddot{\varphi} = \frac{M}{C} \cos(npt + \beta)$$

Integration of this equation, gives:—

$$\varphi = -\frac{M}{C\,n^2\,p^2} \cos(npt + \beta) + Rt + S$$

Since R obviously must be equal to p, the mean angular velocity, and the constant S is unimportant, the fluctuation ϑ in the expression $\varphi = pt + \vartheta$ is given by:—

$$- \frac{M}{C\,n^2\,p^2} \cos(npt + \beta)$$

Substituting this in (2),

$$mx + kx = ma\,\omega^2 \left[\cos pt + \sin pt\,\frac{M}{C\,n^2\,p^2} \cos(npt + \beta) \right]$$

which, since,

$$\sin A - \sin B = 2 \sin \frac{A - B}{2} \cdot \cos \frac{A + B}{2}$$

can be written,

$$m\ddot{x} + kx =$$

$$ma\,\omega^2 \cos pt + \frac{ma\,\omega^2\,M_0}{2\,C\,n^2 p^2} \left[\sin\left\{(n+1)pt + \beta\right\} - \sin\left\{(n-1)\,pt + \beta\right\} \right]$$

Thus, in addition to resonance occurring when $\omega = p$, there also exists the possibility that resonance may occur whenever

$$(n \pm 1)\,p = \omega$$

i.e.   if, $n = 1$, when $p = \dfrac{\omega}{2}$

   $n = 2$, when $p = \dfrac{\omega}{3}$ or ω

   $n = 3$, when $p = \dfrac{\omega}{4}$ or $\dfrac{\omega}{2}$, etc.

Thus, whenever a variable component is present in the driving torque, the shaft may whirl at speeds which are simple fractions of the shaft frequency.

Resonance at half the critical speed is usually observed when horizontal shafts are employed since the force due to gravity, mg in Fig.8.6, always necessitates a fluctuation in driving moment once per revolution.

These fractional whirls were exhibited by both shafts. Although the $\frac{1}{3}$ and $\frac{1}{4}$ whirls could be detected it was not possible to determine the sense of the whirls from the indistinct oscilloscope traces. However, relating these to the frequency plot, Figs.8.4 and 8.5, showed that they could be placed so as to conform with the synchronous whirling (critical) speeds.

8.6 Bearing Excitation

A small resonance was observed when the H.P. shaft speed reached 3560 rpm. Sufficient computer analysis had been done by then to show that no critical speed was to be expected at this speed. Perhaps the effect was caused by a type of bearing excitation noted by Yamamoto (Ref.21).

The ball or roller assembly in a rolling bearing, (Fig.8.7(a)), precesses at a rate α times the shaft speed, where,

$$\alpha = 2.0 + 2.0 \cdot \frac{d}{D}$$

in which,

> d = diameter of the balls or rollers
> D = diameter of the inner track.

Yamamoto showed that if, as a result of manufacturing errors, one ball or roller is larger than the others, the shaft would be subjected to an excitation at a frequency which is α times the shaft speed, and which rotates in the same direction as the shaft rotates. Resonance would occur, therefore, whenever the shaft speed, Ω , attains a value at which $\alpha\Omega$ equals the forward whirling frequency which the shaft exhibits when rotating at a speed, Ω .

Measurement of a spare H.P. rear bearing showed that the mean roller diameter was 0.3124 in, while the inner track diameter was 2.3405 in, and so the roller assembly would precess at a rate 0.441 times the shaft speed. Similar measurements of the H.P. front bearing also suggested a precession rate of 0.441, a value which was confirmed by observation.

The computed variation of H.P. shaft frequency, ω, with rotational speed, Ω, is shown plotted in Fig.8.7(b). It can be seen that the locus, $\alpha = 0.441\Omega$, intersects the frequency curve when the shaft speed is 3500 rpm. However, the computed values of frequency were known to be some $.4^{o}/o$ low. When the experimental values of synchronous and half speed whirl frequencies were extrapolated, bearing excitation was shown to be expected to occur at 3560 rpm, in agreement with the observed resonance.

A similar examination of the L.P. rear bearing showed that the rollers would precess at a rate 0.42 times the shaft speed. When this is compared with the computed variation of L.P. shaft frequency, ω, with speed, Ω, in Fig.8.7(c), it can be seen that bearing excitation was to be expected at a shaft speed of 5620 rpm.

The L.P. shaft had been found to exhibit rough running in the region of 5800 rpm and it therefore seems feasible to suggest that bearing excitation was contributory.

8.7   Higher Modes of Vibration

The L.P. shaft showed a resonance at a speed of 4959 rpm. Although the amplitude was small it was possible to distinguish that the vibration resembled a reverse whirl. The explanation for this behaviour was later shown by computer investigation to be due to vibration in a mode in which the whole rig precessed in an opposite direction to the L.P. shaft rotation.

8.8 Subharmonic Oscillation

The radius of the H.P. disc orbit at speeds just below 4800 rpm was approximately 0.0005 in, although there were frequent fluctuations as large as 0.001 in. But when the speed was raised, the orbit suddenly increased, at a speed of approximately 4800 rpm, to a radius of the order of .012 in with some increase in noise level.

The path of the disc centre, shown by the oscilloscope trace, was peculiar as shown in Fig.8.3. Apparently the disc was traversing an orbit, which was roughly circular, once during the course of three revolutions of the shaft. Professor Robson pointed out that this behaviour was probably a subharmonic vibration caused by some non-linearity within the system. Later work showed that the frequency of forward precession of the shaft was expected to be about 1600 rpm when rotating at this speed, suggesting that it was indeed a subharmonic vibration of order 3.

Several traverses through the speed range 4600 — 5600 rpm produced the results shown in Figs.8.8 and 8.9. The response of the shaft 'jumped' at a speed of about 4800 rpm. It did not appear to be governed by the unbalance of the disc as shown by Fig.8.8. The results of two tests, in which the speed was gradually raised to 5600 rpm and then lowered, showed that the response was quite different to the non-linear response observed when the L.P. shaft was being tested in temporary bearing mountings (see section 5.5). Although a 'jump' occurred at 4800 rpm when the speed was rising, no corresponding 'jump' was observed on lowering the speed from 5600 rpm, until the speed reached 4800 rpm (Fig.8.9).

Professor Robson had pointed out that whereas the existence of a subharmonic vibration could be shown to be possible, it was often extremely difficult to initiate unless appropriate conditions were provided. The behaviour of the model confirmed this nature of subharmonic

vibration. On many occasions the vibration refused to appear at any speed in the range 4800 – 5600 rpm. But it could be shown to be incipient since a blow applied to the model with a large piece of wood often initiated the vibration, although it was usually not maintained.

8.9 Non-linearity of Bearing

In section 5.5 it was shown that the L.P. shaft had exhibited some apparently non-linear behaviour at forward whirl. It was argued that this occurred when the radial acceleration of the disc approached the acceleration due to gravity and was probably due to the shaft crossing the bearing clearance. But a closer examination of the behaviour of the whirling shaft suggested that the support of the shaft at the bearings may exhibit non-linearity at any speed greater than forward whirl.

A diagrammatic representation of the H.P. shaft is shown in Fig.8.10(a). The front bearing is supposed to support the shaft rigidly in a lateral direction only, and to have no clearance. The rear bearing is mounted on a spring and has clearance, and as a result the shaft rests below the horizontal when not rotating. The shaft is assumed for simplicity, to be rigid.

When the shaft operates at a speed just below the whirling speed, the centre of the disc, C, rotates in a circle of radius r. The centre of mass, G, lies outside C by an amount a, and if the damping is zero, the line CG is radial. If the disc is assumed to be well balanced so that $(a + r)\omega^2$ does not approach the value 32 ft/sec^2, then the shaft will always rest at the bottom of the bearing clearance, and the spring bearing will rotate in a circle of radius somewhat less than r.

Now a whirling shaft is a vibrating system subjected to inertial excitation and therefore the variation of radius r with ω will be as shown in Fig.8.10(b). When the

rotational speed exceeds the whirling speed, the radius of the path, r, will approach the value of the eccentricity, a, and will lag the direction of the unbalance by nearly 180°.

Therefore at speeds much larger than the whirling speed the shaft configuration will be as shown in Fig.8.10(c). The centre of mass, G, tends to approach the static centre line of the shaft, while the shaft centre, C, rotates outside it in a path with a radius approaching the value of the eccentricity, a. The shaft, within the bearing, must therefore traverse a circle with a radius somewhat less than the eccentricity, a.

Now the eccentricity was shown to be rather less than 0.0003 in (section 8.4). The radial clearance of the bearing on the other hand is probably less than 0.00025 in — it would be very difficult to determine this exactly. It, therefore, seems likely that under such conditions the shaft no longer rests at the bottom of the bearing but either rolls continuously around the bearing, or only around part of the bearing, as illustrated in Figs.8.11(a) and (b). In either case the support of the shaft will no longer have a linear characteristic and probably resembles that shown in Fig.8.11(c).

8.10 Duffing's Equation

A type of non-linear restoring force which has a characteristic, not unlike the supposed shaft support, was used by Duffing to derive some important properties of non-linear vibrating systems (Ref.20). The equation he solved was of the form

$$\ddot{x} + x + \varepsilon x^3 = F \cos \omega t$$

where the term εx^3 describes the non-linear property of the restoring force (Fig.8.12(a)).

The solution of this equation produces the response curve shown in Fig.8.12(b) for the case when $\varepsilon > 0$. When damping is included in the equation the response is modified, as shown in Fig.8.12(c), and the amplitude will jump from A to B when the frequency is increasing, and from C to D when it is decreasing. This behaviour was suggested by the early tests on the L.P. rotor (section 5.5).

A solution of Duffing's equation can be shown to exist in which the response is at a frequency which is $\frac{1}{3}$ of the excitation, i.e. at $\frac{\omega}{3}$, provided that the excitation is greater than a certain value, which is more than 3 times the linear natural frequency, depending on the magnitude of ε. The amplitude of this subharmonic vibration, in the absence of damping, is indicated in Fig.8.13(a). When damping is included the response is changed to that indicated in Fig.8.13(b),(Ref.25), which suggests that if the frequency ratio is gradually increased beyond 3 then subharmonic vibration may suddenly occur with considerable amplitude.

8.11 Analog Computer Studies

Although Duffing's equation showed that a subharmonic of order 3 might be produced by a particular non-linear spring characteristic, it did not prove that such behaviour would occur with the spring characteristic which had been suggested for the H.P. bearing (Fig.8.11(c)). A brief analog computer study was therefore carried out to investigate possible subharmonic behaviour of a system governed by the equation:—

$$\ddot{x} + d\dot{x} + f(x) = F \cos \omega t$$

where $f(x)$ represents the supposed bearing characteristic shown in Fig.8.11(c).

A symbolic representation of the circuit which was used on an analog computer to represent this equation is shown in Fig.8.14(a). The element marked 'N.L.' is the

diode circuit shown in Fig.8.14(b).   When the diodes
were not biased, so that the characteristic of Fig.8.14(c)
had no backlash, the circuit was found to resonate at
1.63 c/s to represent the forced solution of the linear
equation:—

$$\ddot{x} + 0.02\ \dot{x} + (12 \times \frac{27}{3.1})\ x = F\cos\omega t$$

When the diodes were biased to produce the non—linear
characteristic represented by Fig.8.14(c), sustained sub—
harmonic resonance of order 3 could be obtained on occasions
provided the amplitude of the excitation E was greater than
14 volt, and the frequency greater than 4.4 c/s, and a
certain initial displacement or velocity was imposed.

The computer study thus showed that the supposed non—
linearity of the bearing, due to clearance, was likely to
promote the existence of a subharmonic of order 3 but it
did not seem that further computer studies would be
profitable.

After the computer study had been carried out some
investigations of the behaviour of non—linear systems was
discovered in a book by Hayashi (Ref.26).   He investigated
experimentally the behaviour of an electric circuit
representing Duffing's equation in which the non—linear
element was simulated by a specially constructed saturable—
core inductor.   His work showed that subharmonic oscillations
could only be sustained under certain conditions, and even if
these were obtained, certain ranges of initial conditions,
including the correct phase of the commencement of the
excitation, were necessary in order to initiate the
oscillation.

Evidence of subharmonic oscillation of a shaft carried
in ball bearings was reported in 1957 by Yamamoto (Ref.21).
He showed that the moment restraining the angular motion of
a shaft carried in single—row ball bearings (without self—

aligning housings) increased with angular deflection in
a non-linear fashion.   His tests showed that a sub-
harmonic of order 2 was readily produced but higher order
subharmonics did occur to a small degree.

Table 8.1

TABLE 8.1

VIBRATION SURVEY OF THE L.P. SHAFT

(H.P. Shaft not rotating)

L.P. Shaft Speed — rpm	L.P. Disc Orbit Radius — thou.	Remarks
692	3	$\frac{1}{3}$ Whirl
981	3	$\frac{1}{2}$ Reverse Whirl
1049	6	$\frac{1}{2}$ Forward Whirl
1448	1	H.P. Shaft Lateral
1896	3.5	Synchronous Reverse Whirl
2166	15	Synchronous Forward Whirl
4959	2	Higher mode of Synchronous Reverse Whirl
5800	3	Rough running

Table 8.2

TABLE 8.2

VIBRATION SURVEY OF THE H.P. SHAFT

(L.P. Shaft not rotating)

H.P. Shaft Speed — rpm	H.P. Disc Orbit Radius — thou.	Remarks
353	3.5	$\frac{1}{4}$ Whirl
469	3	$\frac{1}{3}$ Whirl
698	2	$\frac{1}{2}$ Reverse Whirl
730	5	$\frac{1}{2}$ Forward Whirl
1364	3	Synchronous Reverse Whirl
1483	21	Synchronous Forward Whirl
2029	2	L.P. Shaft Lateral
3550	2	Bearing excitation
4800	10	Subharmonic

Table 8.3

TABLE 8.3

OBSERVATIONS AT THE FORWARD WHIRLING

CRITICAL SPEEDS

L.P. Shaft
(H.P. Shaft not rotating)

Speed — rpm	Radius — thou.	Phase Angle
2163	15	45°
2166	15	90°
2168	13	135°

H.P. Shaft
(L.P. Shaft not rotating)

Speed — rpm	Radius — thou.	Phase Angle
1479	19	45°
1483	21	90°
1490	19	135°
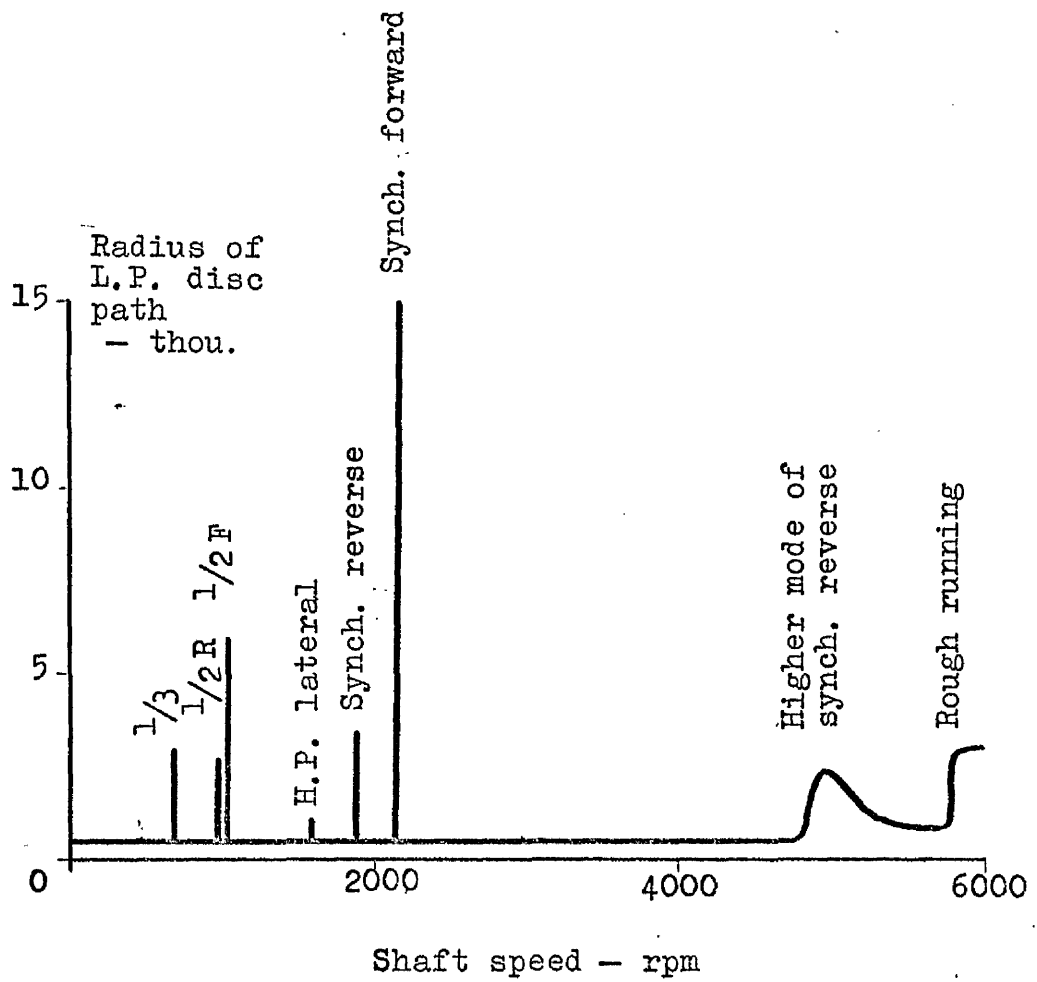
Fig.8.1

Fig.8.1   Whirl amplitudes of L.P. Rotor
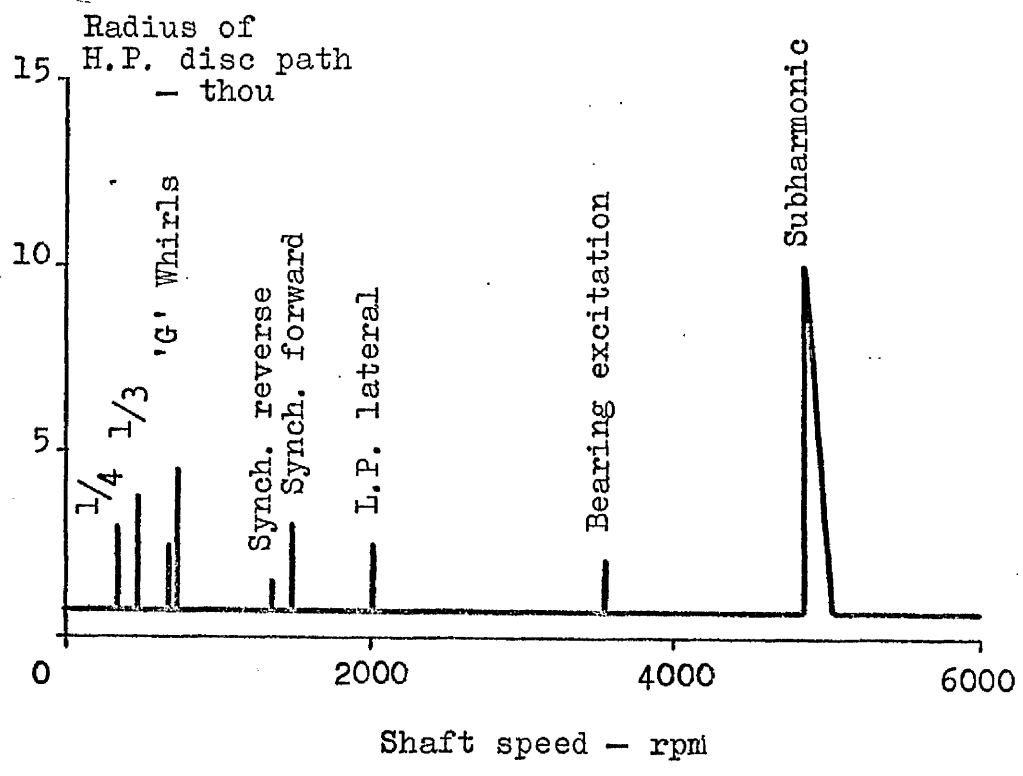
Fig.8.2

Fig.8.2   Whirl amplitudes of H.P. Rotor

Fig. 8. 3

0.006"
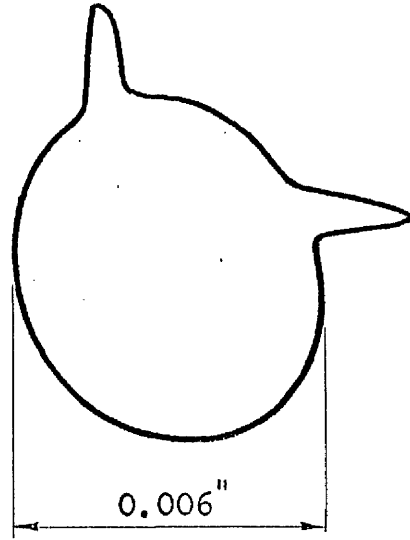
H.P. Forward Whirl at 1490 rpm

0.024"
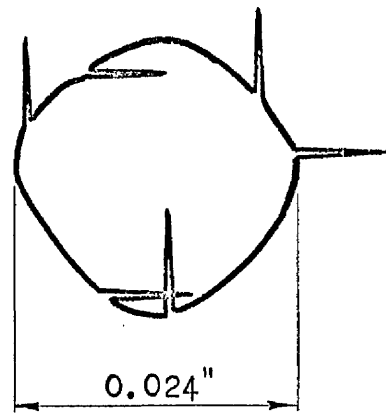
$^1/_3$ Subharmonic at 4785 rpm

Fig.8.3   Tracings of oscilloscope photographs
of path of H.P. disc centre at forward
whirl and during subharmonic vibration.
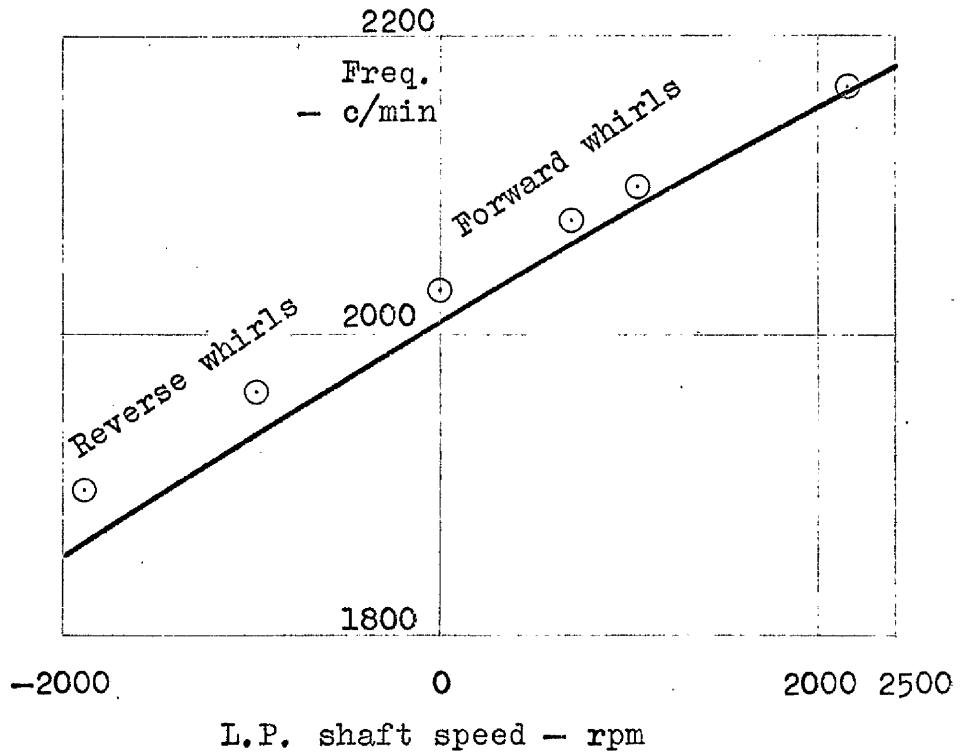
Fig.8.5   Observed L.P. synchronous and fractional
whirls compared with computer predictions.
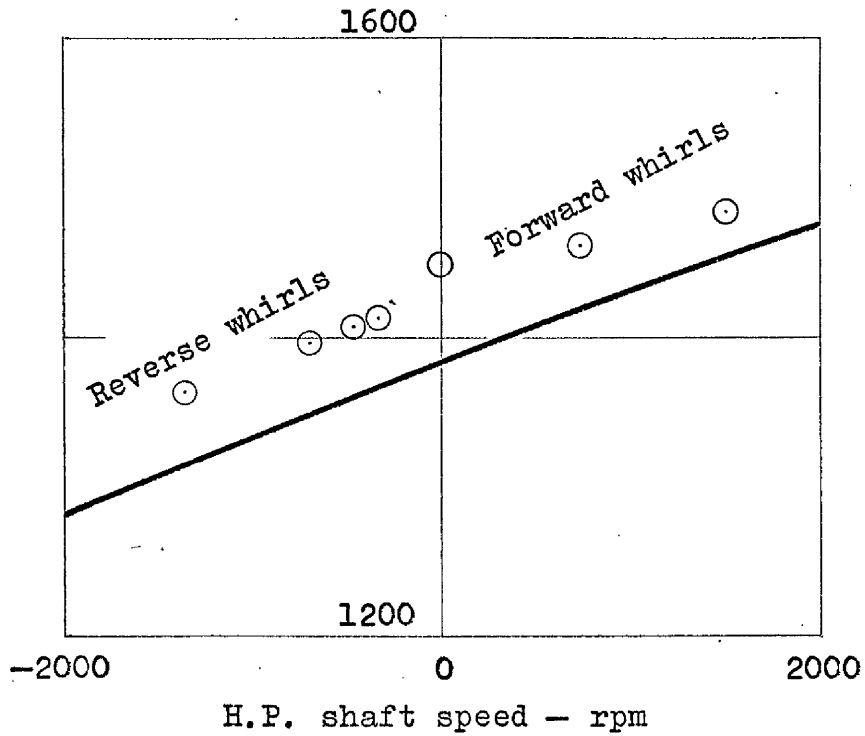
Fig.8.4   Observed H.P. synchronous and fractional
whirls compared with computer predictions.
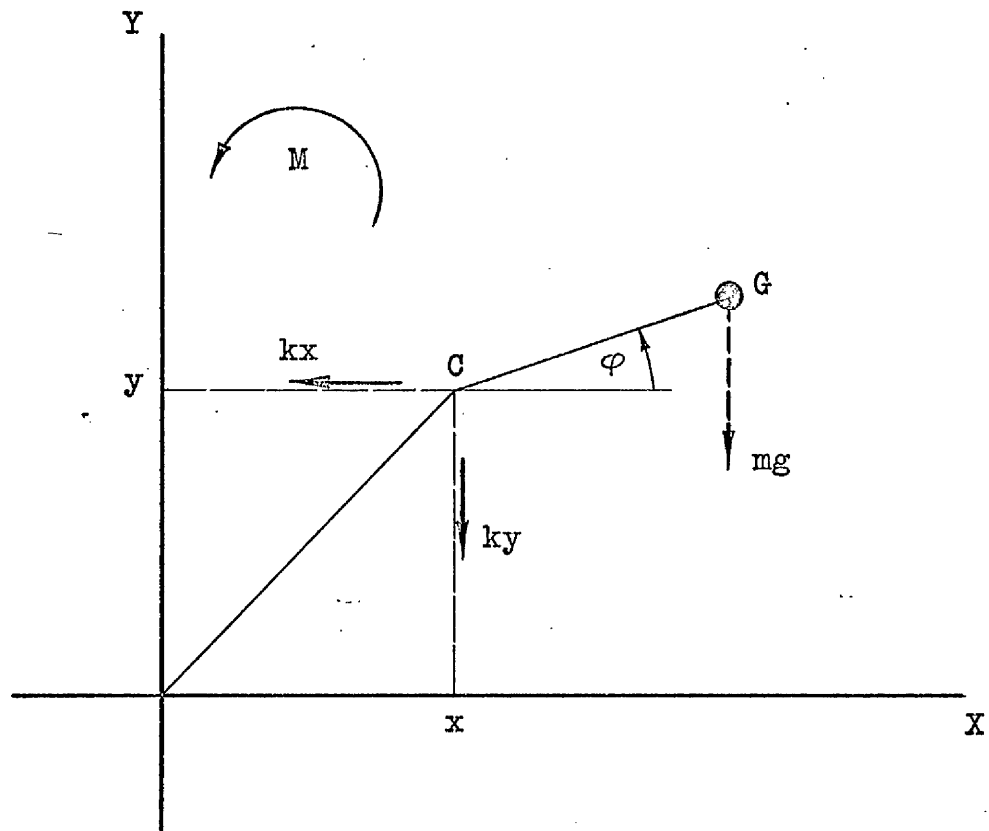
Fig.8.6

Fig.8.6   Motion of centre of disc mounted at mid—point
of a simply supported shaft when subjected to
moment M.
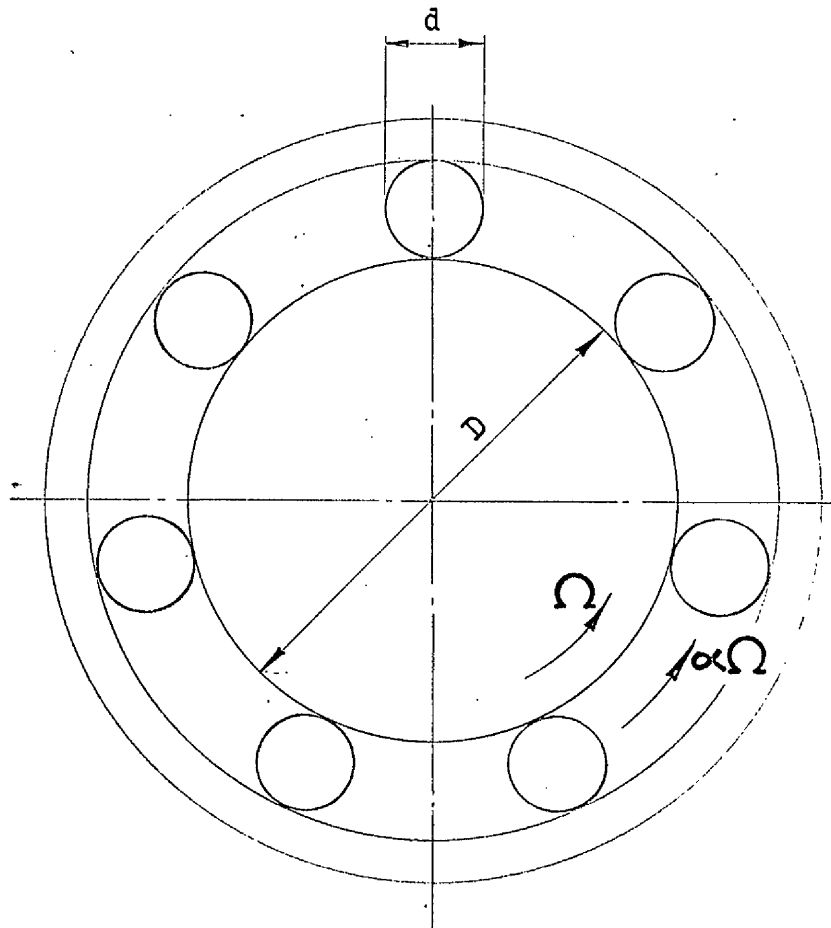
Fig.8.7(a)

Fig.8.7(a)   Precession of ball assembly in a
ball bearing.
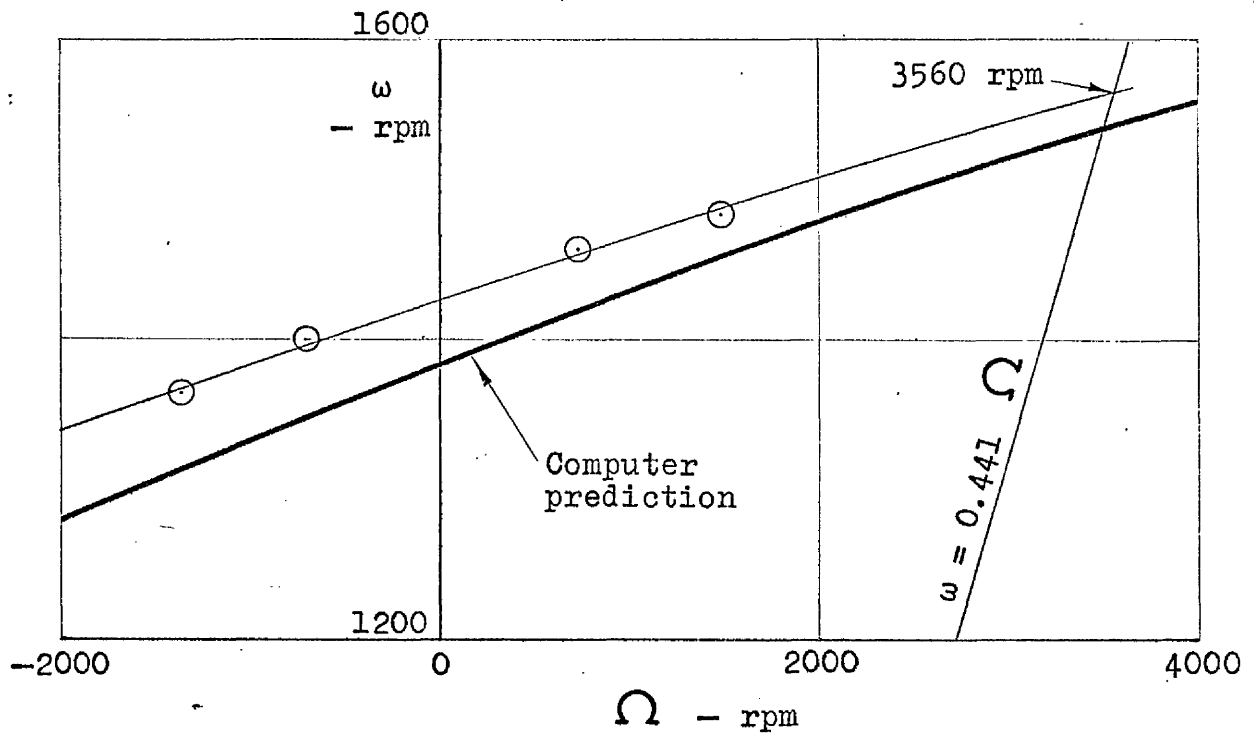
Fig.8.7(b), (c)

Fig.8.7(b)   Bearing excitation of H.P. shaft
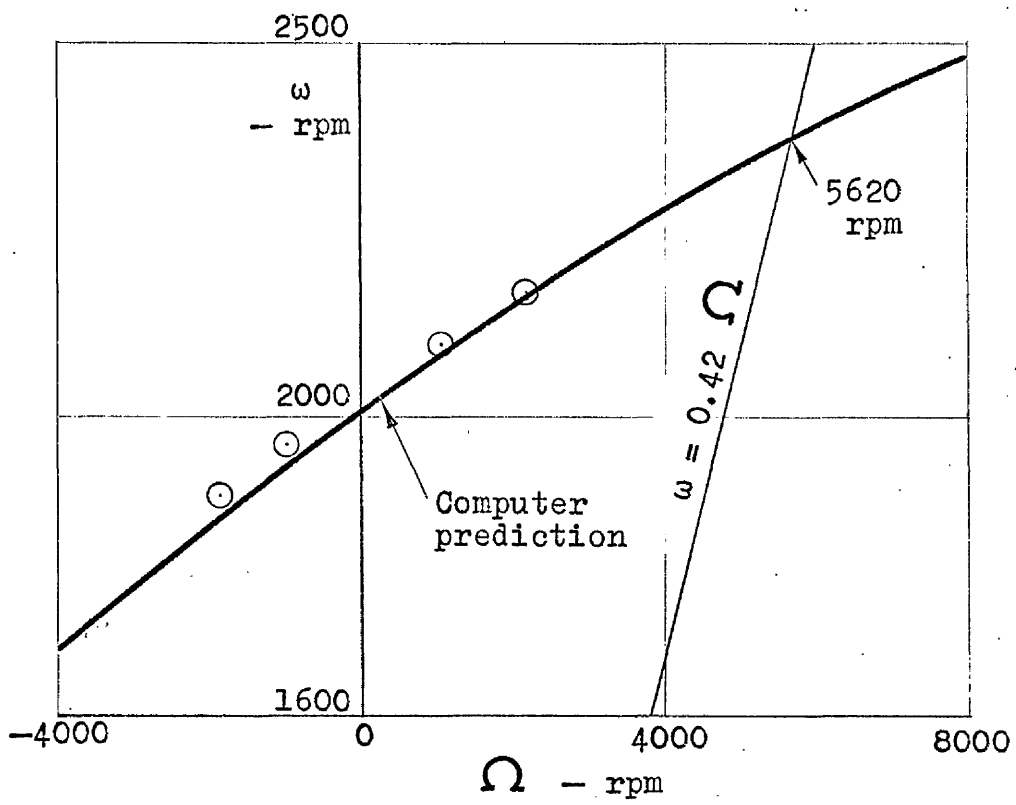
Fig.8.7(c)   Bearing excitation of L.P. shaft
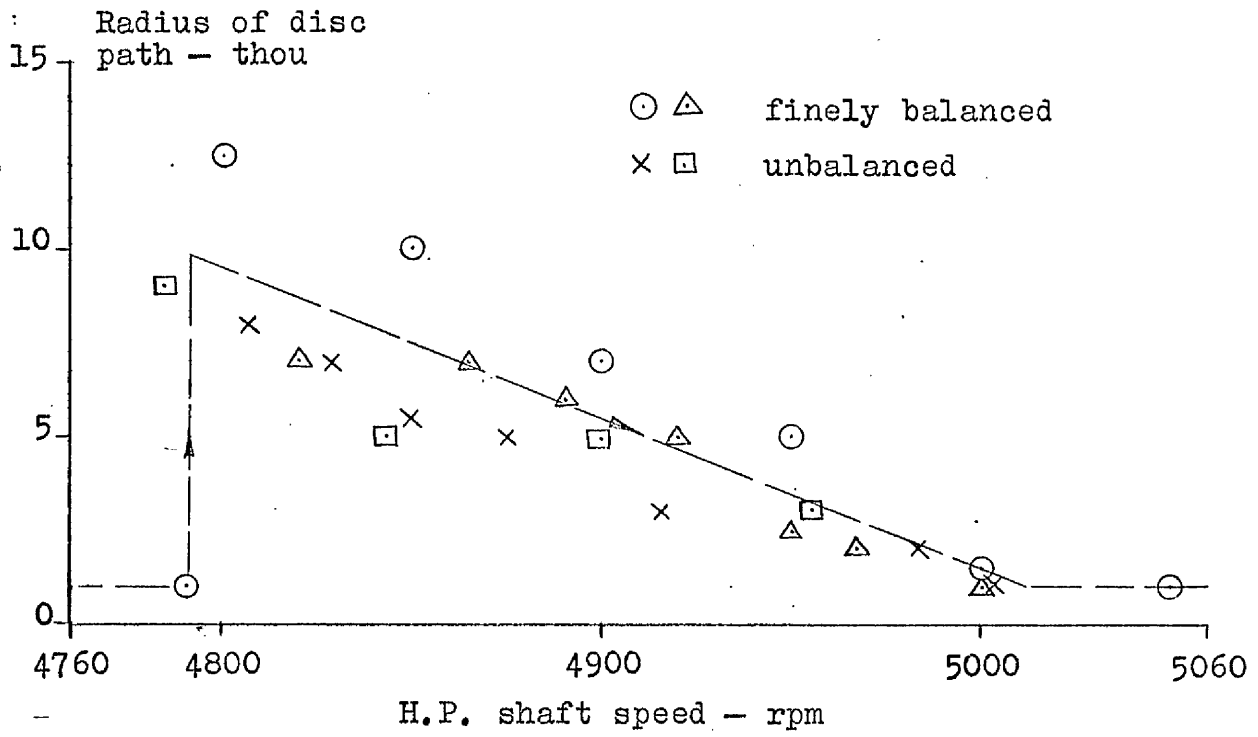
Fig.8.8   Results of four traverses through region
of subharmonic vibration of H.P. rotor.
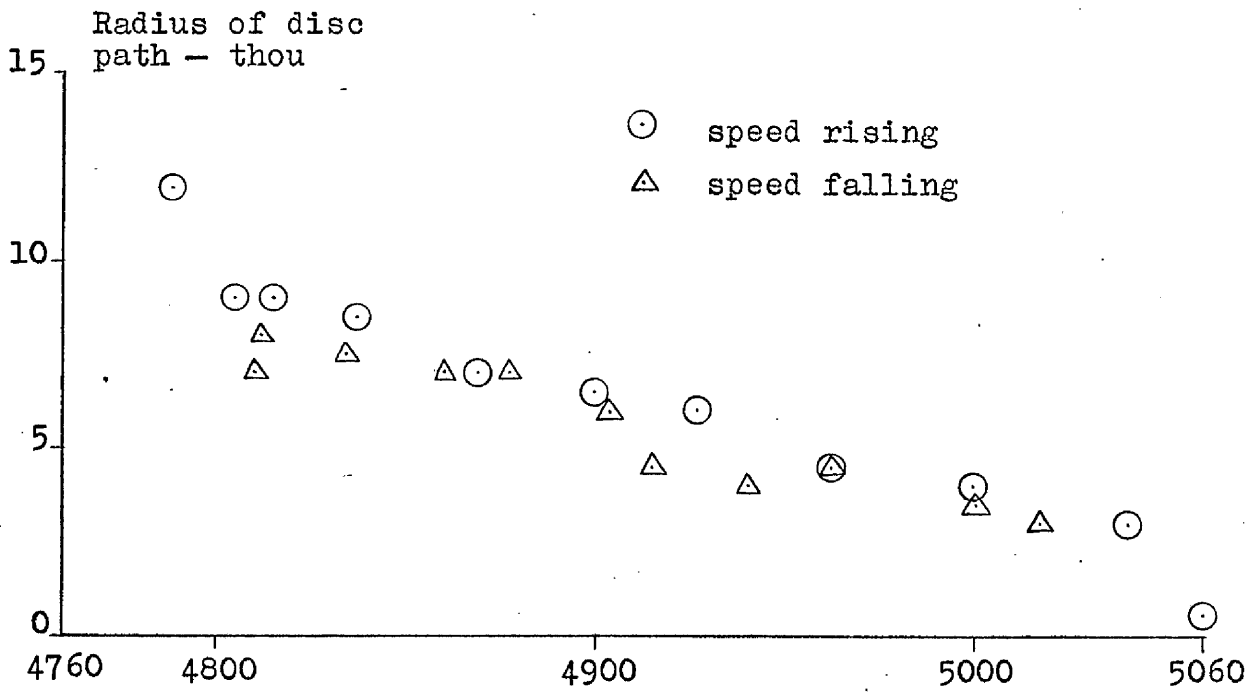
Fig.8.9   Results of traverse up and down the range
of subharmonic vibration of H.P. rotor.

Fig.8.10

Bearing
clearance

r

a

C

G

(a)

r

a

O

Ω

(b)

Bearing
clearance

r

G

C

a

(c)
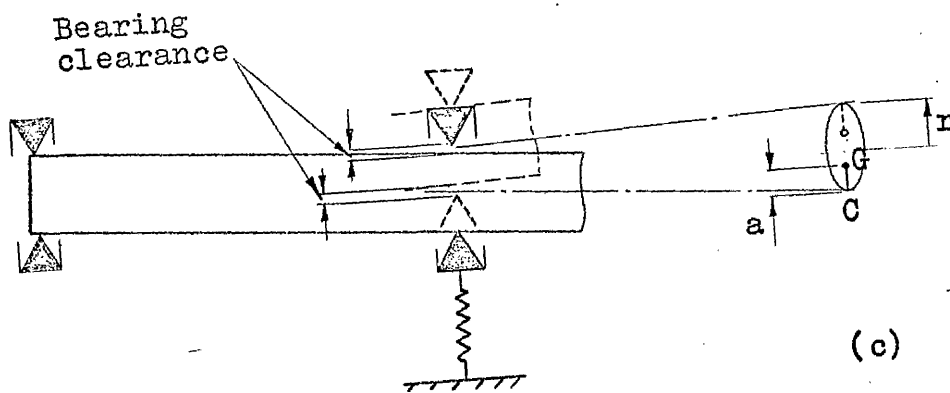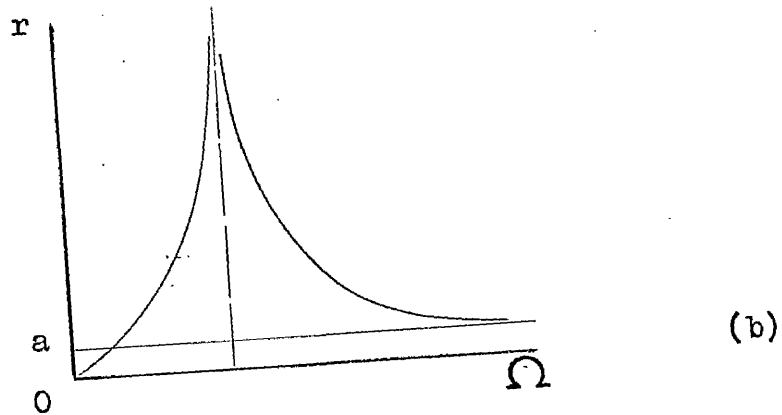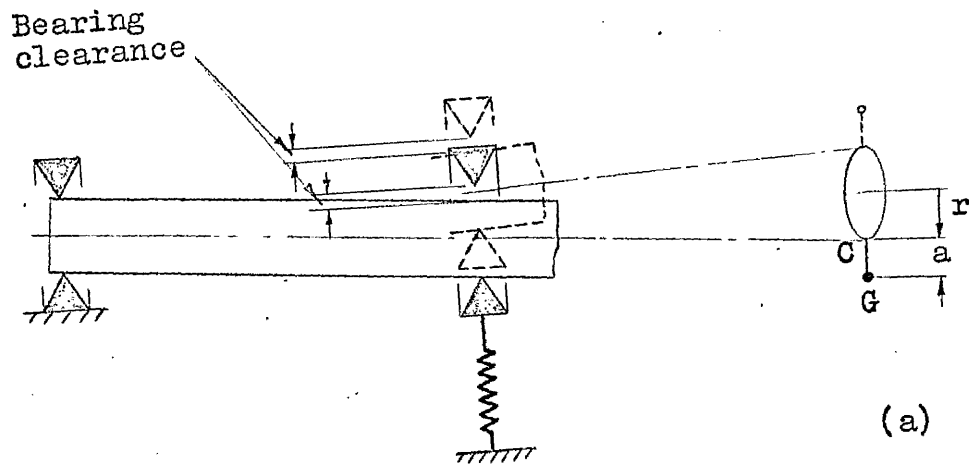
Fig.8.10   Idealised H.P. shaft with sprung
rear bearing with clearance.
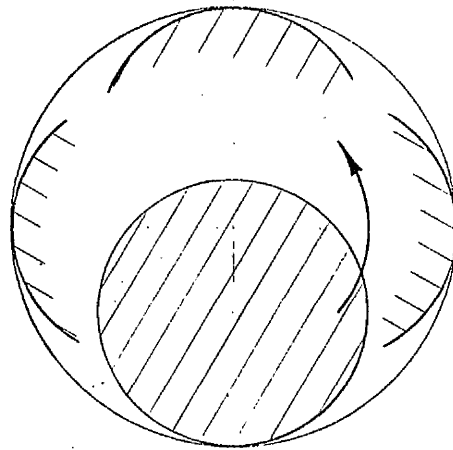
Fig.8.11

Fig.8.11(a)   Shaft maintaining contact with
bearing throughout rotation.
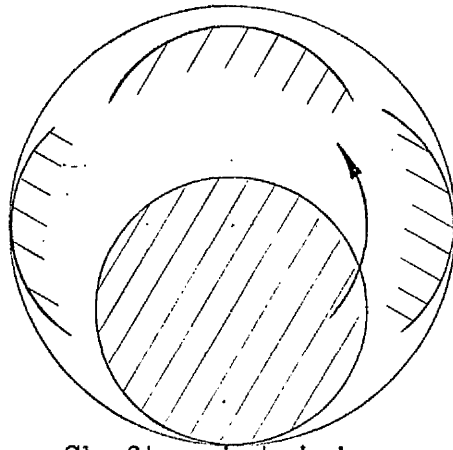
Fig.8.11(b)   Shaft maintaining contact with bearing
throughout only part of rotation.
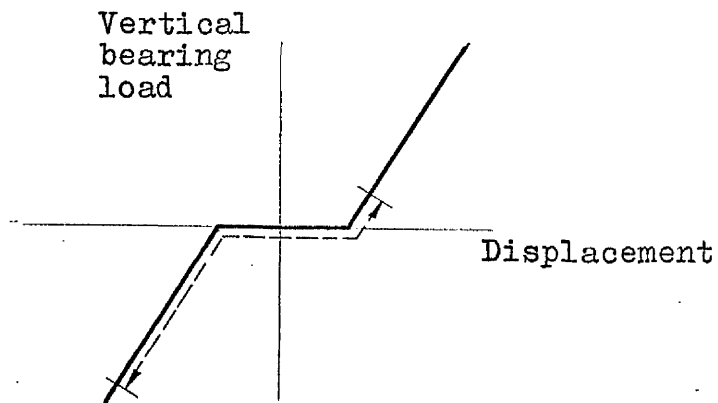
Fig.8.11(c)   Load displacement characteristic of
sprung bearing with clearance.

Fig.8.12

Force
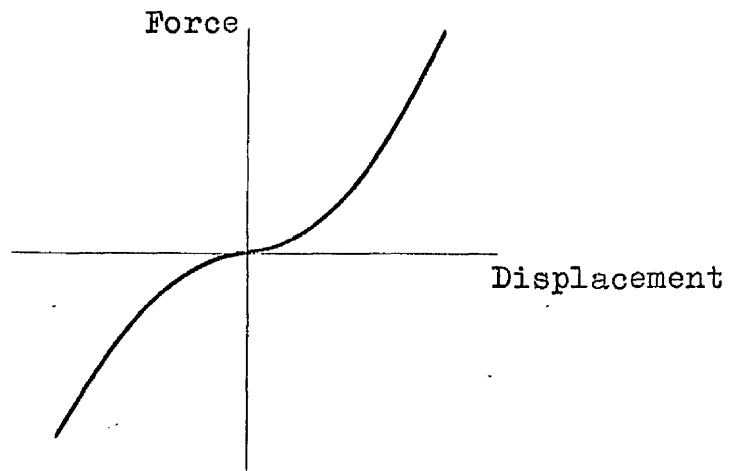
Displacement

<u>Fig.8.12(a)</u>   Force/displacement characteristic $x + \varepsilon x^3$

Amplitude

1 ω
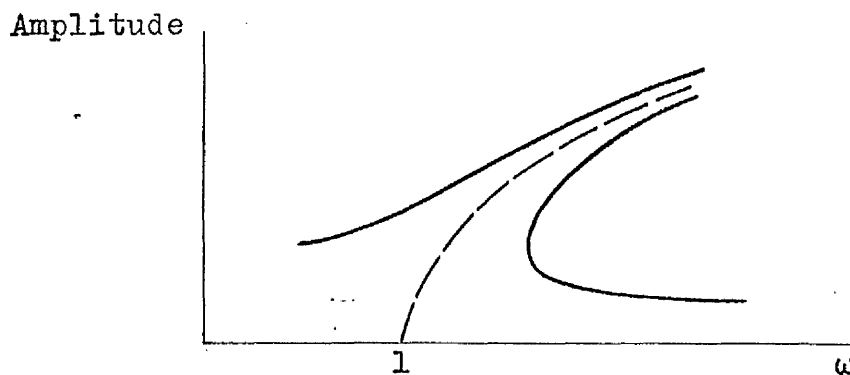
<u>Fig.8.12(b)</u>   Response of system to harmonic excitation
with no damping.

Amplitude

A
D
C
B
1 ω
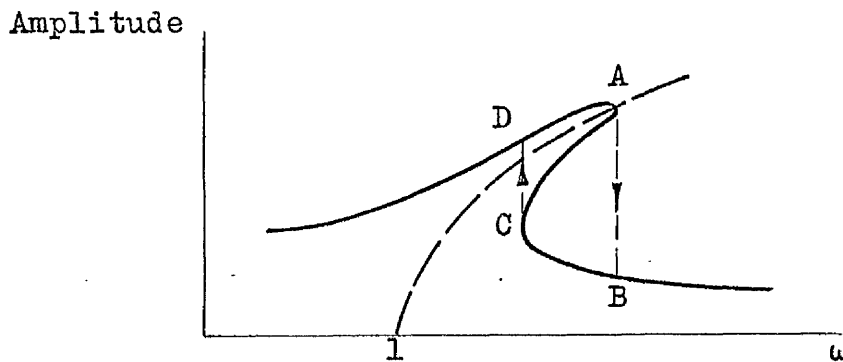
<u>Fig.8.12(c)</u>   Response to harmonic excitation with damping
present, showing 'jump phenomena'.
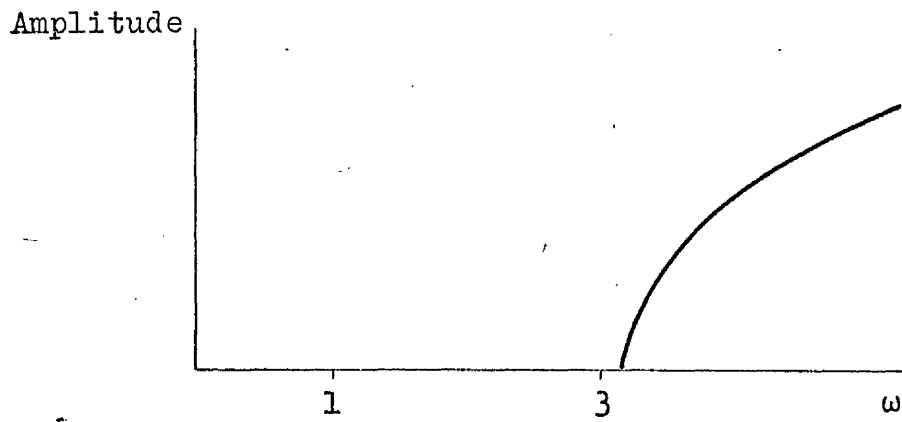
Fig.8.13

Fig.8.13(a) $^1/3$ Subharmonic response without damping
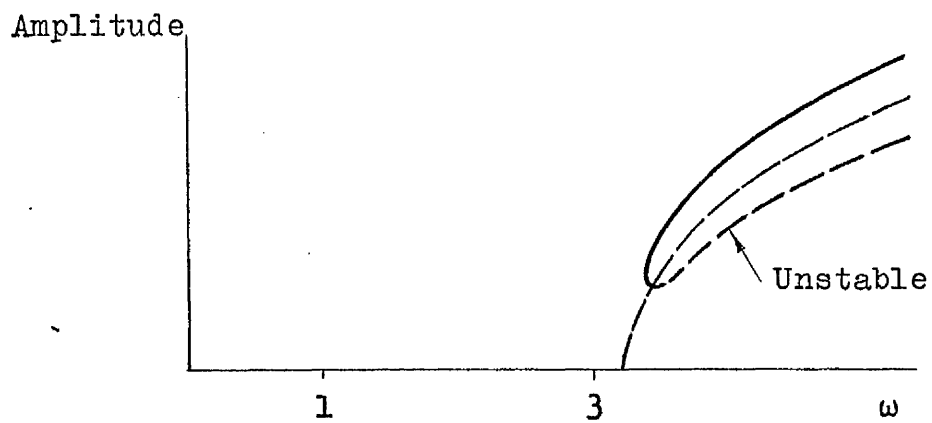
Fig.8.13(b) $^1/3$ Subharmonic with damping
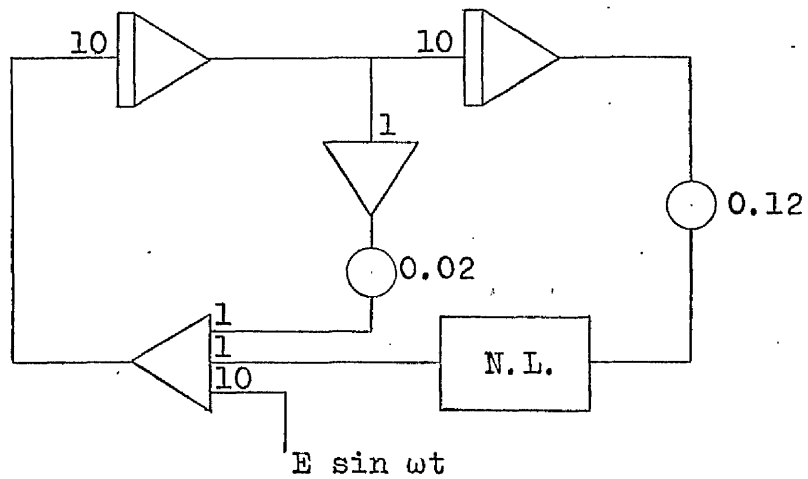
Fig.8.14

Fig.8.14(a)   Analog computer circuit
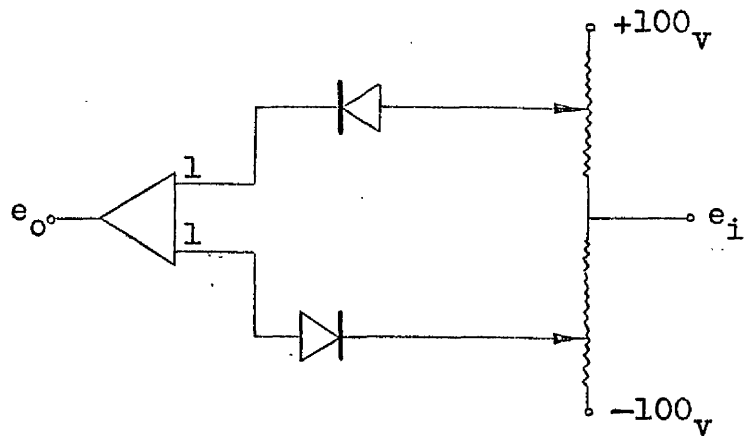
Fig.8.14(b)   Circuit of non-linear element
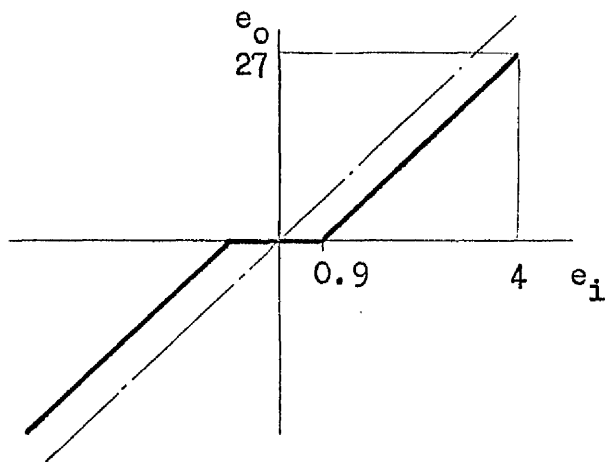
Fig.8.14(c)   Non-linear characteristic
represented by non-linear
element

CHAPTER 9

VARIATION OF THE FREQUENCIES OF THE RIG

WITH SPEED AND SENSE OF THE ROTATION OF THE SHAFTS

SUMMARY

The rig is now regarded as having several frequencies, some of which are characterised by relatively large displacement of one shaft, and each may be excited by the unbalance of either shaft.   The variation of a particular frequency with the shaft speeds can be conveniently represented by a 3-dimensional plot in which the frequency is always positive while the shaft speeds may be positive or negative.

The predicted variation of two lowest frequencies (formerly called H.P. and L.P. whirling speeds) with shaft speeds up to 4000 rpm are presented together with experimental confirmation of the results.

The variation of these two frequencies, and the frequencies of three higher modes of vibration, with shaft speeds up to 12000 rpm are described.   Some limited experimental results show that the computer predictions of the higher frequencies are reasonable.

CHAPTER 9

VARIATION OF THE FREQUENCIES OF THE RIG

WITH SPEED AND SENSE OF THE ROTATION OF THE SHAFTS

9.1   Introduction

The work described in preceding chapters showed that
a reasonably faithful simulation of the rig had been
achieved on the computer.   An examination of the influence
of the rotation of the rotors (both sense and magnitude) on
the frequencies and modes of vibration of the complete rig
could now be made.

Since the vibrational behaviour of the rig depends
on the magnitude and sense of both shaft rotations, it is
no longer correct to use the terms 'forward' or 'reverse
whirling speeds'.   Instead the rig will be regarded as
having several modes of vibration at frequencies, λ_1,
λ_2, λ_3 ..... , each affected to some degree by the speeds
of the shafts.   Some may be characterised by relatively
large motion of one of the rotors.

A particular frequency, λ, will be a function of the
speeds of the H.P. and L.P. shafts, which, for brevity, will
now be called simply H and L, respectively.   The variation
of λ with H and L may be represented as a surface in a
3-dimensional diagram, as shown in Fig.9.1(a).   In this
representation the value of λ is <u>always</u> considered to be
<u>positive</u>.   If a shaft speed, say H, is positive then the
rig is considered to whirl in the same sense as the H.P.
shaft (and to whirl opposite to the H.P. shaft if H is
negative).

In Fig.9.1(a) a plane is shown, passing through the
H-axis, which contains all points at which λ = L.   This

plane will intersect the frequency surface, and the line
of intersection will therefore appear as line AB in the
plan view shown in Fig.9.1(b). When the shaft speed
reaches the value corresponding to a point on this line,
then the rig will be excited, at the frequency λ, by
unbalance of the L.P. rotor.

By similar reasoning another line exists on the
frequency surface, on which $\lambda = H$, shown as CD in
Fig.9.1(b). If the shaft speeds correspond to a point
on this line, excitation at frequency λ (= H) will be
caused by unbalance of the H.P. rotor. (The particular
rotor speed combination existing at the intersection of AB
and CD, (L = H = λ), was used to check the forward whirling
speed prediction in earlier work). The ratio, H/L, of the
rotor speeds obtained in twin spool jet engines varies
throughout the speed range (see Chapter 1). The working
line of such an engine may therefore resemble line P Q R S
in Fig.9.1(b). Vibration will therefore be induced by
unbalance of the H.P. rotor when the shaft speeds reach the
value corresponding to that at point Q, and similarly by
unbalance of the L.P. rotor when the speeds reach the value
obtained at point R.

The question now arises whether the other quadrants
of Fig.9.1(b) are significant. In the third quadrant,
(L and H both negative), similar argument will produce two
shaft speed combinations at which the rig or engine will
vibrate but precess in an opposite sense to that of the
shafts (corresponding to the reverse whirl of a single
shaft).

If the shafts rotate in opposite directions, as
perhaps in a vertical take-off engine, then unbalance of
the L.P. rotor will cause resonance when the shaft speeds
correspond to a point on the line AB in the quadrant where
L is positive, and H is negative. Similarly, excitation
due to unbalance of the H.P. rotor will cause resonance

when the speeds correspond to a point on the line CD, in the quadrant where H is positive and L is negative.

The variation of the lowest two frequencies, λ_1 and λ_2, was explored over a range of rotor speeds which could be obtained on the rig. The investigation was then extended to higher speeds, using the computer. Three higher modes of vibration, at frequencies, λ_3, λ_4 and λ_5, were also explored on the computer and attempts were made to verify these on the rig.

9.2   Variation of λ_1 at low shaft speeds

Although both shafts could be driven at speeds up to 6000 rpm, it seemed advisable to restrict the experimental study of the variation of λ_1 and λ_2 to shaft speeds below 4000 rpm to avoid the ranges in which severe vibration occurred apparently due to non-linear effects.

The computer model of the rig was used to predict the variation of λ_1 for values of H and L from $-$ 4000 to $+$ 4000 rpm. The results were found to be illustrated concisely by plotting λ_1 versus H, as shown in Fig.9.2. The value of λ_1 varied considerably with H, but was independent of L until the latter reached large negative values.

The results were checked on the rig by fixing the H.P. shaft speed, H, and running the L.P. shaft, in either sense, at a speed at which large amplitude of the discs was observed. (The conditions covered are indicated in the small sketch of the plan view of the λ, H, L, diagram). Although the computer model of the rig had been shown to underestimate this frequency by about 4°/o, the results show that the computer predicts faithfully the variation of λ_1 with H.P. rotor speed. The variation of λ_1 with L was predicted to be small. This was confirmed by setting the L.P. speed of the rig and noting the H.P. speed at which large amplitudes of the discs were observed. (The conditions explored are

indicated in the small sketch in Fig.9.3). The
experimental results, shown in Fig.9.3, confirm the
negligible variation of λ_1 with L which had been predicted.

The predicted mode of vibration of the rig when
H = L = 0 is shown in Fig.9.4. The modes occurring at
other combinations of rotor speeds were similar, and are
summarised by the plot of A_H/A_L shown in Fig.9.5. (A_H
now denotes amplitude of vibration of the H.P. disc, while
A_L denotes the amplitude of the L.P. disc). The amplitude
of the H.P. disc is large compared with that of the L.P.
disc. The ratio of the amplitudes appears to be mainly
affected by the L.P. shaft speed.

During the tests conducted to verify the variation
of λ_1 with shaft speeds, the amplitudes of the discs were
recorded. The results are illustrated in Figs.9.6 and
9.7. The unbalance of the H.P. rotor was small since it
exhibited an amplitude of only 0.002 in when H = λ_1 and
L = 0 (i.e. the H.P. 'forward whirling speed'). The L.P.
rotor had a greater degree of unbalance achieving an
amplitude of 0.014 in when L = λ_2 and H = 0 (i.e. at the
L.P. 'forward whirling speed'). The tests illustrated in
Fig.9.6 were therefore the result of relatively strong
excitation by the L.P. rotor and do resemble the predicted
fall of A_H/A_L with increasing H. But the tests (with
excitation by the H.P. disc unbalance) illustrated in
Fig.9.7, do not show the more marked fall of A_H/A_L which
the computer model had predicted. However, the observed
amplitude of the L.P. rotor, A_L, in all these tests was
seldom greater than 0.001 in. Amplitudes less than this
value could not be recorded with accuracy since the
variation of circularity of the disc periphery was of
this order.

9.3 Variation of λ_2 at low shaft speeds

The computer model was used to predict the variation of λ_2 for values of H and L from $-$ 4000 to $+$ 4000 rpm. The magnitude of λ_2 varied little with H and therefore the results could be expressed very simply as a plot of λ_2 versus L, as shown in Fig.9.8.

The tests conducted to verify the predicted variation of λ_2 with L, produced the results shown in Fig.9.8. Similar tests to confirm the predicted independence of λ_2 with H are shown in Fig.9.9. The results confirm the accuracy of the computer model.

The predicted mode of vibration at frequency λ_2, when H = L = 0, is shown in Fig.9.10. The modes at other combinations of L and H were similar and are summarised by the plot of A_L/A_H versus L and H shown in Fig.9.11.

The amplitudes of the discs during the tests conducted to determine the variation of λ_2 with L produced the values of A_L/A_H plotted in Fig.9.12. The ratio A_L/A_H rises with L at a rate similar to that predicted by the computer model.

The ratio of the disc amplitudes recorded when the variation of λ_2 with H was examined was found to be almost constant as shown in Fig.9.13.

9.4 Extended study of vibration at frequency λ_1

An examination of the variation of λ_1 when the shaft speeds were varied up to 12000 rpm was conducted on the computer. The results are shown plotted in Fig.9.14(a) together with an isometric view of the frequency surface, Fig.9.14(b).

The value of λ_1 continues to be influenced by the H.P. shaft speed, H, and under most conditions insensitive to the L.P. rotor speed, L. But when the shafts rotate

in opposite directions the frequency of whirl in the same sense as the rotation of the H.P. shaft, ($\lambda_1 = + H$), falls rapidly as the L.P. shaft speed increases.

Examination of the predicted modes of vibration over the ranges of L and H from − 12000 to + 12000 rpm appeared to show rather perplexing changes. The computer model had been designed to produce the modes in the form of a list of displacements of the elements of the rig when the front bearing had unit positive displacement. This unusual presentation of the results had been adopted in the early development of the computer model to assist in the detection of programming errors.

The computed modes (some 49, at speed intervals of 4000 rpm) were plotted as small sketches in the H, L plane as shown in Fig.9.15. The apparently anomalous behaviour of the modes was resolved by normalising the modes by dividing each displacement by the largest, which in most cases was the deflection of the H.P. disc. A more concise statement of the change in the modes was found to result if the ratio of the H.P. and L.P. disc displacements, A_H and A_L, was plotted versus the shaft speeds, as in Fig.9.16. The main conclusions which may be drawn from this plot are as follows − when both shafts rotate in the same direction the rig may be induced to whirl in the same sense by the unbalance of either shaft when its speed reaches λ_1 (conditions + L + H in Fig.9.16(a)). The mode of vibration will then be characterised by relatively large displacement of the H.P. rotor and resemble the mode of vibration when L = 0, H = 0, shown again in Fig.9.17(a).

If the shafts rotate in opposite directions the rig may be induced to whirl in the same sense as the rotation of the L.P. shaft by its unbalance (conditions, + L, − H in Fig.9.16(a)). The character of the mode will be still similar to that for L = 0, H = 0.

If the shafts still rotate in opposite directions
the rig may also be induced to whirl, at a different value
of λ_1, in the same direction as the H.P. shaft by its
unbalance (conditions − L, + H, in Fig.9.16(b)).   But now,
rather surprisingly the mode of vibration changes markedly
to one characterised by relatively large displacement of
the L.P. shaft − a typical mode, for L = −12000, H = +12000
being shown in Fig.9.17(b).

9.5   Extended Study of Vibration at λ_2

An examination on the computer of the variation of
λ_2 with shaft speeds up to 12000 rpm produced the results
plotted in Fig.9.18(a), also illustrated in an isometric
view of the frequency surface in Fig.9.18(b).

The value of λ_2 continues to be influenced to a large
degree by the rotation of the L.P. shaft.   But when the
shafts rotate in opposite directions λ_2 is influenced
considerably by the speed of the H.P. shaft.

When the predicted modes of vibration were compared
it was found that the change in character of the modes
could be conveniently expressed in the same way as had been
done with the lower frequency λ_1.

When the shafts rotate in the same direction, the rig
may be induced to whirl in the same direction by the
unbalance of either shaft when the speed reaches the
appropriate value of λ_2.   Fig.9.19(a) shows that under
these conditions (both L and H positve) the mode will be
characterised by relatively large displacement of the L.P.
shaft and generally similar to the mode at L = H = 0
repeated in Fig.9.20(a).

If the shafts rotate in opposite directions,
excitation by unbalance of the L.P. shaft will cause whirl
in which the displacement of the L.P. rotor may become
relatively larger (conditions, + L, − H, in Fig.9.19(a)).

But, when the shafts still rotate in opposite directions, and the speed of the H.P. shaft approaches the appropriate value of λ_2, its unbalance will cause the rig to whirl in the same sense as the H.P. shaft. Fig.9.19(b) then shows that the mode of vibration will change markedly to one characterised by relatively large displacement of the H.P. rotor and resemble that shown in Fig.9.20(b) which occurs when H = 12000, L = —12000.

9.6   Vibration at Frequency λ_3

The predicted variation of λ_3, the frequency of the next higher mode of vibration, is shown plotted versus H and L in Fig.9.21(a).   An isometric view of the λ_3 surface is shown in Fig.9.21(b).

When the shafts rotate in the same direction the variation of frequency of whirl in the same sense is not affected greatly by the speed of the shafts (conditions L +, H +).   But the frequency of whirl in the opposite sense (conditions L —, H —) falls very rapidly with increasing H.P. shaft speed.

When the shafts rotate in opposite directions the frequency at which unbalance of the L.P. shaft would excite whirl (conditions L +, H —) falls rapidly with H.   On the other hand the frequency at which unbalance of the H.P. shaft would cause excitation (conditions L —, H +) falls with increasing L.

An attempt was made to check the predictions by shaking the rig with an electromagnetic vibrator mounted above the front plate of the casing.   When both shafts were stationary resonance was observed at a frequency of 5460 c/min, which agreed well with the computed value of 5429 c/min.   The observed mode of vibration, indicated in Fig.9.22, showed striking agreement with the predicted mode.

When the L.P. shaft was rotating at 4000 rpm, resonance was produced at frequencies of 5280 and 5860 c/min. These frequencies appeared to correspond with the predicted values of 5066 ($L = -\lambda_3$, $H = 0$) and 5580 ($L = +\lambda_3$, $H = 0$) c/min. Extrapolation of the experimental frequencies suggested that the rig would be expected to vibrate synchronously in a reverse whirl sense when the L.P. shaft speed reached a value of 5240 rpm. In the survey of the whirling behaviour of the L.P. shaft (described in section 8.2) it was noted that such whirling had been observed at 4959 rpm.

When the rig was excited by the vibrator with the H.P. shaft rotating at 4000 rpm (while the L.P. shaft was stationary), resonance was observed at 5050 and 5720 c/min. These frequencies appeared to correspond to the predicted values of 4569 and 5491 c/min. Extrapolation of the experimental frequencies suggested that the H.P. shaft should have induced synchronous reverse whirl of the rig when the H.P. speed reached 4950 rpm. However, this behaviour seemed to have been hidden within the non-linear region of vibration of H.P. shaft (section 8.3).

The predicted mode of vibration of the rig when both shafts were stationary is shown in Fig.9.22. Both discs show relatively little displacement compared with that of the front bearing. The agreement with the experimental mode can be seen to be satisfactory.

An examination of the modes of vibration predicted at various combinations of shaft speeds produced the variations of A_L and A_H with L and H shown in Fig.9.23. (A_L and A_H now being referred to unit positive displacement of the front bearing).

When the shafts rotated in the same direction, and whirl of the rig was in the same sense, (conditions L +, H +), the mode of vibration was very similar to that shown in Fig.9.22.

But when the rig whirled in an opposite direction to the H.P. shaft ($\lambda_3 = -$ H, with L + or $-$) the H.P. shaft displacement was predicted to be relatively large compared with other parts of the rig. The mode for the condition L = + 12000, H = $-$ 12000 rpm shown in Fig.9.24 was typical of the modes under these conditions.

When the shafts rotate in opposite directions, and the rig whirls in the same sense as the H.P. shaft (conditions H +, L $-$) the mode changed to one which was characterised by relatively large displacement of the L.P. rear bearing, associated with considerable movement of the L.P. disc. The mode at the conditions L = $-$ 12000, H = + 12000 rpm, shown in Fig.9.25, was typical.

9.7   Vibration at Frequency λ_4

The predicted variation of the frequency λ_4, of the next highest mode of vibration, is shown plotted versus L and H in Fig.9.26(a) and isometrically in Fig.9.26(b).

The results show that when the shafts rotate in opposite directions the rig may vibrate in the same sense as the L.P. shaft, or in the same sense as the H.P. shaft, at frequencies which are not in general far from the frequency of 6380 c/min exhibited when the shafts are stationary.

But when the shafts rotate in the same direction the rig may vibrate at two widely separated frequencies, of the order of 8000 and 5000 c/min in the same or opposite sense respectively.

When the rig, with both shafts stationary, was shaken by a vibrator connected to the front plate, it was found to resonate at 6600 c/min, a value which compared well with the predicted value of 6380 c/min. But when either shaft was driven at a speed of 4000 rpm, resonance was not found to occur at any frequency which could be related to the predicted values.

The predicted mode of vibration at λ_4 when both shafts are stationary, is shown in Fig.9.27(a). The agreement of the measurements made during the resonance test is very good. Considerable bending of the shafts is evident although the disc movement is relatively small.

The mode of vibration when both shafts rotate in the same direction and the rig whirls in the same sense, is typified by that predicted for L = + 12000, H = + 12000 rpm, shown in Fig.9.27(b). The bending of the casing is now more apparent.

The predicted mode of vibration when the rig vibrates at λ_4 with the shafts rotating in opposite directions was in general similar to that shown in Fig.9.27(c) where both shafts are rotating at 12000 rpm. Once again there is considerable bending of both shafts with only minor movement of the discs.

When the shafts rotate in the same direction the rig may whirl in an opposite sense. The mode predicted for these conditions was similar to that shown in Fig.9.27(c) but the largest displacement was at the L.P. rear bearing.

9.8   Vibration at Frequency λ_5

The predicted variation of the frequency λ_5, of the highest mode of vibration which was examined, is shown graphically in Fig.9.28(a) and isometrically in Fig.9.28(b).

The results show that the frequency at which the rig will whirl is influenced mainly by the speed of the shaft which is rotating in the same sense, particularly if the shafts are contra-rotating. The frequency λ_5 is nearly always separated from the lower frequency λ_4 by at least 1000 c/min but when the shafts rotate in the same sense at almost the same speed the separation of λ_4 and λ_5 falls to only about 500 c/min (e.g. at L = H = + 12000, λ_4 = 8964 while λ_5 = 9434).

When the rig was excited by the vibrator connected to the front plate, it was found to resonate at a frequency of 7580 c/min which compared well with the predicted value of 7400 c/min.   The measured mode showed striking agreement with the predicted mode plotted in Fig.9.29(a).

When the rig was excited with the H.P. shaft rotating at 4000 rpm, resonance was recorded at 7040 and 8500 c/min, which appeared to correspond with the predicted values of 7279 and 8333 c/min for the conditions $H = -$ and $+ 4000$ rpm, $L = 0$.

When the L.P. shaft was rotating at 4000 rpm, while the H.P. shaft was stationary, resonance was observed at 7450 and 7900 rpm.   These frequencies appeared to correspond to the predicted values of 6895 and 8274 c/min for the conditions $H = 0$, $L = -$ or $+ 4000$ rpm.   Thus the observed variation of λ_5 with L appeared to be less than the predicted variation, as had also been found to be the case when the rig vibrated in the λ_3 mode (section 9.6).

The predicted mode of vibration when both shafts are stationary is shown in Fig.9.29(a).   Considerable bending of both shafts was evident, with the front bearing showing the largest displacement.   The discs, however, showed only minor displacement.

Examination of the modes of vibration at other combinations of shaft speeds showed that when the rig whirled in an opposite sense to the H.P. shaft the modes were remarkably similar to the above (at $L = H = 0$), until the L.P. shaft reached very high speeds in the same sense as the whirl.

When the L.P. shaft rotated at speeds greater than 4000 rpm, and the whirl was in the same sense, the character of the mode changed slightly to one in which the bending of the L.P. shaft was the major feature, as typified by the mode at $L = 12000$, $H = 0$, shown in Fig.9.29(b).

When the rig whirled in the same sense as the
H.P. shaft the mode of vibration changed to one in which
there was relatively small movement of the L.P. and H.P.
shafts but considerable bending of the casing centred about
the front plate.   A typical mode, for the condition
H = + 12000, L = 0, is shown in Fig.9.29(c).

9.9   Conclusions

When the single rotor system treated in Section 1.3
is regarded in the manner adopted in this chapter, it has
two natural frequencies which rise as the rotor speed
increases from large negative values, through zero to large
positive values.   The investigation of a two rotor system
shows that it displays a similar trend — each frequency
rises to a greater or lesser extent with each rotor speed,
as shown in Figs. 9.14, 9.18, 9.21, 9.26 and 9.28.

A feature which is not obvious in these diagrams is
the close approach of some frequencies at certain com-
binations of shaft speeds.   The most notable example of
this condition was found to occur when the shafts were
rotating in opposite directions.   Since λ_1 increases most
rapidly with H, while λ_2 increases markedly with L, the two
frequencies approach in the region where H is positive while
L is negative, as suggested by the isometric views shown in
Figs. 9.14(b) and 9.18(b).   The condition is shown more
clearly in an alternative presentation of the computer
predictions shown in Fig. 9.30.   The frequencies λ_1 and
λ_2, which were computed at intervals of 4000 rpm (in H and
L) are placed on a grid map of the HL plane.   The results
shown in Fig. 9.30 show clearly that the two frequencies
λ_1 and λ_2 approach to within about 100 rpm at certain
combinations of shaft speeds (e.g. at H = 8000,
L = − 4000).

Formerly it has been usual to regard whirling as
the occurrence of severe vibration when the speed coincides
with the natural frequency of the rotor (fractional and
reverse whirls were noticed long ago but did not appear to
result in serious vibration.)   However, in a two rotor
system either rotor may be induced to whirl when the speed
of the other rotor coincides with its natural frequency.
The conditions under which excitation of the present system
would occur due to unbalance of each rotor is shown in
Fig. 9.31 (the computed version of the diagram sketched in
Fig. 9.1(b)).   The full lines are loci of points at which
H coincides with λ_1, λ_2, λ_3, λ_4 and λ_5, and as a result
vibration would be induced by unbalance of the H.P. rotor.
Similarly, the dashed lines show the loci of points at which
unbalance of the L.P. rotor would excite vibration.

A hypothetical jet engine shaft speed characteristic
has been superimposed on Fig. 9.31 as chain dotted lines.
The characteristic drawn in the top right quadrant is for
an engine in which the shafts rotate in the same direction.
At each intersection of the characteristic with the
frequency loci vibration will be induced by the appropriate
rotor.   At point Q the system will be excited by the
unbalance of the H.P. rotor, rotating at a speed equal to
λ_2, while at R excitation is caused by the L.P. rotor
rotating at a speed equal to the current value of λ_2.
Thus each mode of vibration is encountered twice in a two
rotor system.   If the engine characteristic had been a
little higher then points Q and R would coincide and it
would be possible for the unbalance of each rotor to excite
whirl of the system at frequency λ_2.

The same engine characteristic has also been drawn
in the top left and lower right quadrants to indicate the
critical points for a contra-rotating shaft system.   Since
each frequency falls with the speed of the shaft which

rotates in opposite sense to the whirl, the characteristic now crosses the λ_4 lines. Thus it would appear that more critical points of vibration are likely to be encountered in the speed range of a contra-rotating shaft engine.

The modes of vibration which were predicted by the computer, and confirmed to an extent by experimental observations, showed that a two rotor system was likely to possess some unusual changes in modes of vibration. Originally the frequencies λ_1 and λ_2 were regarded as H.P. and L.P. rotor frequencies since the modes showed relatively large displacements of the respective rotors.

The lowest frequency of vibration, λ_1, produced modes of vibration which showed large displacement of the H.P. rotor under most conditions. But when the shafts rotated in opposite directions relatively large displacement of the L.P. rotor could be produced by excitation due to the H.P. rotor (conditions H + , L −).

Vibration at frequency λ_2 usually showed relatively large movement of the L.P. rotor, but again when the shafts rotated in opposite directions and vibration was induced by the H.P. rotor (conditions H + , L −) the mode changed to one displaying large movement of the H.P. rotor.

The mode of vibration at frequency λ_3 showed considerable bending of the shafts with little movement of the discs. Again it seemed that changes in modal shape were most marked when the shafts rotated in opposite directions.

Vibration at frequency λ_4 was also characterised by modes in which there was considerable bending of the shafts. But now the shafts were bent in opposite directions which, in practice, might result in shaft rubbing.

The mode of vibration at λ_5 showed no great change in character with rotor speeds but was notable in showing more marked distortion of the casing.
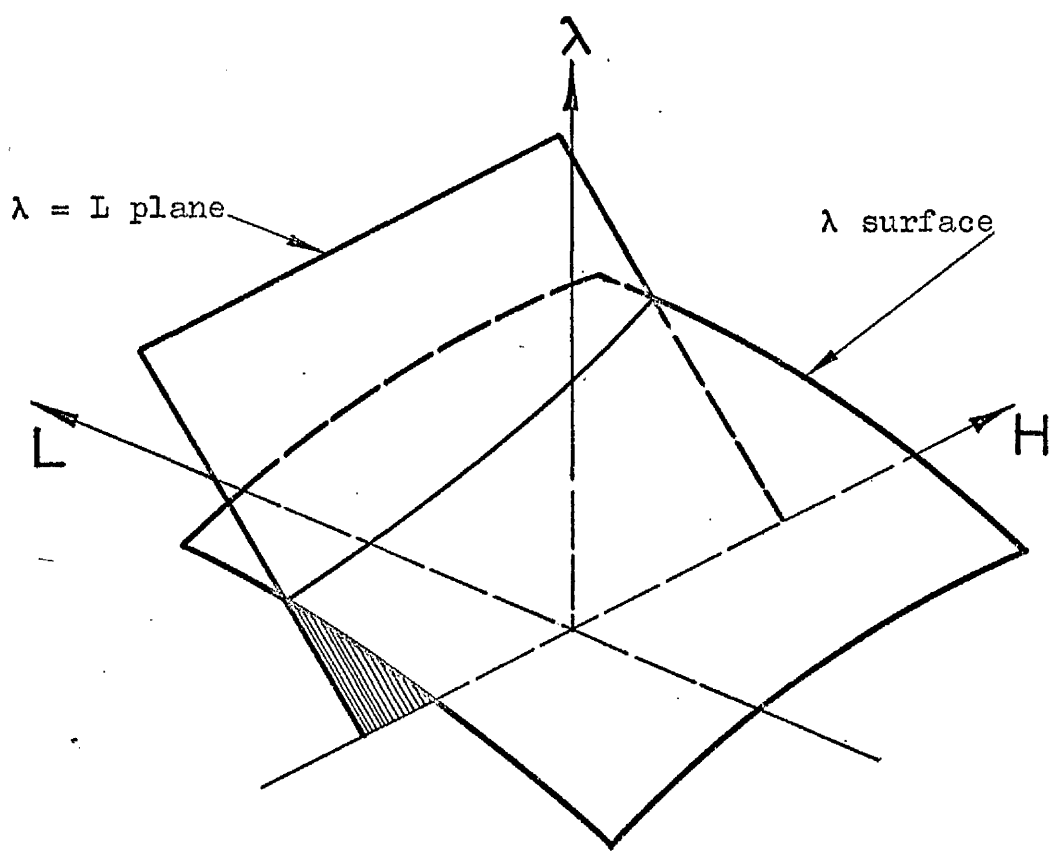
Fig.9.1

Fig.9.1(a) Representation of variation of frequency λ with shaft speeds H and L.
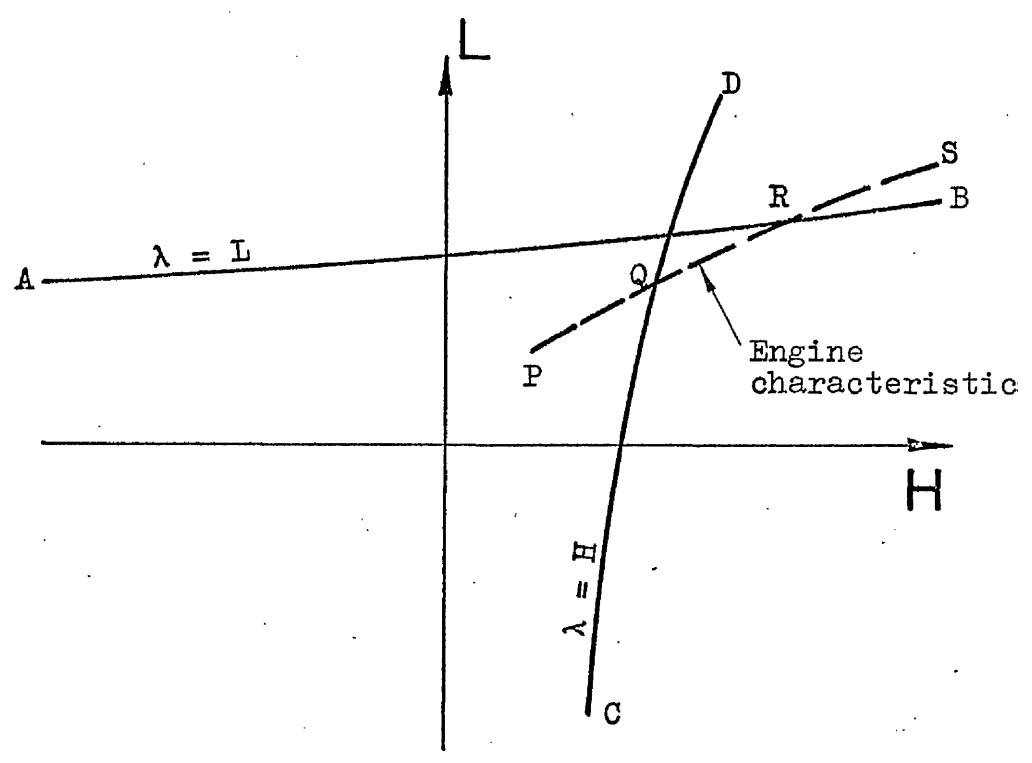
Fig.9.1(b) Plan view of Fig.9.1(a).
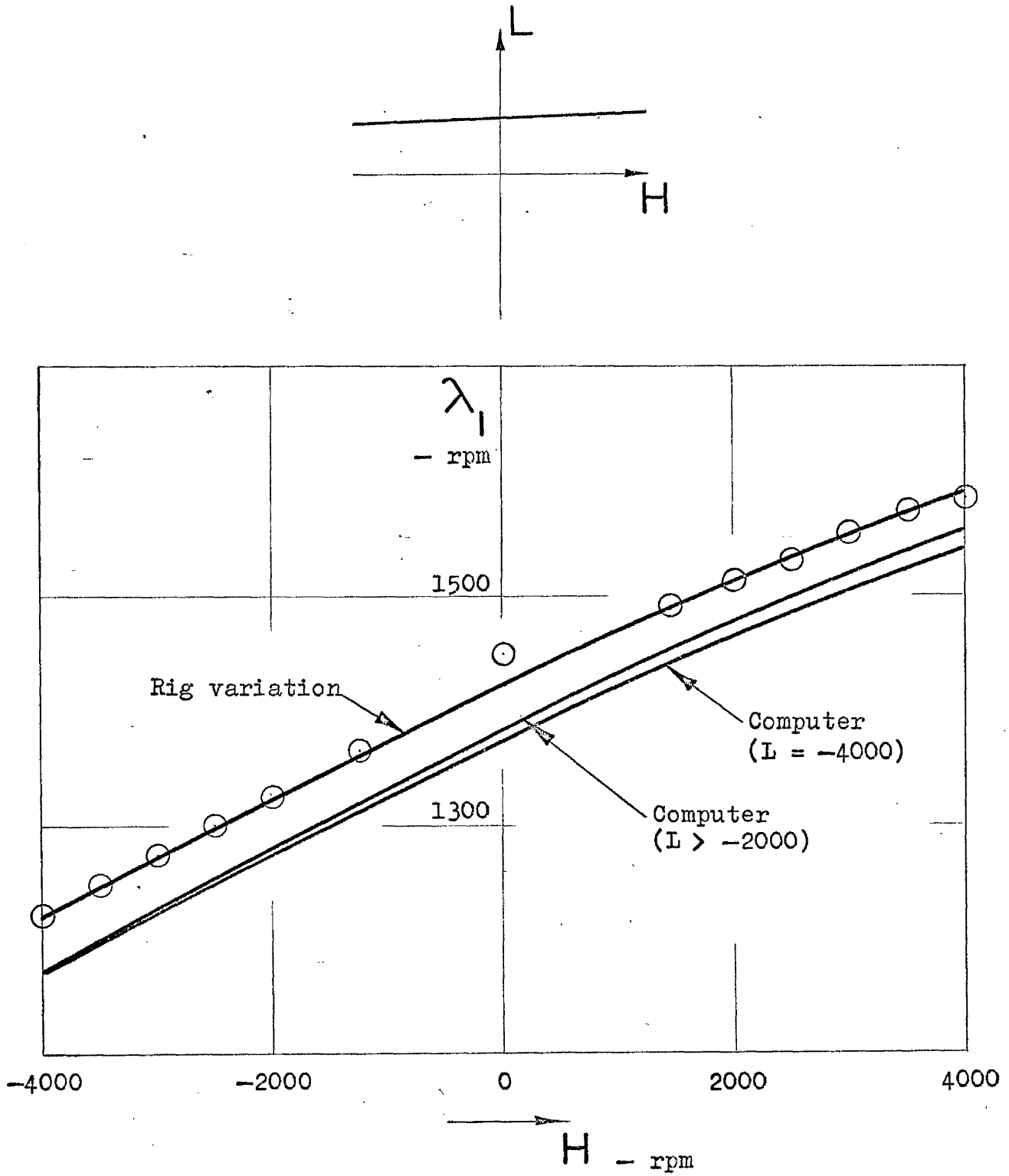
Fig.9.2

Fig.9.2   Variation of λ_1 with H and L
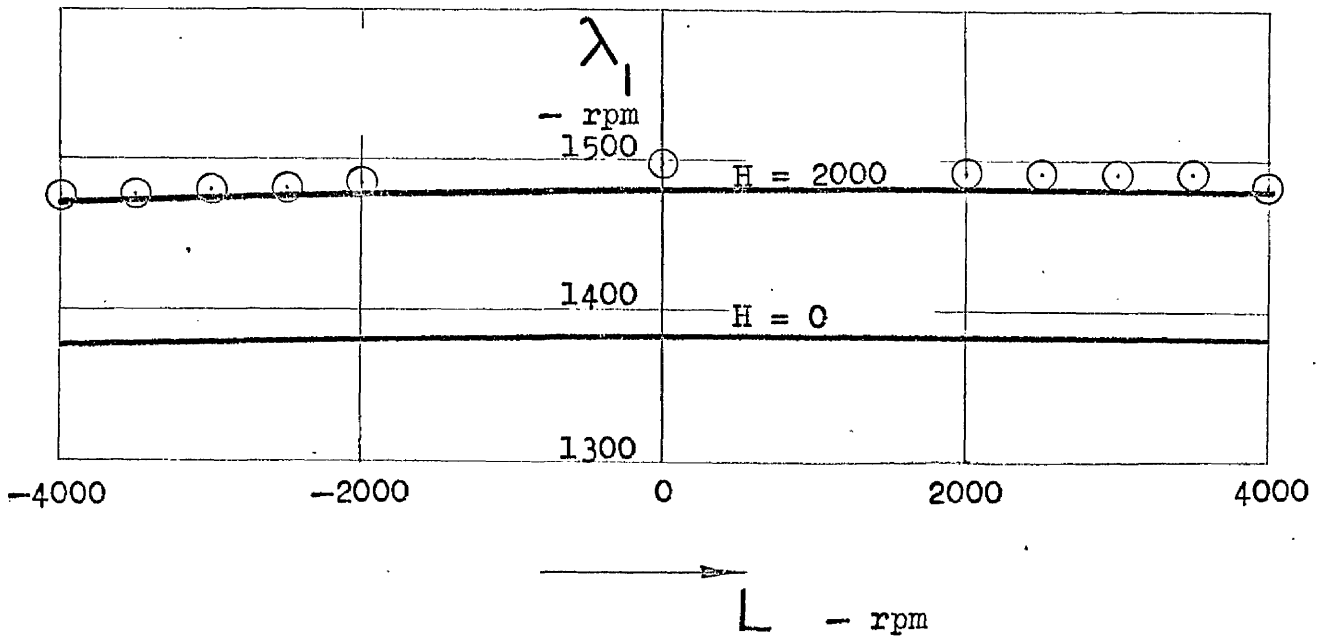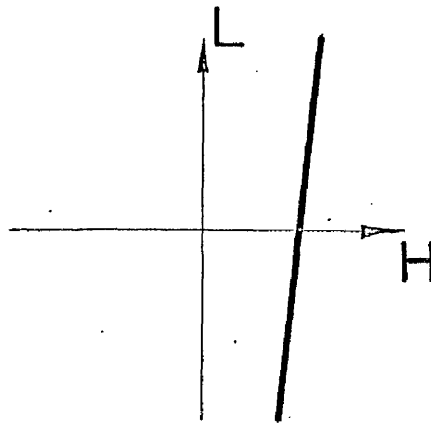
Fig.9.3

Fig.9.3   Variation of λ_1 with L
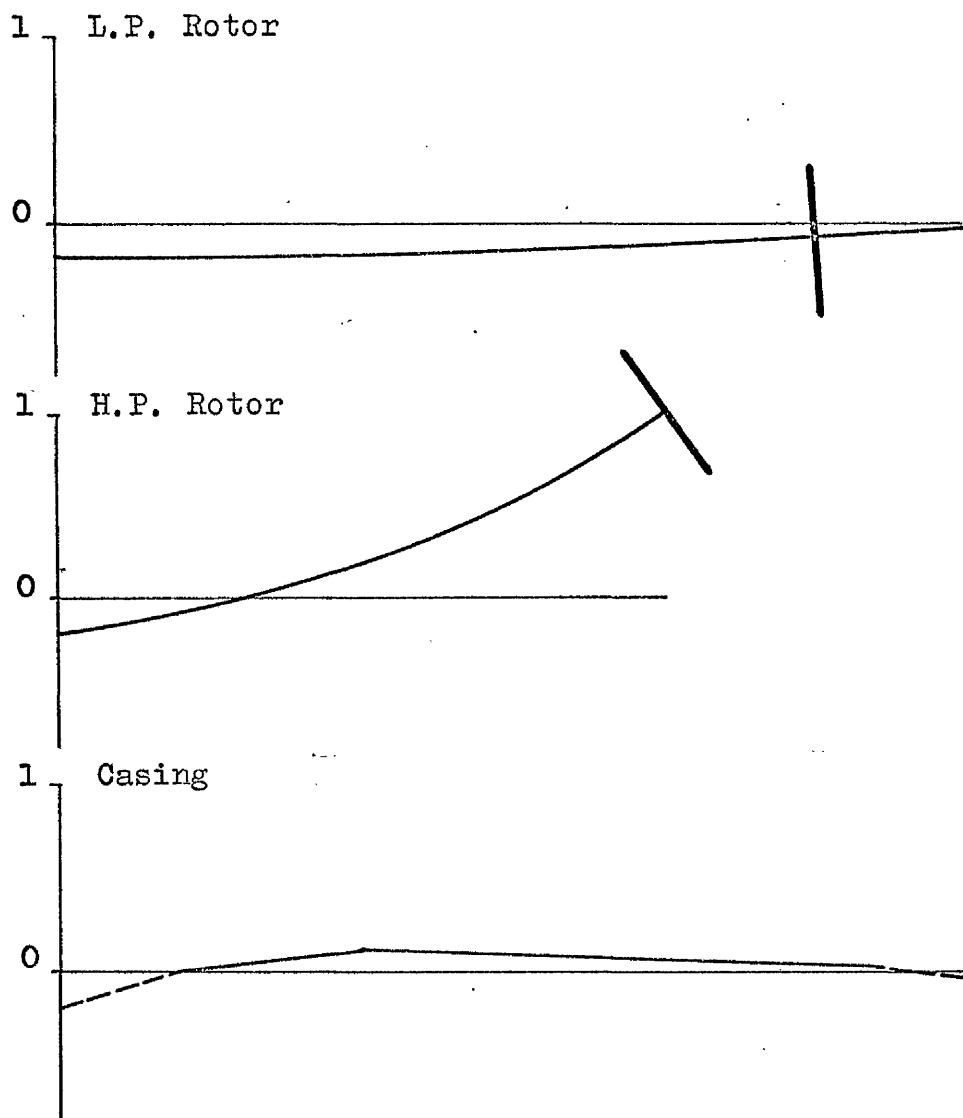
Fig.9.4

Fig.9.4   Mode of vibration at λ_1
when H = L = 0.
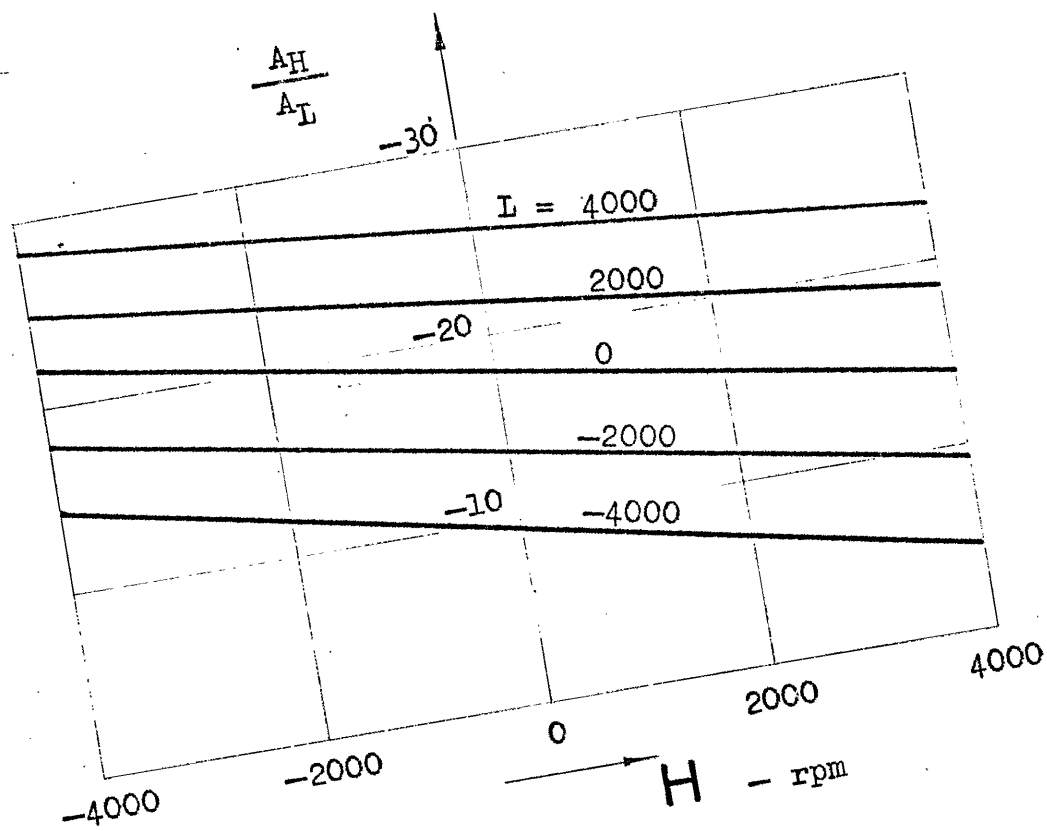
Fig.9.5

Fig.9.5   Ratio of disc amplitudes
A_H/A_L v. H and L
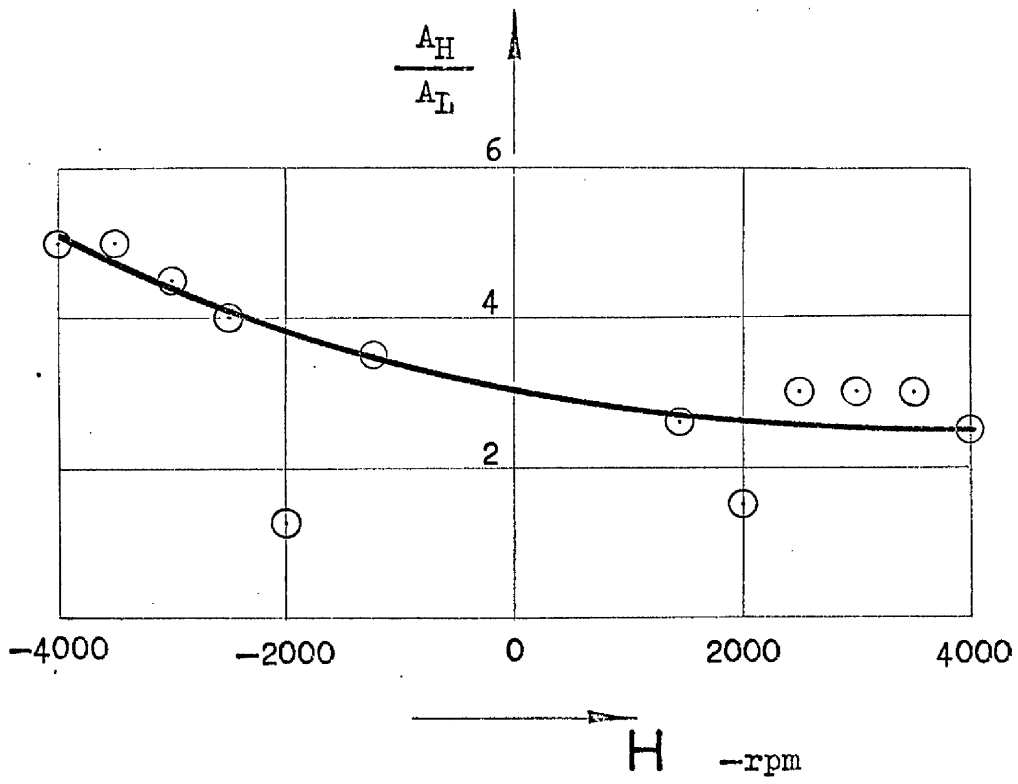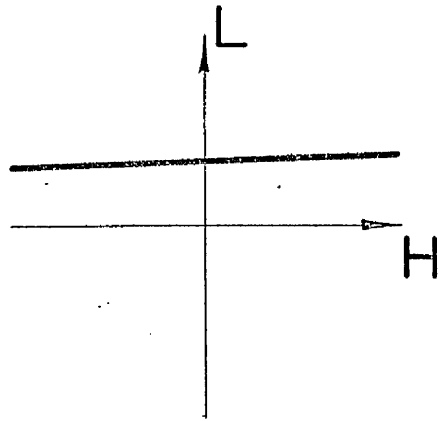
Fig.9.6

Fig.9.6   Ratio of disc amplitudes, A_H/A_L, observed when $L = \lambda_1$
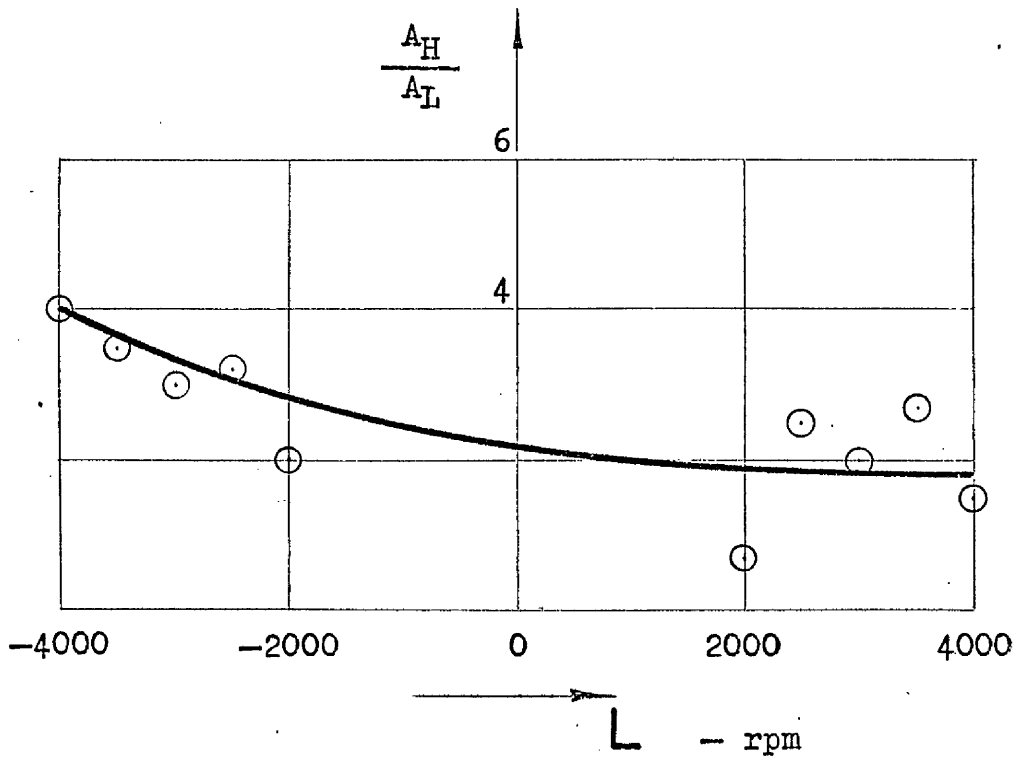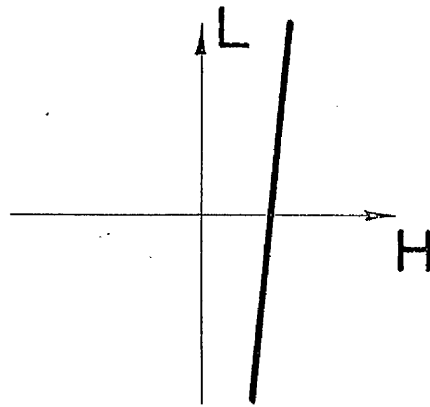
Fig.9.7

Fig.9.7   Ratio of disc amplitudes, A_H/A_L, observed when $H = \lambda_1$

Fig.9.8

Fig.9.8   Variation of λ_2 with L

Fig.9.9

Fig.9.9   Variation of λ_2 with H

Fig.9.10

1 | L.P. Rotor

0

1 | H.P. Rotor

0

1 | Casing

0
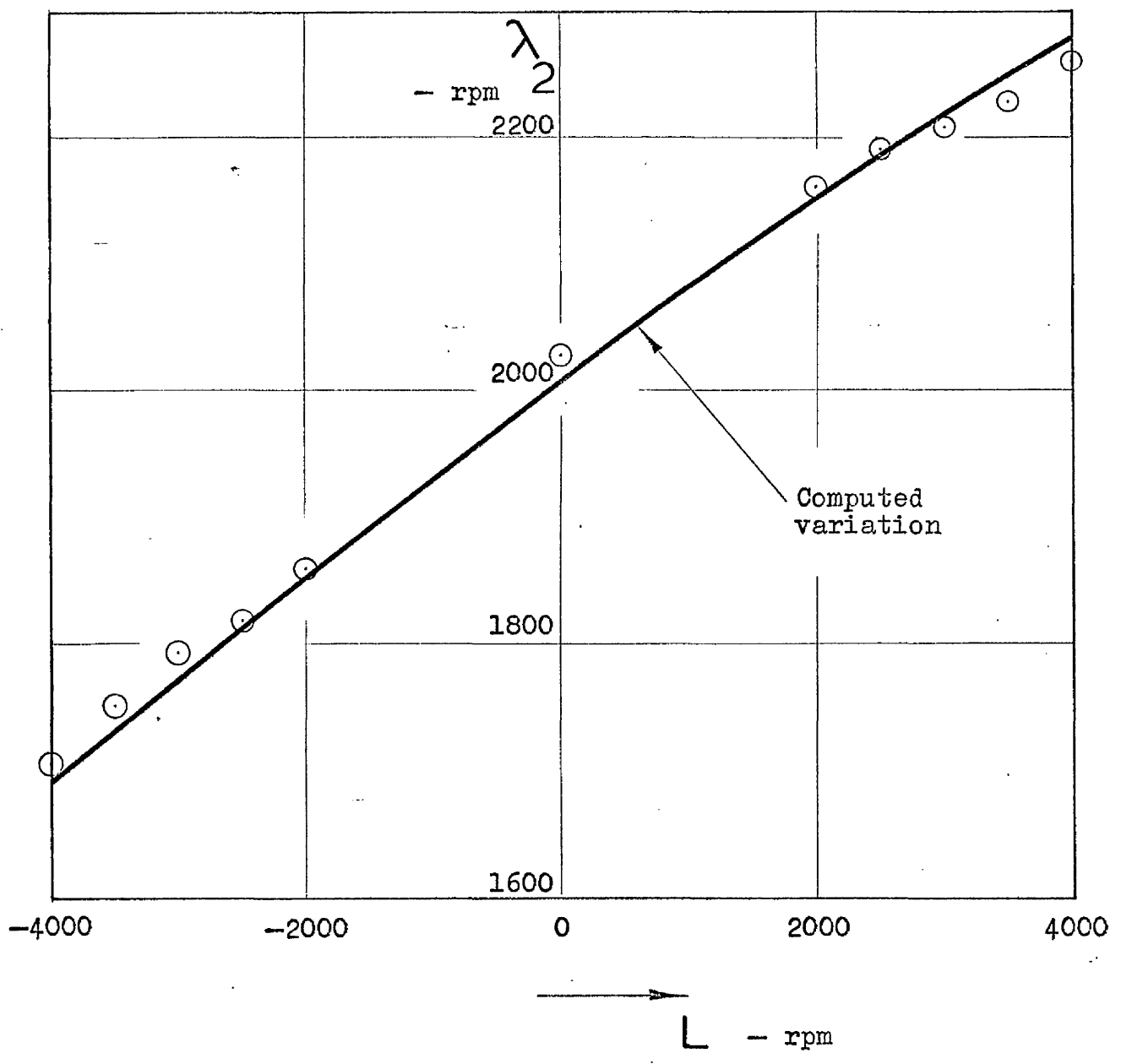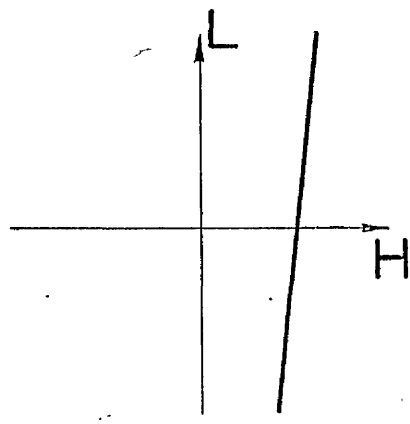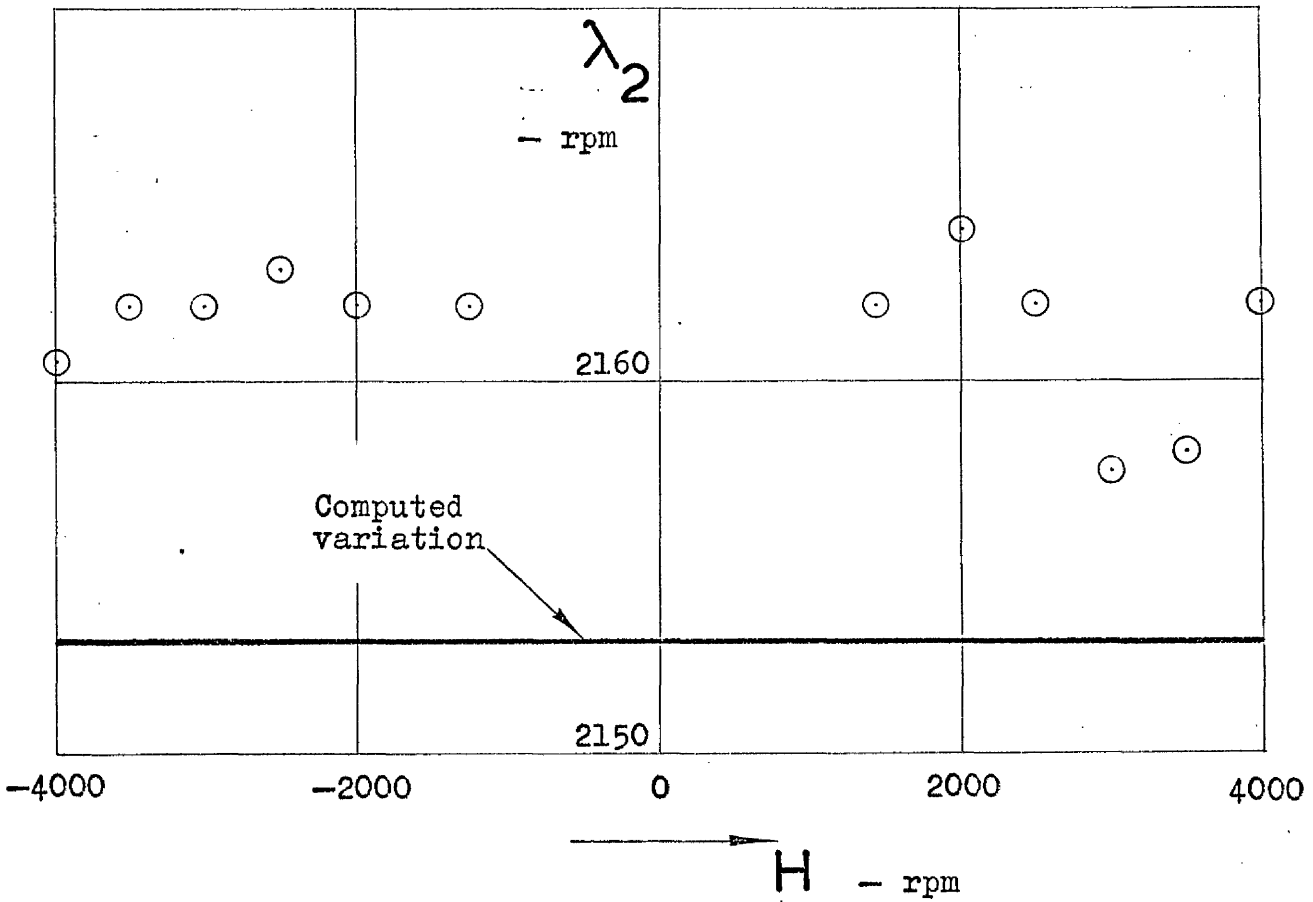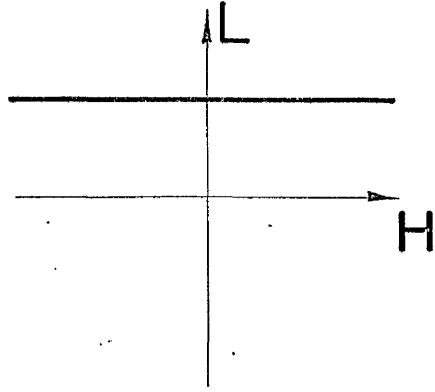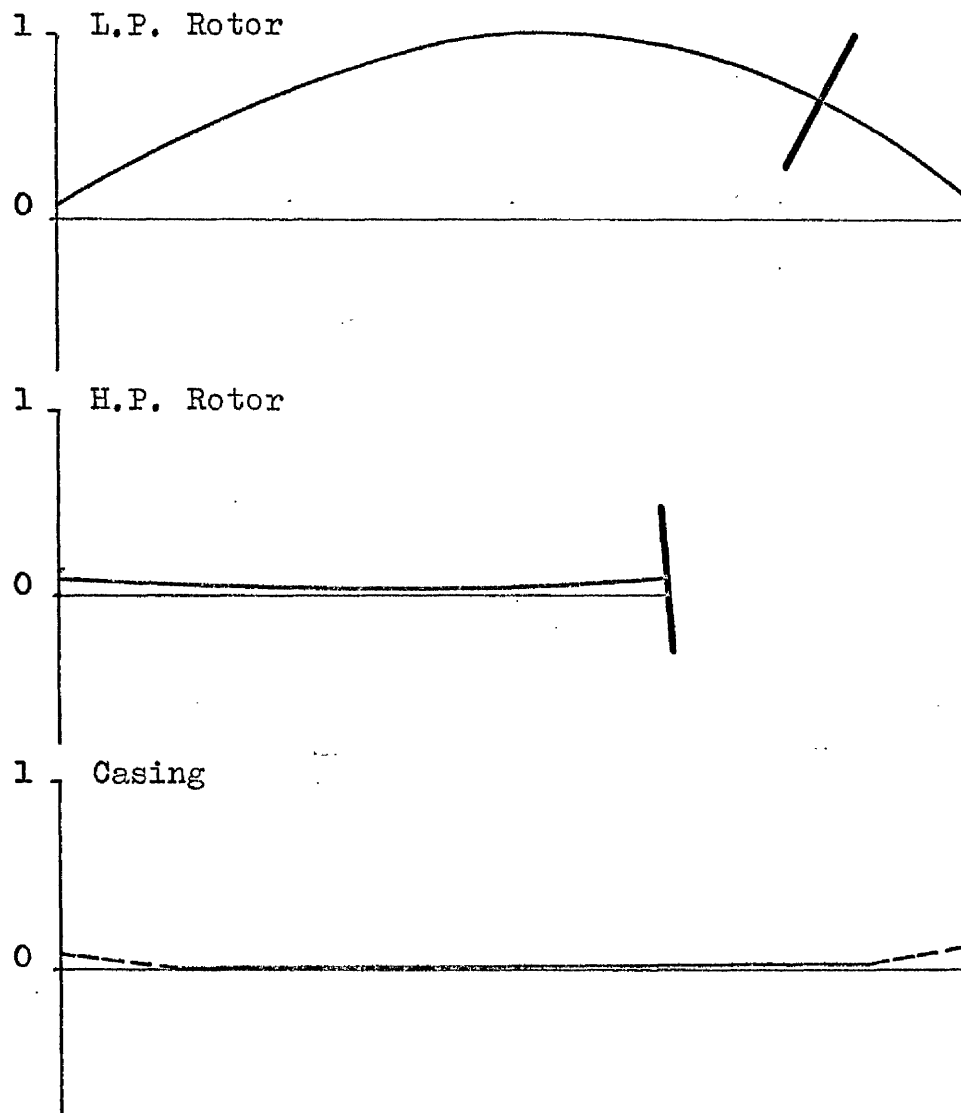
<u>Fig.9.10</u>   Mode of vibration at λ_2
              when $H = L = 0$.
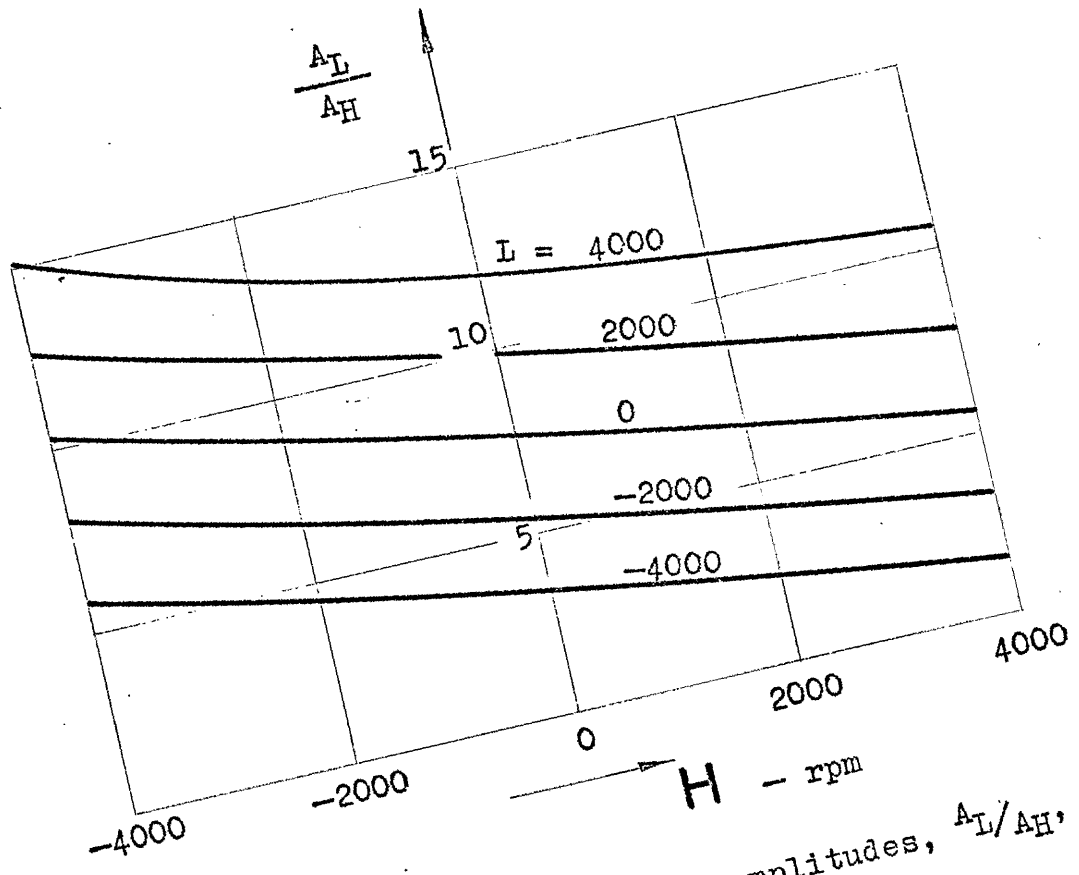
Fig.9.11

Fig.9.11   Ratio of disc amplitudes, A_L/A_H, v. H and L
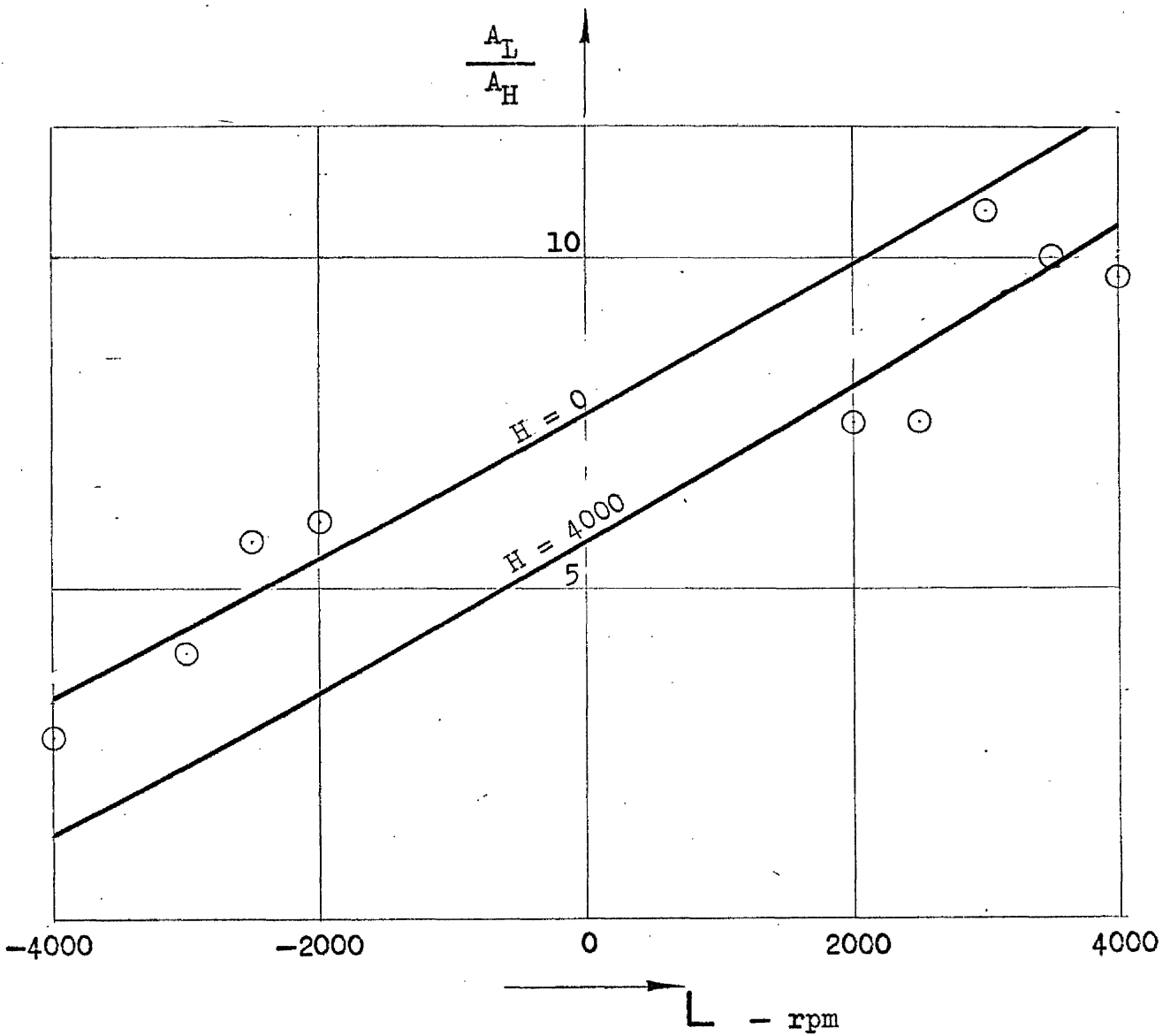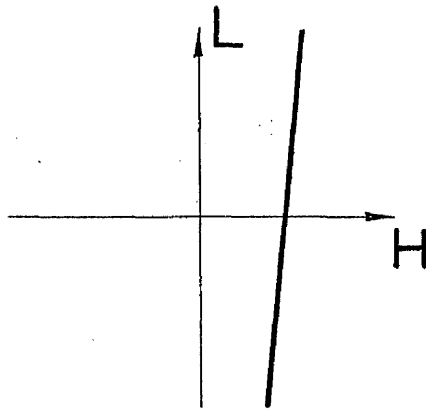
Fig.9.12

Fig.9.12   Ratio of disc amplitudes, A_L/A_H, observed
            when $L = \lambda_2$.
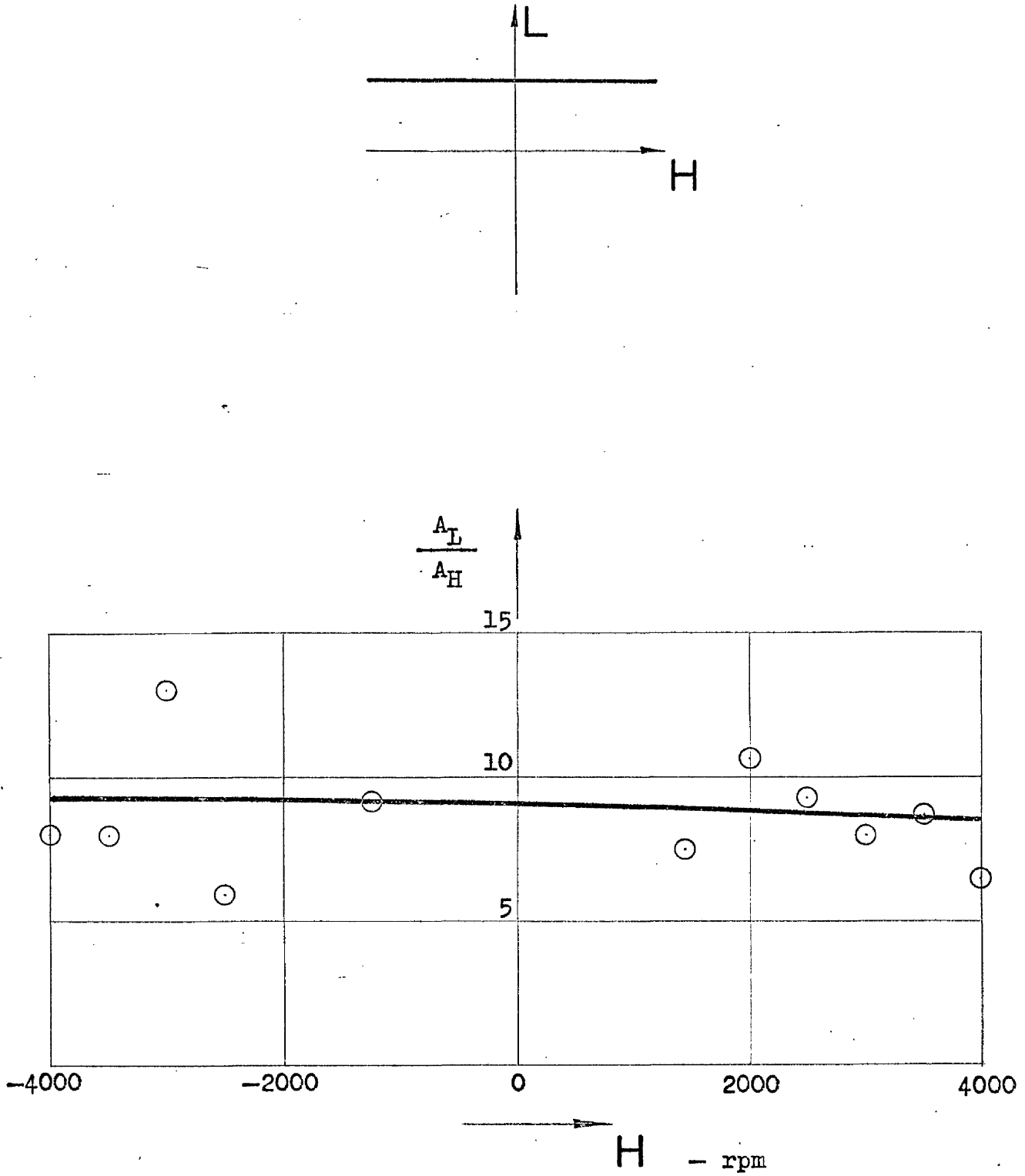
Fig.9.13

Fig.9.13 Ratio of disc amplitudes, A_L/A_H, observed when $H = \lambda_2$.
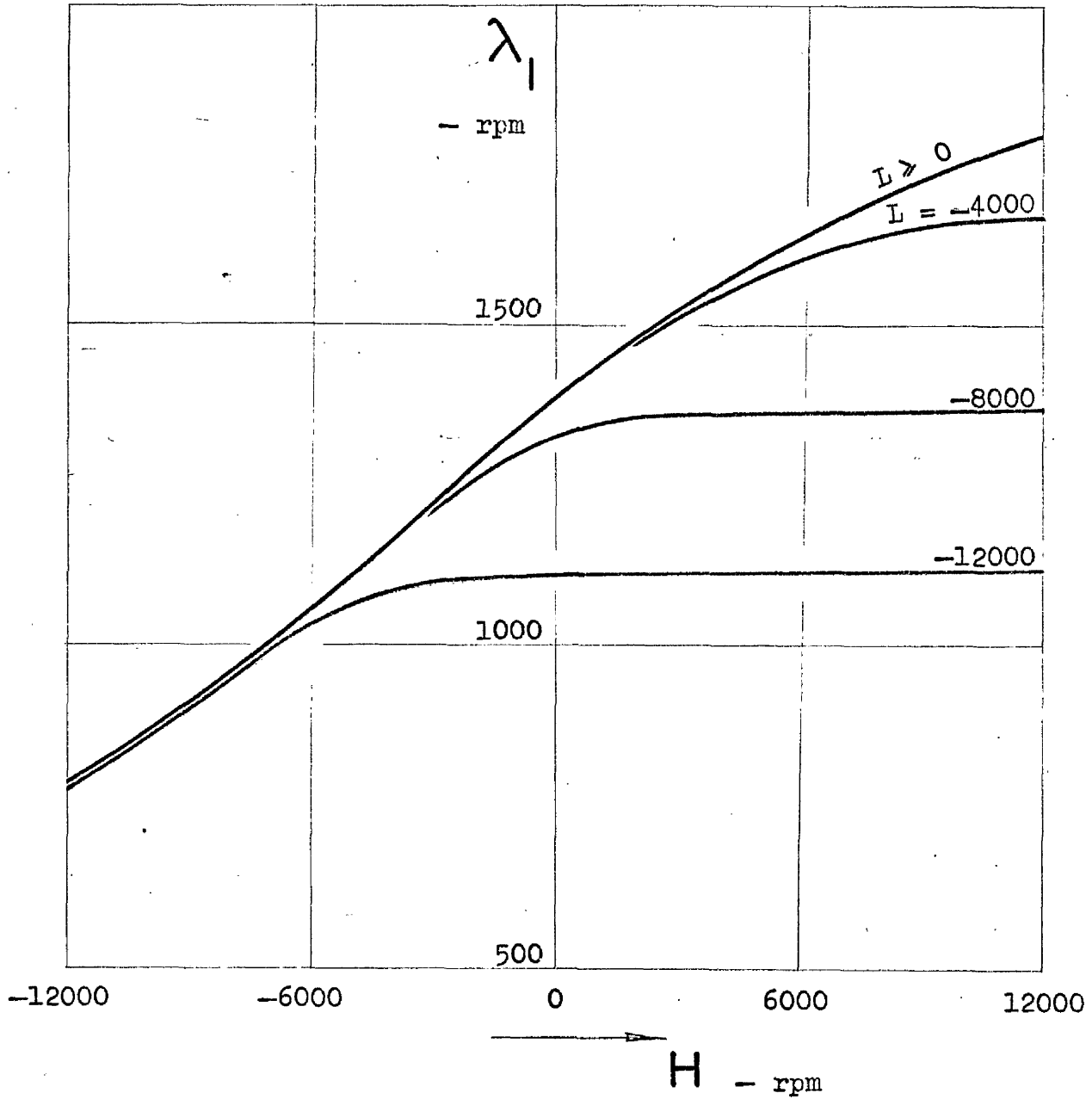
Fig.9.14(a)

Fig.9.14(a)   Variation of λ_1 with H and L
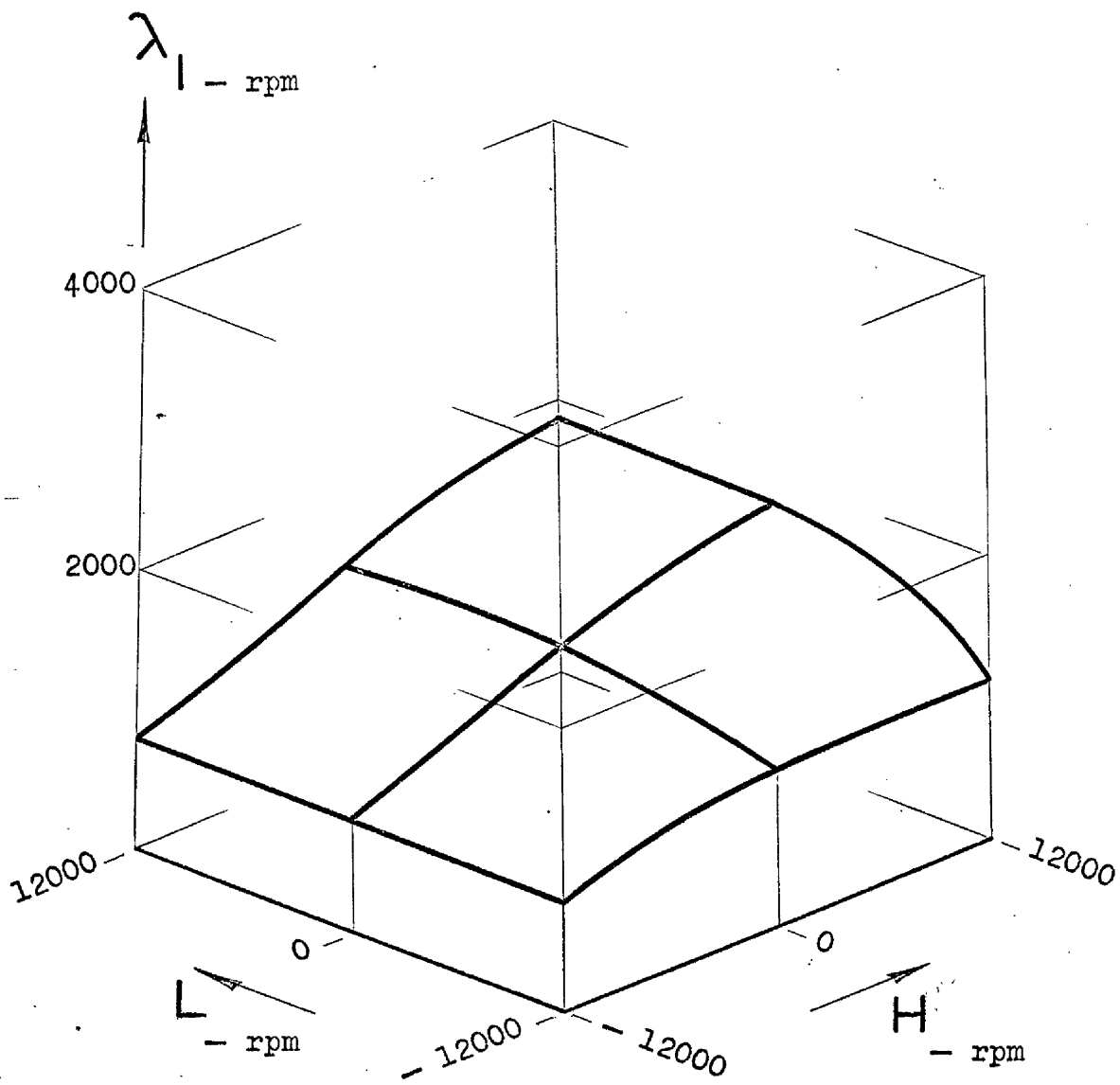
Fig.9.14(b)

Fig.9.14(b)   Isometric plot of variation of
λ_1 with H and L.
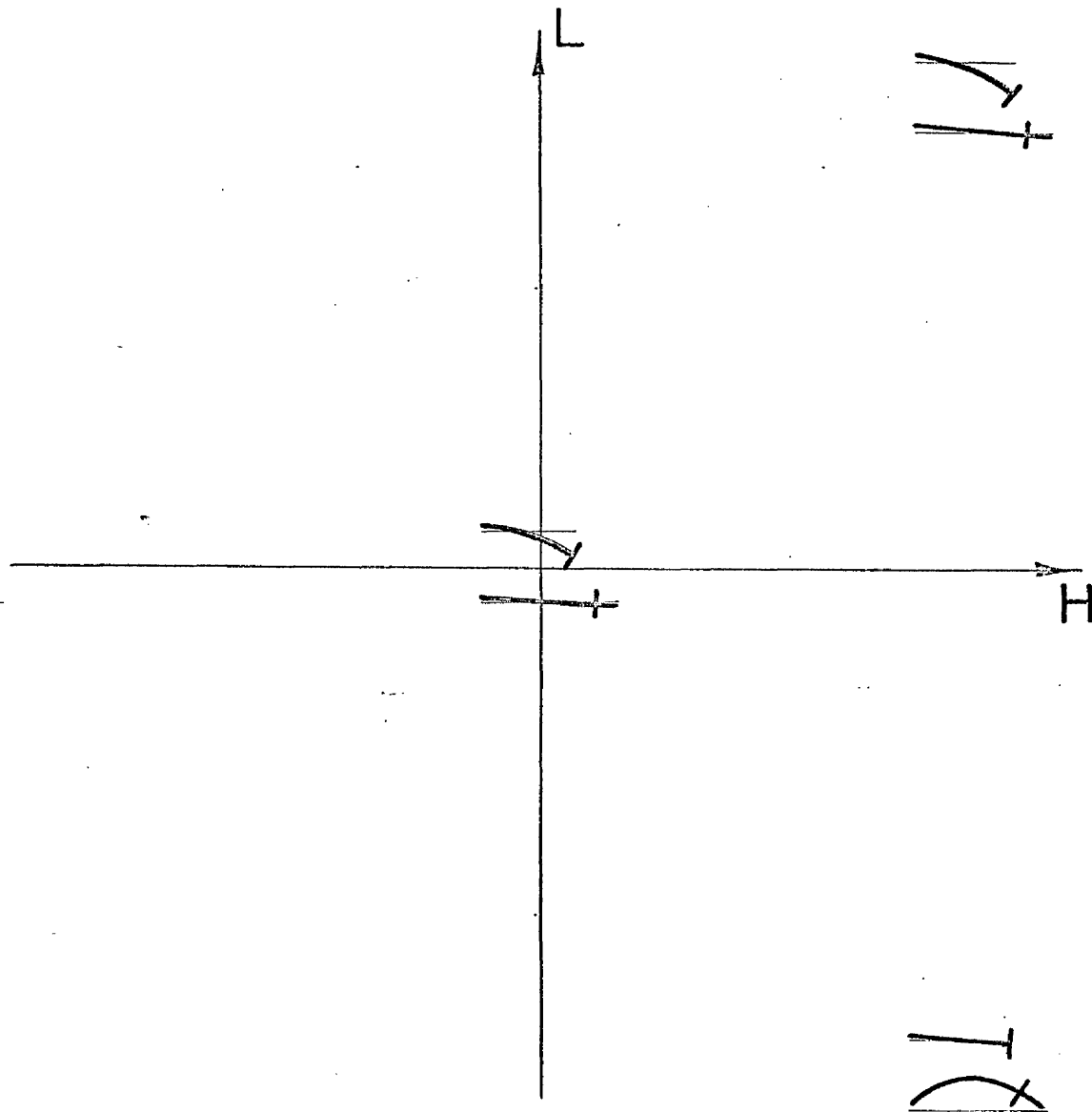
Fig.9.15

Assembly of sketches of computed modes of vibration at frequency λ_1 (based on unit displacement of front bearing).
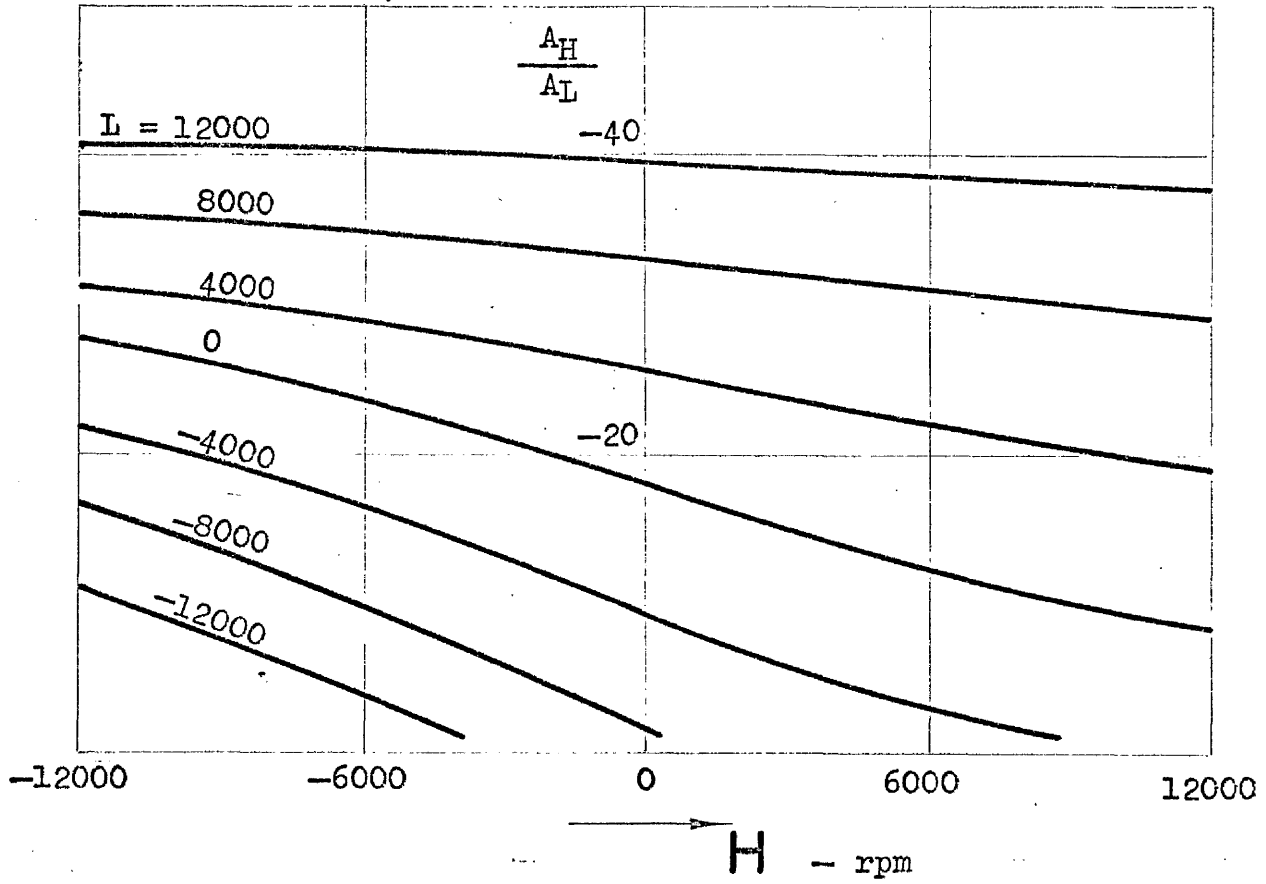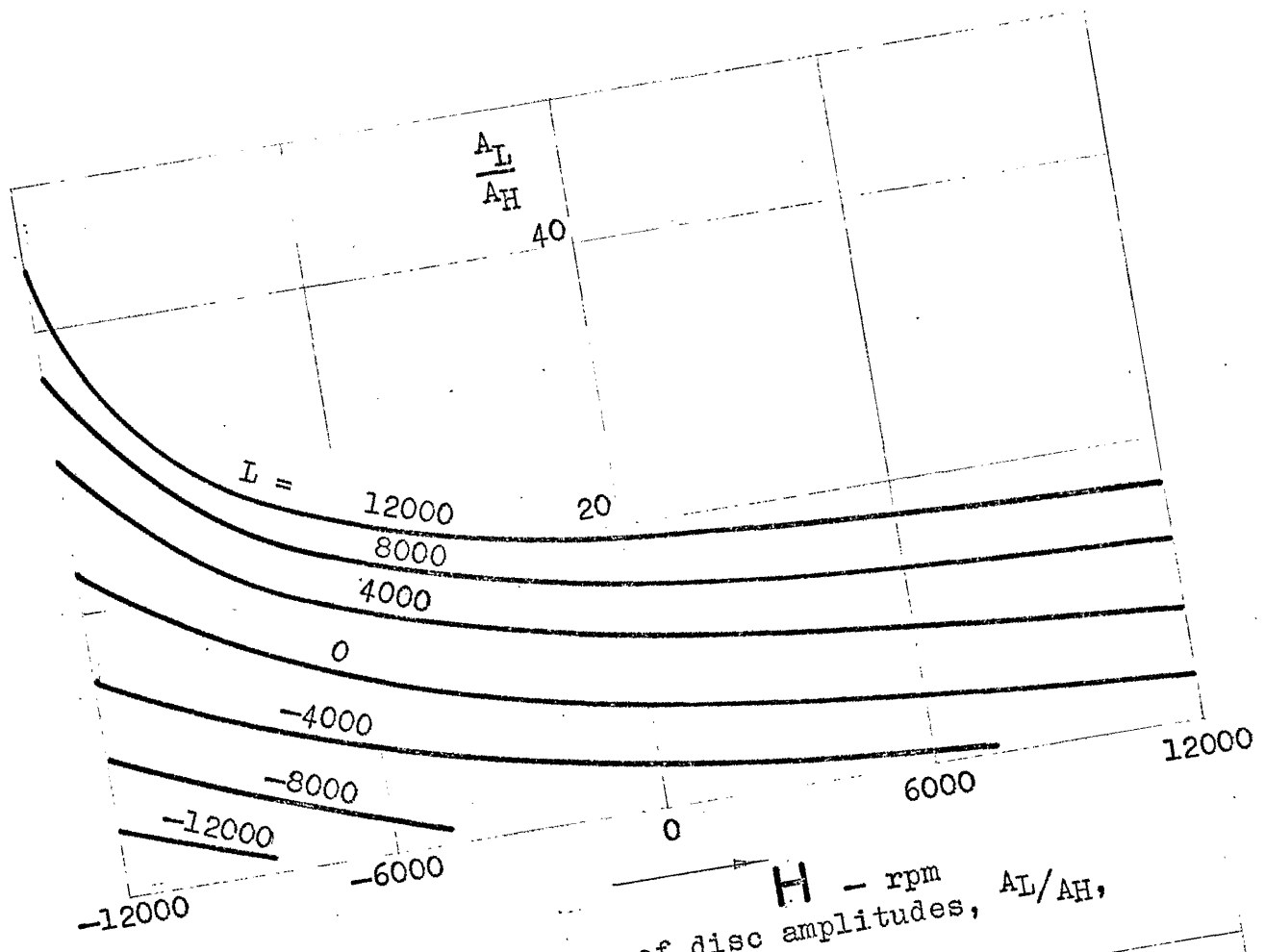
Fig.9.16

Fig.9.16(a)   Ratio of disc amplitudes, A_H/A_L,
v. H and L.
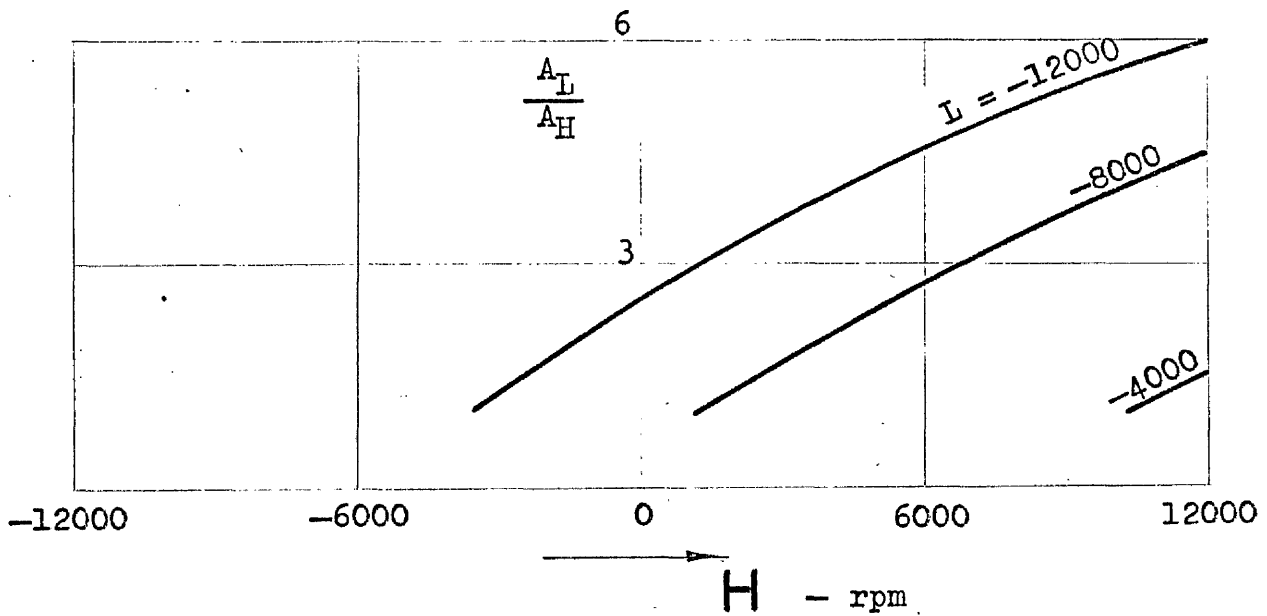
Fig.9.16(b)   Ratio of disc amplitudes, A_L/A_H,
v. H and L.
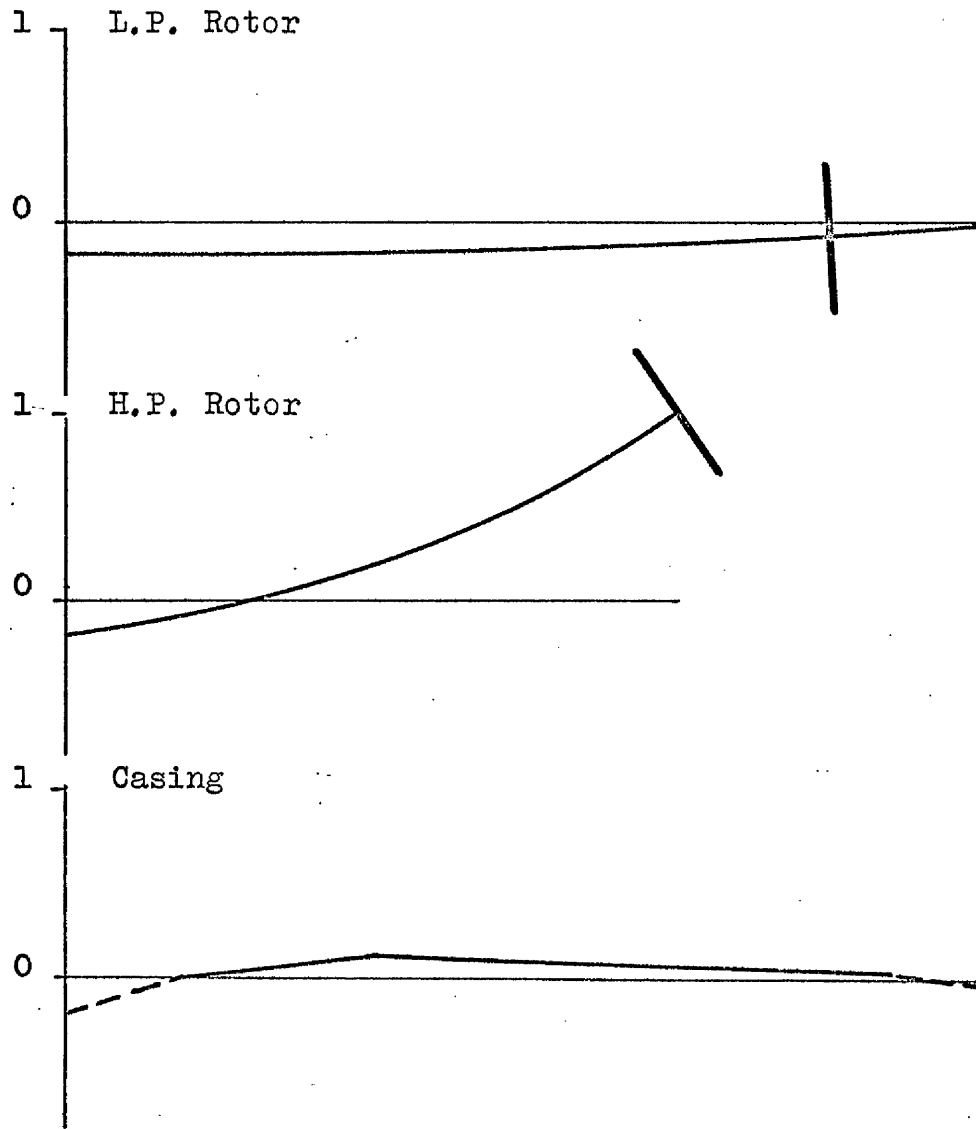
Fig.9.17(a)

Fig.9.17(a)   Mode of vibration at λ_1
when $H = L = 0$.
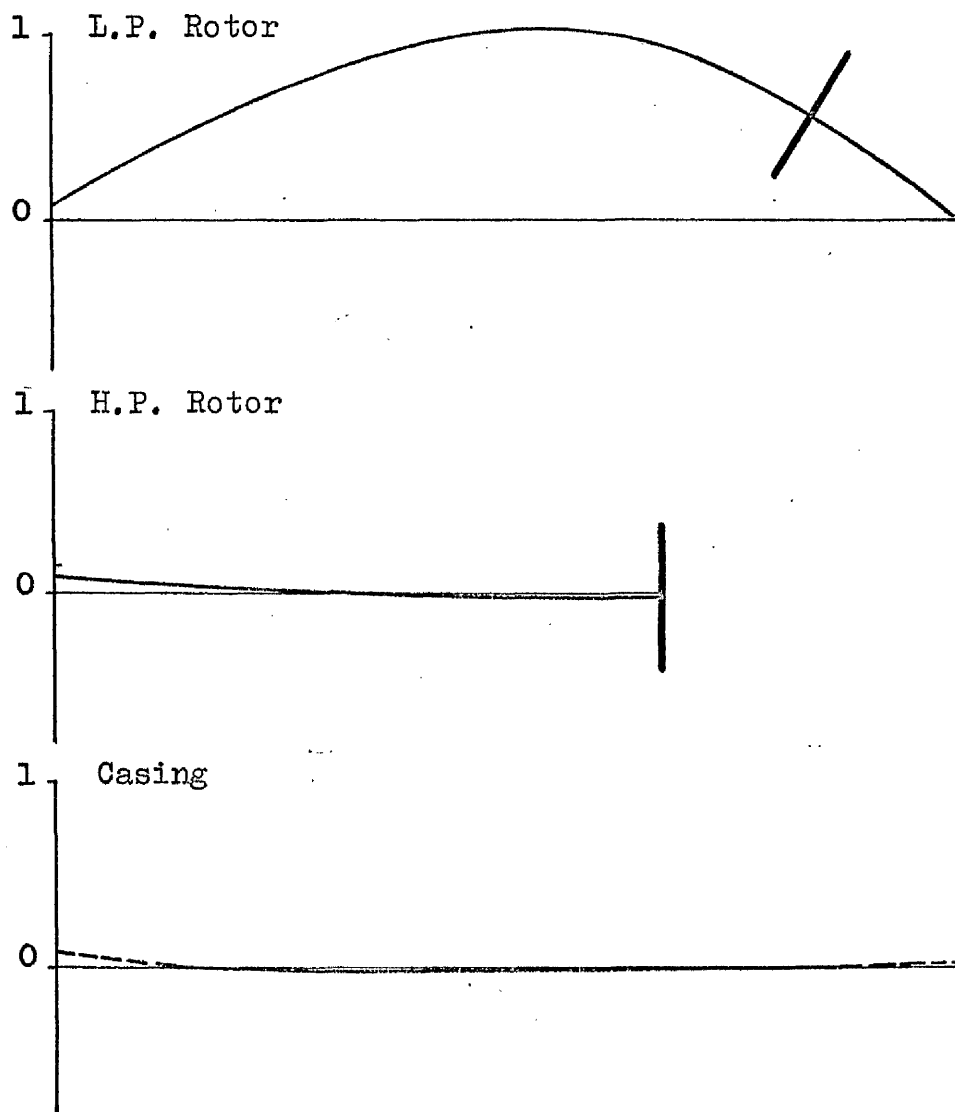
Fig.9.17(b)

Fig.9.17(b)   Mode of vibration at λ_1
when H = +12000, L = −12000.
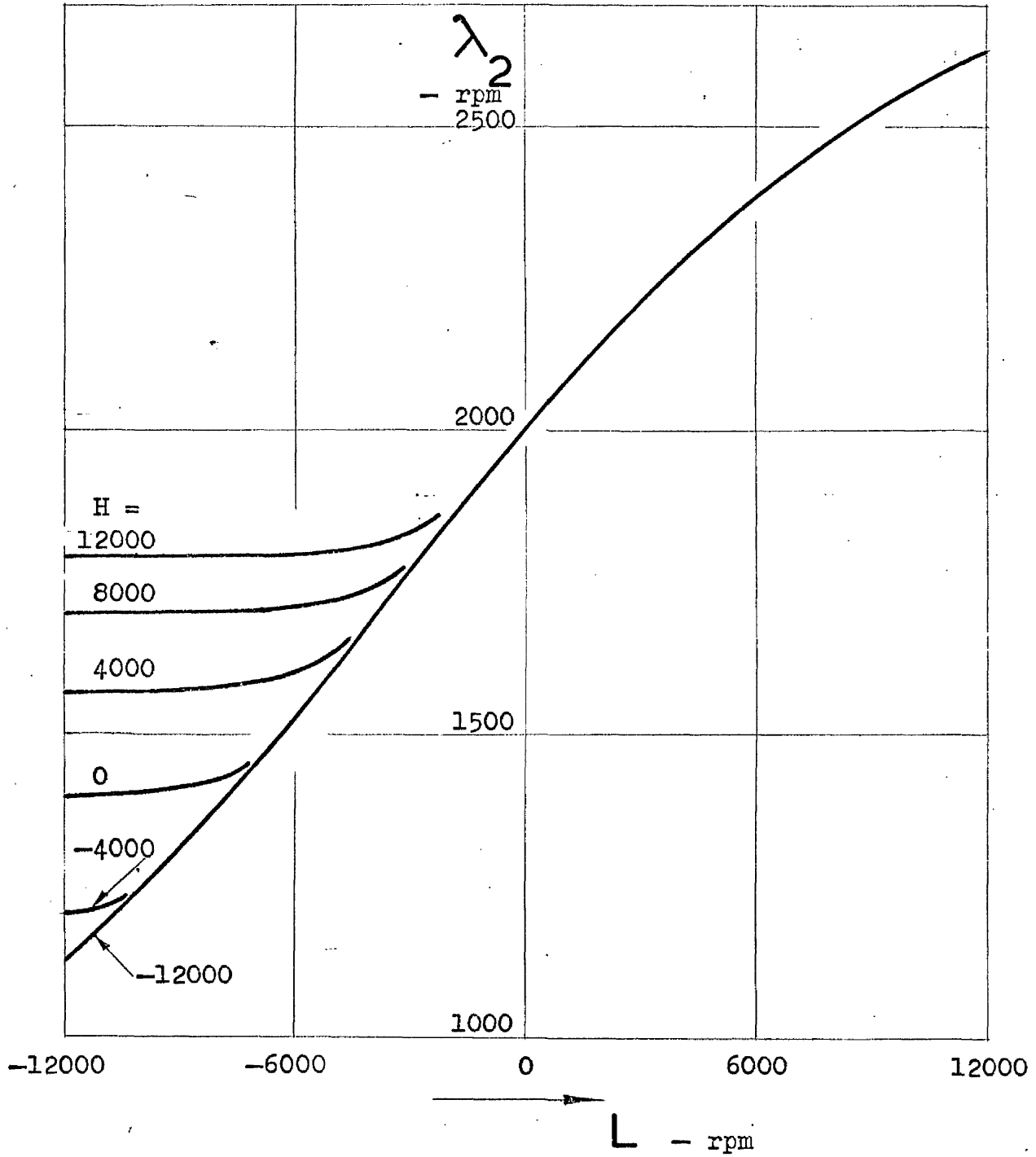
Fig.9.18(a)

Fig.9.18(a)

Fig.9.18(a)   Variation of λ_2 with H and L
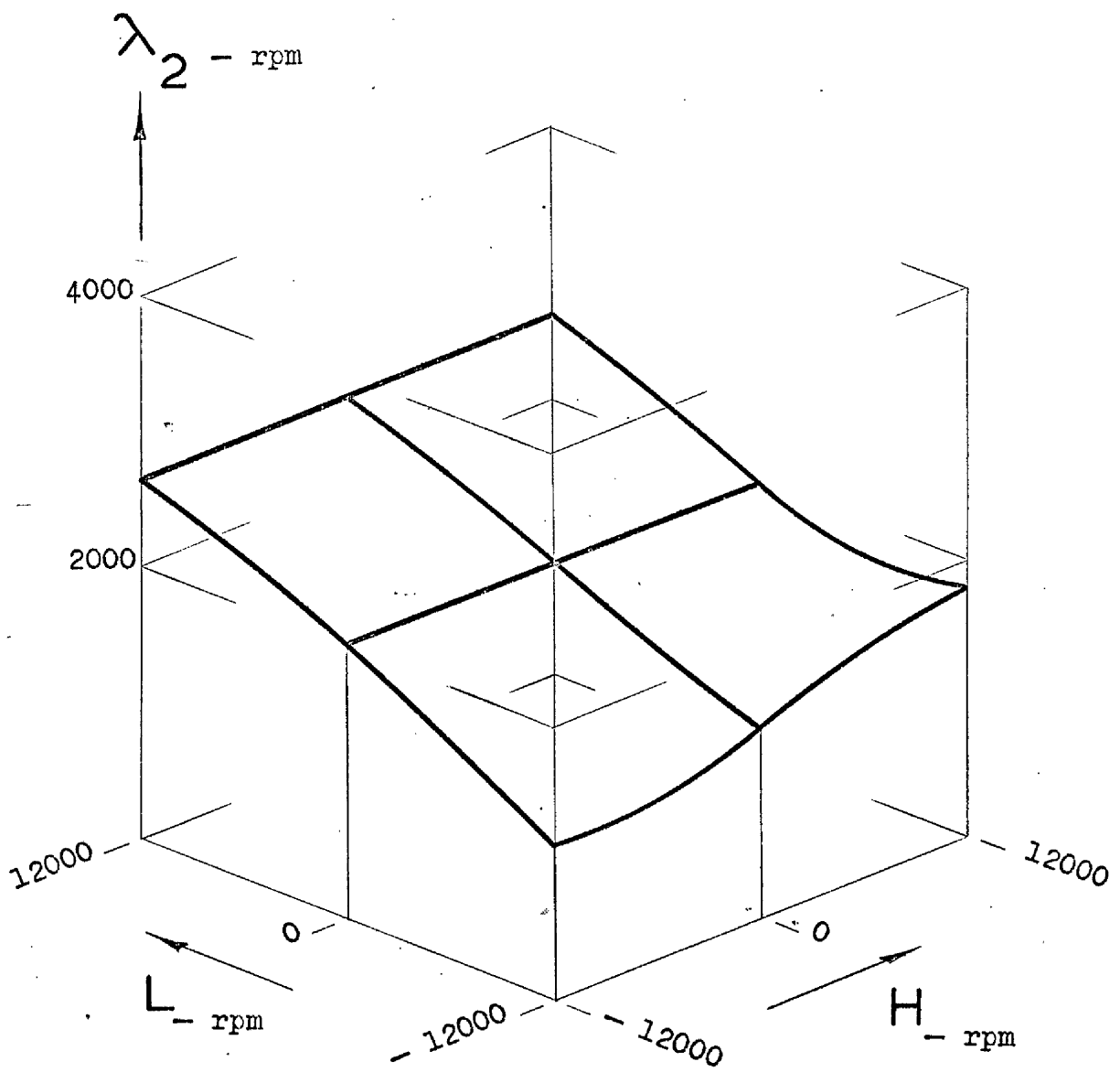
Fig.9.18(b)

Fig.9.18(b)   Isometric plot of variation of
λ_2 with H and L.

Fig.9.19

Fig.9.19(a)   Ratio of disc amplitudes, A_L/A_H,
v. H and L.
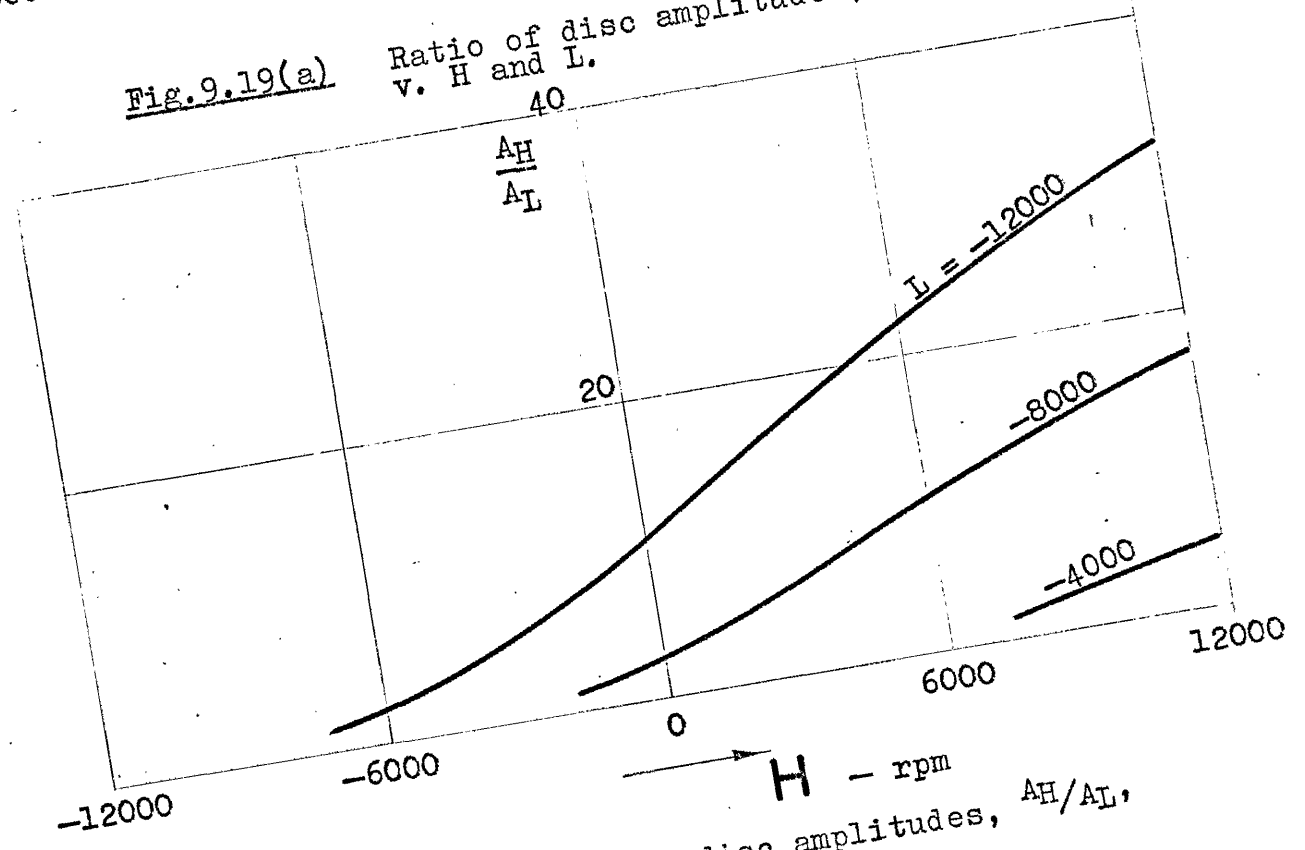
Fig.9.19(b)   Ratio of disc amplitudes, A_H/A_L,
v. H and L.
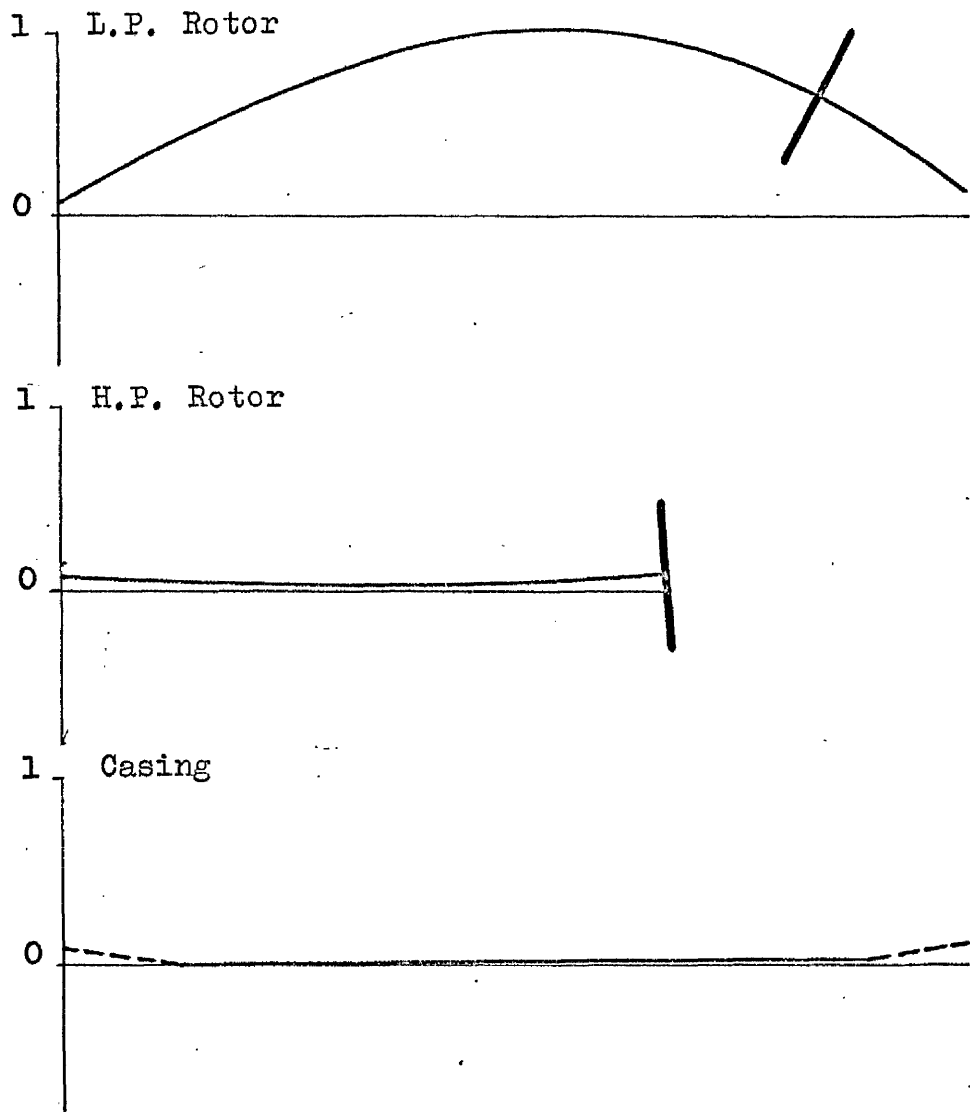
Fig. 9. 20(a)
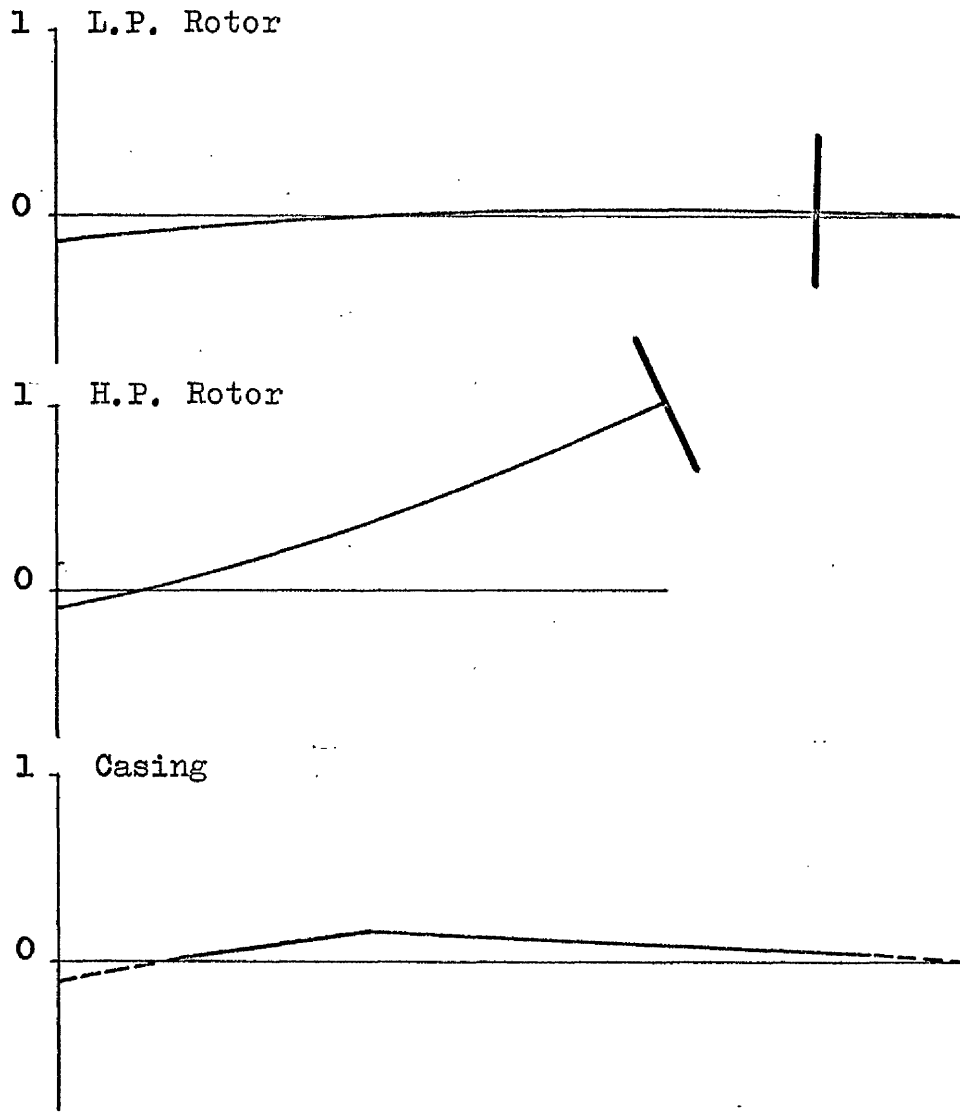

Mode of vibration at λ_2
when $H = L = 0$.

Fig. 9.20(b)

Fig.9.20(b) Mode of vibration at λ_2
when H = +12000, L = —12000.
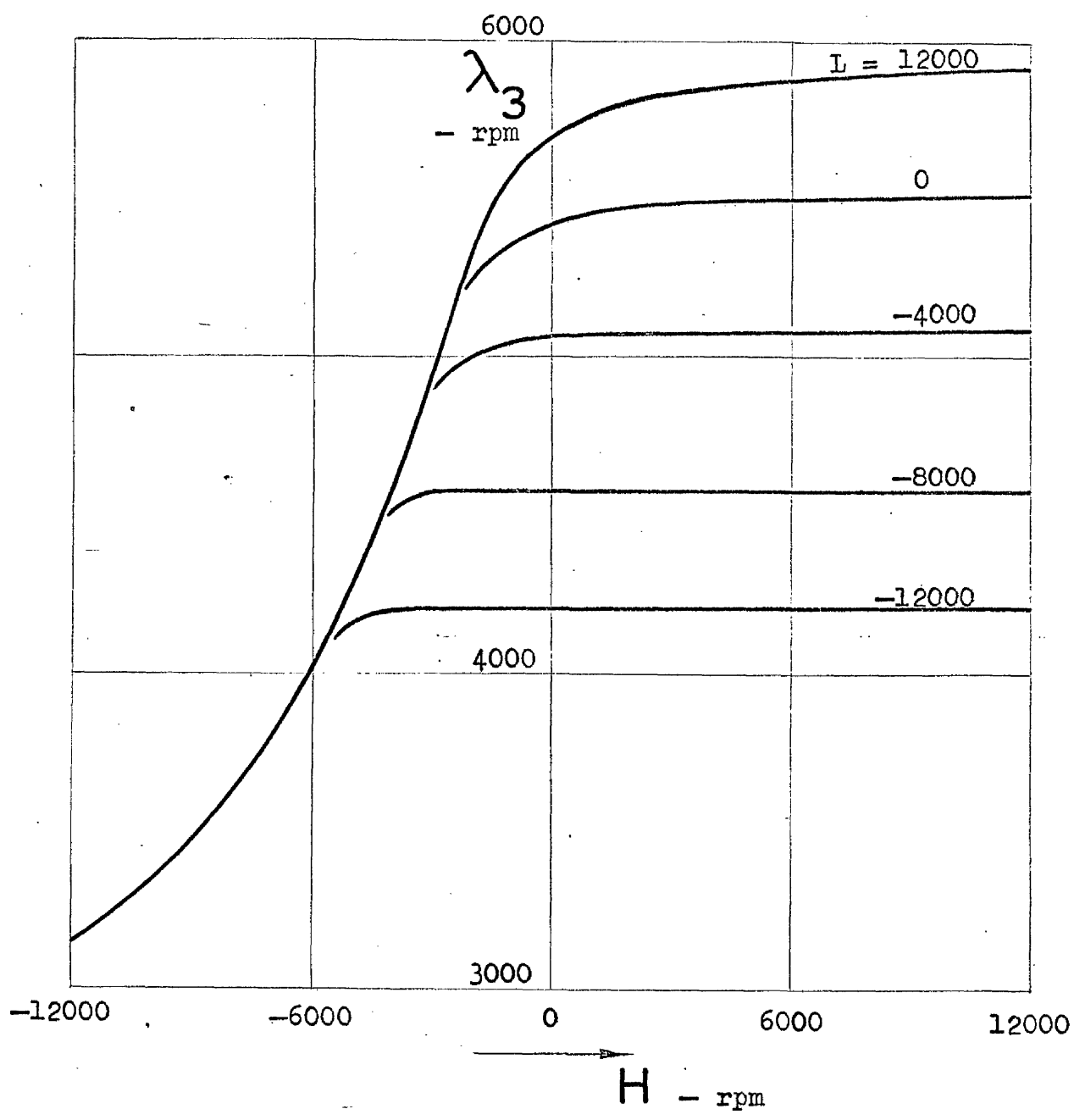
Fig.9.21(a)

<u>Fig.9.21(a)</u>   Variation of λ_3 with H and L
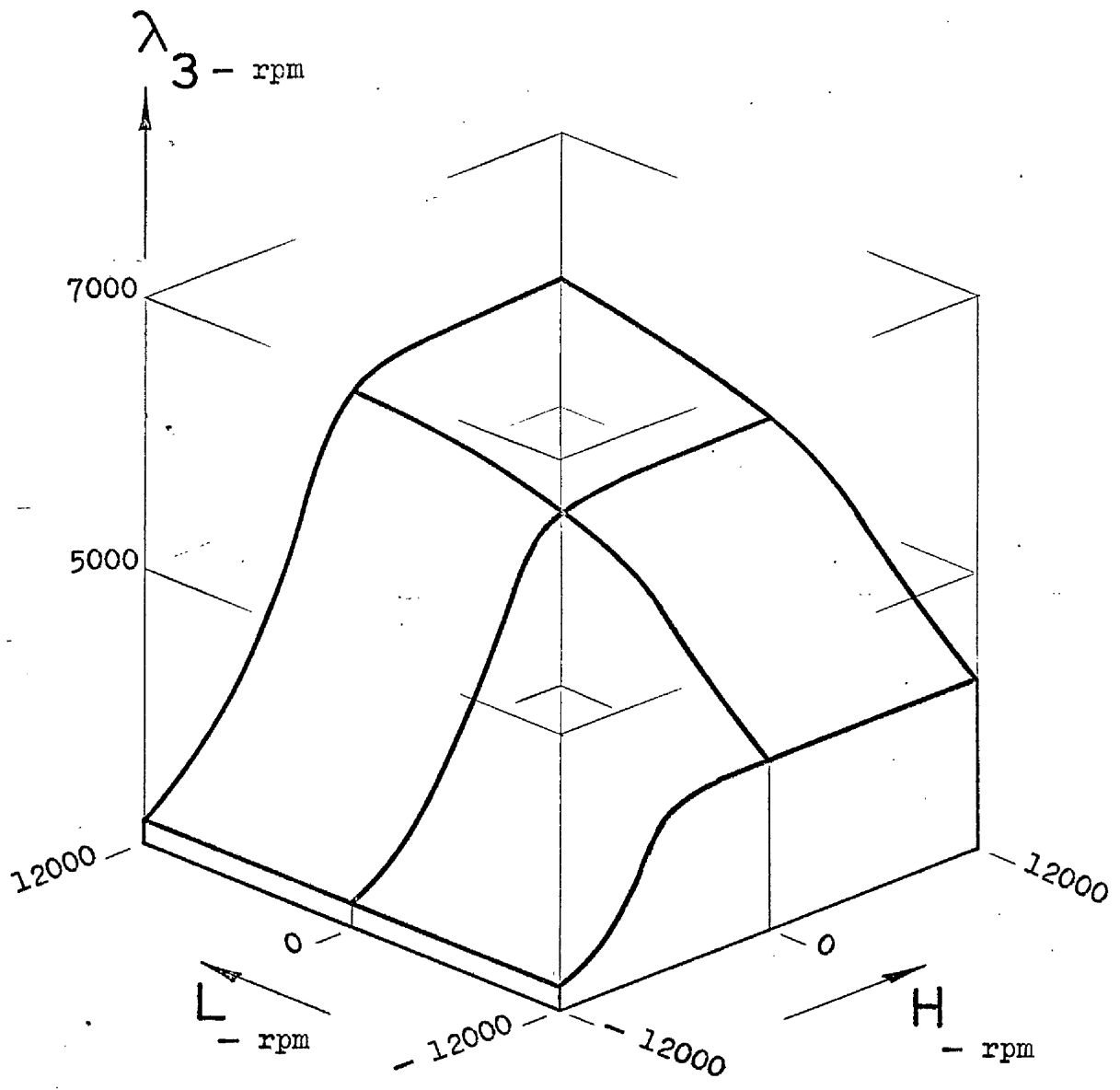
Fig.9.21(b)

Fig.9.21(b)   Isometric plot of variation of
λ_3 with H and L.

Fig.9.22

L.P. Rotor

1

0

1   H.P. Rotor

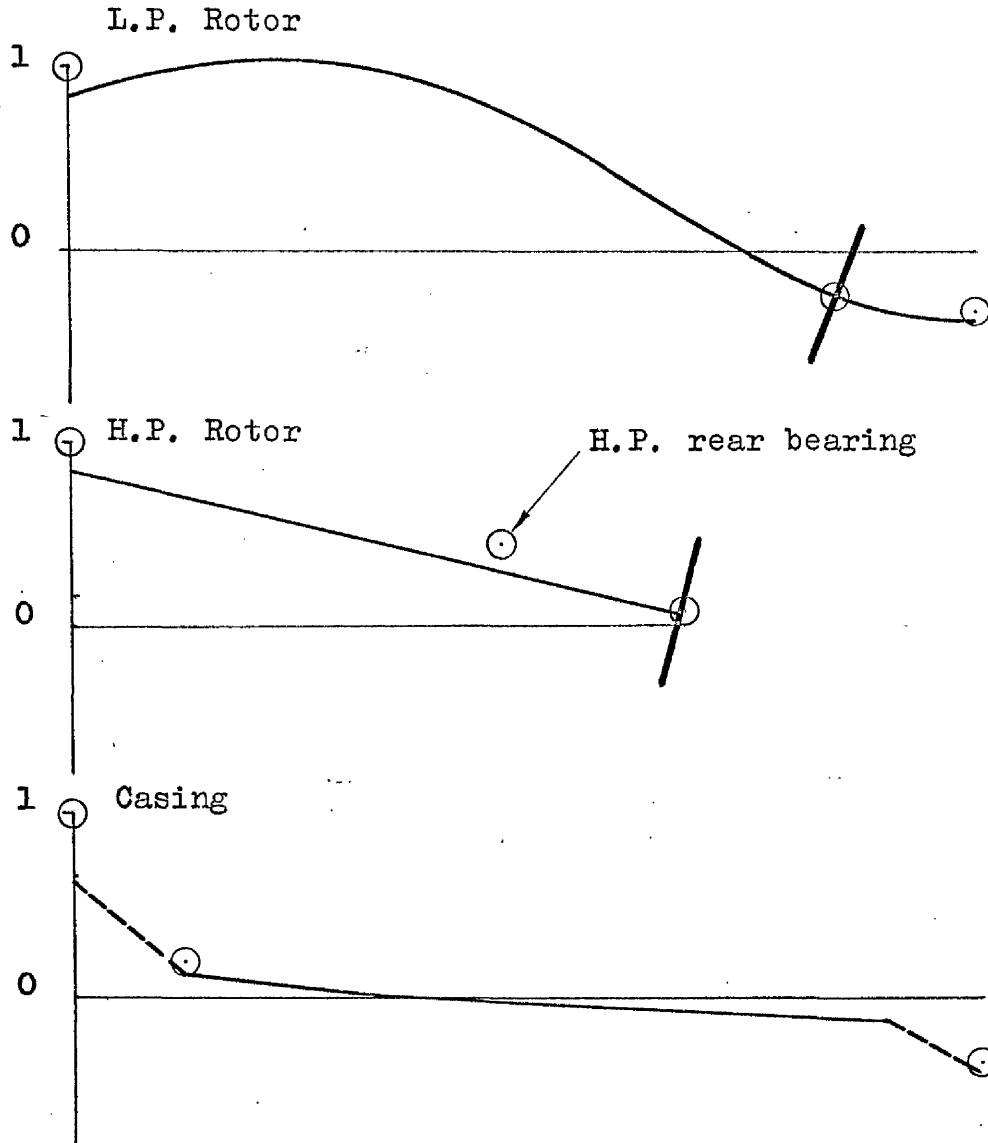H.P. rear bearing

0

1   Casing

0

Fig.9.22   Computed mode of vibration at λ_3
when H = L = 0.   (Circled points
show experimental amplitudes referred
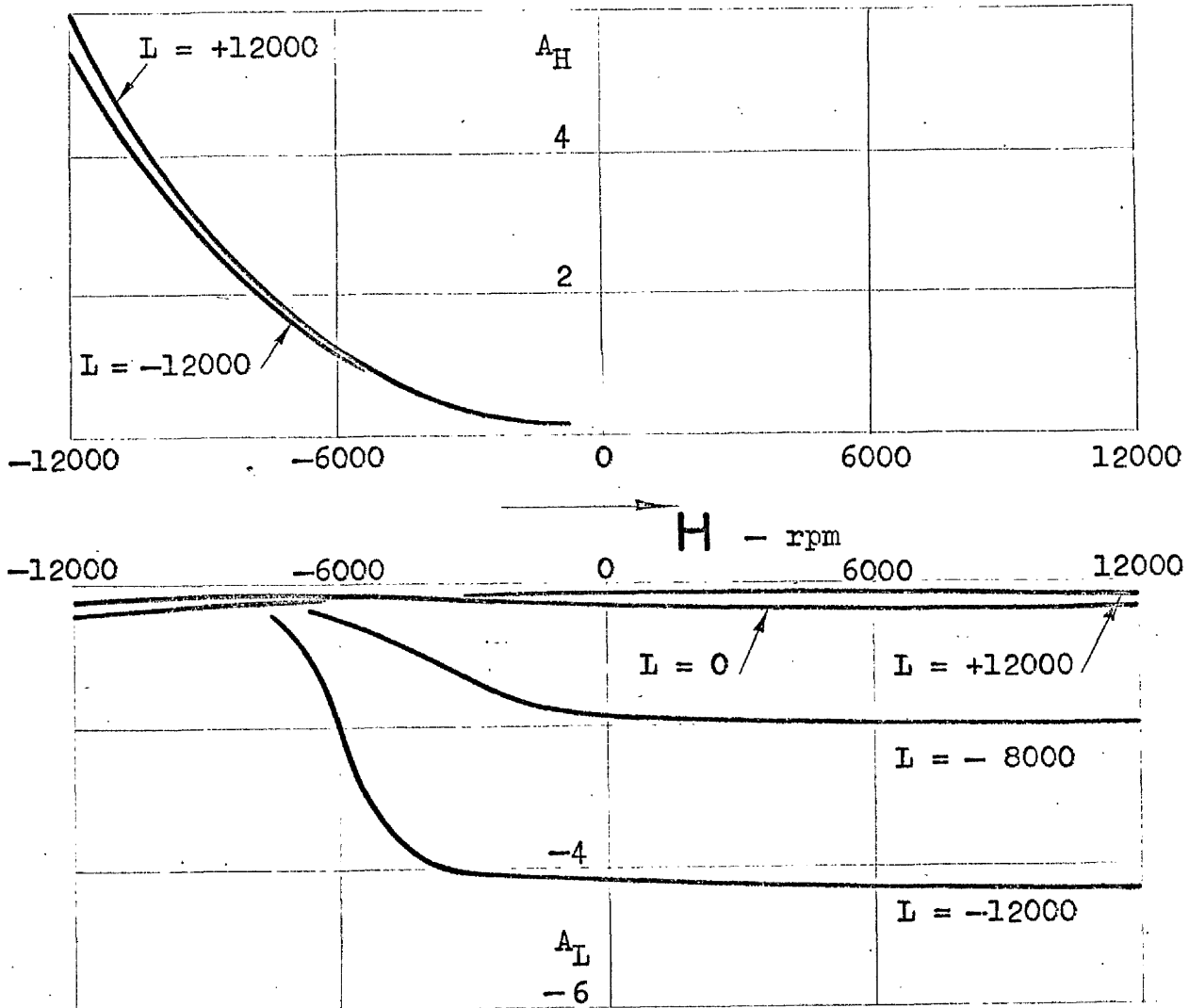to unit amplitude of front bearing).

Fig.9.23

Fig.9.23   Disc amplitudes A_H and A_L, referred to unit displacement of front bearing, plotted v. H and L.
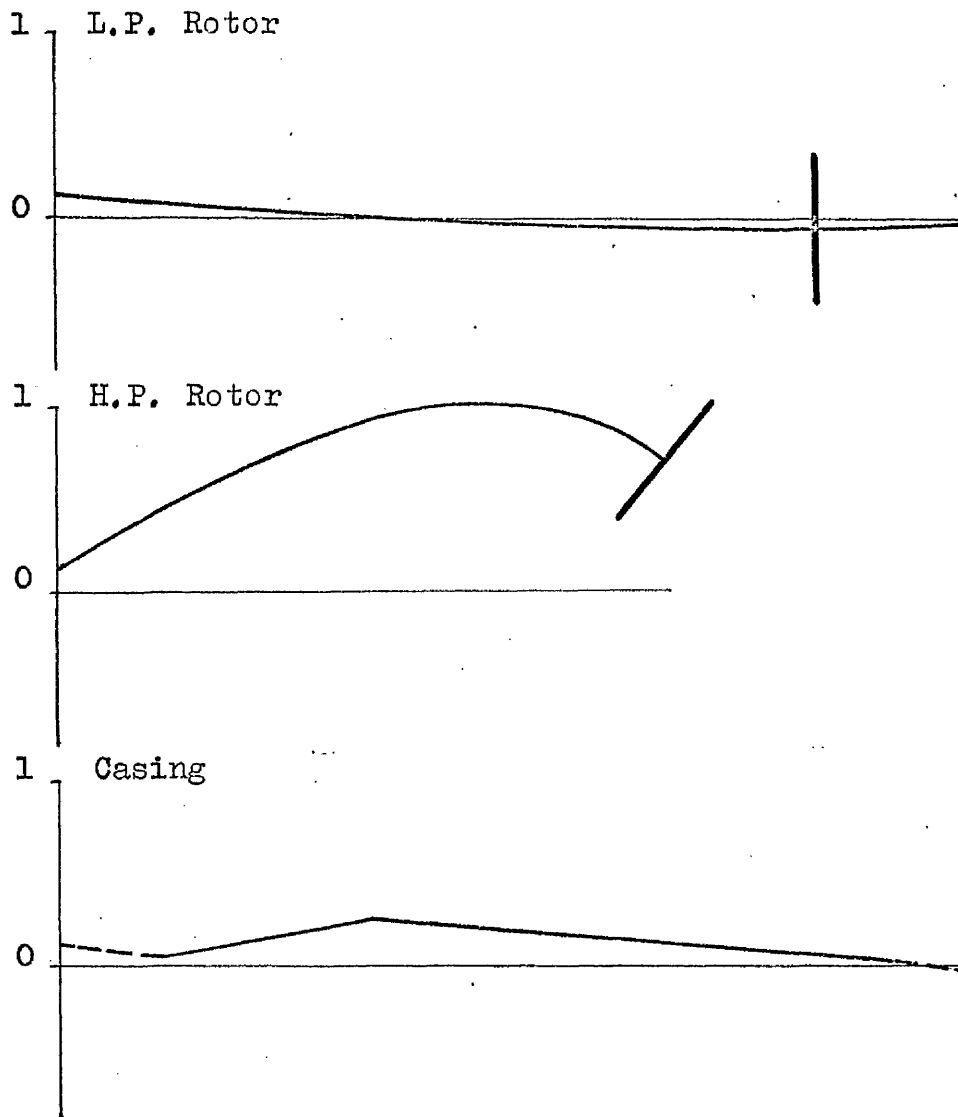
Fig.9.24

1 — L.P. Rotor

0 —

1 — H.P. Rotor

0 —

1 — Casing

0 —

<u>Fig.9.24</u>   Mode of vibration at λ_3 when
           H = −12000 and L = +12000.
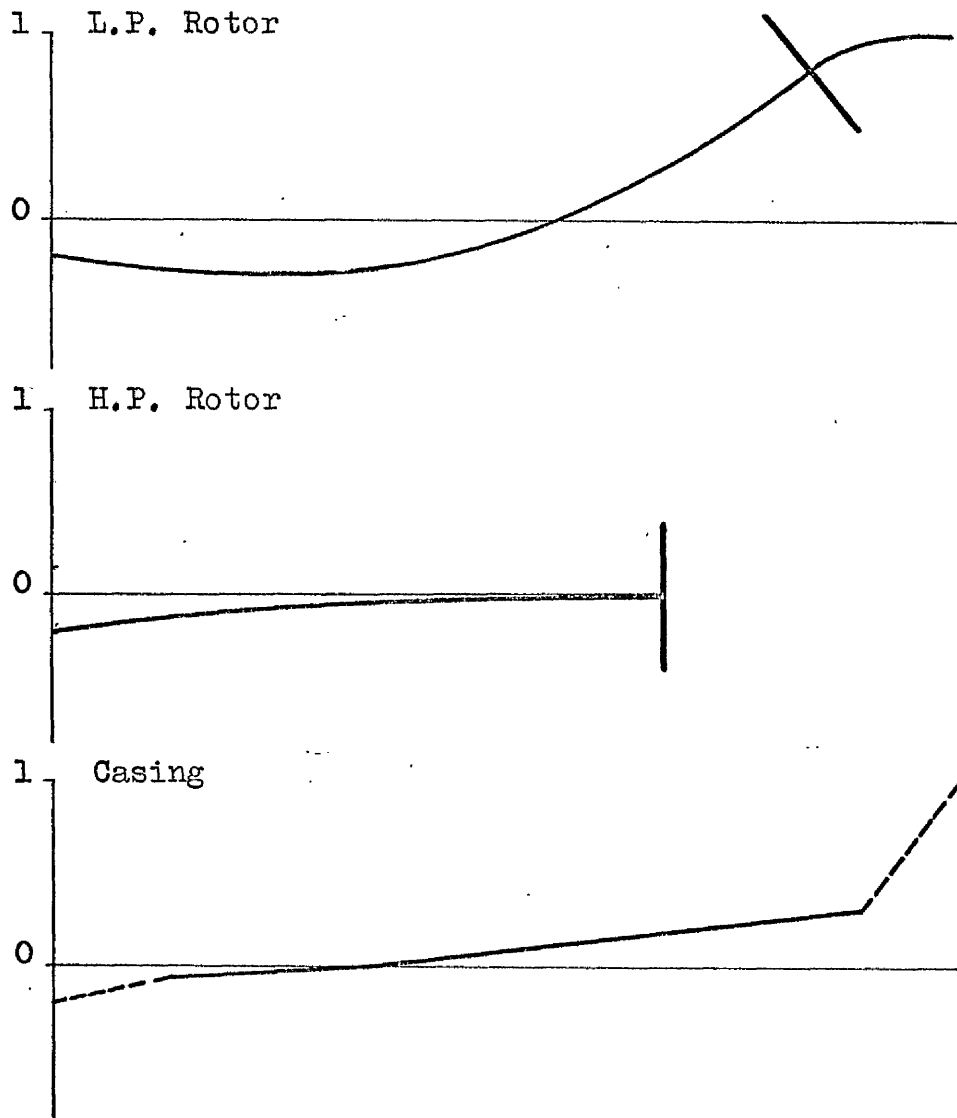
Fig. 9.25

Mode of vibration at λ_3 when
H = +12000 and L = −12000.
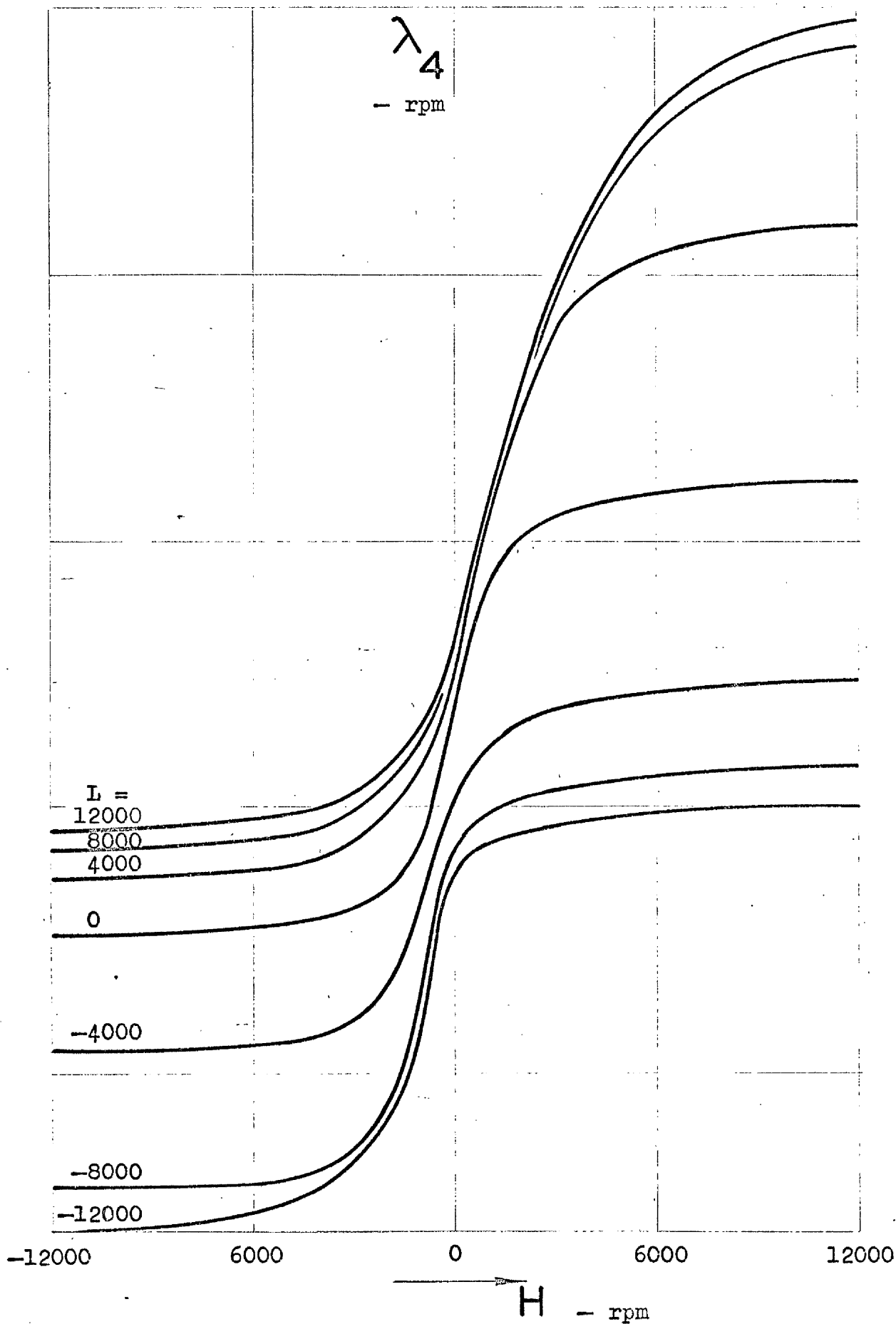
Fig. 9.26(a)

Fig.9.26(a)   Variation of λ_4 with H and L
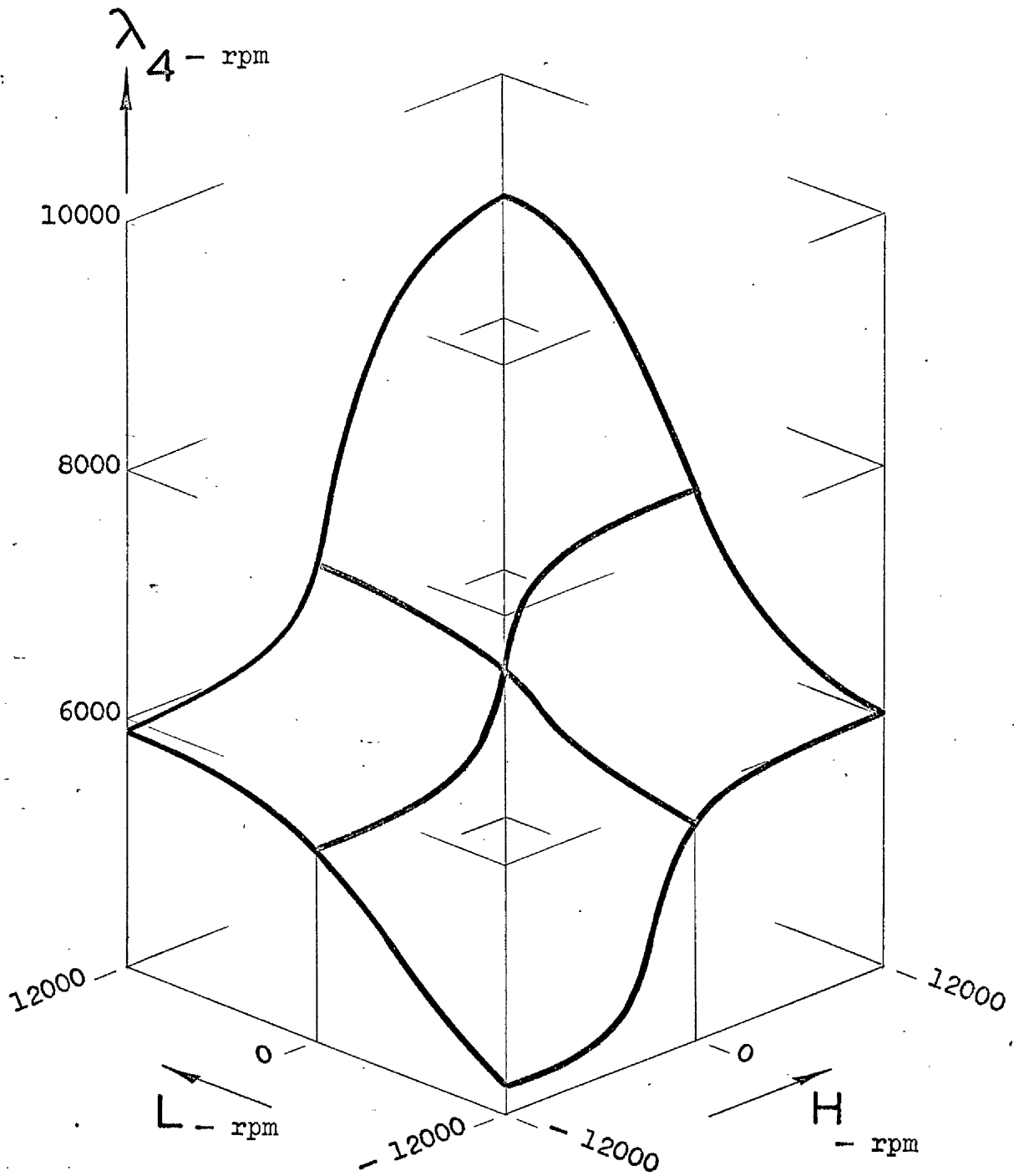
Fig.9.26(b)

<u>Fig.9.26(b)</u>   Isometric plot of variation of
λ_4 with H and L.

Fig.9.27(a)

Fig.9.27(a) Computed mode of vibration at λ_4 when H = L = 0. (Circled points show experimental amplitudes referred to unit amplitude of H.P. rear bearing).
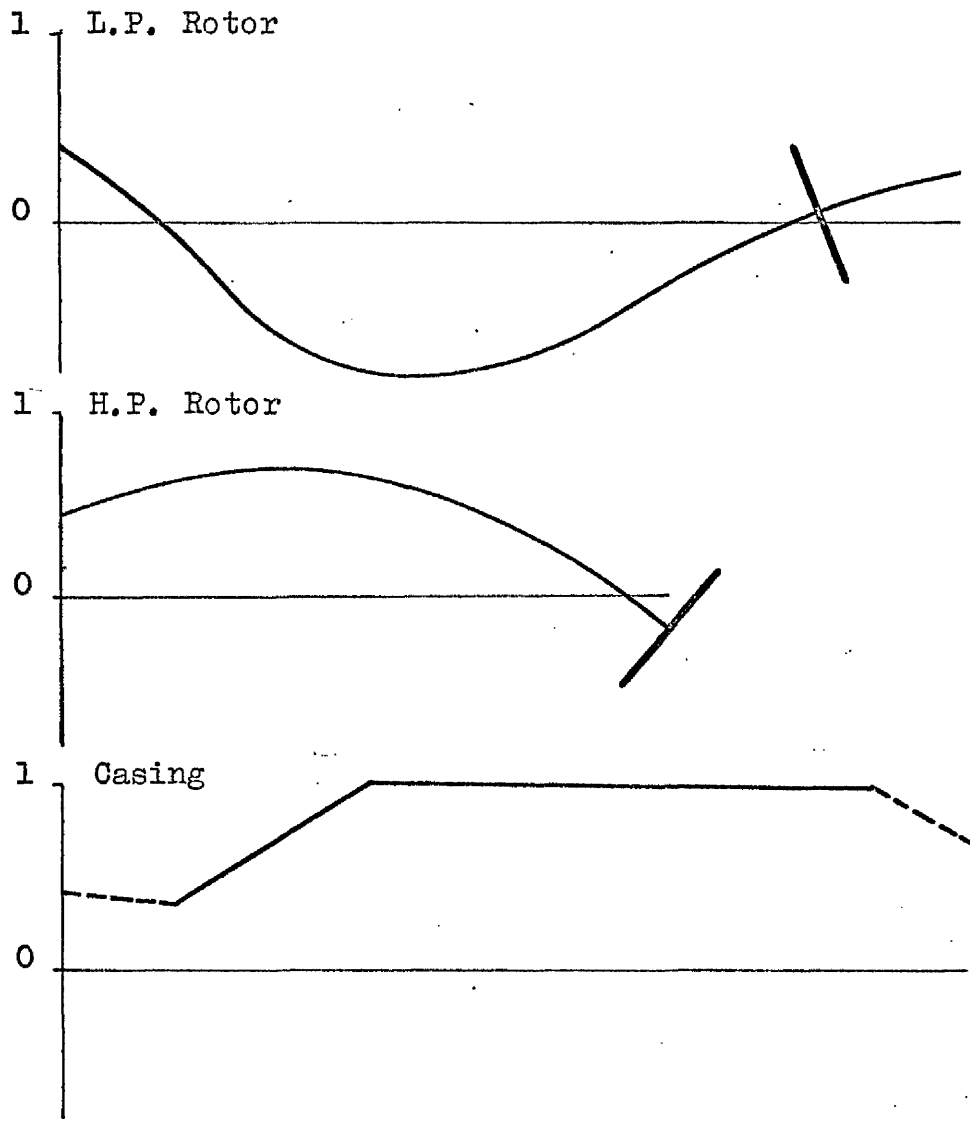
Fig. 9.27(b)

Mode of vibration at λ_4 when
H = L = + 12000.
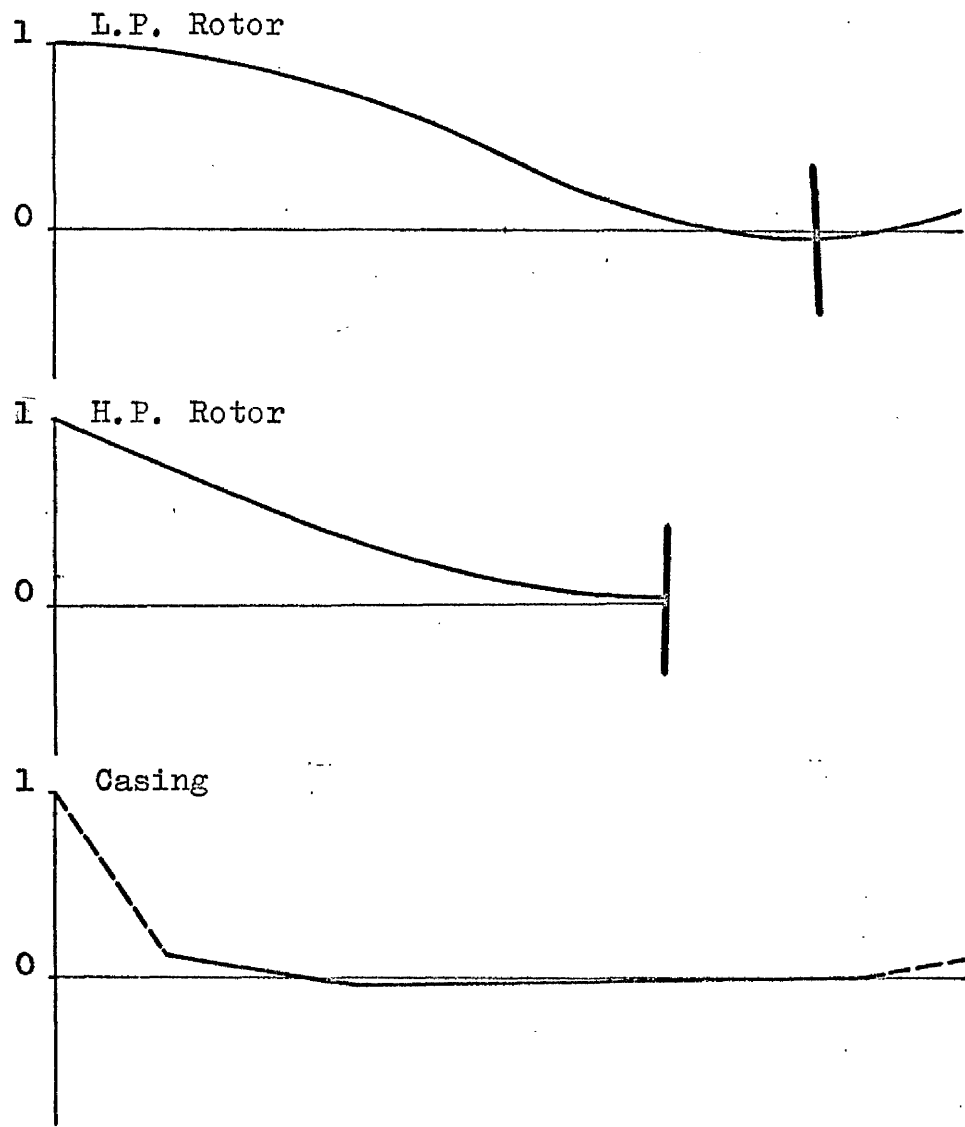
Fig.9.27(c)

Fig.9.27(c)   Mode of vibration at λ_4 when
              H = +12000 and L = −12000.
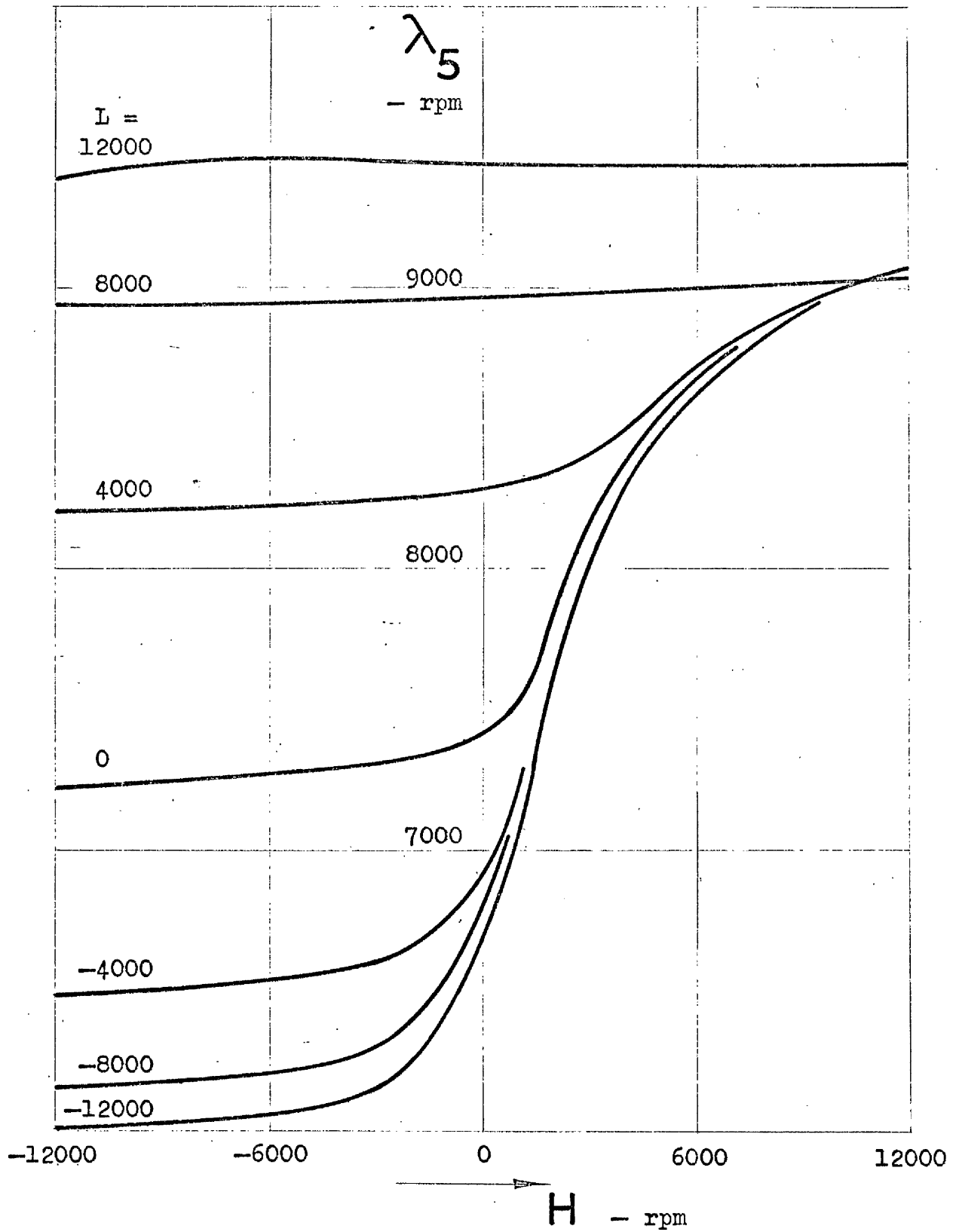
Fig.9.28(a)

Fig.9.28(a)   Variation of λ_5 with H and L
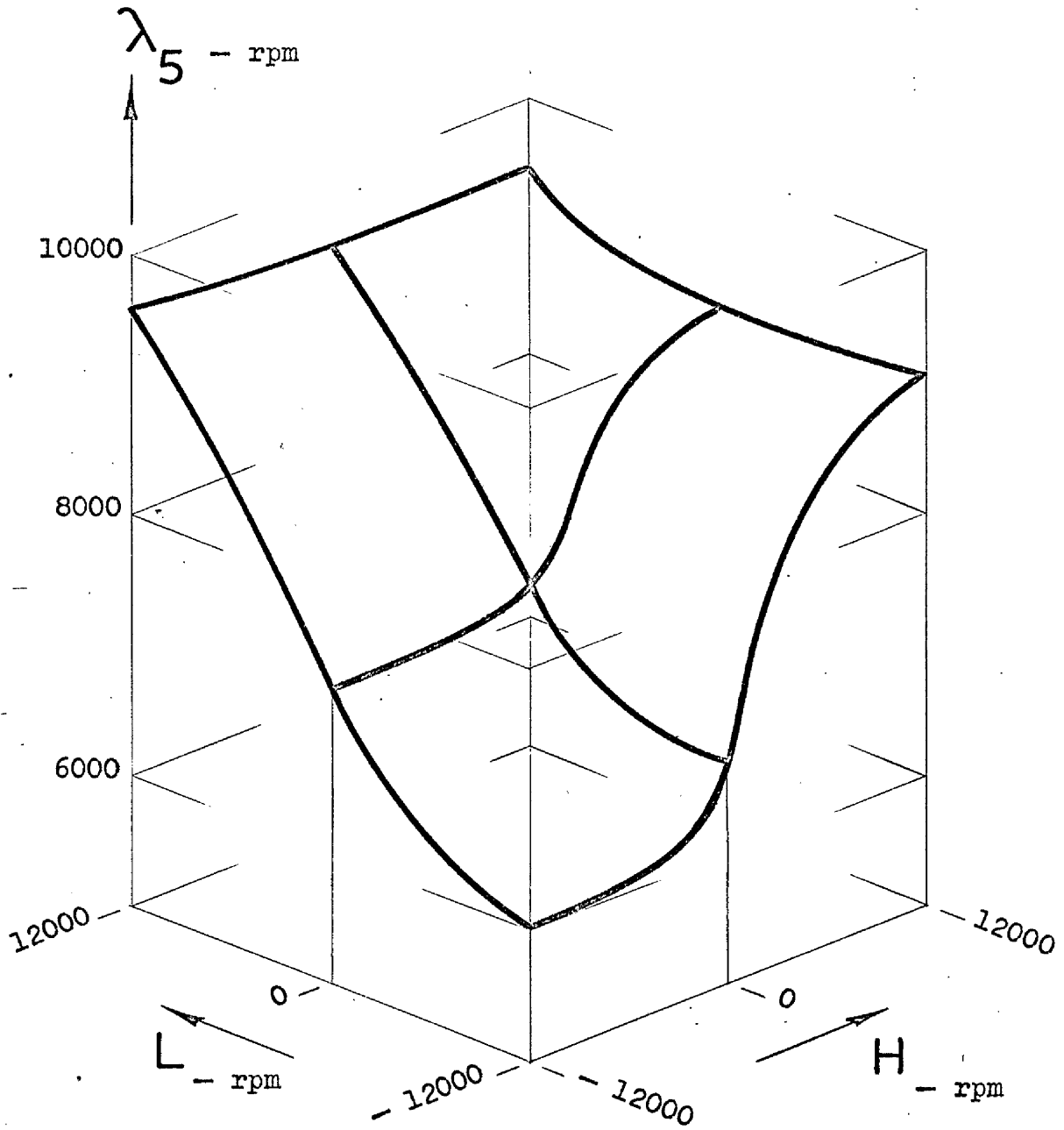
Fig.9.28(b)

<u>Fig.9.28(b)</u>   Isometric plot of variation of
λ_5 with H and L.

Fig.9.29(a)

1   L.P. Rotor

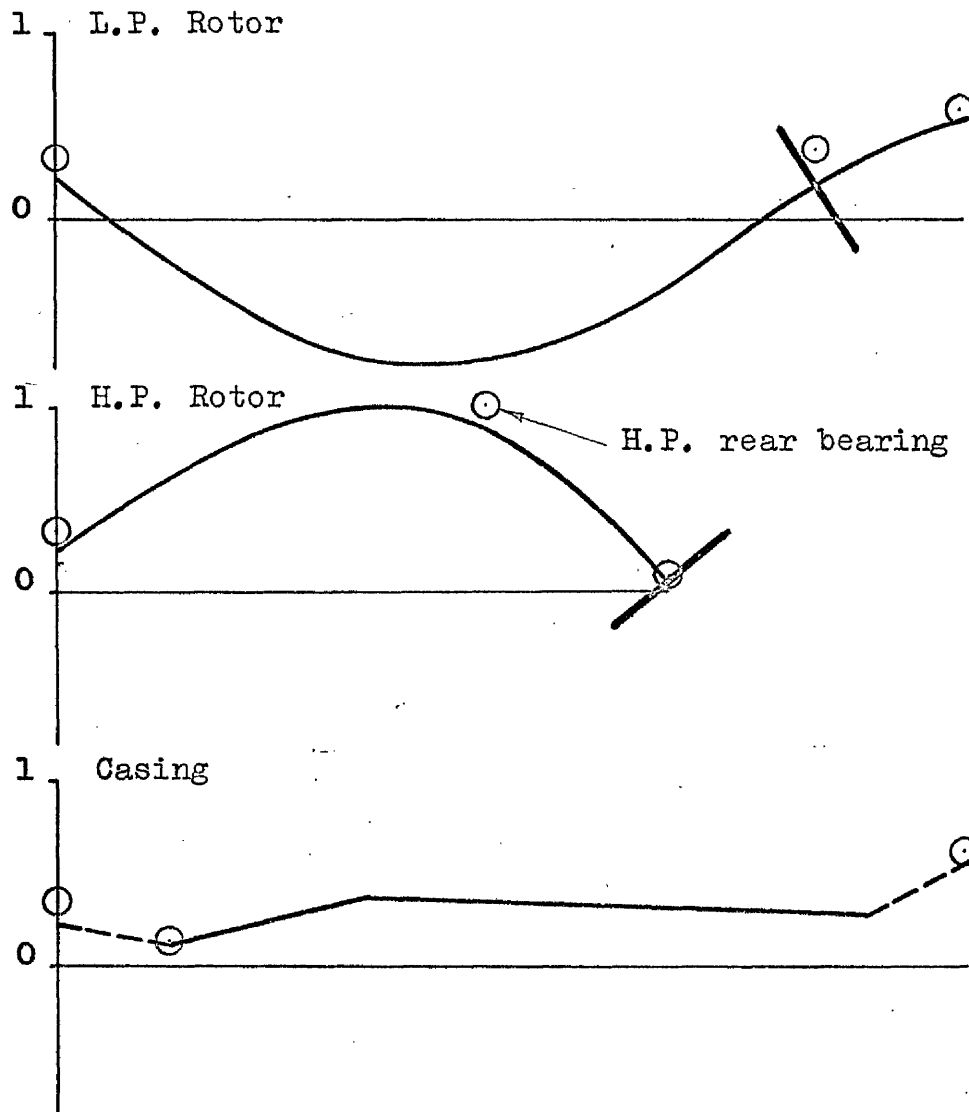0

1   H.P. Rotor

0

H.P. rear bearing

1   Casing

0
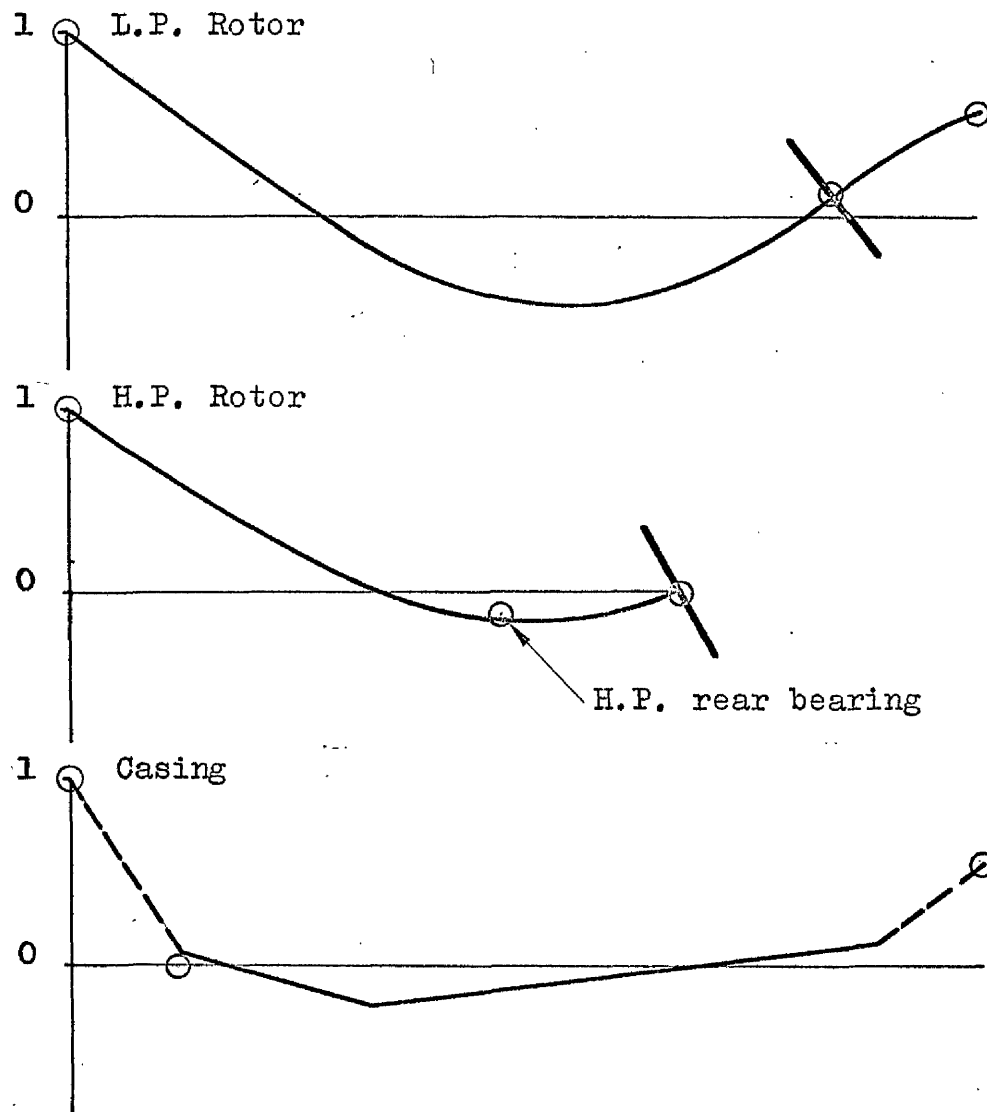
Fig.9.29(a)   Computed mode of vibration at λ_5
when H = L = 0.   (Circled points
show experimental amplitudes referred
to unit amplitude of front bearing).
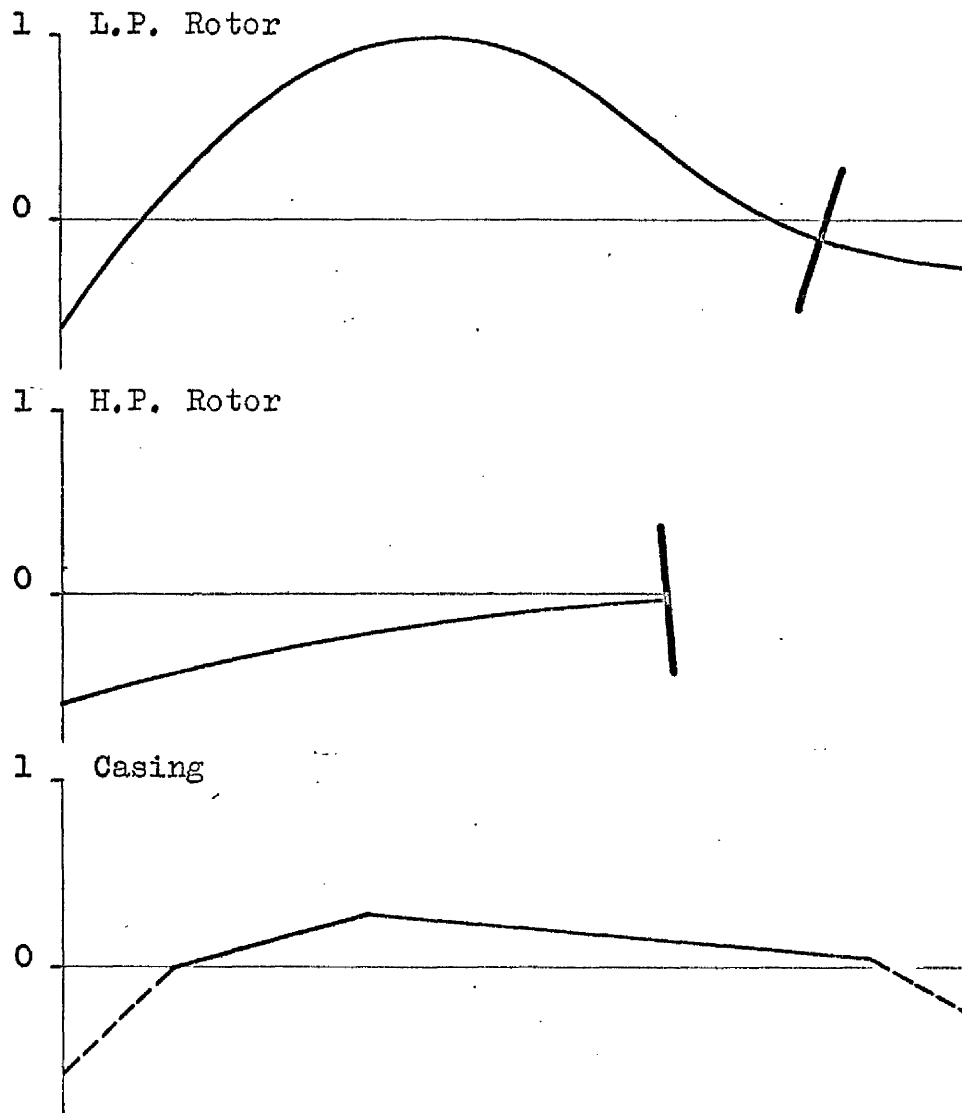
Fig.9.29(b)

Fig.9.29(b) Mode of vibration at λ_5 when
H = 0 and L = 12000.

Fig.9.29(c)

1 | L.P. Rotor

0

1 | H.P. Rotor

0

1 | Casing

0
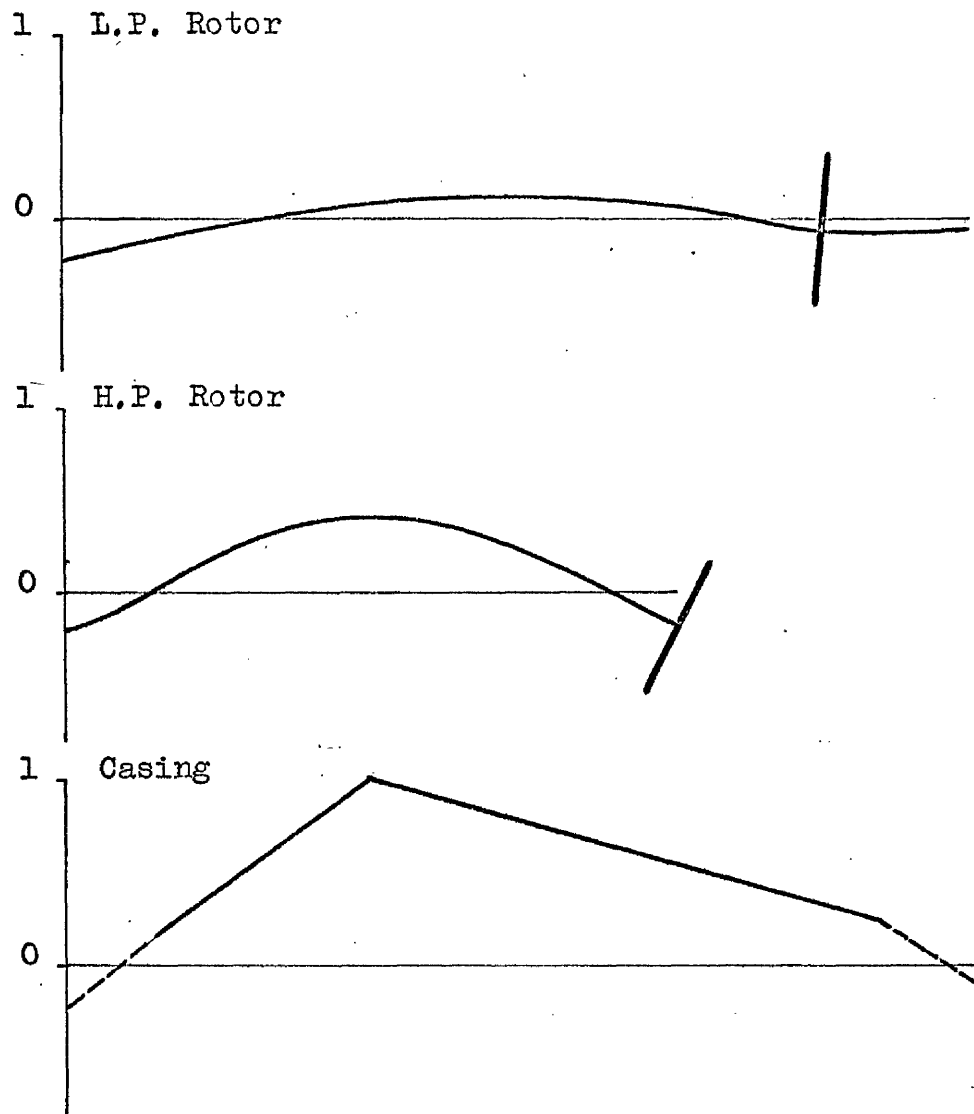
<u>Fig.9.29(c)</u>   Mode of vibration at λ_5 when
                      $H = + 12000$ and $L = 0.$

Fig.9.30

L – rpm

H – rpm

	-4000	0	4000	8000	12000
0	1172	1383	1558	1690	1782
	2008	2010	2010	2011	2013
-4000	1168	1377	1544	1640	1667
	1690	1693	1703	1739	1807
-8000	1160	1325	1361	1367	1369
	1389	1437	1578	1703	1795
-12000	1089	1111	1115	1117	1118
	1208	1387	1570	1699	1793
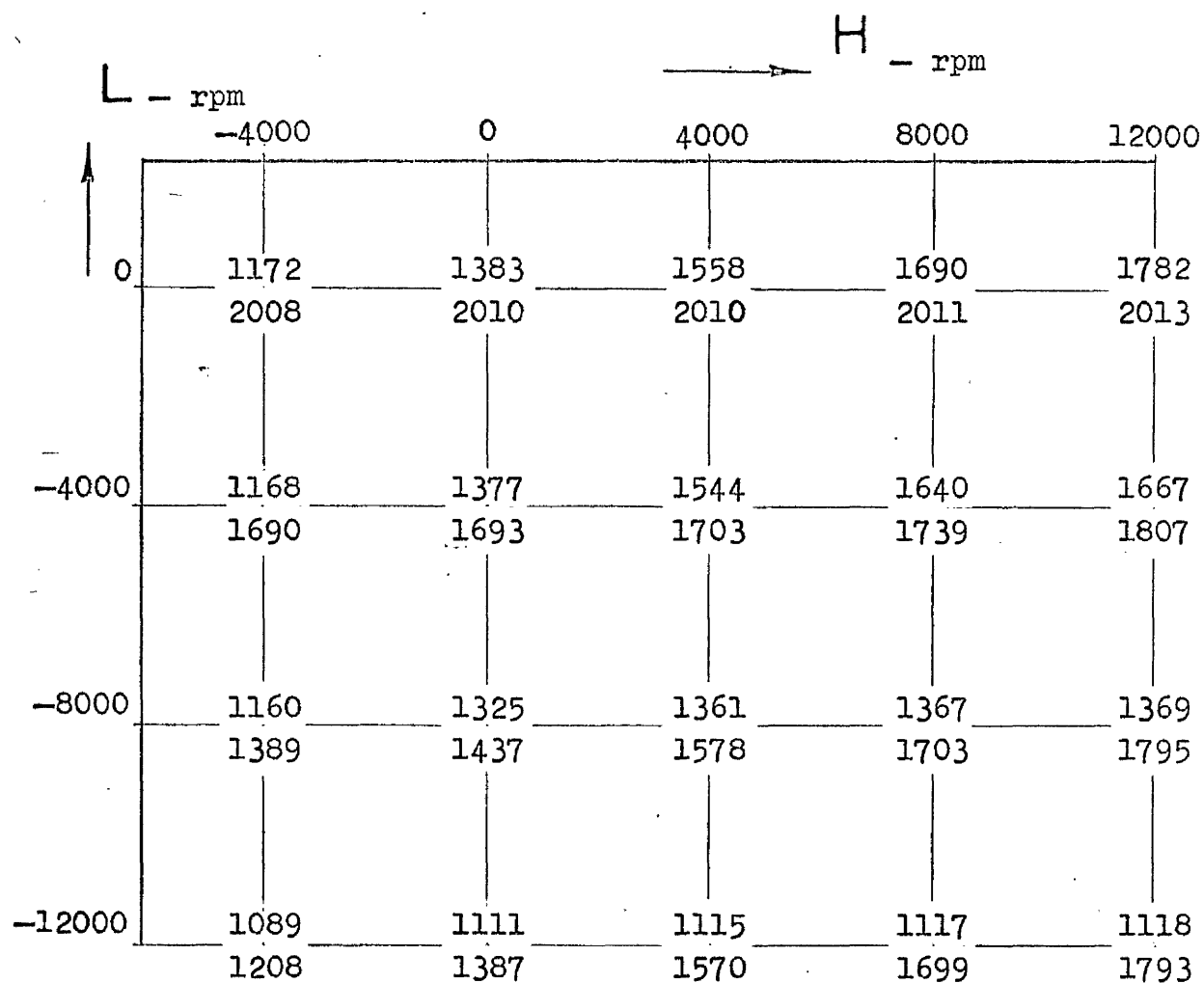
Fig.9.30   Grid map of HL plane showing close
approach of frequencies λ_1 and λ_2.

Fig.9.31

Fig.9.31 Loci of $H = \lambda_i$ and $L = \lambda_i$ with hypothetical engine characteristic superimposed.

CHAPTER 10

CONCLUSIONS AND SUGGESTIONS

FOR FURTHER WORK

SUMMARY

The transfer matrix method has proved to be ideally suited to the problem of predicting the natural frequencies of multi-shaft systems.

The difficulty experienced in producing a faithful computer simulation of the experimental rig suggests that it is not possible to predict the natural frequencies of jet engine systems with the accuracy demanded in practice.

The possibility that severe vibration of a sub-harmonic nature, similar to that observed on the rig, may well occur in a jet engine system suggests that this phenomenon demands urgent attention by research workers in the aero engine industry.

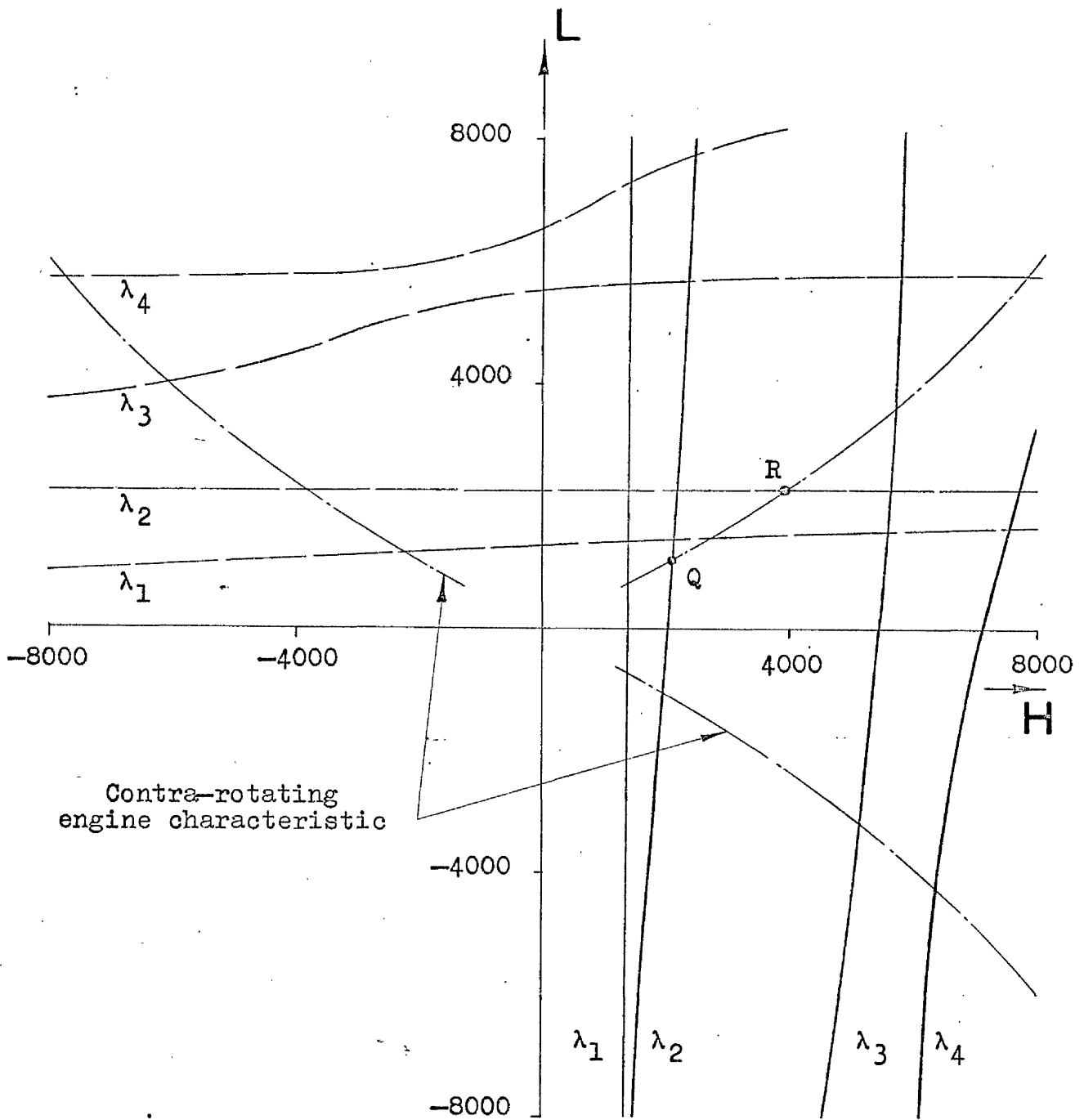It would seem that if the postulated cause of the excitation of reverse whirl is correct it may well be significant in shaft systems which use relatively large rolling element bearings.

The examination of the variation of natural frequencies with the speeds of the shafts has shown that appreciable variations do occur, particularly in systems which contain contra-rotating shafts. The studies have also shown that the character of a particular mode can change drastically at certain combinations of shaft speeds.

It was not practicable to include an examination of the effect of rotor damping, particularly that caused by friction at the splines connecting sections of a shaft, in this investigation. An examination of the implications of this effect is required.

CHAPTER 10

CONCLUSIONS AND SUGGESTIONS

FOR FURTHER WORK

10.1 Computer Analysis

It is the writer's opinion that in many computer studies of engineering problems much effort is devoted to mathematical or programming elegance while avoiding the real problem of ascertaining the accuracy of the numerical representation of the physical properties of the system — perhaps because it is often tedious or difficult to obtain this information experimentally.   In this investigation the experimental results — the natural frequencies of the rig — were not subject to variations in experimental technique and therefore discrepancies could only be blamed legitimately on the accuracy of the numerical representation of the rig.

The transfer matrix method of determining the natural frequencies was adopted because it appeared to be the most straightforward and therefore easiest to check for programming errors.   The properties of each section were contained within a simple 4 x 4 matrix, usually formulated by a standard procedure, thus reducing possible programming errors.

The method was ideally suited to the assembly of proved sub-programmes, representing each component, into a programme representing the whole rig with only little modification to the scheme of the calculation.

The adaptation of the transfer matrix method to produce the deflection of the casing under a static lateral load (which revealed the omission of the flexibility of the aluminium plates) was simple.   (Alternative methods of

frequency calculation, outlined in Chapter 3, could, of course, have been modified to produce the same result.) This simple technique is considered to be a valuable method of checking the numerical representation of a complex system which is being examined for natural frequencies.

When the mode of vibration was calculated it was a simple matter to produce, in addition, a tabulation of the slope, bending moment and shear force occurring at each section. These results, particularly the shear forces at the connections of the components, were invaluable in the detection of errors in the formulation of the calculation.

The transfer matrix method does suffer from numerical difficulties. At times these were thought to be serious and the modified matrix method was adopted with success. Other methods of frequency analysis also suffer from numerical difficulties. In the iteration technique used in the eigen-value approach special rinsing techniques often have to be employed to remove all traces of a known mode before the iteration will converge on the next mode.

In the writer's opinion the transfer matrix method is the best method of predicting the natural frequencies of multi-shaft systems. It has an appealing lack of mathematical abstraction. The assembly of the properties of each section is relatively simple thus reducing the likelihood of programming errors. Finally, the method can be adapted readily to provide several useful checks on the validity of the mathematical representation of a complex engineering structure such as a jet engine.

10.2 Accuracy of Prediction

Part of this investigation was devoted to attempting to assess the possible accuracy of prediction of the whirling speeds of jet engines. The model was a relatively simple structure compared with that of a jet engine and

despite the effort devoted to improving the computer
simulation of the model some of the measurable whirling
speeds were as much as $4^o/o$ higher than predicted.

It would therefore seem that, despite the use of
powerful computers, the whirling speeds of jet engines
cannot be predicted very accurately. The main difficulty
lies in the prediction of the stiffness of the structure
in the design stage. Admittedly some help is gained by
rig testing mock-ups of the major components — but the
results of these tests are of limited value unless they
are supplemented by tests designed to reveal the stiff-
nesses of the connections between the components.

If whirling speeds cannot be predicted accurately
then there is always the possibility that the actual speeds
will lie in the most unfavourable part of the engine speed
range. Therefore more effort should be devoted to design-
ing mechanisms which can be utilised to shift the whirling
speeds to less critical parts of the speed range — and new
designs should incorporate such features at the outset in
case they are found to be needed.

The conclusion that whirling speed calculations are
inevitably inaccurate does not mean that they should not be
attempted. Instead they should be regarded as a guide,
particularly as regards the variation of whirling speeds
with shaft speed due to gyroscopic effects. If an engine
is expected, from the computer studies, to exhibit whirling
within the speed range then it would be wise to perform a
lateral shaking test on the prototype before its first run.
The results of such a test, when compared with the computer
studies, ought to produce a very accurate assessment of
the true whirling speeds.

10.3 Bearing Excitation

The experimental work showed that slight excitation of the rig was caused by non-uniformity of the rolling elements of the bearings. But a serious vibration, of the nature of a sub-harmonic, was discovered which was not affected by unbalance of the rotor and was attributed to non-linearity of the support of the rotor as a result of the bearing clearance. Although a similar type of vibration had been reported by Yamamoto, the writer is not aware of any further investigation of this problem. The serious nature of this vibration would be disastrous if it were encountered in the course of development of a new engine.

A development which was introduced into some jet engines while this investigation was in progress is known as the squeeze film bearing. It is a revival of the technique of cushioning the roller bearing at the bottom end of a connecting rod, by means of an oil film, used in some motor cycle engines of the 1930's. In the jet engine application the outer track of the bearing is mounted in the housing with a small clearance of about 0.003 in and the annulus is fed with lubricating oil at a moderate pressure of about 30 psi. Remarkable reductions in vibration amplitude have been found to result when this technique is adopted — presumably as a result of the damping effect produced by the oil film.

An understanding of the properties of squeeze film bearings is being pursued in various establishments. It would appear to be important to ensure that some of this effort is devoted to examining the possibility of alleviating sub-harmonic whirl by this means.

10.4 Reverse Whirl

Reverse whirl has formerly been regarded as unimportant or even fictitious by some authorities. This is understandable since it is usually of very small amplitude and, as this investigation has shown, not caused by unbalance of the rotor.

Reverse whirl has been shown to be important in systems which contain two contra-rotating shafts. The experimental work showed that it was possible for one rotor to excite reverse whirl of the other. The degree of excitation could perhaps have been more extensively explored, with varying amounts of unbalance, but the results obtained would of course only be relevant to this system.

The writer has introduced the concept that reverse whirl, of even a single rotor system, is caused by non-circularity of the journal, or inner track of the bearing. The reverse whirl amplitudes of the rotors, when the other rotor was stationary, were certainly small. However, the bearings were not large and not subjected to influences which would distort them to any great degree. But in large jet engines (e.g. the Rolls-Royce RB-211 engine) large diameter bearings are used to support the H.P. rotor system. It would seem that there is a real possibility that the control of circularity of the inner tracks of these bearings may not be sufficient to prevent excitation of reverse whirl being greater than the excitation of forward whirl due to rotor unbalance.

There is therefore a strong case for an investigation of the magnitude of reverse whirl caused by controlled non-circularity of the bearing — which could of course be conducted adequately on a single rotor rig.

10.5 Support stiffness

No attempt was made in this investigation to examine the influence of the stiffness of the supports of the rig.   Since jet engines are usually mounted on the wings of multi-engined aircraft, and therefore mounted flexibly, it would be of value to investigate the influence of such flexibility on the whirling behaviour.

10.6 Damping effects

At the outset of this investigation damping due to friction within the splines connecting the shaft sections was suggested as a possible source of internal damping which could lead to instability.   This aspect was not included in this investigation for the difficulties described in Chapter 1.   The writer believes that this aspect is important enough to justify a separate investigation which could be conducted more easily on a single rotor system.

10.7 Gyroscopic effects

The novelty of this investigation lay in the co-axial shaft system.   Despite the almost universal adoption in modern jet engines of this arrangement no investigation of its whirling behaviour appears to have been reported.

The natural frequencies of a two shaft system have been shown to vary, sometimes considerably, with the speeds of both shafts.   Graphical methods of presenting the variations of the frequencies with shaft speed have been devised.   The introduction of a hypothetical engine characteristic showed that in a two shaft system a particular mode of vibration is likely to be encountered twice in the speed range of the engine.

The mode of vibration was found to be influenced quite markedly in some cases by the speeds of the rotors.

The results suggested that contra-rotating shaft systems are likely to encounter more points of vibration in a given speed range, and show peculiar changes in vibration modes, than systems in which the shafts rotate in the same direction.

REFERENCES

1. RANKINE, W.J.M.

    'On the centrifugal force of rotating shafts'

    The Engineer, vol.27, 1869.

2. GREENHILL, A.G.

    'On the strength of shafting when exposed both
        to torsion and to end thrust'

    Proc. Inst. of Mech. Engrs., 1883.

3. DUNKERLEY, S.

    'On the whirling and vibration of shafts'

    Roy. Soc. Phil. Trans. A, vol.185, 1894.

4. STODOLA, A.

    'Steam and Gas Turbines'

    McGraw-Hill, New York, 1927.

5. CHREE, C.

    'The whirling and transverse vibration of
        rotating shafts'

    Phil. Mag., vol.7, 1904.

6. LEES, S.

    'Whirling of an overhung eccentrically
        loaded shaft'

    Phil. Mag. (6), vol.45, 1923.

7. JEFFCOTT, H.H.

'The lateral vibration of loaded shafts in the neighbourhood of a whirling speed and the effect of want of balance'

Phil. Mag. (6), vol.37, 1919.

8. SMITH, D.M.

'Motion of a rotor carried by a flexible shaft in flexible bearings'

Proc. Roy. Soc. A, vol.142, 1933.

9. NEWKIRK, B.L. and TAYLOR, H.D.

'Shaft whipping due to oil action in journal bearings'

Gen. Elec. Rev., vol.28, 1925.

10. NEWKIRK, B.L.

'Journal bearing instability'

Proc. Conf. Lub. and Wear, 1957, 179 (Inst. Mech. Engrs.)

11. DIMENTBERG, F.M.

'Flexural vibrations of rotating shafts'

Butterworths, London, 1961.

12. DEN HARTOG, J.P.

'Mechanical vibrations'

(4th ed.) McGraw-Hill, New York, 1956.

13. KIMBALL, A.L.

'Internal friction theory of shaft whirling'

Gen. Elec. Rev., vol.27, 1924.

14.   MORRIS, J.

'The Escalator Method'

Chapman and Hall, London, 1947.

15.   PROHL, M.A.

'A general method for calculating critical
speeds of flexible rotors'

J. Appl. Mechs., vol.12, 1945.

16.   SHEPHERD, D.G.

'Principles of Turbomachinery'

- Macmillan, New York, 1956.

17.   PURDY, J.F.

'Model investigations into the critical
speeds of turbomachinery'

Thesis, Cambridge University, 1956.

18.   TSE, F.S., MORSE, I.E. and HINKLE, R.T.

'Mechanical vibrations'

Prentice-Hall International, London, 1963.

19.   PESTEL, E.C. and LECKIE, F.A.

'Matrix methods in elasto-mechanics'

McGraw-Hill, New York, 1963.

20.   STOKER, J.J.

'Nonlinear vibrations'

Interscience Publishers, New York, 1963.

21.   YAMAMOTO, T.

                'On the vibrations of a rotating shaft'

            Mem. Fac. Eng. Nagoya Univ., vol.9, 1957.

22.   BLACK, H.F.

                'Synchronous whirling of a shaft within
                a radially flexible annulus having small
                radial clearance'

            Proc. Inst. Mech. Engrs., vol.181, part 3A, 1967.

23.   ROARK, R.J.

                'Formulas for stress and strain'

            McGraw-Hill, London, 1954.

24.   BIEZENO, C.B. and GRAMMEL, R.

                'Engineering dynamics', Vol.3.

            Blackie, London and Glasgow, 1954.

25.   LAWDEN, D.F.

                'Mathematics of engineering systems'

            Methuen, London, 1961.

26.   HAYASHI, C.

                'Nonlinear oscillations in physical systems'

            McGraw-Hill, New York, 1964.

_____